Key mechanisms of surface water pCO_2 variability in the North Atlantic Ocean

Justin Krijnen

Thesis submitted in fulfilment of the requirements for the degree of Doctor of Philosophy

University of East Anglia
School of Environmental Sciences

May 2013

Abstract

A proxy for the North Atlantic gyre circulation has been developed, using sea-surface height from altimetry. In conjunction with the winter North Atlantic Oscillation (NAO) index, statistical analysis has been applied to understand the key mechanisms of surface water partial pressure of CO_2 (pCO_2) variability, both on the seasonal and inter-annual timescale.

With respect to the seasonal amplitude of surface pCO_2 in temperate regions (>40°N), it is found that the gyre circulation strength, in response to the winter NAO index, drives this seasonal amplitude. Under positive NAO index winters, the formation of mode waters is favoured through strong surface cooling. This deepens the mixed layer, entraining carbon and nutrient-rich subsurface waters into the surface layer and increasing the surface pCO_2 in winter. This deep winter mixing, bringing up nutrients in combination with enhanced advection of nutrients from the subpolar region, may also enhance and prolong the following spring bloom, decreasing the pCO_2 in both spring and early summer. Thus, the seasonal amplitude of surface pCO_2 under a positive NAO phase would increase.

Under negative NAO winters, surface cooling is not as pronounced compared to a positive NAO winter and therefore the mixed layer is not as deep. Thus, both vertical and horizontal (via advection) carbon and nutrient entrainment are reduced thereby decreasing the pCO_2 in winter and potentially weakening the following spring bloom. Thus the seasonal amplitude of surface pCO_2 under a negative NAO phase would decrease. The subtropical regions (25 - 40°N) are also subjected to similar processes as the temperate regions, under both positive and negative NAO winters.

However, the above-mentioned lagged effect of carbon-rich sub-surface water and nutrient entrainment in winter on the intensity of the spring bloom has to be treated with caution given the lack of statistically significant correlations between the surface pCO_2 in winter and the proxy for carbon-rich subsurface water in spring.

On inter-annual timescales, the phase of the winter NAO alters the ocean circulation in all regions. Under a positive NAO index, the subtropical gyre is more spun-up and with increased SST, increasing the annual mean pCO_2. In the temperate zone, the interplay between carbon entrainment and biological drawdown dominates, dampening the inter-annual pCO_2 variability.

Contents

List of Figures

Acknowledgements

First and foremost I would like to thank my wonderful wife Kathrin for the continued emotional support she has given me over these years. She has had to endure my complaining and whining (especially during the first couple of years) when MATLAB was giving me headaches. However, we've also experienced short, intense periods of glee (e.g. when MATLAB began to do what I wanted it to and of course when the scientific results began to materialise). So, if it wasn't for her calming influence I probably would have fallen off the roller coaster ride that is a PhD a long time ago. Thanks for being there for me whenever and whatever the circumstances!

Equally important, on an academic front, was the support I received from my supervisors Andrew Watson, Ute Schuster and Samantha Lavender over the past four years. I am also grateful to Corinne Le Quéré and Erik Buitenhuis for providing me with their model output data. In addition many thanks go to Dimitrios Efthymiadis for his useful comments and academic advice.

I would also like to thank the National Centre for Earth Observation (NCEO) and the Natural Environmental Research Council (NERC) for their financial support throughout my doctoral studies.

Outside of the academic arena, my sincere thanks go to my friends who have also played a major part in keeping my spirits high. I certainly enjoyed the games of golf we played on the pitch and putt, especially since I won (most of the time!). Many thanks also go to Julian and Lina, and their two children, Alex and Christopher with whom my wife and I have spent many joyful moments. My thanks also extend to the Norwich Orthodox parish. In particular I would like to thank Fr. Patrick and Fr. Julian for their spiritual support and advice. Many thanks also go to Mary and Natasha (their wives, respectively) for inviting us to their wonderful dinners! Last but certainly not least, I would like to sincerely thank my parents for their belief in me and boundless understanding and support.

Chapter 1: Introduction

1.1 Background and Importance

1.1.1 The North Atlantic carbon sink

The world's oceans are an important sink of atmospheric CO_2, and their role in the carbon cycle has been increasingly investigated in the light of the rapid growth of anthropogenic CO_2 emissions over the last three decades. From 2000 to 2006, the atmospheric growth rate was ~1.93 ppm yr^{-1} compared to ~1.49 ppm yr^{-1} during the 1990s and ~1.58 ppm y^{-1} during the 1980s (Canadell et al. 2007). The global oceans were reported to have taken up an estimated 118 ± 19 PgC (petagram Carbon) by 1994 (Sabine et al. 2004), which represented half of the global anthropogenic CO_2 emissions of 244 ± 20 PgC since the onset of the industrial revolution (Sabine et al. 2004). The North Atlantic in particular is a strong sink for atmospheric CO_2, storing 23% of the global anthropogenic CO_2 inventory whilst covering only 15% of the global ocean area (Sabine et al. 2004). Continuous uptake of atmospheric CO_2 through the simultaneous surface cooling of waters whilst travelling northwards (mainly via the Gulf Stream and North Atlantic current), in addition to relatively high biological activity, are the main reasons for the intense ocean sink of the basin (Takahashi et al. 1993).

However, recent studies have pointed to a decrease of the oceanic carbon sink (Lefèvre et al. 2004; Olsen et al. 2006; Omar and Olsen 2006; Corbière et al. 2007; Metzl et al. 2010). While most of the increase in the growth rate of atmospheric CO_2 over the last 30 years has been attributed to the amount of fossil fuel CO_2 released, 18 ±15% is considered to be a result of a decline in the efficiency of the land and ocean sinks (Canadell et al. 2007). Furthermore, superimposed on this wider ocean CO_2 sink decrease, observational studies have shown that there is also significant seasonal and inter-annual variability of the ocean CO_2 sink in the North Atlantic between the 1990s and 2000s (Schuster and Watson 2007; Watson et al. 2009) with a decrease in the uptake of CO_2 by the eastern temperate North Atlantic of ~50% from the mid-1990s to the 2000s (Schuster et al. 2009). However, it should be noted that globally, the ocean carbon sink has not decreased but has continued

to take up CO_2 since the 1960s (Ballantyne et al. 2012). Thus, natural climate variability may have masked a continued upward trend in global ocean carbon uptake.

1.2 Thesis aim

This thesis focuses upon identifying the drivers of the seasonal and inter-annual variability of the CO_2 in seawater in the North Atlantic. By understanding the mechanisms of seawater CO_2 variability in this dynamically active basin on these time-scales, it will be possible to better predict how this oceanic carbon sink is likely to respond to future climate change. This is especially important given that anthropogenic CO_2 emissions are likely to continue to increase and potentially result in warming of between 1.1 to 6.4°C by the year 2100 (IPCC 2007).

Before reviewing further studies with respect to the ocean carbon sink variability, the mechanism that allows for uptake of atmospheric CO_2 will briefly be discussed (section 1.3). In addition, the inorganic carbon chemistry of CO_2 in seawater will be examined and the controls on the oceanic CO_2 discussed (section 1.4).

Section 1.5 provides an overview of the North Atlantic Oscillation (NAO) and its effect on the ocean circulation. In addition, the mean seasonal cycle of surface pCO2 for the two regions studied in this thesis is described. Section 1.6 outlines the current understanding of the mechanisms associated with the long term trends of the oceanic CO_2 (and seasonal to inter-annual variability thereof where applicable), which provides the foundation for the research hypotheses that are presented in section 1.7. Finally, section 1.8 provides an outline of the thesis structure.

1.3 Air-sea flux of CO_2

The mechanism that allows for uptake of CO_2 in the ocean is the air-sea flux of CO_2. It is driven by ΔpCO_2, which represents the difference between atmospheric and sea surface partial pressures of CO_2 (pCO_2) (Sarmiento and Gruber 2006). As will be discussed, variations in the surface pCO_2 are determined by sea surface temperature (SST), salinity, dissolved inorganic carbon (DIC) and total alkalinity

(ALK). There is a complex interplay of factors that causes the surface water pCO_2 to change depending on the location and timescale. For example, on timescales of decades to centuries, atmospheric CO_2 dissolves into the sea surface and is transported at depth through intermediate and deep waters, such as the North Atlantic Deep Water (NADW) (Sarmiento and Gruber 2006). A fraction of the DIC is used up by phytoplankton and the detritus thereof sinks to the bottom of the sea as particulate organic carbon (POC) and is stored in sediments over thousands of years. On seasonal to inter-annual timescales, SST, DIC and biology all interact to influence the surface pCO_2 (Gruber et al. 2002).

Atmospheric measurements have been made at Mauna Loa since ~1958 (Keeling et al. 1976). Seawater pCO_2 measurements have been undertaken since the 1970s (Watson and Orr 2003). Research vessels as well as an increasing number of commercial ships have been used as platforms on which to carry out these measurements (Schuster and Watson 2007).

Syntheses of these data have been published (see for example Takahashi et al., (1993; Takahashi et al. 2002; Takahashi et al. 2007; Takahashi et al. 2009) with the latter publication using up to 3 million point measurements. The recent establishment of the Surface Ocean CO_2 Atlas (SOCAT; (Pfeil et al. 2012)) however consists of 6.3 million point measurements (Bakker et al. 2012).

The intensity and sign of the air-sea flux of CO_2 can be expressed as the flux (F) of CO_2 into either the atmosphere or the ocean across the air-sea boundary:

$$F = k_v \alpha \, \Delta pCO_2 \qquad (1.1)$$

where ΔpCO_2 is the difference in partial pressure of CO_2 in the air and surface water and k_v is the gas transfer coefficient, primarily a function of wind speed (Watson and Orr 2003), and α the solubility of CO_2, which is a function of temperature and salinity (Weiss 1974). The determination of k_v has been intensely debated, however. For example, the parameterization of k_v from the use of wind-wave laboratory experiments (Liss and Merlivat 1986) compared with an empirically formulated version (Wanninkhof 1992) produced different parameterizations of k_v.

Equation 1.1 expresses the air-sea flux as a product of a readily measurable chemical gradient across the sea surface and a variable gas transfer velocity k_v that expresses the ease with which a molecule of gas can pass from the gaseous to the dissolved phase or vice versa (Watson and Orr 2003).

The following section examines the inorganic carbon chemistry and the controls on the surface pCO_2.

1.4 Inorganic carbon chemistry

1.4.1 The carbonate system in seawater

Atmospheric CO_2 (its gaseous form) dissolves in the surface ocean. This is expressed as an "accommodation":

$$CO_{2(gas)} \leftrightarrow CO_{2(aq)} \tag{1.2}$$

The aqueous CO_2 hydrates with the seawater to form carbonic acid (H_2CO_3). This is the hydration/dehydration reaction.

$$CO_{2(aq)} + H_2O \leftrightarrow H_2CO_{3(aq)} \tag{1.3}$$

As it is difficult to make an analytical distinction between the two species $CO_{2(aq)}$ and $H_2CO_{3(aq)}$, they are usually combined and their sum is expressed as the concentration of a hypothetical species $CO^*_{2(aq)}$ (Dickson et al. 2007). The latter then dissociates first to form bicarbonate $HCO^-_{3(aq)}$ ions and then carbonate $CO^{2-}_{3(aq)}$ ions (Sarmiento and Gruber 2006):

$$CO_{2(gas)} + H_2O \leftrightarrow CO^*_{2(aq)} \tag{1.4}$$

$$CO^*_{2(aq)} \leftrightarrow H^+_{(aq)} + HCO^-_{3(aq)} \tag{1.5}$$

$$HCO^-_{3(aq)} \leftrightarrow H^+_{(aq)} + CO^{2-}_{3(aq)} \tag{1.6}$$

The sum of the concentrations of the dissolved inorganic carbon species in seawater (Dickson 1981) represents the DIC, as expressed in the following equation:

$$DIC = \left[CO^{*}_{2(aq)}\right] + [HCO_3^-] + [CO_3^{2-}] \quad (1.7)$$

However, only a very small fraction of the dissolved inorganic carbon exists as dissolved CO_2 (~0.5%). Most of the carbon exists as bicarbonate ion (~89%) and a smaller proportion (~11%) as carbonate ion (Sarmiento and Gruber 2006). As such, DIC can be approximated as the sum of carbonate and bicarbonate ions only:

$$DIC \approx [HCO_3^-] + [CO_3^{2-}] \quad (1.8)$$

Apart from the DIC, the marine carbonate system is defined by the pCO_2, which refers to the partial pressure of carbon dioxide of a sample of seawater that is in equilibrium with a gas. This partial pressure is determined either through a gas chromotograph, an infrared analyzer or by Cavity Ringdown Spectrometers (CRDS). Corrections for differences in pressure, temperature and moisture between the in-situ and analytical conditions need to be taken into account (see chapter 2, section 2.2.1 for a description of the calculation of surface pCO_2). Other factors that control the marine carbonate system are ALK, hydrogen ion concentration $[H^+]$, reported as pH, SST, and salinity.

The focus of this thesis is on understanding the variability of the surface pCO_2 in the North Atlantic Ocean. Tjiputra et al. (2012) calculate that the primary factors responsible for the variability in surface pCO_2 in the open North Atlantic Ocean are SST and DIC (through biological processes) with ALK and salinity of minor importance. Thus, ALK and salinity have been excluded as parameters which affect the surface pCO_2 in this thesis.

The following section discusses how the main parameters mentioned previously (e.g. SST and DIC primarily) may alter the surface pCO_2.

1.4.2 Factors controlling sea surface pCO_2 in the North Atlantic Ocean

Temperature affects the surface pCO_2 by increasing or decreasing the solubility of CO_2 in seawater. Takahashi et al. (1993) described the temperature-dependence of surface pCO_2 and further details are reported in chapter 2, section 2.4.4.

Biological processes form the second fundamental set of surface water pCO_2 drivers. The key processes that affect the concentration of DIC are the photosynthetic uptake of CO_2 to form organic matter and the reverse process of respiration and remineralization (Sarmiento and Gruber 2006). The formation of organic matter decreases the concentration of DIC.

The production of organic matter occurs through the process of photosynthesis in the euphotic zone (i.e. the uppermost sunlit layers of the oceans). Through settling particles or advection of dissolved organic carbon, a proportion of the organic matter is transported to the deeper layers which leads to a net consumption of CO_2 in the surface layers. The organic matter is then remineralized in the deeper layers and CO_2 is thus returned to the seawater. These processes result in a net transfer of DIC from the surface into the deep ocean, which is often referred to as the "soft tissue pump" (Volk and Hoffert 1985). Another important result is a vertical gradient in DIC, such that mixed layer deepening will usually entrain higher DIC water.

The second biological control on surface DIC is the biogenic formation and dissolution of calcite and aragonite (also known as calcification):

$$Ca^{2+} + 2HCO_3^- \leftrightarrow CaCO_3 \qquad (1.9)$$

Mineral calcium carbonate shells are formed in the upper layers of the ocean primarily by three groups of planktonic organisms: coccolithophorids, foraminifera and pteropods. Upon the death of these organisms, their shells sink and eventually dissolve. The net effect of this process is a downward transport of DIC and ALK into the deep ocean, known as the "carbonate pump" (Sarmiento and Gruber 2006).

Inputs of freshwater may also have an effect on the DIC and ALK by diluting the concentration of all chemical species present in seawater in direct proportion to the

dilution of salinity (Sarmiento and Gruber 2006). The opposite effect occurs if an excess of evaporation over precipitation leads to a net removal of freshwater from the surface ocean.

In summary, the variations in surface ocean pCO_2 in the North Atlantic Ocean (excluding the coastal zone) are primarily determined by temperature and secondly by biological processes, such as photosynthesis and remineralisation that affect the concentrations of DIC.

The following section describes the North Atlantic atmospheric circulation and how it affects the oceanic circulation. Important concepts that are used in this thesis are also defined (e.g. the subtropical and temperate regions) and an overview of the seasonal cycle of surface ocean pCO_2 within these regions is given.

1.5 The North Atlantic Oscillation and the seasonal cycle of pCO_2

1.5.1 The North Atlantic Oscillation and its effect on the ocean circulation

In the North Atlantic, the dominant mode of climate variability is the North Atlantic Oscillation (NAO) (Marshall et al. 2001). The NAO is defined as an index of normalized, time-averaged pressure differences between the stations representing its two centres of action, the Azores and Iceland (Marshall et al. 2001). Pressure differences between Gibraltar, Spain and Reykjavik, Iceland are also used (e.g. Osborn 2011) as are pressure differences between Lisbon, Portugal and Reykjavik, Iceland (e.g. Hurrell et al. 2003). The NAO index has varied significantly over the last century as shown in Figure 1-1.

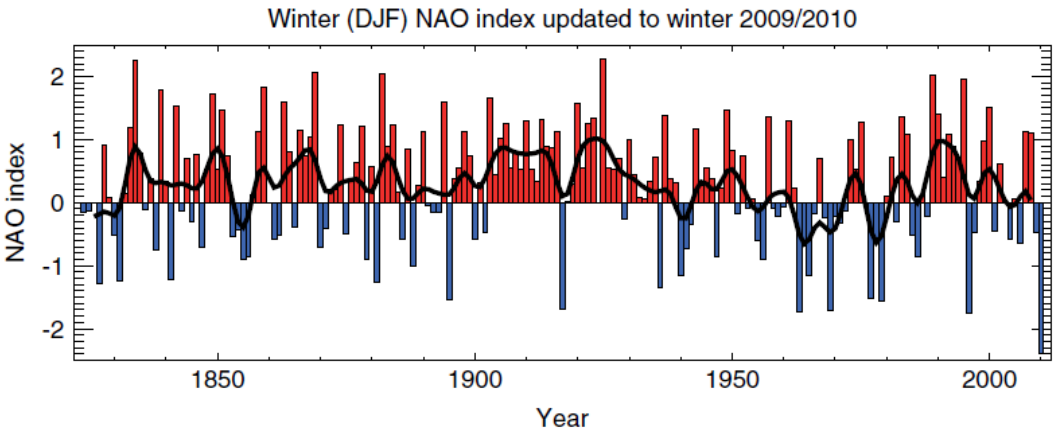

Figure 1-1: Winter NAO index based on the difference between normalised sea-level pressure observations at Gibraltar and southwest Iceland. The thick black line shows smoothed values from a 10-year Gaussian weighted filter (Osborn 2011).

The positive NAO index winters depicted in red (Figure 1-1) are associated with a strengthening of the westerly winds in the subpolar region of the North Atlantic (north of 45°N), (Marshall et al. 2001), as illustrated by Figure 1-2. The north-east trade winds also increase in the tropical Atlantic (between the equator and 30°N). In both these regions, the ocean loses energy to the atmosphere due to the strengthening of these wind fields (Deser et al. 2010). As a result, negative SST anomalies are evident in both the subpolar and tropical Atlantic (Deser et al. 2010), see Figure 1-2.

In the mid-latitude regions (i.e. between 30°N and 45°N), wind speeds decrease during a positive NAO index winter, due to the location of this zone beneath the enhanced Azores High (Deser et al. 2010). Hence energy is gained by the ocean, thereby resulting in positive SST anomalies throughout the mid-latitude North Atlantic (Figure 1-2).

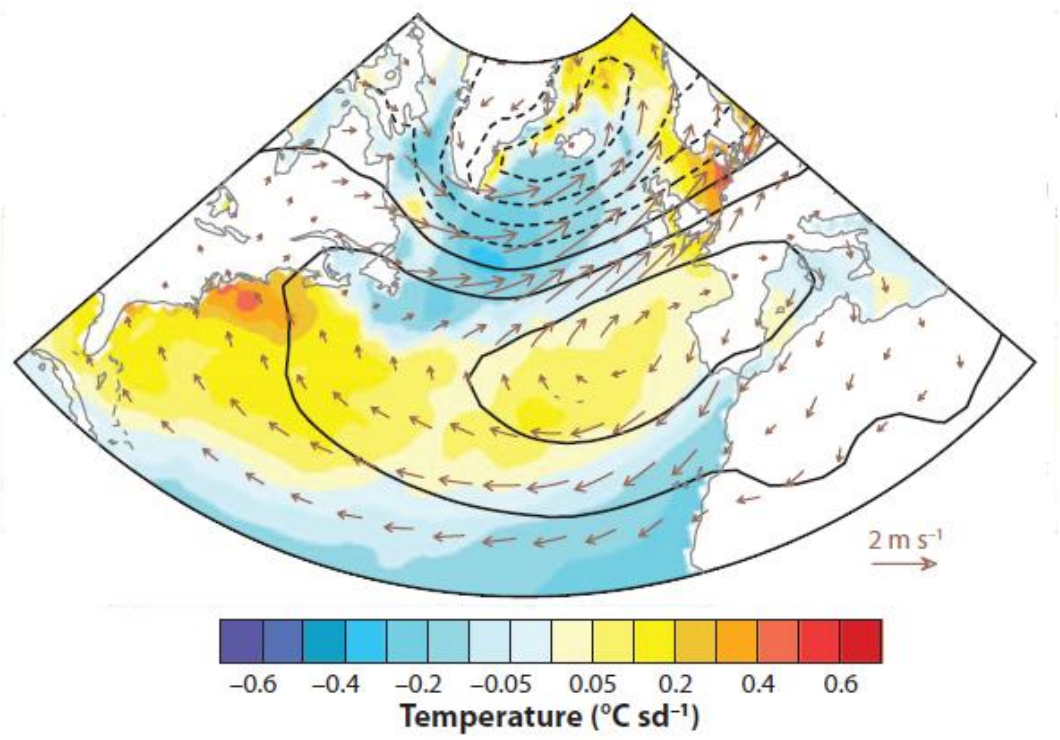

Figure 1-2: Anomaly patterns associated with a +1 standard deviation departure of the North Atlantic Oscillation (NAO) Index during winter (December-March) defined using stations at Lisbon, Portugal and Reykjavik, Iceland. Sea-surface temperature (SST) (shading), sea-level pressure (SLP) (contours), and surface wind (arrows). The SLP contours are 1hPa, with negative values dashed (Deser et al. 2010).

In regions where energy is lost to the atmosphere through strong surface cooling, formation of mode waters is favoured. One such water mass is the Eighteen Degree Water (EDW) that forms south of the Gulf Stream in winter (Marshall et al. 2009), in addition to the Subpolar Mode Water (SPMW) in the subpolar gyre region (Levine et al. 2011), see Figure 1-3. Furthermore, the polar and subtropical Eastern North Atlantic Central Water, ENACWp and ENACWt, respectively (Padin et al. 2011), form at the eastern flank of the North Atlantic Current (NAC), see Figure 1-4. The outcrop area, extent and formation rate of these mode waters is related to the phase of the NAO: high formation rates, large outcrop areas in addition to large extents of both of these mode waters occur during positive NAO years, when heat loss to the atmosphere is high (Bates et al. 2012, Levine et al. 2011). The opposite occurs during low NAO index years (Bates et al. 2012, Levine et al. 2011).

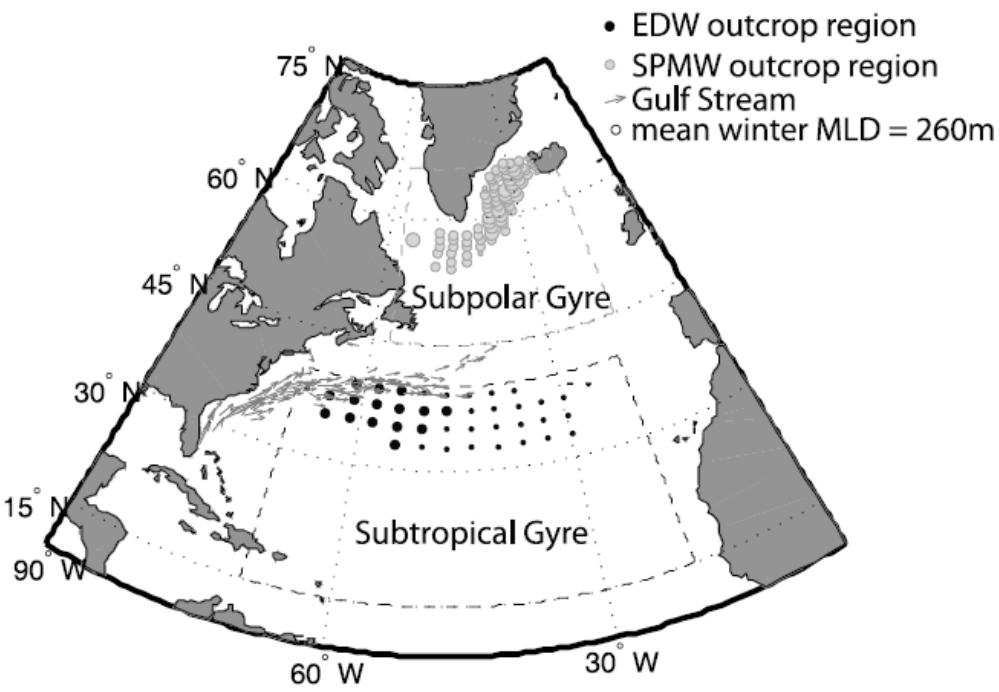

Figure 1-3: Schematic of the outcrop regions for the Eighteen Degree Mode water, EDW and the Subpolar Mode Water, SPMW, shown using black circles and grey circles respectively. The size of the circle corresponds to the average wintertime mixed layer depth (MLD). From Levine et al. (2011).

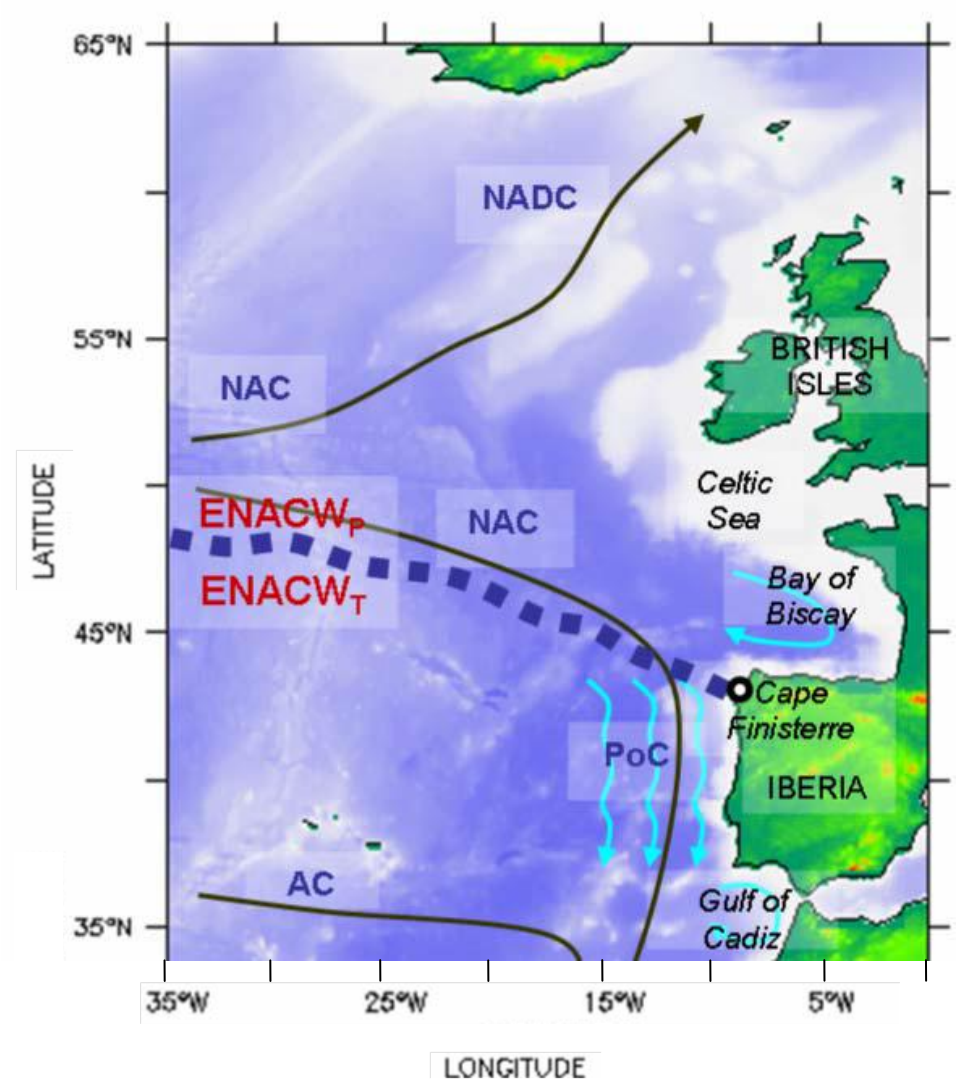

Figure 1-4: Schematic of the Eastern North Atlantic region. The principal mode waters are the subpolar Eastern North Atlantic Central Water (ENACWp), and the subtropical Eastern North Atlantic Central Water (ENACWt). The main surface currents within the region are the North Atlantic Current (NAC), the North Atlantic Drift Current (NADC), the Azores Current (AC), and the Portuguese Current (PoC). The blue arrows indicate the general circulation of the Bay of Biscay, Gulf of Cadiz and the region off the coast of Portugal. Adapted from Mason et al. (2006).

The wind circulation patterns orchestrated by the NAO drive the surface currents of the North Atlantic. This is achieved through turbulent transfer of momentum across the atmospheric boundary layer, known as the wind stress (Marshall and Plumb, 2007). A schematic of the main surface currents found in the North Atlantic is given in Figure 1-5. In addition, two main gyre systems are evident in the North Atlantic: the subtropical and subpolar gyre.

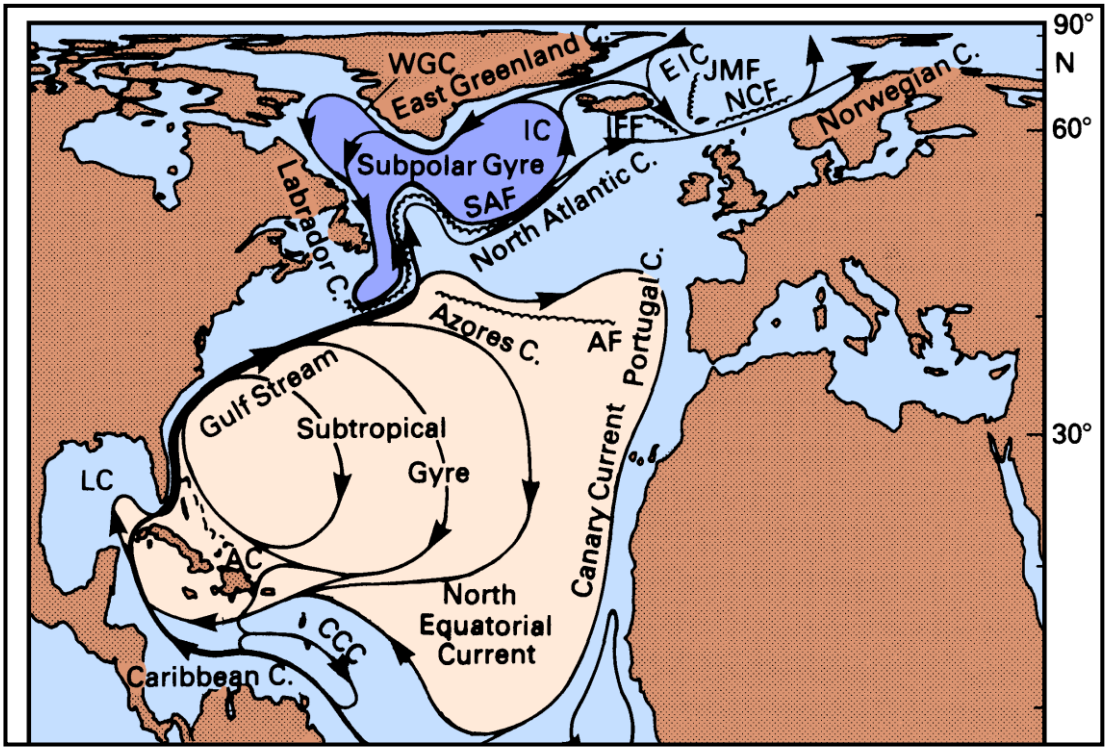

Figure 1-5: Surface currents of the Atlantic Ocean. Abbreviations are used for the East Iceland (EIC), Irminger (IC), West Greenland (WGC), and Antilles (AC) Currents and the Caribbean Countercurrent (CCC). Other abbreviations refer to fronts: JMF: Jan Mayen Front, NCF: Norwegian Current Front, IFF: Iceland - Faroe Front, SAF: Subarctic Front, AF: Azores Front. Adapted from Tomcak and Godfrey (2001).

The subtropical gyre is driven by the westerly winds on its northern flank and the north-easterly trade-winds on its southern flank. The rotation of the Earth, which produces the Coriolis force, creates an Ekman transport that is perpendicular to the direction of the wind (Bigg, 2003). This is to the right in the northern hemisphere and to the left in the southern hemisphere. Thus, within the subtropical gyre, water is transported to the centre of the gyre, where this results in a doming of the sea surface (Bigg, 2003). Therefore, sea-surface heights (SSH) are climatologically high in this region.

The subpolar gyre is driven by polar easterlies on its northern flank and the mid-latitude westerlies on its southern flank (Figure 1-5). As a result of the Coriolis force, Ekman transport carries water to the south of the subpolar region towards the mid-latitudes. Therefore, SSH are climatologically low in this region (see Figure 1-6).

Several authors have used the gradient in SSH between two reference points to determine the transport of western boundary currents. For example, Imawaki et al. (2001) determined the transport of the Kuroshio (Japan's western boundary current)

by calculating absolute geostrophic velocities from the gradient in SSH across the boundary current. A similar method has also been used to obtain the transport of the Agulhas current, off the eastern coast of South Africa (van Sebille et al 2010). Furthermore, Curry and McCartney (2001) use the potential energy anomalies (PEA) at the centres of both the subtropical and subpolar gyres for calculating the basin-scale baroclinic mass transport of the North Atlantic gyre circulation.

A similar approach to Curry and McCartney (2001) is used in this thesis for the purpose of identifying a proxy for the gyre circulation strength. Hence, the SSH difference between the centres of the subpolar and subtropical gyres is used as a proxy of the oceanic circulation strength.

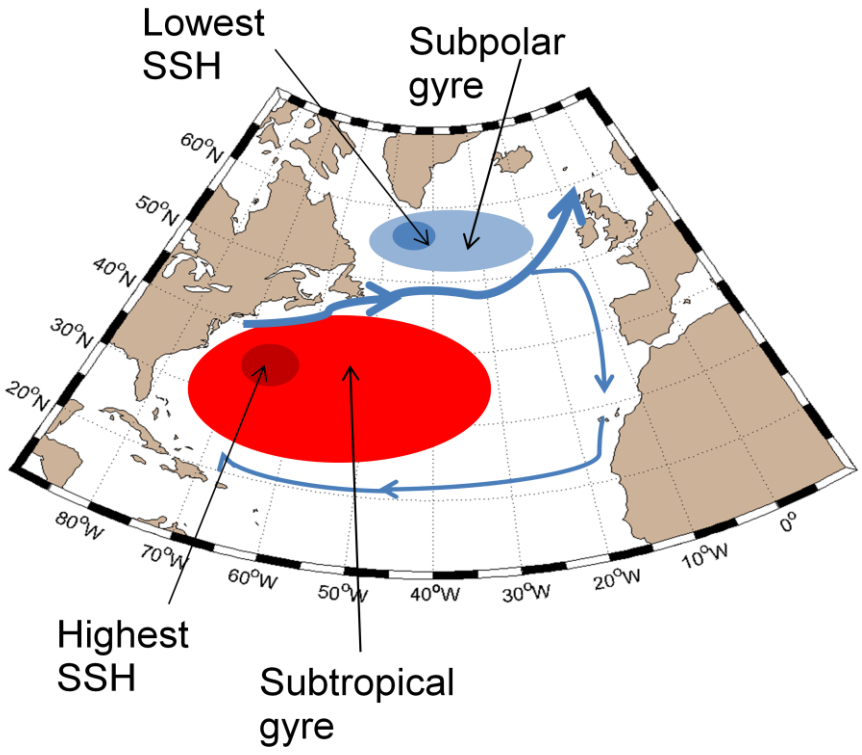

Figure 1-6: Schematic of the location of the highest and lowest SSH in the North Atlantic.

Variations to the strength of the North Atlantic gyre circulation have been linked with the NAO (Curry and McCartney 2001). These authors found that the greatest change in mass transport within the Gulf Stream-North Atlantic Current region occurred at a maximum 1 to 2 years after a positive NAO episode. Similarly, Frankignoul et al. (2001) and Flatau et al. (2003) relate changes to the sign of the NAO index to variations in the meridional SSH gradient with increased surface flow along 50°N during positive NAO phases. Thus, there is a tight coupling between the

atmospheric circulation and ocean circulation primarily through the wind-driven response to the NAO.

Air-sea heat flux changes in response to the NAO also occur, although these are of minor importance compared to the wind-driven element described previously (Esselborn and Eden 2001). For example, during positive NAO phases, a stronger westerly wind field effects changes to latent and sensible heat fluxes which result in a tripolar structure of SST anomalies throughout the North Atlantic with negative anomalies (i.e. cooler SST) in the subpolar gyre and tropical North Atlantic and positive anomalies (i.e. warmer SST) in the temperate to subtropical latitudes (Visbeck et al. 2003). The opposite pattern of SST anomalies would occur during a negative NAO phase. Esselborn and Eden (2001) showed that during the 1995 to 1996 strong decline of the NAO index, a heat gain of 1.0 G J/m^2 occurred in the subpolar gyre, corresponding to a 4cm increase in SSH in this region. However, these authors attribute this SSH increase and hence heat gain primarily to wind-induced circulation changes rather than local air-sea heat flux alterations.

Thus, variations in the atmospheric circulation, often expressed as the NAO index in the North Atlantic, as described previously, will also affect the ocean circulation strength. In turn, this will affect the SST and thus the extent and intensity of convective mixing throughout the North Atlantic. Therefore, the centres of the subpolar and subtropical gyres respectively act as dynamic centres of action through which one can explore the large scale-circulation strength through the ΔSSH and its potential impact upon the surface water pCO_2 variability.

1.5.2 The seasonal cycle of pCO_2 in the subtropical and temperate region of the North Atlantic

Two key regions will be focused upon in this thesis: the subtropical and temperate regions. The subtropical region primarily studied in this thesis extends roughly between 20°N and 40°N and 60°W and 30°W (boxes 1 and 2, see chapter 2, section 2.5.2). Surface waters are characterised by high salinity (>37) (Antonov et al. 2006), a result of the excess of evaporation over precipitation in the region. The average temperature exceeds 22°C (Locarnini et al. 2006).

The temperate region is bounded to the north by the North Atlantic Current (NAC) and to the south by the Azores Current (AC) and thus acts as a transitional latitudinal band between subpolar waters to the north (>43°N) and subtropical waters to the south (<43°N) (Padin et al, 2011).

The distinct geographical positioning of the above two zones means that the surface water pCO_2 seasonal cycles will be different. These are now briefly discussed and illustrated. Figure 1-7 illustrates the seasonal variation associated with the surface water pCO_2 and DIC within the temperate region.

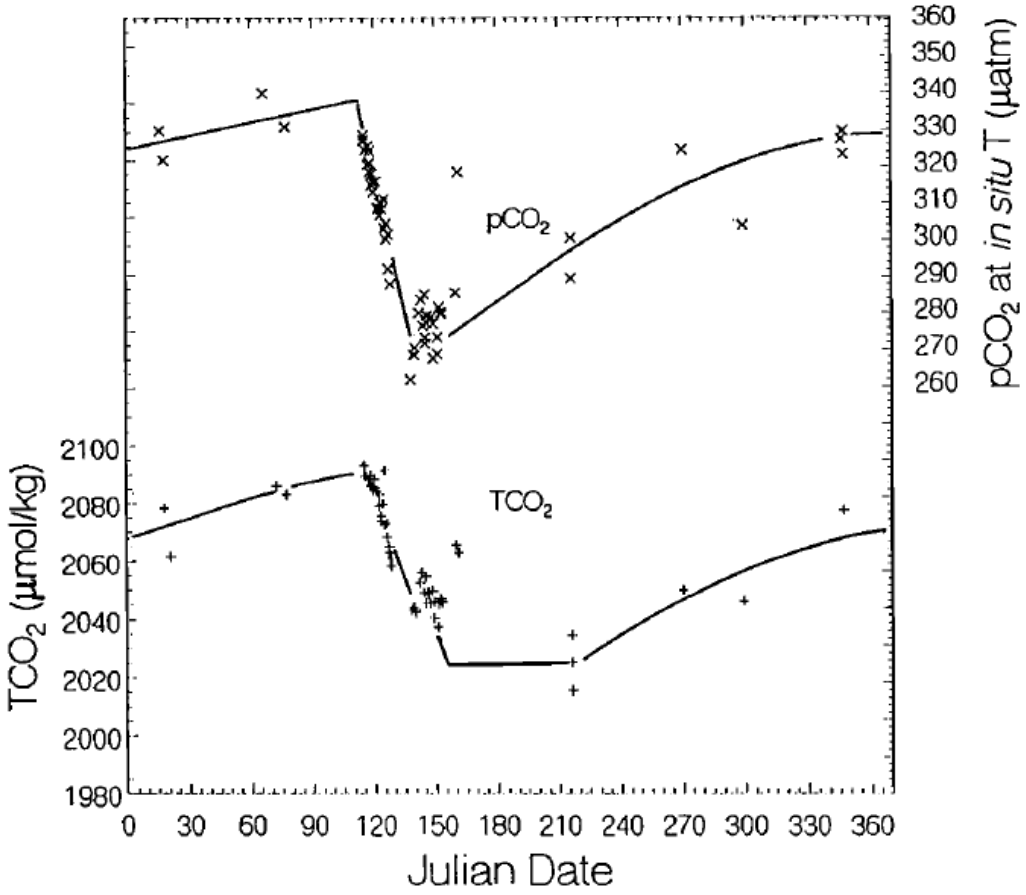

Figure 1-7: Seasonal changes of the surface pCO_2 and total CO_2 concentration (TCO_2), referred to as DIC in this thesis, observed in the North Atlantic, 45 - 49°N and 15 - 25°W during 1973-1989. From Takahashi et al (1993). The cluster of data points between Julian days 115 and 152 represents the data obtained during the Joint Global Ocean Flux Study (JGOFS)/North Altantic Bloom Experiment (NABE) study at 47°N, 20°W in April-June 1989 by D. W. Chipman and J.Goddard of Lamont Dohert Earth Observatory (LDEO). The curves indicate a general seasonal trend.

During winter, deep convective mixing within the northeast North Atlantic occurs (the mixed layer depth can reach to 500m, Takahashi et al. 1993). Thus, as mentioned in section 1.4, subsurface waters, rich in DIC and nutrients will be entrained to the surface, thereby increasing the seawater pCO_2 (see Figure 1-7).

In spring, the nutrients entrained the previous winter will be used by phytoplankton, reducing the concentration of DIC thereby decreasing the surface pCO_2 (Takahashi et al. 1993), see Figure 1-7.

The surface pCO_2 increases soon after the phytoplankton bloom ceases due to the seasonal warming of the surface water (Takahashi et al. 1993). The DIC concentration remains low until the end of the summer, and then increases to a maximum in late winter as a result of the deepening of the mixed layer in autumn (Takahashi et al. 1993).

In the subtopics, winter mixing is generally not as deep as in the temperate regions, thereby the entrainment of DIC from the depths to the surface will be less. Surface cooling during the winter months results in a net decrease of surface pCO_2 in winter in this region (Bates et al. 1996), see Figure 1-8.

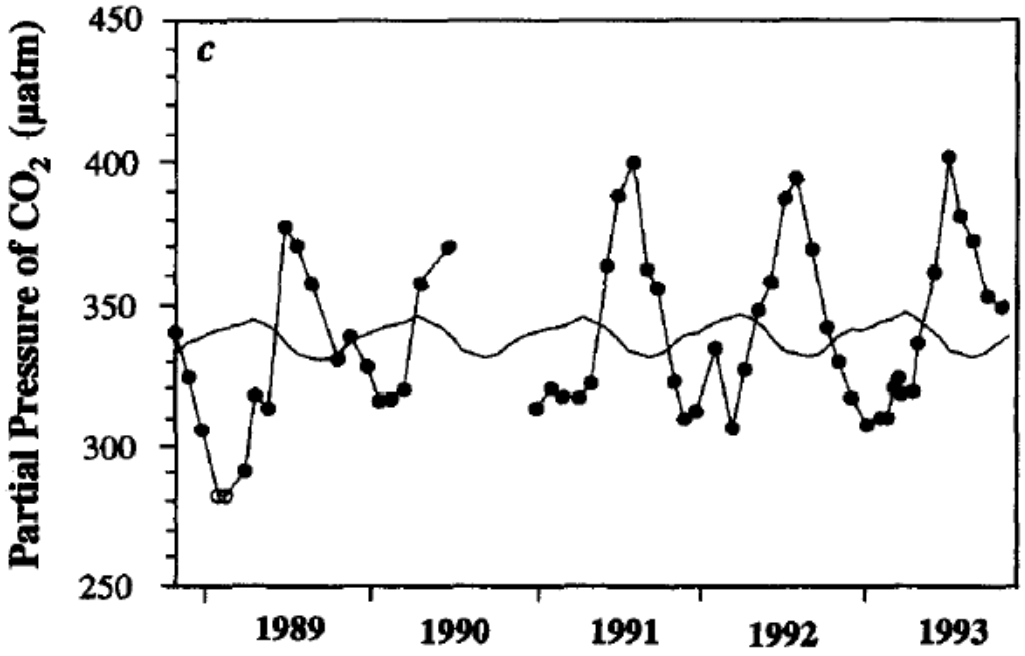

Figure 1-8: Surface ocean pCO_2 (filled circles) and atmospheric pCO_2 (solid line) at the Bermuda Atlantic Time Series (BATS) station between October 1988 and December 1993. The open circles denote atypically low surface pCO_2 observed in spring 1989. From Bates et al. (1996).

Although winter mixing is generally less intense than in the temperate region, nutrients and DIC-rich subsurface waters are entrained to the surface. The nutrients

enable phytoplankton blooms to occur (Bates et al. 1996, Gruber et al. 2002). However, the increase in SST during the spring to summer period dominates, thereby resulting in a net increase in surface pCO_2 during this period (Bates et al. 1996).

During autumn, surface cooling results in a decrease of the surface pCO_2, even though the mixed layer depth increases (Bates et al. 1996).

1.6 Current understanding of the mechanisms of sea surface pCO_2 variability in the North Atlantic

This section outlines the different mechanisms of surface pCO_2 variability in the North Atlantic that have been discussed in the literature. These include small-scale factors that control sea surface pCO_2, such as SST, vertical mixing and DIC, biology, and mode water formation, as well as the large-scale atmospheric circulation, that in the North Atlantic is dominated by the NAO, which impacts the aforementioned parameters.

Several studies have investigated how the inter-annual variability of surface water pCO_2 for differing regions of the North Atlantic can be altered through the atmospheric circulation (embodied within the NAO as discussed in section 1.5). Gruber et al. (2002) stipulate that in the subtropics, during a positive NAO, warmer surface waters are expected during the year which in turn gives rise to positive SST anomalies in this region (see also Figure 1-2). Winter vertical mixing is therefore limited, thereby entraining fewer nutrients to the surface. This results in less net community production and hence less CO_2 uptake by the ocean. Thus positive pCO_2 anomalies over and above the annual cycle occur.

During negative NAO periods, there is an enhanced frequency of winter storms which deepens the winter mixed layer (Gruber et al. 2002). This entrains more nutrients to the surface, which fuels greater biological activity the following spring (Gruber et al. 2002). In addition, due to the enhanced winter storminess associated with negative NAO events in the subtropics, negative SST anomalies are likely to be prevalent in these years (Gruber et al. 2002). In combination with enhanced biological activity, annual surface pCO_2 anomalies are therefore also likely to be

negative (Gruber et al. 2002). Furthermore, the coupled eco-system circulation model of Oschlies (2001) illustrated mechanistically that the subtropics experience less winter mixing during a high NAO phase. As a result, fewer nutrients are entrained to the surface. This then causes a weakening of the seasonal cycle of sea-air fluxes of CO_2, leading to weaker carbon sinks. The opposite would be true during a negative NAO phase. This model prediction was confirmed by the observations from BATS (Gruber et al. 2002).

However, as explained in section 1.5, the outcrop area, extent and rates of mode water formation are found to be higher during positive NAO winters than negative NAO winters, both in the subtropics (e.g. Levine et al. 2011) and the temperate regions (e.g. Padin et al. 2011). It is therefore conceivable that the surface pCO_2 in winter is likely to be (strongly) affected by the formation of these mode waters, through excessive deepening of the MLD entraining DIC-rich subsurface waters to the surface (Padin et al. 2011). Therefore, the surface pCO_2 in winter may be greater than the climatological mean in the temperate regions (see Figure 1-7) as a result of excessive DIC entrainment through mode water formation and advection (Padin et al. 2011) into the temperate region. A modelling study by Ullman et al. (2009) that focused on the subpolar region showed that high NAO winters coincided with an increased supply of DIC to the surface due to deeper MLD. Thus, this may be a plausible mechanism by which surface pCO_2 can increase during winter.

Although Padin et al. (2011) focus on the temperate regions, it is possible that the aforementioned increase in winter surface pCO_2 could occur in the subtropics as a result of the EDW formation zone infiltrating further south within the subtropical region. Therefore, positive pCO_2 anomalies with respect to the subtropical mean seasonal cycle (see Figure 1-8) could arise in winter in the subtropics as a result of increased DIC entrainment. Gruber et al. (2002) stipulate that under positive NAO events, the subtropics would be subjected to higher surface pCO_2 in winter through higher SST (as a result of a decrease in wind speed under the enhanced Azores High). In addition, they state that the spring bloom may be weak due to a reduction in the nutrients entrained the previous winter, thereby reducing the amplitude of the seasonal cycle. However, it is equally possible that due to the infiltration of the EDW further south, with its inherently higher MLD (Levine et al. 2011 and Figure 1-3), enhanced nutrient entrainment would occur in winter thereby fuelling stronger phytoplankton blooms the following spring.

Therefore remote effects such as the formation of mode water which occurs north of the subtropics may take precedence over the local atmospheric effects within the same region, as was illustrated for the temperate regions (Padin et al. 2011).

Furthermore, given the limited phytoplankton stocks within the subtropics (Strom et al. 2000), the DIC and nutrients entrained the previous winter may not be completely used up during spring. Given that surface cooling begins to occur in autumn, a renewed DIC pool may be entrained to the surface. Coupled with higher than normal surface pCO_2 the previous winter and despite a negative pCO_2 anomaly in spring, due to anomalously high biological activity, the seasonal amplitude of surface pCO_2 is likely to be dampened. A similar process is also likely to occur within the temperate regions, although as will be explained, the renewal of DIC during autumn is also likely to be driven by the ocean circulation rather than just the vertical gradient in DIC.

As described in section 1.5, the ocean circulation is wind driven, thus the NAO will affect the ocean circulation strength. A modelling study by Thomas et al. (2008) has attributed high NAO index periods such as the mid 1990s with increased transport of low-DIC waters from the subtropics into the subpolar gyre region. The transport of low-DIC waters would have decreased the surface ocean pCO_2, thereby increasing the ΔpCO_2 and allowing uptake of atmospheric CO_2 into the ocean. Compared to the mid 2000s, when the NAO index was predominantly neutral/negative, the transport of low-DIC subtropical waters decreased, thereby increasing the DIC content of the waters in the eastern subpolar gyre. Thus, the oceanic uptake of CO_2 is reduced. This agrees well with observational studies that also concluded that the surface ocean pCO_2 within the eastern subpolar gyre increased at a faster rate than that of the atmospheric pCO_2 (Lefèvre et al. 2004; Omar and Olsen, 2006; Olsen et al, 2006; Corbière et al. 2007, Schuster and Watson 2007). Thus, the ocean sink for atmospheric CO_2 has decreased by ~50% in the eastern subpolar region from the mid 1990s to the mid 2000s (Schuster et al. 2009).

Whilst the variations in both horizontal and vertical transport in DIC are certainly important mechanisms through which the surface pCO_2 can vary, it is also necessary to highlight how horizontal nutrient advection may affect biological activity and hence surface pCO_2 variability.

As mentioned in section 1.5, Frankignoul et al. (2001) and Flatau et al. (2003) demonstrate that during high NAO index periods, higher wind speeds will induce stronger surface currents and hence Ekman transport will occur. Since Ekman transport occurs perpendicular and to the right of the wind in the Northern Hemisphere (Bigg, 2003), cold, nutrient rich waters from the subpolar region could be advected to the temperate regions further south.

Hence, even though transport of low-DIC waters from the subtropics to the subpolar region may occur as evidenced within the Thomas et al. (2008) study, it is important to note that these authors focused on multi-decadal trends, rather than seasonal to inter-annual variability of surface pCO_2. Thus, it is considered that over time, a build-up of low-DIC waters from the subtropics may well occur if a persistently positive NAO was occurring as Thomas et al. (2008) illustrated, but that on shorter time-scales, other water mass sources, in closer proximity to the temperate region may dominate.

Häkkinen and Rhines (2004) and Häkkinen and Rhines (2009) report an increase in the subpolar gyre circulation during a positive NAO. Thus, it is plausible that in the temperate region, during high NAO periods, cold, DIC and nutrient-rich waters would penetrate into the region. As a result, stronger spring blooms may result during positive NAO winters due to the horizontal transport of high-nutrient waters southwards, thereby decreasing the surface pCO_2 through enhanced biological activity.

The spin-up of the subpolar gyre during a positive NAO phase may also enable a renewed DIC pool to be produced in autumn. As surface cooling begins in autumn, the MLD deepens (bringing up DIC-rich subsurface water to the surface). Given that the subpolar gyre would still be spun up, horizontal advection of high-DIC waters from the subpolar region into the temperate region may occur, increasing the surface pCO_2. During negative NAO periods, a reduced horizontal supply of DIC and nutrients would be advected into the region, thereby leading to negative pCO_2 anomalies in autumn. In addition, surface cooling in autumn, although not as excessive as during a positive NAO would still decrease the SST and thus contribute to lower surface pCO_2 in autumn.

Combining the winter, spring and autumn processes as described above for the temperate region, may result in negative annual pCO_2 anomalies during positive NAO periods (as biological drawdown of CO_2 dominates through both vertical and horizontal transport of nutrients). A positive annual pCO_2 anomaly would be expected to occur under a negative NAO in the temperate region as biological activity is less intense and of shorter duration.

Within the subtropical region, it would be expected that during high NAO periods, the subtropical gyre circulation would increase due to enhanced wind speeds around the gyre system as a result of an enhanced Azores High (Marshall et al, 2001) (see section 1.5). Thus, despite infiltration of cold, EDW during winter into the region, thereby decreasing the surface pCO_2 in winter, during the remainder of the year, e.g. spring, summer and autumn, convergence of warm subtropical waters in this region would dominate. The SSH in the region would thereby increase. Since high (low) SSH is indicative of high (low) heat content (Cabanes et al. 2006), this convergence of warm waters is expected to lead to positive SST anomalies during these months. In addition, wind speeds would be relatively low away from the northern and southern periphery of the subtropical gyre due to the enhanced Azores High, especially during summer when much of the North Atlantic is covered by it (Hurell and Deser, 2009). Zonal geostrophic velocities would therefore be predominantly low in the region. Thus, stratification of the water column is likely, thereby contributing to the positive SST anomalies during summer in the subtropics. Thus, it would be expected that in this region under a high NAO phase, the surface pCO_2 anomalies are also positive in summer and most likely dominate on the inter-annual timescale, despite the cold winter SST associated with the formation of the EDW.

Under a negative NAO, the gyre circulation would not be as strong due to a weaker Azores High system, decreasing the wind speeds around the system (Hurrell and Deser, 2009). Thus convergence of warm subtropical waters would decrease, reducing the SSH and hence the heat content and thus leading to negative SST anomalies. However, although the Azores High would be weaker, it would also be displaced further south (Hurrell, 1995), enabling the (weaker) westerly wind field to affect the area and aiding in the surface cooling of the region during winter. Thus, zonal geostrophic velocities would be higher in this instance. Surface pCO_2 anomalies would therefore also be negative in winter and the following spring,

summer and autumn as a result of the decrease in SST convergence due to a weaker subtropical gyre circulation. Thus, on an annual timescale, negative pCO_2 anomalies would be most likely in this case.

It should be noted that there may be occasions when under strongly negative NAO winters, winter storms in both the subtropics and temperate regions deepen the MLD sufficiently and entrain high volumes of DIC and nutrients to the surface, thereby resulting in positive pCO_2 anomalies. It is considered that these would be exceptional cases however and if they did occur, only apply to winter.

Thus there are several possible processes that affect the variability of surface pCO_2 within the subtropical and temperate regions of the North Atlantic. Several studies have identified possible mechanisms of surface water pCO_2 variability. On the inter-annual timescale, MLD and SST variability associated with the different phases of the NAO are likely to affect the surface pCO_2 variability in the subtropics (Gruber et al. 2002).

However, the ocean circulation strength is also likely to affect the oceanic pCO_2 variability. For example, within the temperate regions horizontal DIC and nutrient advection are likely to be important factors that affect the surface pCO_2 variability on inter-annual timescales.

In terms of the seasonal variability of surface pCO_2, the formation of mode waters (e.g. the EDW in the subtropics (Levine et al. 2011) and the ENACW in the temperate regions (Padin et al. 2011) will modify the mean seasonal cycle of surface pCO_2 through vertical DIC and nutrient entrainment in both regions.

Whilst several other studies identify potential mechanisms of the variation in the oceanic carbon sink, their focus is on long-term trends of this sink through NAO forcing (e.g. Schuster and Watson, 2007, Thomas et al. 2008, Schuster et al. 2009; Ullman et al. 2009). Although the NAO is certainly an important contributor, as will be highlighted in this thesis, the role of the ocean circulation in explaining the variability of the ocean sink of CO_2 also needs to be taken into account. As such, an index of the ocean circulation strength based on sea surface height SSH differences between the centre of the subpolar and subtropical gyre will be used in this thesis. From here on the term ΔSSH is used to denote the SSH differences.

The following section identifies scientific hypotheses which will be tested in this thesis and outlines the main effects of the NAO and ocean circulation strength on the seasonal and inter-annual variability of surface pCO_2 in the subtropics and temperate regions.

1.7 Hypothesis and research approach

The following hypotheses will be tested in this thesis:

- That the phase of the NAO affects the ocean circulation strength (i.e. ΔSSH).
- That the NAO affects the surface pCO_2 on seasonal timescales.
- That the ΔSSH affects the surface pCO_2 on both seasonal to inter-annual timescales.
- That the NAO and/or ΔSSH affect the SST, MLD, CHL, DIC on either seasonal to inter-annual timescales.
- That the SST, MLD, CHL, DIC affect the surface pCO_2 on either seasonal to inter-annual timescales.

The following schematics identify the hypothesised main effects of the NAO on surface water pCO_2 on both seasonal and inter-annual timescales for the subtropics. Figure 1-9 refers to the hypotheses for the subtropics and Figure 1-10 refers to the hypotheses for the temperate region. Section 1.6 describes the basis and links for the schematics outlined below, hence these shall not be repeated here.

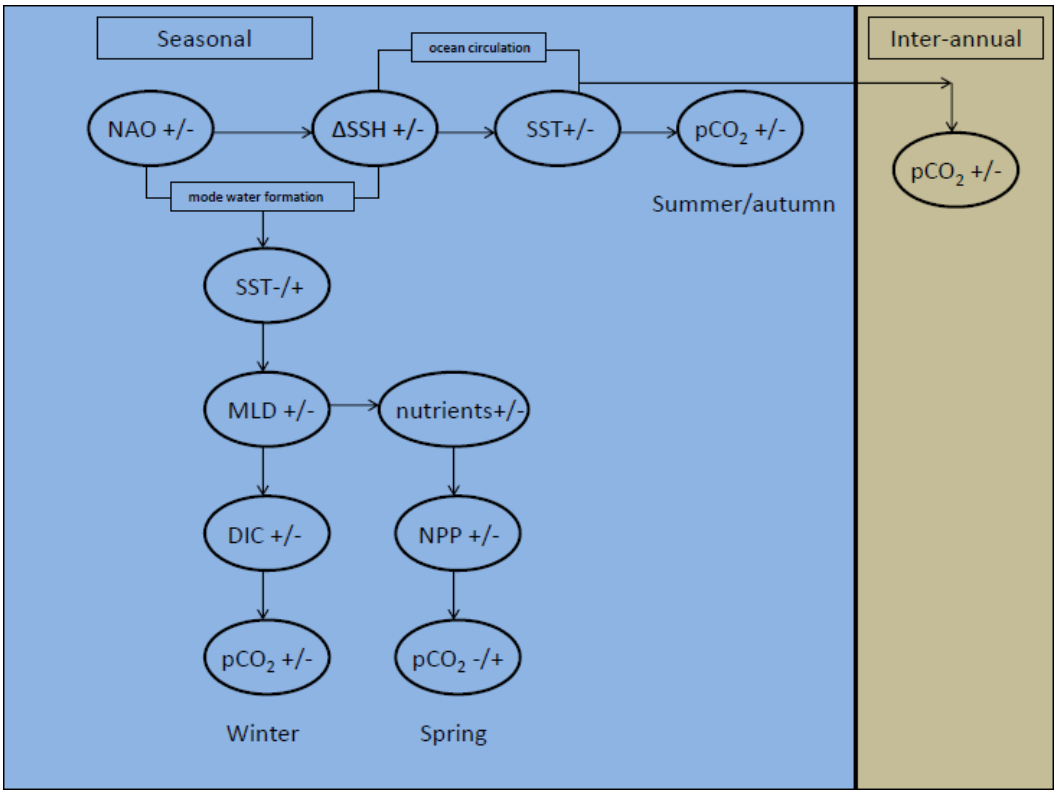

Figure 1-9: Schematic of hypothesized main mechanisms of seasonal and inter-annual surface pCO_2 anomalies in the subtropics under different NAO regimes. The sign (+/ -) within the ovals indicates the effect of a positive and negative NAO on the surface pCO_2 respectively. NPP stands for net primary productivity.

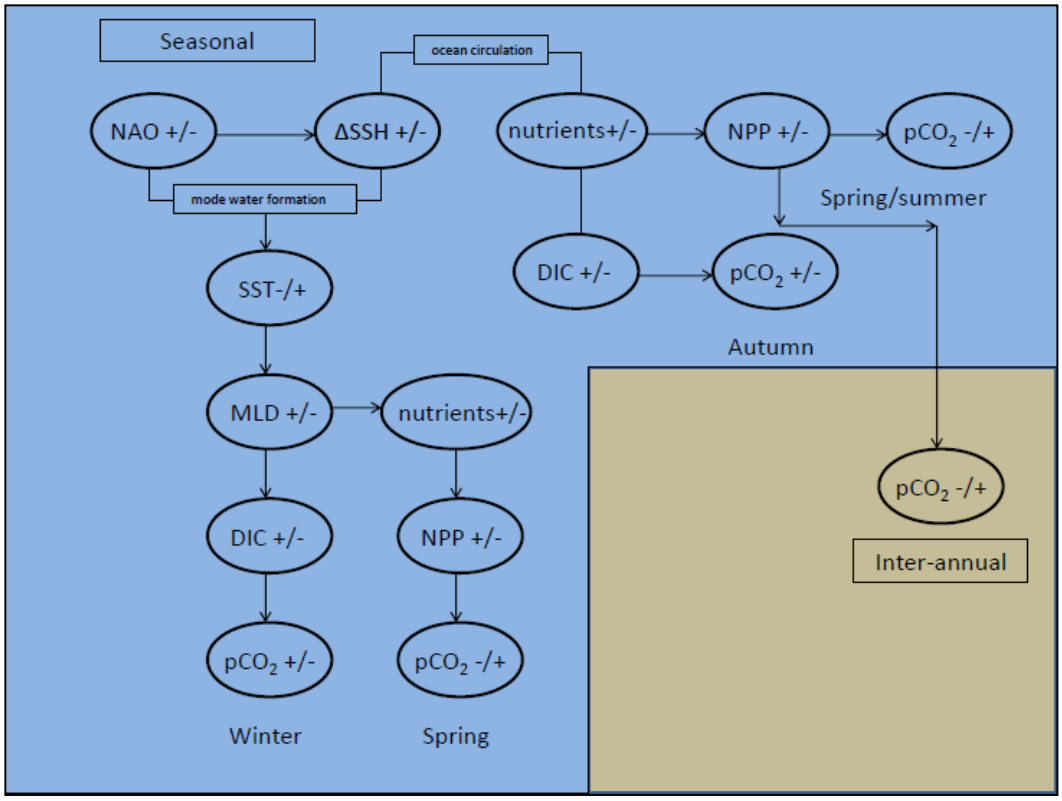

Figure 1-10: Schematic of hypothesized mechanisms of seasonal and inter-annual surface water pCO_2 anomalies in the temperate region under NAO positive/negative regimes. The sign (+/ -) within the ovals indicates the effect of a positive and negative NAO on the surface pCO_2 respectively. NPP stands for net primary productivity.

These hypotheses will be tested by using satellite altimetry to elucidate the variability of the ocean circulation strength and its ultimate impact on the surface water pCO_2 variability through the small-scale parameters discussed previously, which is an approach that has not been used before. Coupled with the in-situ measurements of the surface water pCO_2 in the North Atlantic (see chapter 2, section 2.2.1), model output will be used to mechanistically assess the drivers of seasonal to inter-annual variability of surface water pCO_2.

There are inherent differences between model predictions of surface water pCO_2 variability and those stemming from observations and the main reasons for this are as follows:

- Although considerable efforts have been made to increase the observational network of oceanic CO_2 in the North Atlantic, the temporal and spatial extent of these observations are limited to the tracks taken by voluntary observing ships (VOS) lines (i.e. see chapter 2, section 2.2.1, for the location of the ship tracks used in this thesis).
- Global coupled bio-geochemical models are coarse in resolution and do not yet correctly parameterize biological processes (see chapter 3 for a discussion of this with respect to the model output used in this thesis) (Schuster et al. 2012).

Nonetheless, it is important to compare both observations and models when assessing changes to the oceanic sink of CO_2 and the variability of that sink. This is because observations are still sparse in space and time and thereby need to be compared to ocean models that are not limited by this temporal or spatial constraint (even though the parameterization of biological processes is deficient). This is the approach taken in the thesis and details of the methods used can be found in chapter 2.

1.8 Thesis outline

The thesis is structured as follows:

- Chapter 2 details the methods used to undertake the research and outlines the sources of data used.
- Chapter 3 describes the data for both observations and model output in terms of the seasonal and inter-annual variability of the surface water pCO_2 and related parameters such as SST, MLD, DIC and chlorophyll-a (CHL). Limitations of the model are also discussed.
- Chapter 4 examines the drivers of the seasonal anomaly of the surface water pCO_2 for both the observations and model output in relation to the hypothesis outlined in section 1.7 of this chapter.
- Chapter 5 examines the drivers of the inter-annual variability of the surface water pCO_2 in relation to the observations and model output with respect to the aforementioned hypothesis in section 1.7 of this chapter.
- Chapter 6 summarizes the findings of the research and provides suggestions for future research.

Chapter 2: Methods

2.1 Introduction

As was discussed in chapter 1, much research has been undertaken on identifying the causes of the variability of the surface water pCO_2 in different regions and on different time-scales. The international community has made enormous efforts during recent decades to increase the number of *in-situ* pCO_2 measurements through various EU-funded projects such as CarboOcean (www.carboocean.org) and CarboChange (http://carbochange.b.uib.no). There is, however, still an uneven distribution of these measurements in both time and space, and this also applies to the relatively well sampled North Atlantic.

This chapter describes the data used, the data preparation, and the statistical techniques applied in this study of the variability of surface pCO_2 in the mid-latitude North Atlantic in view of the variability of large scale surface and atmospheric circulation.

2.2 Sources of surface water pCO_2

2.2.1 Observations

The measurement of the surface water pCO_2 in this study followed the approach taken by Cooper et al. (1998), incorporating changes to this surface water pCO_2 measuring system as reported in Schuster and Watson (2007). A summary of how the in-situ partial pressure (pCO_2) measurements are made is given here.

The equilibration of seawater CO_2 with gaseous CO_2 within the 'equilibrator' (also known as equilibration chamber) of the ship is the key principle by which in-situ seawater pCO_2 measurements are calculated. This is achieved by maintaining a constant flow of seawater from the ships' seawater inlet to the equilibrator. The equilibrator is also vented to the atmosphere which ensures that equilibration takes place at ambient pressure. Once equilibration is reached, the mole fraction of CO_2 in dry air (xCO_2) is determined by a non-dispersive IR analyzer (Li7000, LiCor Inc.,

USA). This is based on the absorptive properties of CO_2 molecules within the IR spectrum. The partial pressure of an ideally behaving gas is determined by this mole fraction and the total pressure of the gas phase. The fugacity is normally used, since this accounts for the non-ideal behaviour of CO_2. It is based on the 'modified version of Henry's Law' (Weiss 1974) and can be calculated from equations in Weiss (1974). The difference between pCO_2 and fCO_2 is less than 1.5 µatm (Dickson et al. 2007), hence the abundant use of pCO_2 in the literature. To obtain the true mole fraction of CO_2 in dry air, corrections need to be applied to the xCO_2 to account for pressure band broadening and water vapour pressure interference of the Li7000. In addition, the xCO_2 is corrected for the drift of the IR analyzer by the calibration of CO_2 to a set of known CO_2 concentrations (i.e. standard gases) provided by NOAA-CMD_CCGG (http://www.esrl.noaa.gov/gmd/ccgg/index.html).

The equilibrator pCO_2 is then calculated by correcting the true xCO_2 to equilibrator temperature and pressure by using the saturated water vapour pressure appropriate to seawater as given in Cooper et al. (1998):

$$pH_2O = 0.981 \exp\left(14.32602 - \frac{5306.83}{T_{equ}}\right) \quad (2.1)$$

where T_{equ} is in Kelvin and represents the absolute temperature of the equilibrator. A further correction needs to be applied to account for the ambient pressure. Hence equilibrator pressure is corrected to the ships' barometer (p). Thus, the equilibrator pCO_2 is calculated as follows:

$$pCO_2{}^{100\%\, humidity} = xCO_2{}^{dry}\, x\, \left(p - \left(0.981\, x \exp\left(14.32602 - \frac{5306.83}{T_{equ}\,[\text{Kelvin}]}\right)\right)\right) \quad (2.2)$$

Lastly, the in-situ sea surface pCO_2 is calculated by incorporating the difference in temperature (ΔT) between the equilibrator temperature and SST (measured at the seawater inlet) based on the empirical relationship of Takahashi et al. (1993):

$$pCO_2 = pCO_2{}^{100\%\, humidity} x\, exp\, \left(0.0423\, \left(T_{SST} - T_{equilibrator}\right)\right) \quad (2.3)$$

In-situ measurements of surface pCO_2 were made between 2002 and 2007 on board the *MV Santa Maria* and *MV Santa Lucia* between the U.K. and Caribbean (Figure 2-1).

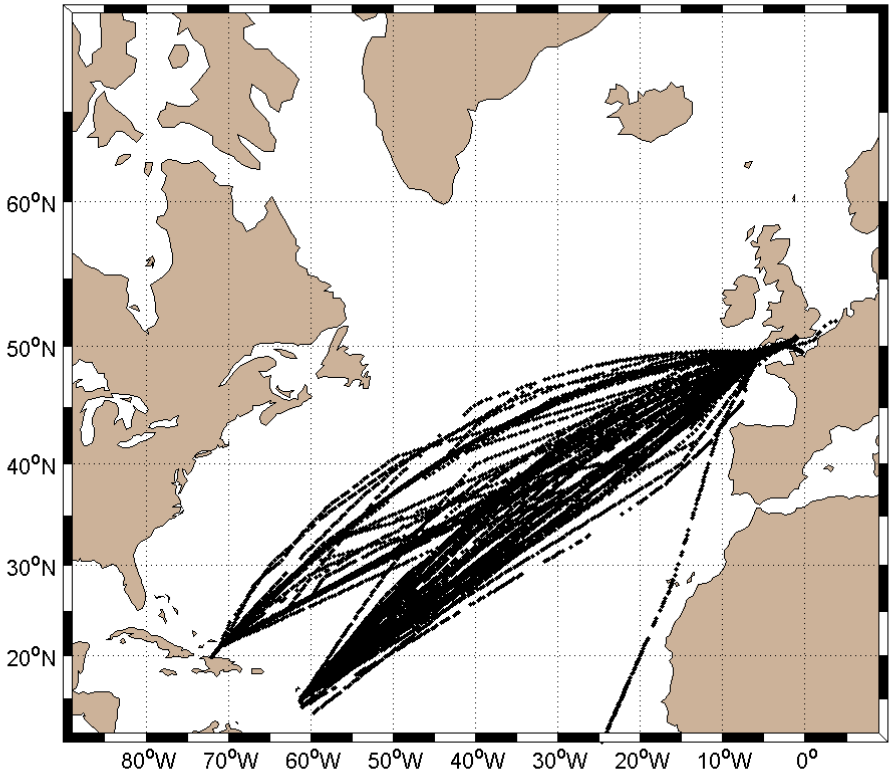

Figure 2-1: Locations of in-situ measurements of surface pCO_2 onboard the MV Santa Maria and MV Santa Lucia between 2002 and 2007

2.2.2 Model output

Model output from the biogeochemical model PlankTOM5.2 was used (Buitenhuis et al. 2010). This has been developed as part of the Dynamic Green Ocean Model (DGOM) initiative which aims to improve the representation of ecosystem dynamics in global ocean biogeochemistry models (Le Quéré et al. 2005). The version of PlankTOM5.2 used in this thesis was forced with the increase in atmospheric pCO_2 from 1990 to 2009 (Le Quéré et al. 2007). The current version of the model includes five Plankton Functional Types (PFTs) (Buitenhuis et al. 2010). These are based on three phytoplankton types (mixed phytoplankton, silicifiers and calcifiers) and two zooplankton functional types (micro and mesozooplankton) (Manizza et al. 2010). The model implements the ballasting effect of biogenic calcite and opal on large sinking particles (Manizza et al. 2010). In addition, phytoplankton growth is co-limited by light, phosphorus, iron and silicate for silicifiers (Manizza et al. 2010).

The PlankTOM5 biogeochemical model is run within the Nucleus for European Modelling of the Ocean (NEMO) physical model, version 2.3 (Madec 2008). The horizontal resolution is 2° longitude and on average 1.1° latitude (the resolution increases to 0.5° latitude at the equator) and a vertical resolution of 10m in the top 100m increasing to 500m at 5km depth (Buitenhuis et al. 2010). The model has a free surface height (Roullet and Madec 2000), a necessary precursor to ocean salt content conservation. Vertical mixing is calculated at all depths from a turbulent kinetic energy model (Gaspar et al. 1990) and sub-grid eddy induced mixing is constrained according to Gent and McWilliams (1990).

The PlankTOM5 model is forced by river inputs of DIC, alkalinity, Dissolved Organic Carbon (DOC), phosphate (PO4), sodium silicate (SiO_3) and iron (Fe) (Cotrim da Cunha et al. 2007), sediment input of Fe and dust input of Fe and SiO_3 (Aumont et al. 2003). The NEMO physical model is forced by daily winds and precipitation from the National Centre for Environmental Prediction and National Centre for Atmospheric Research (NCEP-NCAR) reanalysis (Kalnay et al. 1996) from 1948 to 2007. The model was initialised with observations of sea-surface temperature (SST), sea-surface salinity (SSS), PO_4, SiO_3 and oxygen (O_2) from the World Ocean Atlas 2005 in addition to DIC and alkalinity (Buitenhuis et al. 2010). Excluding the Arctic Ocean, gridded DIC and alkalinity were obtained from the Global Ocean Data Analysis Project (GLODAP). DIC concentrations were corrected for anthropogenic increases since 1948 (Buitenhuis et al. 2010). Modelled surface water pCO_2 was calculated from DIC, alkalinity, SSS, and SST (Cotrim da Cunha et al. 2007).

These parameters were provided on a 1° latitude by 1° longitude grid so that the spatial resolution was the same between modelled output and observations (see section 2.5 for a description of the data preparation procedure).

2.3 Sources of related parameters

Potential parameters that influence surface water pCO_2 in the North Atlantic were collected from satellite observations and reanalysis data.

2.3.1 Satellite observations

Satellites have the major advantage of acquiring data from all over the world with high spatial resolution, and a large number of data points can therefore be obtained. Satellite observations can, for example, provide chlorophyll *a* values and sea surface temperature (SST). Specific satellite data products used in this study are reported in Table 1 and briefly discussed in section 2.4.2.

2.3.2 Reanalysis data

Another way in which data on the biological and physical processes of the ocean can be accessed is through reanalysis data (in addition to biogeochemical models as described in section 2.2.2).

Reanalysis systems use observational and remotely sensed data from both atmospheric (e.g. global rawinsonde data for measuring wind speed and direction) and oceanic sources (e.g. SST from ships, buoys, near-surface data from ocean station reports such as Expendable bathythermographs (XBTs)). The observed and remotely sensed data are then fed in to a data assimilation scheme which uses a state of the art model that represents atmospheric physics (e.g. convection, large-scale precipitation, vertical and horizontal diffusion processes to name but a few). The output is a gridded product of many important climate variables such as sea level pressure, temperature at 2 metres, meridional and zonal winds at 10m, surface and skin temperature and many more (Kalnay et al. 1996). Specific descriptions of the reanalysis datasets used are given in sections 2.4.1 and 2.4.2.

2.4 Related parameters used

Related satellite and reanalysis parameters used were NCEP-NCAR SST, Mercator mixed layer depth (MLD), SeaWiFS Chl-a, Sea-Surface Height (SSH), geostrophic zonal velocities and the North Atlantic Oscillation (NAO). The model output variables used were surface water pCO_2, SST, MLD, total CHL, Dissolved Inorganic Carbon (DIC) and SSH. The initial spatial resolution of the model output corresponds to the resolution of the parameters provided for this study, and not the actual spatial resolution of the model (see section 2.2.2). Table 1 shows the source of each parameter used and its spatial resolution.

Parameter(s)	Source	Initial Spatial Resolution [°] or [km]	Initial Temporal frequency	Website/FTP address/Reference
SST	NCEP-NCAR reanalysis project	1.875° x 1.875°	Daily	http://www.cdc.noaa.gov/data/reanalysis/ Kalnay et al (1996)
MLD	Mercator ocean reanalysis	1/4° x 1/4°	Monthly	www.mercator-ocean.fr Ferry et al (2011)
Chlorophyll a	SeaWiFS satellite	9km x 9km	8-daily	http://oceancolor.gsfc.nasa.gov/cgi/l3 McClain et al (1998)
pCO_2, SST, MLD, DIC, CHL, SSH	NEMO-PlankTOM5 model output	1° x 1°	Monthly	N/A Le Quéré et al (2007)
Sea-surface height	TOPEX-Poseidon and JASON	1/3° x 1/3°	Weekly	http://www.aviso.oceanobs.com/en/data/products/sea-surface-height-products/global/index.html Dibarboure et al (2009)
Geostrophic zonal velocities	TOPEX-Poseidon and JASON	1/3° x 1/3°	Weekly	http://www.aviso.oceanobs.com/en/data/products/sea-surface-height-products/global/index.html Dibarboure et al (2009)
NAO index	Climatic Research Unit (CRU)	N/A	Monthly	http://www.cru.uea.ac.uk Osborn (2011)

Table 1: Sources of data and their spatial resolution

2.4.1 NCEP-NCAR SST

The NCEP/NCAR have collaborated with scientists worldwide to develop their 40-year reanalysis product – from 1948 to present (Kalnay et al. 1996), for the purpose of continued climate monitoring as described above (section 2.3.2). It is one of the most comprehensive databases of reanalyzed climate data for use by the research community worldwide. In addition, as described in section 2.2.2, the global biogeochemical model output used is forced by NCEP-NCAR reanalysis. Thus in order to directly compare model output with observations, it was decided to use the NCEP-NCAR SST product.

2.4.2 Mercator MLD

Mercator MLD is a global reanalysis product of the MyOcean Global Monitoring and Forecasting Centre (Ferry et al. 2011). The goal of this reanalysis product is to provide accurate global simulations of ocean state variables, such as MLD and SST, constrained by assimilation of observations in:

- temperature and salinity,
- meridional and zonal wind speed and direction,
- sea surface height (SSH),
- sea-ice features (concentration, thickness)

The reanalysis product uses the NEMO physical model (described in section 2.2.2) coupled to an assimilation scheme constrained by in-situ observations. As with NCEP-NCAR, in-situ temperature and salinity come from XBTs, argo floats and buoys. In addition, satellite SST (daily Reynolds SST blended with AVHRR) and sea-level anomalies (from the TOPEX-Poseidon, Jason satellites) form part of the data assimilation scheme (Ferry et al. 2011).

The spatial resolution of the global reanalysis system is eddy permitting (1/4° x 1/4°, see Table 1), thus able to resolve synoptic scale processes (e.g. fronts or storms) which would affect the MLD. The observed MLD is defined as the deviation in temperature of 0.2 °C from the surface temperature (Steinhoff et al. 2010) as it is for the model (Sinha et al. 2010).

In addition, given that the MLD is determined by the NEMO model (in combination with an assimilation scheme), the effect of the MLD on the observed pCO_2 versus the modelled pCO_2 can be directly compared.

2.4.3 SeaWiFS Chlorophyll-a

Satellite data from the Sea-Viewing Wide-Field of View Sensor (SeaWiFS) was used to obtain chlorophyll a concentrations. This parameter is widely used to determine biological productivity (primary production), see Gregg and Conkright (2002). Since photosynthesis is involved in this process, as CO_2 is fixed by phytoplankton, this parameter was also included in the study as a potential proxy for biological activity that influences surface water pCO_2.

2.4.4 Temperature versus non-temperature driven pCO_2

The surface water pCO_2 was normalised to a constant temperature by using the equation developed by Takahashi et al. (2002):

$$pCO_2T_{norm} = pCO_{2\,(obs)}\; x\; exp[0.0423\; x\; (T_{mean} - T_{obs})] \qquad (2.4)$$

where pCO_2 T_{norm} is the pCO_2 normalised to the long term mean SST from all available years (i.e. 2002 to 2007) within each grid box (see section 2.5.2), $pCO_{2\,(obs)}$ is the observed surface pCO_2 (in this case monthly means) within each grid box, T_{mean} is the long term SST mean and T_{obs} is the monthly mean SST.

The resulting temperature-normalised pCO_2 represents the biochemical component of the surface water pCO_2, which is mainly influenced by dissolved inorganic carbon (DIC). The secular trend in surface pCO_2 between 1970 and 2007 in the North Atlantic basin is 1.8 ± 0.4 µatm y^{-1} through anthropogenic increase in atmospheric CO_2 (Takahashi et al. 2009). The SST-driven component of the surface water pCO_2 was also calculated based on Takahashi et al. (2002):

$$pCO_2T_{obs} = pCO_{2\,(mean)}x\; exp\;[0.0423\; x\; (T_{obs} - T_{mean})] \qquad (2.5)$$

where pCO_2 T_{obs} is the observed monthly temperature-driven pCO_2 calculated from altering the long term mean pCO_2 from all available years within each grid box (pCO_2 $_{mean}$), with the differences between the monthly mean SST (T_{obs}) and the long-term mean SST (T_{mean}) from all available years within each grid box.

The resulting normalised pCO_2 acts as the temperature-driven component of the surface water pCO_2. Colder water has higher CO_2 solubility and thereby lower seawater pCO_2, whereas warmer water has lower CO_2 solubility and thus higher seawater pCO_2.

However, it should be noted that the Takahashi et al. (1993) thermodynamic relationship only applies to isochemical conditions: in the well mixed layer of the upper ocean, total DIC concentration is uniform and isochemical conditions can be assumed (Woolf et al. 2012). However, when water from beneath the seasonal thermocline is entrained with the upper mixed layer water, the assumption of

isochemical conditions does not apply (Woolf et al. 2012). This is because the total DIC concentration beneath the thermocline is greater than that in the well mixed layer. Thus, the change in surface water pCO_2 in this case will not only result from a temperature change but also from increased DIC from the depths.

Therefore, application of equation (2.5) is more accurate when determining how the surface pCO_2 of a water parcel changes due to surface warming or cooling in the upper mixed layer. However, it is nevertheless considered reasonable to apply equation (2.5) to calculate the temperature dependence of pCO_2 since the climatological average of surface pCO_2 is used (i.e. the long term mean over the study period). This will dampen the seasonal non-isochemical effect of DIC entrainment on the surface pCO_2. Equally, it is recognised that even so, isolating temperature related changes on surface pCO_2 will not be exact. For the purposes of this thesis, however, it is considered an adequate approach which has also been used in other studies investigating temperature versus biological effects on surface pCO_2 (e.g. Tjiputra et al. 2012, Jones et al. 2012).

Separating the temperature-driven from the non-temperature driven mechanisms enables the net effect of temperature versus biochemical processes on the surface water pCO_2 variability to be established. This was also done for the model output, so that a direct comparison with the observations could be made. Chapter 4 and chapter 5 further discuss these potential seasonal and inter-annual mechanisms, respectively.

2.4.5 Sea-surface height

As seen in Table 1, the TOPEX-Poseidon and Jason satellites were used to derive the SSH in this thesis. The SSH is calculated by subtracting the height of the satellite from a reference ellipsoid which is the rough approximation of the Earth's shape from the altimeter range which corresponds to the distance from the satellite to the sea surface (Kubrayakov and Stanichny 2011). The SSH thus corresponds to the height of the sea above the reference ellipsoid. It consists of two terms: the geoid (G) and dynamic topography (h) (Kubrayakov and Stanichny 2011). Thus to estimate the absolute dynamic topography directly, subtraction of G from SSH is undertaken. However, the shape of the geoid is not accurately known and hence the calculation of absolute dynamic topography is performed as follows:

SSH is averaged over a specific time period (in this thesis from 1993 to 1999 – www.aviso.oceanobs.com). The instantaneous SSH is then subtracted from the time-averaged SSH to yield the sea-level anomaly (SLA) (Kubrayakov and Stanichny, 2011). In addition, estimation of the mean dynamic topography (MDT) is required which is computed from the difference between the time-averaged SSH and the geoid. As mentioned, although the geoid is not accurately known, gravity models have been developed and estimates of the geoid are improving (e.g. Bingham et al. 2008). Thus, the absolute dynamic topography corresponds to the addition of the SLA with the MDT. It should be noted that the term 'SSH' used in this thesis corresponds to the absolute dynamic topography. The latter can be used to calculate zonal and meridional geostrophic velocities as shown in section 2.4.6.

As described in the Introduction (chapter 1, section 1.5), the subpolar gyre exhibits a low SSH compared to that of the subtropical gyre, meaning that the greater the SSH difference between the two gyres, the stronger the relative transport across the temperate regions. The geostrophic zonal velocities were used to determine this relationship (see chapter 3, section 3.2.1). ΔSSH can therefore act as a proxy for the large-scale ocean circulation (see Figure 1-6, section 1.5). Using this principle, the monthly mean sea-surface heights of the centre of the subpolar gyre [55° - 59°N; 48° - 43°W] and the centre of the subtropical gyre [23° - 28°N; 68° - 73°W] were calculated for the study period (2002 to 2007). ΔSSH was obtained from subtracting the monthly mean SSH between the subtropical and subpolar centres (see Figure 1-6, section 1.5). The ΔSSH from the model output were calculated in exactly the same way and at the same locations.

2.4.6 Geostrophic zonal velocities

As mentioned in section 2.4.5, the geostrophic zonal velocities will provide an indication of the strength of the ocean circulation. The zonal velocities were chosen rather than the meridional since the major current systems in the North Atlantic (the Gulf Stream, North Atlantic current and Azores current) are dominantly zonal.

The calculation of zonal geostrophic velocities is based on the absolute dynamic topography (section 2.4.5). They are based on the geostrophic balance equation (in the zonal direction):

$$u_g = -\frac{g}{f}\frac{\partial h}{\partial y}\ ; \qquad (2.6)$$

where u_g is the zonal geostrophic velocity, g is the gravitational acceleration, f is the Coriolis parameter, h is the absolute dynamic topography and y is latitude (Kubrayakov and Stanichny 2011).

2.4.7 North Atlantic Oscillation index

The North Atlantic Oscillation (NAO) index (Osborn et al. 2011) is an important climate mode of the North Atlantic, explaining ~37% of the winter (December, January and February) 500 hPa pressure variance of the North Atlantic (Marshall et al. 2001). Thus, as detailed in the Introduction (section 1.6), the large-scale atmospheric circulation will affect the oceanic circulation and the parameters mentioned above (i.e. SST, MLD and Chl-a). Therefore, the NAO index was included in this research. As seen in section 1.5, the NAO between 2002 and 2007 is generally in a neutral to negative state until the winter of 2006/7 where it reverts to a positive NAO phase.

2.5 Data preparation

The following section(s) describe the process of data preparation and data filtering/reduction undertaken.

2.5.1 Initial binning and co-locating daily and monthly values

Satellite and reanalysis products with a spatial resolution of less than 1° x 1° (e.g. SeaWiFS Chl-a, TOPEX-Poseidon ΔSSH, geostrophic zonal velocities and Mercator MLD) would pick up highly localized processes. Although it is important to capture local effects, very small-scale processes are not the focus of this study. In order to eliminate these processes, a 1 day by 1° latitude by 1° longitude grid was used in this research.

Satellite and reanalysis products that were available at daily, 8-daily and weekly frequency (i.e. NCEP-NCAR SST, SeaWiFS Chl-a and TOPEX-Poseidon ΔSSH, geostrophic zonal velocities respectively) were either binned or regridded depending

on the initial spatial resolution of the product into 1 day by 1° latitude by 1° longitude grids. With respect to the ΔSSH, a monthly mean spatial average of the centre of the subpolar gyre and centre of the subtropical gyre was calculated (see section 2.4.5). Mercator MLD, in addition to the model output parameters, which were available only at monthly frequency, were regridded onto a 1 month by 1° latitude by 1° longitude grid, at the same latitudes and longitudes as the daily values. The NAO index which was available at monthly frequency with no spatial resolution was gridded onto a 1 month grid.

Related parameters available at 1 day x 1 ^{o} latitude x 1 ^{o} longitude were then co-located with the surface pCO_2 observations (which were made at frequencies up to one per minute). With respect to the geostrophic zonal velocities, it should be noted that these were not co-located with the surface water pCO_2 measurements. This was done in order to capture the strength of the ocean circulation, which is not dependent on surface water pCO_2 measurements. The monthly MLD values in addition to the monthly model output parameters were also co-located with the surface water pCO_2 measurements. There were instances when surface pCO_2 measurements could not be made (e.g. due to a failure of the pCO_2 instrument) but the ship was still in operation. In these cases, related parameters were still co-located with the ship track position. In this way, the maximum number of related parameters was obtained. This also meant that where there were no in-situ pCO_2 measurements, the model output pCO_2 was still co-located to where the ship track was located at a given point in space and time. This maximised the use of model output pCO_2 and related modelled parameters within the ship track region.

2.5.2 Monthly averaging into seven sub-regions

Subsequently, monthly (temporal) and spatial means of the daily and monthly regridded / co-located values were obtained within a total of seven 20° latitude by 20° longitude grid boxes as shown in Figure 2-2. Again, with respect to the zonal geostrophic velocities, these were monthly and spatially averaged over the entire grid boxes in order to capture the strength of the ocean circulation within these boxes and not just where pCO_2 measurements were made. These large boxes were selected to ensure that as many measurements and data of ocean parameters as possible were included in the research.

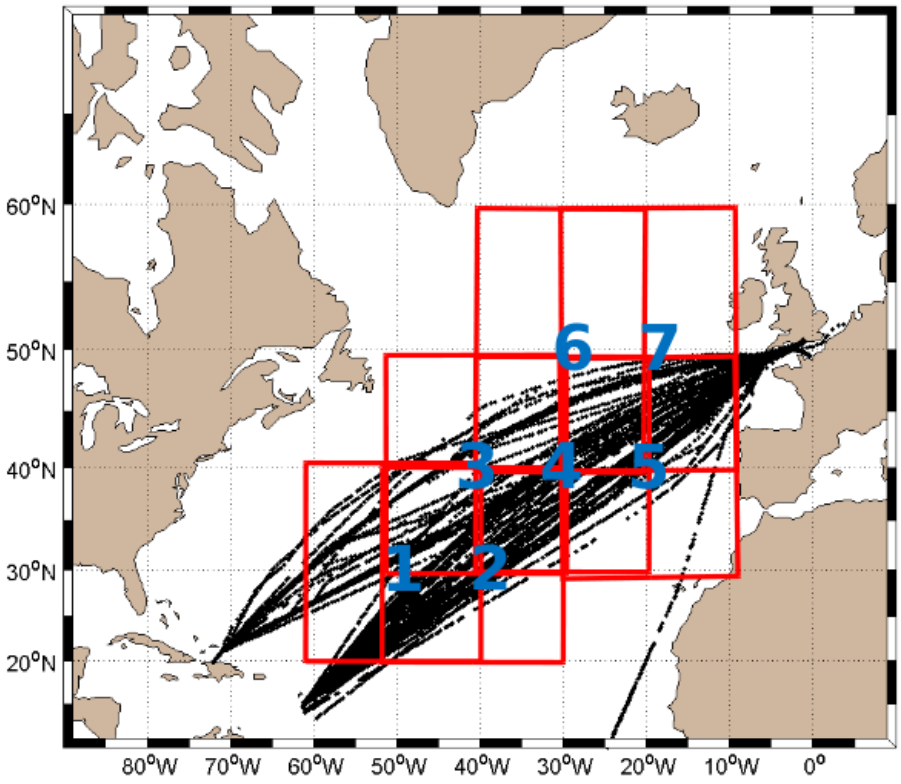

Figure 2-2: Illustration of the seven 20° latitude by 20° longitude grid boxes used in this research. Box 1 (20-40°N; 40-60°W); box 2 (20-40°N; 30-50°W); box 3 (30-50°N; 30-50°W); box 4 (30-50°N; 20-40°W); box 5 (30-50°N; 10-30°W); box 6 (40-60°N; 20-40°W); box 7 (40-60°N; 10-30°W).

Thus, the monthly mean co-located values had the same temporal frequency and spatial resolution as the ΔSSH and temporal frequency as the NAO index. Therefore, a direct comparison between the large-scale atmospheric and oceanic circulation with the related parameters and surface water pCO_2 could be made. In all subsequent sections and chapters, the term “grid boxes” is indicating the 20^o latitude by 20^o longitude boxes.

It should be noted that particularly within the temperate regions (boxes 6 and 7 in Figure 2-3), the spatial average did not encompass the whole 20° latitude by 20° longitude grid box because there were no *in-situ* pCO_2 measurements north of 50°N.

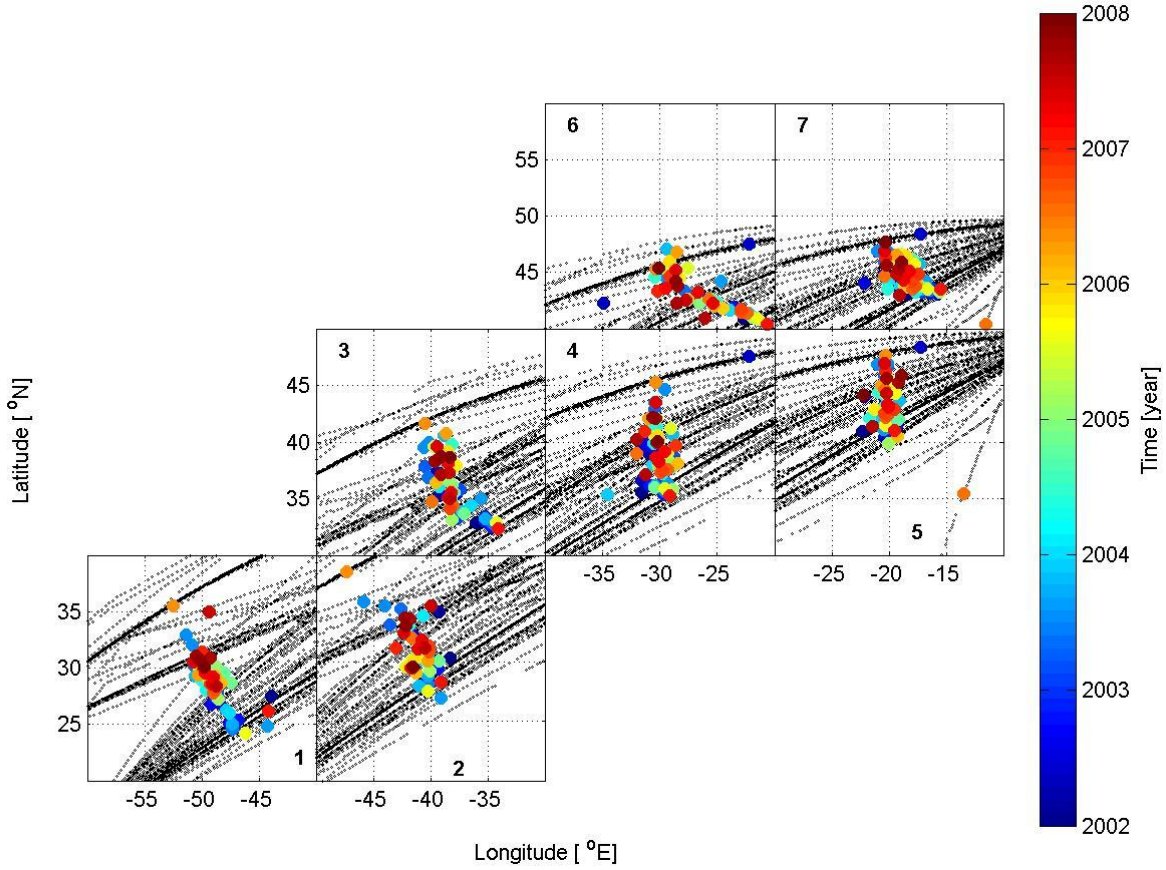

Figure 2-3: The mean location of monthly means (colour) together with the locations of the original measurements (black) in each grid box. These are arranged according to the grid's centre position shown in Figure 2-2.

2.5.3 Linear interpolation of related parameters and surface pCO_2

Inevitably, there were gaps in the monthly mean time series of the surface pCO_2 observations, as measurements could not be done in each grid box in each month. Surface pCO_2 was therefore linearly interpolated in time across the data gaps for each grid box. Gaps were also present in the co-located monthly related parameters time series, despite the greater number of monthly mean related parameters available compared to the surface water pCO_2 (see section 2.5.1). The related parameters were also linearly interpolated across the data gaps for each grid box, although fewer gaps were present than with the surface water pCO_2 measurements (see Figure 2-5). No linear interpolation was performed on the observed or modelled

ΔSSH, zonal geostrophic velocities or on the NAO index, since no gaps were present in these data sets.

The number of months of missing surface pCO_2 data for each calendar month for each grid box is shown in Figure 2-4. The maximum recurrence of missing months possible during the study period is six, given the six years of the study period (2002 to 2007).

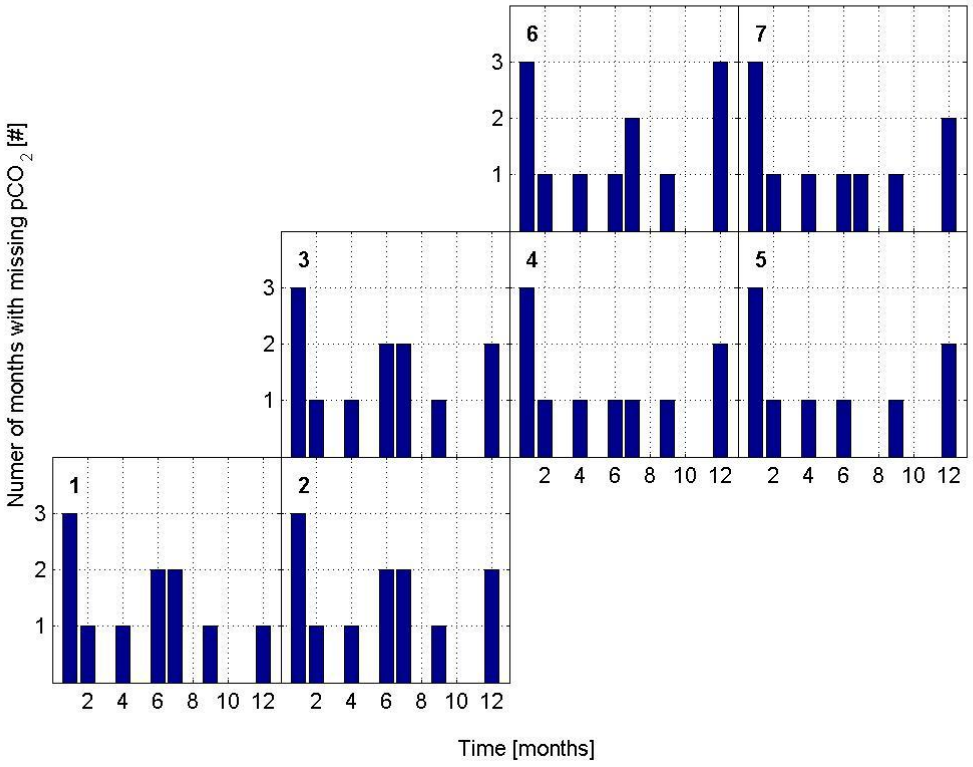

Figure 2-4: The number of times a monthly mean surface pCO_2 is missing from the monthly mean dataset for each grid box. The study period starts in 2002 and ends in 2007, thus a maximum of 6 recurrences could take place. The number in the top left corner of each plot corresponds to the grid box number shown in Figure 2-3.

It is clear that January is the month that has the least complete data record throughout the study region with all grid boxes exhibiting three years missing data. December is the second most data poor month, with one to three years revealing missing months in all of the boxes. July is another month that shows missing data with three years exhibiting lack of data in box 6 and 7. The other boxes show that data is not available two out of a possible six times. Data in June is also not available in two years for the whole study region. February, April, May, September

and October do not possess data in only one out of six years in boxes 5, 6 and 7. In boxes 1 to 4, there is data in May throughout the duration of the study period. March, August and November hold a complete data set for all boxes. Reasons for the lack of data in certain months include the docking of the ship at port and the occurrence of hurricanes in the subtropical regions during the summer months. Although some monthly data is missing, there is a relatively complete data set throughout the study region. Linear interpolation of the missing data points was justified in that there were observed data either side of the missing value in most cases, rendering a realistic representation of what the actual data might have looked like, if data was available.

The number of months of missing parameter data (e.g. NCEP-NCAR SST, Mercator MLD, SeaWiFS Chl-a) and of the model output data (e.g. SST, MLD, DIC, CHL, surface pCO_2) for each calendar month for each box during the study period is shown in Figure 2-5.

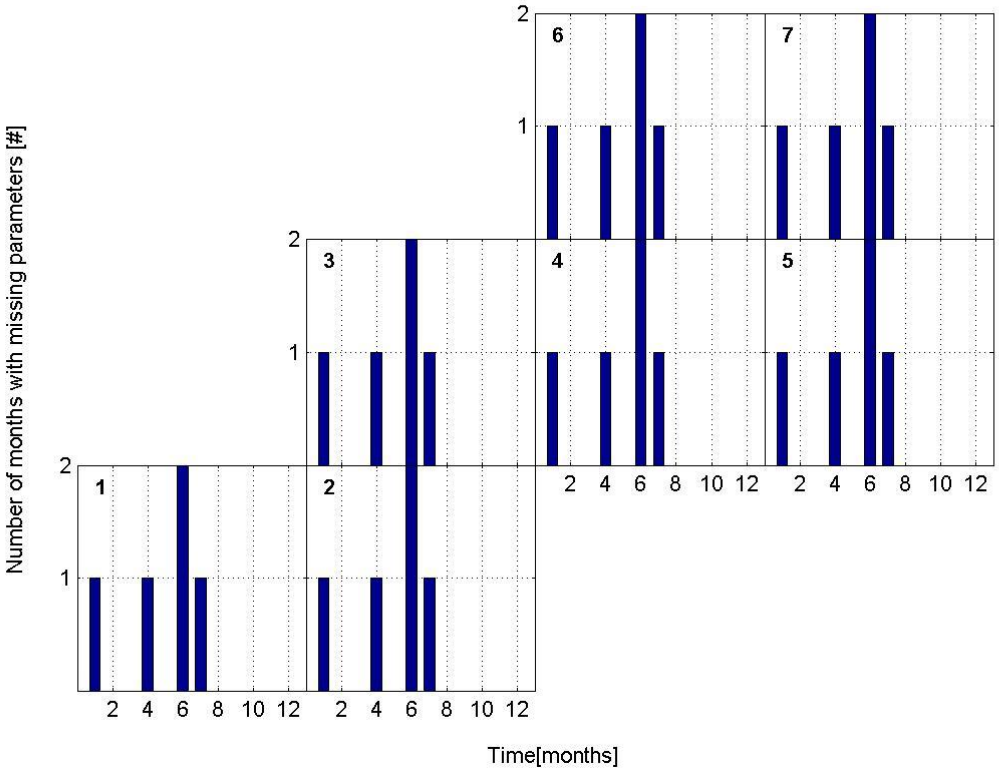

Figure 2-5: The number of times that either a monthly mean related parameter or a model output pCO_2 or modelled related parameters is missing from the monthly mean dataset for each grid box. The study period starts in 2002 and ends in 2007, thus a maximum of 6 recurrences could take place. The number in the top left corner of each plot corresponds to the grid box number shown in Figure 2-3.

Compared to Figure 2-4, there is a significant reduction in the number of missing related parameters, as these occur only when the ship is not in operation, for which explanations have been given previously.

January, in particular, exhibits more related parameters and modelled surface pCO_2 over the study period than surface water pCO_2 measurements, and February, March, May and August to December are free from gaps in the related parameters and model output pCO_2 and related parameters.

2.6 Time-series analysis

The objective of the research was to identify potential processes that influence the variability of the surface water pCO_2. To this end, a statistical analysis of the co-located variables with pCO_2 measurements was made. In order to achieve meaningful results, the following data procedures were undertaken.

2.6.1 Obtaining long-term variability

An approximate 12 month running mean was calculated for the surface pCO_2 and each co-located parameter. It is 'approximate' because the original pCO_2 measurements and co-located parameters were used which had gaps in the data. This was done so that the long-term variability of the surface water pCO_2 and related parameters could be assessed based on the actual monthly mean measurements/parameters. This does not apply to the observed and modelled ΔSSH, however, which do not have any gaps. In this case, a full 12-month running mean was calculated. In addition, for the NAO, only the winter January, February, March, (JFM) NAO index was used in the research since this is the time period that the NAO is most active (Marshall et al. 2001). Implementing a 12-month running mean on the NAO index would dampen the winter signal and was thus not undertaken. The surface water pCO_2 and key related parameters are illustrated for both observed and modelled data in chapter 3, section 3.3.1 for inter-annual variability and section 3.3.2 for the seasonal variation (i.e. the mean seasonal cycle. In addition, chapter 3 also illustrates the 12 month running means of the observed and modelled ΔSSH in addition to the winter NAO index (section 3.2.2).

2.6.2 Obtaining seasonal anomalies

In order to obtain the seasonal anomalies of the surface water pCO_2 along with the related parameters, the long- term variability was first removed by subtracting the 'approximate' (for the available observations and related parameters) and actual 12-month running mean (for the linearly interpolated observations and related parameters) from the monthly mean data. For the model output, no linear interpolation was undertaken as this would potentially misrepresent the model output surface pCO_2 and related parameters. Furthermore, fewer gaps were present in the model output than the observations. Note that this was done for all related parameters except the NAO index, since seasonal variability was already present in the time series, particularly in winter (December – February). Removing the long-term variability, as described above, in this instance would have altered the NAO index winter signal. However, in general, removing the long-term variability and the mean seasonal cycle needed to be performed in order to prewhiten the time-series (Chatfield 2004). If this is not undertaken, then it is likely that 'large' cross-correlation coefficients will result, which are spurious as they are caused by autocorrelations within the two series (Chatfield 2004). Additionally, another example illustrates the importance of removing the anomalies' mean seasonal cycle or any harmonic from the data (Chelton 1982): the inclusion of the mean seasonal cycle within two separate time series results in the degrees of freedom equalling 2, even if the number of observations increases without bound. This limits the number of independent observations in the data and hence reduces the statistical significance of the cross-correlation coefficient. Therefore, removal of the long-term variability and the mean seasonal cycle (described below) were undertaken to ensure statistical robustness as demonstrated in the literature.

A 3-month running mean was then calculated in order to eliminate sub-seasonal scale processes which are not the focus of this study. Thus what remains are 3-month running mean smoothed anomalies with respect to the long-term variability of the data. It should be noted that for the original data sets where there were gaps in the monthly mean data these were taken out of the 3-month running mean anomalies in order to avoid an unrealistic representation of the original data.

After the removal of the long-term variability and the implementation of a 3 month moving average onto the data, there remained the task of removing the mean seasonal cycle from the 3 month running mean smoothed anomalies.

The mean seasonal cycle was produced by calculating the mean of each individual parameter (e.g. surface pCO_2) for every calendar month throughout the entire study time period (i.e. 2002 to 2007) from the 3-month running mean smoothed anomalies. It should be noted that in chapter 3, the mean seasonal cycle was calculated from the original monthly mean data. Thus, in this case a 12-month running mean was not subtracted from the monthly mean data nor was a 3-month running mean implemented. This was undertaken in order to highlight the seasonal variations in the parameters in relation to their original monthly values.

The mean seasonal cycles of the pCO_2 and parameters were then subtracted from the 3-month moving average anomalies of each data set (i.e. surface pCO_2 and related parameters) to yield anomalies with respect to the mean seasonal cycle. These are termed seasonal anomalies from here on.

The following diagram summarises the procedures undertaken to calculate the mean seasonal cycle, seasonal anomalies and the inter-annual variability and outlines in which chapter of this thesis these terms are examined.

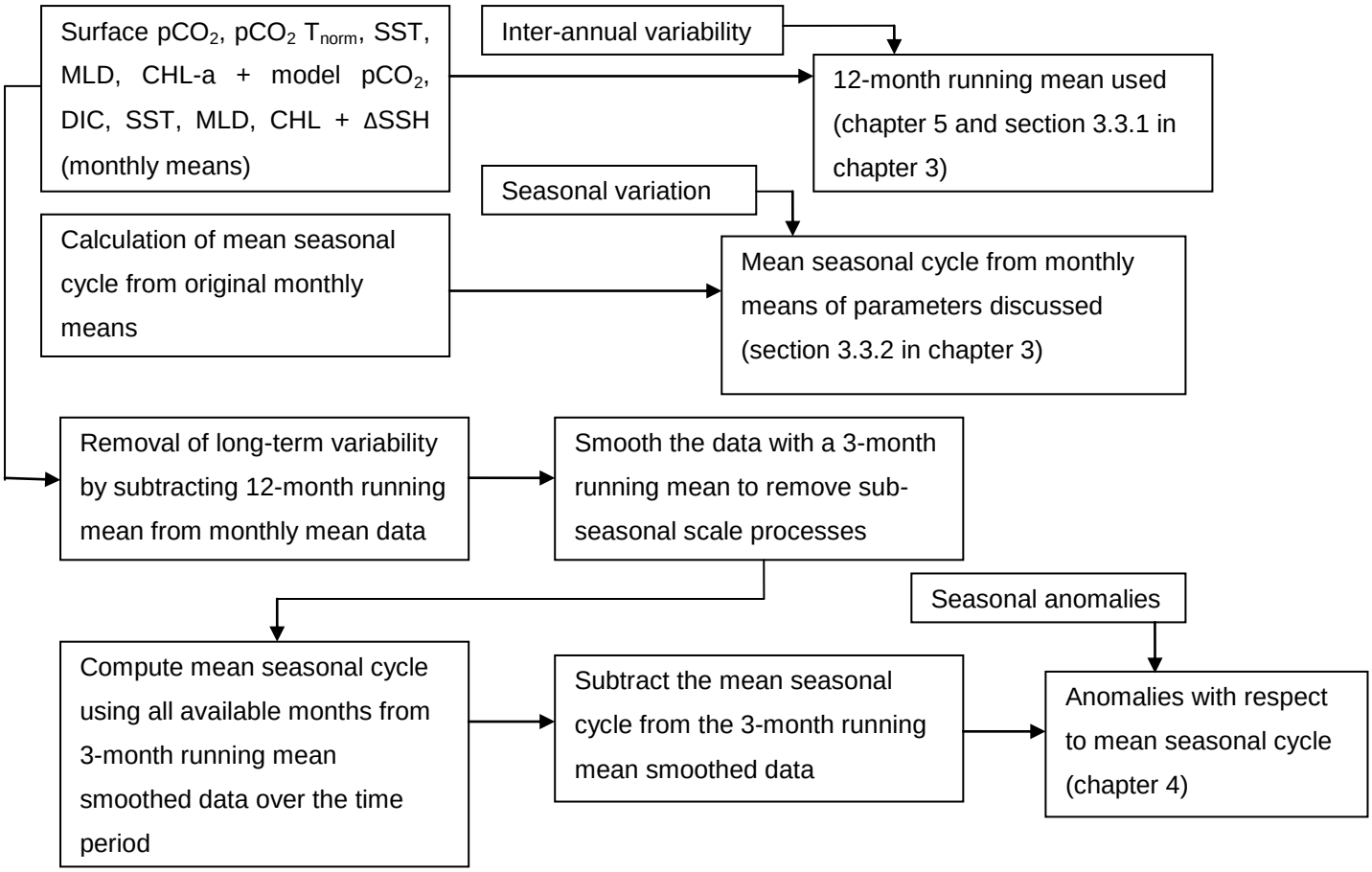

Figure 2-6: Process diagram of methods used to calculate inter-annual variability, seasonal variation and seasonal anomalies.

It should be noted that in section 1.7, in Figure 1-9 and Figure 1-10 the term inter-annual anomalies is used. The inter-annual anomaly is not calculated in this thesis due to insufficient data and thus the research hypothesis is not explicitly tested in this respect. However inference as to whether a parameter is likely to exhibit a positive or negative inter-annual anomaly can still be made from the 12-month running means (i.e. inter-annual variability). For example, when the 12-month running mean of a given parameter during a particular year or several years exhibits a peak or upward trend, it can be inferred that the inter-annual anomaly is likely to be positive. The opposite is likely to be true when a trough or downward trend is evident in the parameters (see chapter 5).

The following section describes the methods used to establish relationships between the surface water pCO_2 and the related parameters.

2.7 Correlations

The objective of the research was to identify relationships between the surface water pCO_2 and the local and large-scale parameters. As such, the statistical technique of correlating the (a) inter-annual variability and (b) seasonal anomalies of the surface water pCO_2 with sea surface parameters (i.e. SST, MLD, CHL, pCO_2 T $_{norm}$) and large-scale circulations (i.e. ΔSSH and NAO index) was applied.

A correlation coefficient is a statistic that is used to measure the strength of a relationship (Wheater and Cook 2000). These have values that lie between +1 (perfect positive relationship) and -1 (perfect negative relationship); values around 0 indicate that there is likely to be no relationship at all. Both the Pearson's product moment correlation coefficient (section 2.8.1), and the Spearman rank correlation coefficient (section 2.8.2) were determined. It should be noted that a correlation implies association but does not imply causality (a driver).

To elucidate whether the correlation coefficient (r) is statistically significant, the probability of obtaining the computed r value by chance needs to be calculated. This is usually achieved by looking at tables of critical values using the degrees of freedom calculated as the number of data pairs minus 2 (Wheater and Cook 2000).

2.7.1 Correlation of inter-annual variability

The approximate 12-month running means (section 2.6.1) of both the observed and modelled monthly mean surface water pCO_2 were correlated with the observed and modelled monthly means of the related parameters from 2002 to 2007, respectively. Chapter 5 discusses the results of these correlations in relation to the interannual variability of the surface water pCO_2.

2.7.2 Cross-correlation of seasonal anomalies

Two types of cross-correlations were calculated; a) with a full set of anomalies (i.e. all months included in the year) and b) seasonal cross-correlations where three-month pairs were correlated against one another (e.g. JFM). In both cases, one of the variables was kept constant in time (the leading variable such as the ΔSSH).

The other variable was then lagged by 1 to a maximum of 12 months from the reference point of the lead variable. It should be noted that for the observations, this was undertaken for both original and linearly interpolated data sets. The model output used only the available data that could be co-located.

In addition, when cross-correlating either the NAO index or the ΔSSH with the surface water pCO_2 and related parameters, the time period of the large-scale parameters was set to be 1 year longer either side of the surface pCO_2 and related parameters time period (i.e. from 2001 to 2008) so that potential lagged effects of the large-scale atmospheric and oceanic circulation on the surface pCO_2 and related parameters could be taken into account. Furthermore, the number of monthly mean related parameters (i.e. NCEP-NCAR SST, Mercator MLD, SeaWiFS Chl-a) exceed the number of surface water pCO_2 observations (see Figure 2-5 and Figure 2-4 respectively). Where these related parameters were correlated with the surface water pCO_2 (e.g. NCEP-NCAR SST), the monthly means of the related parameters were removed where there were no monthly mean surface water pCO_2 data. However when the large-scale parameters (e.g. NAO index and ΔSSH) were correlated with the related parameters, all of the available data were used. This was done so that the atmospheric and oceanic impact on these variables within the ship track region could be gauged as best as possible. The linearly interpolated data sets were also used so that a comparison with the original data sets could be performed. With respect to the three month pair seasonal analysis, only the linearly interpolated observations were used, since the original data set of the surface water pCO_2 (and to a lesser extent the related parameters) had a relatively large number of data gaps. For the model output, no linear interpolation was undertaken for this analysis for reasons described previously. Thus, model output correlations were undertaken only when both variables had data available.

The lead variable was kept constant in time at a given reference period (i.e. JFM). The other variable also exhibited 1 to 12 month lag times (e.g. ΔSSH JFM correlated with surface water pCO_2 February, March, April (FMA), then March, April, May (MAM)) and so on until there was a year lag between the two variables. Chapter 4 discusses these two types of cross-correlation and infers what they could mean in terms of drivers of surface water pCO_2 variability.

2.8 Correlation coefficients and their significance

After filtering of the data, cross-correlations or lead/lag correlations were performed to identify whether any relationship existed between the surface water pCO_2 and the aforementioned local and large-scale parameters. Both the Pearson's product moment correlation coefficient and Spearman's rank were used to identify the potential relationships.

2.8.1 Pearson's product moment correlation coefficient

Pearson's product moment correlation coefficient is often used to establish whether there is a linear dependence on a set of variables and assumes that the data are normally distributed.
It is calculated as follows:

$$r = \frac{n\sum xy - \sum x \sum y}{\sqrt{[n\sum x^2 - (\sum x)^2\ ][n\sum y^2 - (\sum y)^2]}} \tag{2.6}$$

where $\mathbf{n}$ is the number of data pairs; $\sum \mathbf{x}$ and $\sum \mathbf{y}$ are the sums of $\mathbf{x}$ and $\mathbf{y}$, respectively; $\sum \mathbf{xy}$ is the sum of the products of $\mathbf{x}$ and $\mathbf{y}$ (i.e. each value of $\mathbf{x}$ multiplied by its associated value of $\mathbf{y}$ and then all summed) (Wheater and Cook 2000).

2.8.2 Spearman rank correlation coefficient

The Spearman's rank test is used if the variables to be examined may not exhibit a linear relationship but still show an increase (or decrease) of a variable with an increase in another (Wheater and Cook 2000). It is also used when data are non-normal. It is calculated as follows:

$$r_s = \frac{1 - 6\sum d^2}{n^3 - n} \tag{2.7}$$

where d is the difference between the ranks within each pair of data points; and n is the number of data pairs (Wheater and Cook 2000). The ranks themselves are

determined in ascending order (i.e. from the lowest value to the highest) for both variables. Thus, the lowest value will have a rank of 1, and the highest a value of 72, given that we are examining monthly means from 2002 to 2007 (thus a total of 72 months).

Although both correlation coefficients were computed, the Spearman's rank correlation coefficient was primarily used in this study. Only where significant differences between the two correlation coefficients were apparent, was this detailed and explained. Significant differences may arise due to the different treatment of 'outliers' (i.e. extreme values that lie outside the main clustering of data values) between Spearman's rank correlation coefficient and Pearson's correlation coefficient. With the Pearson's method, these outliers will heavily influence the relationship between the two variables sought whereas the Spearman's rank will effectively ignore them. Thus, when the Spearman's rank correlation coefficient is statistically significant, this means that the majority of data values between the variables are related, whilst this may not be the case with the Pearson correlation statistic, since the effect of a few extreme values may be the cause of the significant relationship. Therefore to determine the most robust relationships between the related parameters and surface water pCO_2, the Spearman's rank correlation coefficient was chosen. It should also be noted, however, that extreme values could also be important and meaningful and hence the Pearson method was included in the research.

2.8.3 Determination of statistical significance

The determination of whether a correlation coefficient is statistically significant depends on the degree to which the data are temporally independent of one another (Wheater and Cook, 2000). In many instances, one can assume that there is no noticeable temporal dependence of the data within a given time series.

However, due to the use of 12 month and 3 month running means in the analysis, the data are unlikely to be temporally independent. This means that the degrees of freedom cannot be calculated by assuming that there is no temporal autocorrelation present within the two time series. Consequently, throughout this thesis, the loss of degrees of freedom from the implementation of the 12-month and 3-month running means is taken into account. This is achieved by using the Bretherton et al. (1999)

equation for calculating the effective degrees of freedom, which takes into account the temporal autocorrelation of the two time series being compared:

$$N_{eff} = N\left(\frac{1-r_1 r_2}{1+r_1 r_2}\right) \tag{2.8}$$

Where N_{eff} is the number of effective degrees of freedom, N is the total number of data points in common with the two time series, r_1 and r_2 are the autocorrelation of time series 1 and 2 respectively between zero lag and the first time lag (in this thesis 1 month, since monthly time series are used).

This formula was used in almost all of the analysis, with the exception of the calculation of the statistical significance of the correlation coefficient between the winter NAO index and winter ΔSSH, where no smoothing was implemented (section 3.2.2).

Chapter 3: Comparison of seasonal variation and inter-annual variability of observations and model output

3.1 Introduction

This chapter describes and illustrates some key results of the research. The first section addresses how the ΔSSH can act as a proxy for the gyre circulation strength in addition to illustrating the connection between the winter NAO index and winter ΔSSH.

The sections thereafter discuss the differences between the observed and modelled surface water pCO_2 and related parameters in terms of both inter-annual (section 3.3.1) and seasonal (section 3.3.2) variability. This includes an analysis of the model deficiencies in reproducing some of the related parameters' inter-annual and seasonal variability. This is important to note, as this will enable an understanding of why differences between modelled and observed surface water pCO_2 exist and therefore aid in comprehending the mechanisms of seasonal and inter-annual variability of the surface water pCO_2, which are discussed in Chapters 4 and 5 respectively.

3.2 Large-scale atmospheric and oceanic circulation

3.2.1 ΔSSH as a proxy for gyre spin up/down

As explained in the Introduction, the NAO is the dominant mode of climate variability in the North Atlantic. As such it is likely to affect the seasonal and inter-annual variability of the surface water pCO_2 through changes in ocean circulation (ΔSSH) and related parameters (see Introduction, section 1.6).

This section highlights how the ΔSSH can act as a proxy for the gyre spin up/down in addition to illustrating the link between the NAO index and the ΔSSH. As explained in the Introduction (section 1.6) the spin-up/down of the subtropical and subpolar gyres can be inferred from the relation between the ΔSSH and the zonal geostrophic velocities: years of high ΔSSH will correspond to years of weak zonal

geostrophic velocities and thus weaker surface transport in the central subtropical regions (i.e. boxes 1 to 2). Conversely, the opposite is true for the northern subtropical and temperate regions (i.e. boxes 3 to 7). To illustrate this, the 12-month running means of the ΔSSH and the zonal geostrophic velocities in each box were correlated. The patterns and associated statistically significant correlations are shown in Figure 3-1 and Figure 3-2, respectively, for two of the seven sub-regions, representing the subtropical and temperate regions: box 1 and box 6 respectively.

Figure 3-1 illustrates the high ΔSSH during 2002 and the early part of 2003, which then decrease steadily until January 2006. A rise in the ΔSSH from 2006 to 2007 is observed, before decreasing slightly during 2007, reaching a dip in September of that year, before increasing slightly during the remainder of the year. The geostrophic zonal velocities within box 1, on the other hand, show an opposing pattern to the ΔSSH, i.e. a trough during 2002 and a rise in 2003 which levels off in 2004 before increasing slightly during the first part of 2005. There then follows a slight decrease from the latter part of 2005 to January 2007 before a steady increase during 2007. Therefore, an anti-correlation between the ΔSSH and the zonal geostrophic velocities in the subtropical regions is evident as hypothesised previously (see Introduction, section 1.6 for an explanation as to why this is the case).

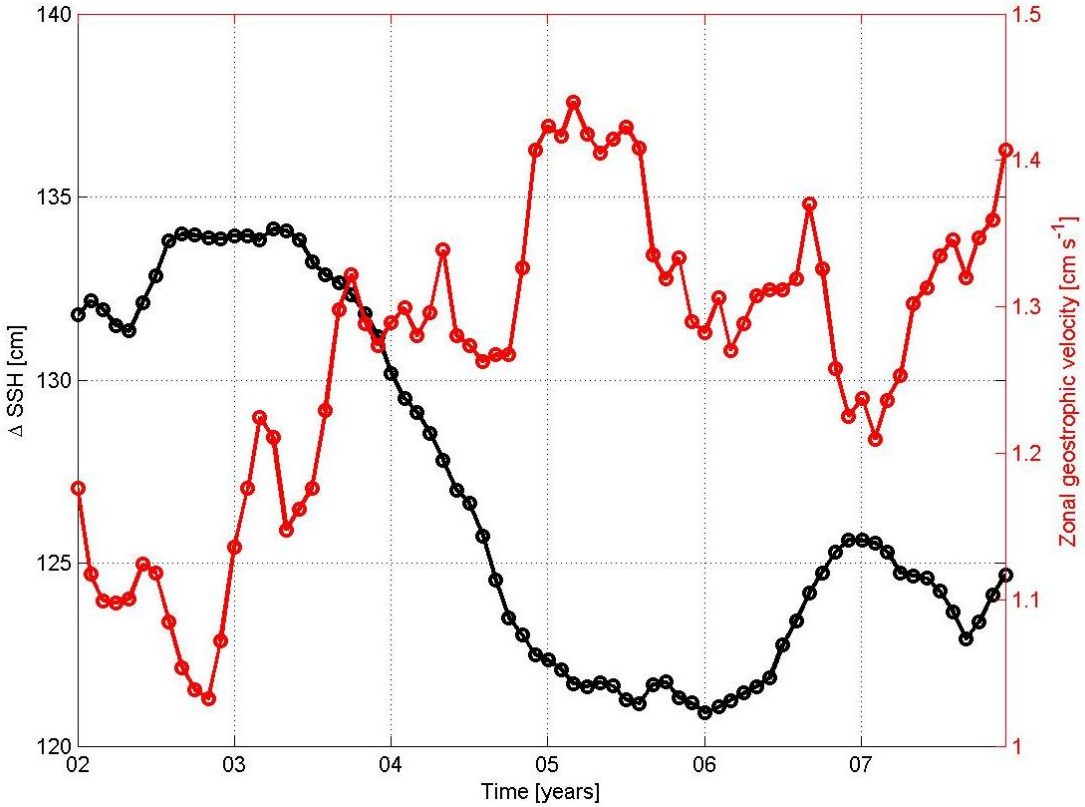

Figure 3-1: The ΔSSH inter-annual variability (black line) during the study period (2002-2007) with the inter-annual geostrophic zonal velocities in box 1 (red line). The correlation coefficient between the two time series is -0.75, which is statistically significant accounting for the loss of degrees of freedom by the implementation of the 12-month running mean.

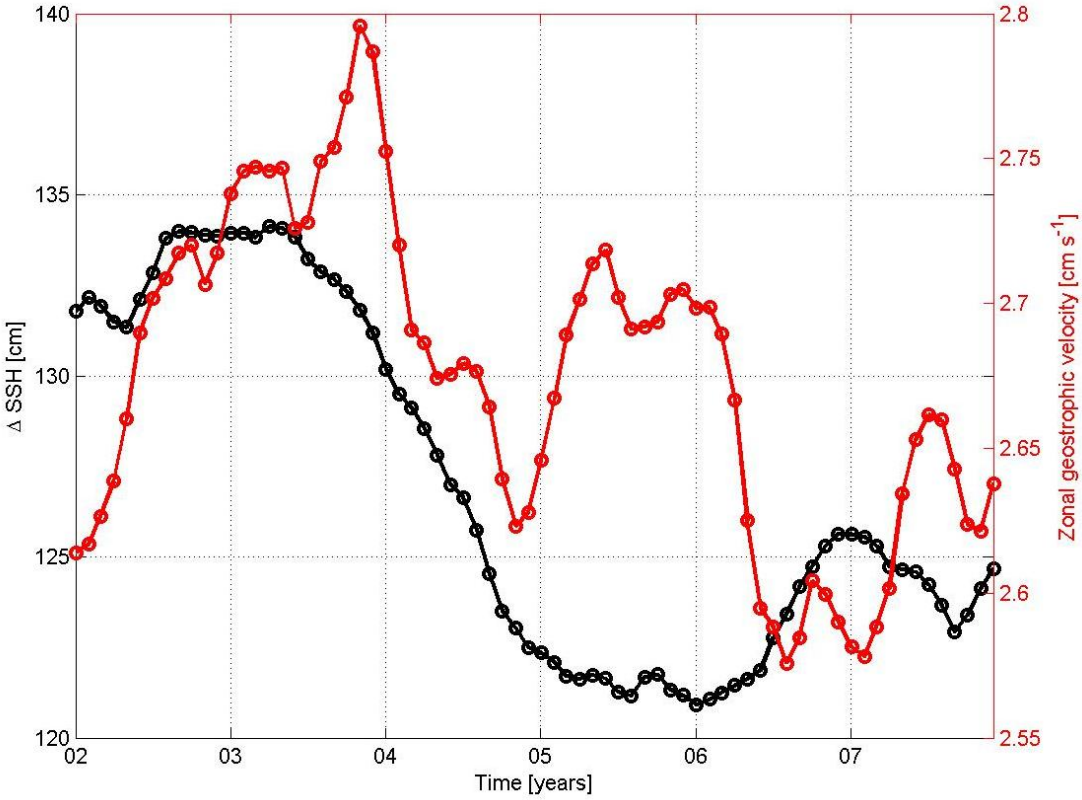

Figure 3-2: The ΔSSH inter-annual variability (black line) during the study period (2002-2007) with the inter-annual geostrophic zonal velocities in box 6 (red line). The correlation coefficient between the two time series is 0.90,which is statistically significant accounting for the loss of degrees of freedom by the implementation of the 12-month running mean.

Figure 3-2 illustrates the close co-variability between the ΔSSH and the geostrophic zonal velocities in box 6. Given that box 6 lies within the Azores current region, which originates as a branch of the Gulf Stream, it is expected that greater (lower) ΔSSH would result in faster (slower) zonal geostrophic currents. The above figure proves this claim is broadly correct.

The following section discusses the connection between the atmospheric circulation (embedded within the NAO index) and the ΔSSH.

3.2.2 The NAO as driver of the ΔSSH

The NAO index is most dominant during the winter months (Hurrell 1995). As such, the winter (DJF and JFM) NAO index was correlated with the winter (DJF and JFM) months of the ΔSSH. The best correlations were found during the JFM time period and these are shown in Figure 3-3.

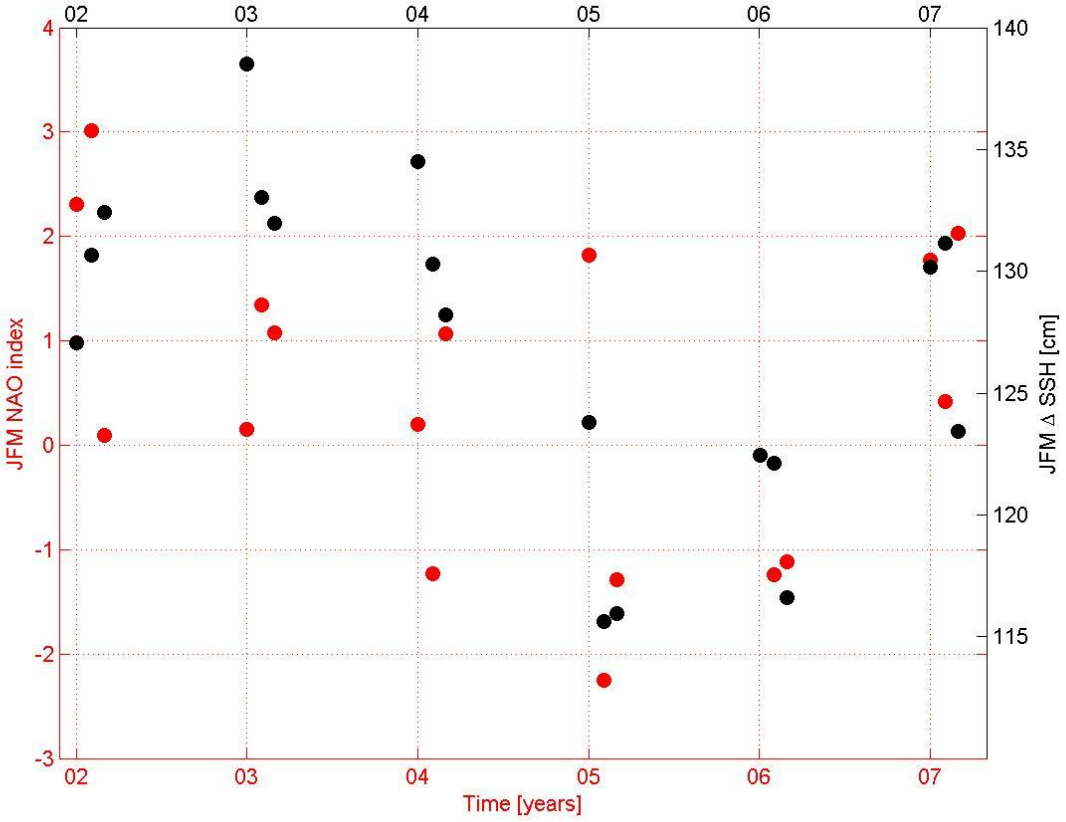

Figure 3-3: The JFM NAO index (red) plotted with the observed JFM ΔSSH (black) between 2002 and 2007. The Pearson correlation coefficient is statistically significant (0.46, p=0.05). The Spearman's correlation coefficient is not statistically significant (0.37, p > 0.05).

As can be seen, overall there is good agreement between the two variables with strong(er) NAO indices corresponding with higher ΔSSH and vice-versa. Thus, the winter NAO index does influence the winter ΔSSH and hence the strength of the ocean circulation.

Although the Spearman and Pearson correlation coefficients are slightly different, Figure 3-4 illustrates that in practice the differences are indistinguishable and the link between the NAO index and ΔSSH is maintained.

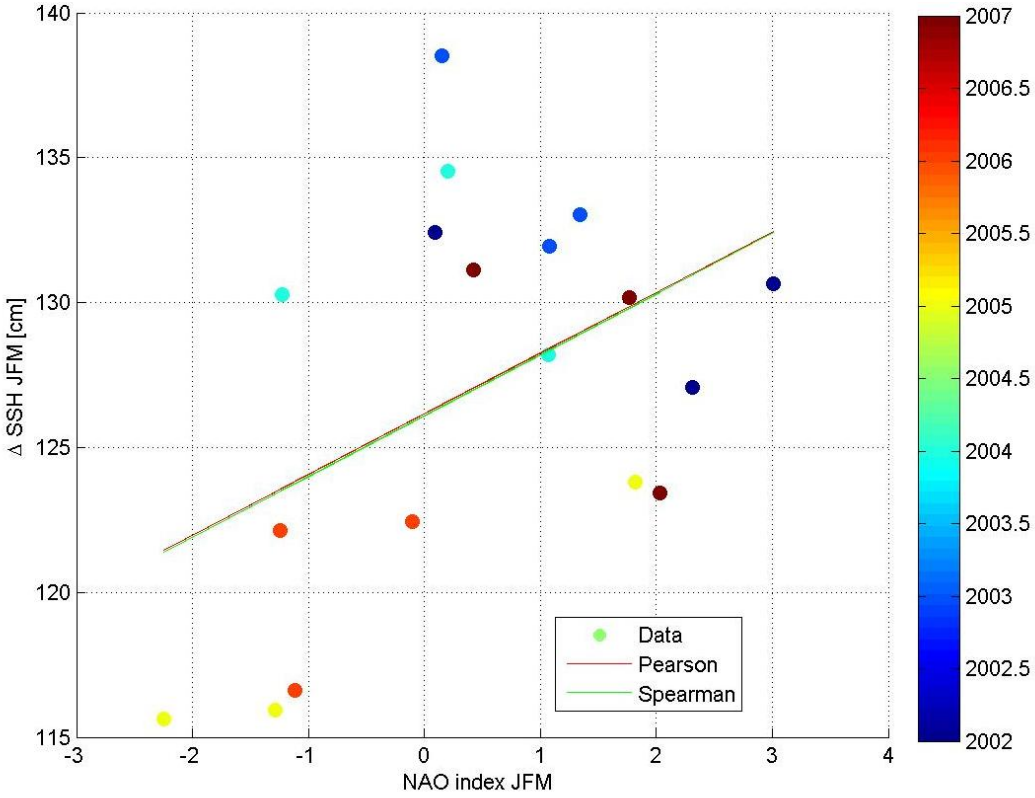

Figure 3-4: winter (JFM) ΔSSH versus winter (JFM) NAO index from 2002 to 2007. The data correspond to the monthly means of each winter-pair. The slope of both the linear and robust techniques (i.e. Pearson versus Spearman) is almost identical.

3.3 Observed and modelled surface water pCO_2 variability and related parameters

In section 3.2.1 and section 3.2.2 it was shown that the atmospheric circulation affects the oceanic circulation, particularly in winter. In this section, a comparison between the observed and modelled inter-annual and seasonal variability of the surface water pCO_2 and the related parameters is made. This underlies the differences between observations and model output in terms of the surface water pCO_2 and related parameters on these timescales. The data-model similarities substantiate the claims made in chapter 4 (seasonal anomalies) and chapter 5 (inter-annual variability) with respect to the potential large-scale drivers on pCO_2 variability in the study region. Equally, data-model differences highlight where the model can be improved and explain the reasons why the pCO_2 variability is simulated differently in certain regions of the study area.

This section is divided into two sub-sections. The first sub-section examines the inter-annual variability whilst the second focuses on the seasonal variability.

3.3.1 Inter-annual variability

3.3.1.1 Surface water pCO_2

Figure 3-5 illustrates the observed and modelled inter-annual variability of the surface water pCO_2 for each grid box. There is good agreement between the observed and modelled variability, particularly in the subtropics (i.e. boxes 1 to 3) but with a decreasing similarity in the temperate regions (e.g. boxes 6 and 7). In the subtropics (e.g. boxes 1 and 2), both the modelled and observed SST (see section 3.3.1.2) co-vary with respect to the modelled and observed surface pCO_2. This is likely to be due to a very weak inter-annual CHL signal in this region (section 3.3.1.4) thereby enabling the SST effect to dominate. However, within the temperate regions (e.g. boxes 6 and 7), even though both the modelled and observed SST co-vary well with each other, this does not apply to the CHL signal (Figure 3-8 in section 3.3.1.4). In addition the CHL concentration is (far) greater in this region than in the subtropics (Figure 3-8, section 3.3.1.4). Thus, this is likely to give rise to differences in the observed versus modelled inter-annual variability of surface water pCO_2 in the temperate region.

For example, in box 1, the surface pCO_2 starts off relatively high in 2002/3 and then decreases steadily until 2004 (model) and 2005 (observations). This is followed by a slight increase in the surface pCO_2 during 2004 (model), which is then slightly decreasing again in 2005 (model). The observations show a continued decrease in pCO_2 during 2004 and a very slight decrease in 2005. Both model and observations reveal a steady increase from 2006 through to 2007. The observations indicate that the annual surface pCO_2 during 2007 was the highest of the entire study period, whilst the modelled pCO_2 remains (slightly) below the 2002 pCO_2 maximum.

In terms of the observations, the pattern described in the last paragraph alters slightly in boxes 2, 3 and 4. This is most likely due to the increase in CHL concentration within these boxes (Figure 3-8, section 3.3.1.4) which in turn would affect the inter-annual variability of surface pCO_2 more than in the subtropics where the SST is most likely to dominate. For example, there is an increasing tendency for

the surface water pCO_2 to start at lower levels to those observed in box 1 (see box 4) and for the surface pCO_2 to increase from 2005 through to 2007, rather than from 2006 to 2007. From boxes 5 to 7, the surface pCO_2 exhibits lower values at the start of the study period (i.e. under 360 µatm) and remains around that level until the early part of 2004, before decreasing to a minimum in early 2005. Thereafter, the annual surface water pCO_2 recovers and reaches its highest values towards the end of the study period as described for the subtropics (e.g. boxes 1 to 3).

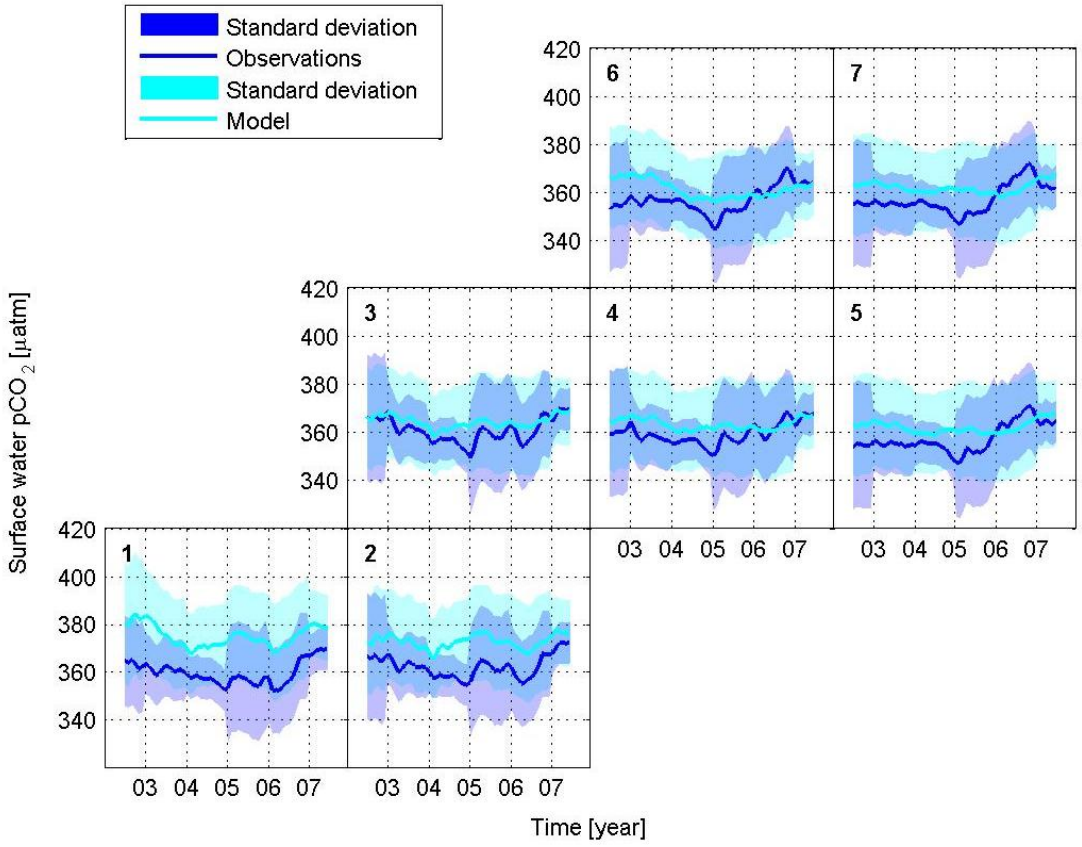

Figure 3-5: Inter-annual variability and standard deviation of the surface water pCO_2 for the observations (dark blue and shading respectively) and model output (light blue and shading respectively).

The modelled pCO_2 pattern of box 1 is broadly repeated in boxes 2, 3 and 4, albeit with a reduced pCO_2 magnitude and a reduced or negligible increase of the surface water pCO_2 during 2004, in addition to a reduced decrease in 2005. From boxes 5 to 7, the increase in surface water pCO_2 seen in the observations from 2005 to 2007 is not as marked and overall the inter-annual variability of the surface water pCO_2 is less pronounced in the temperate regions (boxes 5 to 7) than it is in the subtropics (boxes 1 to 4).

In summary, the variability of the model pCO_2 compares well with the observed pCO_2 in the subtropical regions (i.e. boxes 1 to 3, with box 3 showing the best fit). In the temperate regions, the modelled pCO_2 exhibits a similar pattern to that of the modelled pCO_2 in the subtropics, although the inter-annual variability is dampened in comparison, especially in boxes 4, 5 and 7. The sharper pCO_2 increase from 2005 in the observations in boxes 5 to 7 is not mirrored in the model, however.

3.3.1.2 Sea-surface temperature

Figure 3-6 illustrates the inter-annual variability of the observed and modelled SST. What is immediately striking is the close co-variability between the model and observations. As mentioned in Chapter 2, the model is forced with NCEP-NCAR SST and thus the SST product used for the observations was also NCEP-NCAR SST to enable a direct comparison to be made. This close co-variability between model output and observations is unsurprising, however, given that the source of the SST product is the same.

What is less obvious are the reasons for the slight differences between the model and observed SST (see Figure 3-6), despite originating from the same data source. This is likely to stem from the differences in initial spatial resolution of the modelled versus observed NCEP-NCAR SST: all model output parameters were provided on a 1° latitude by 1° longitude grid whereas the NCEP-NCAR SST product was interpolated onto a 1° latitude by 1° longitude grid from an initial spatial resolution of 1.875° latitude by 1.875° longitude (see also Table 1, chapter 2, section 2.4). Consequently, this interpolation would have resulted in the inclusion of data from a wider swath, thereby resulting in slight differences between the model output and observations.

Equally though, the temporal resolution of the model output was only available at monthly increments, even though the spatial resolution of the model output was lower than that of the observations. Hence, the observed SST would have picked up a larger number of data points (given the initial daily temporal resolution of the observations), which the model output could not have done. Therefore, the initial spatial and temporal resolution of the products used for both the observations and model output will result in slightly different monthly mean values (even though the final spatial and temporal resolution is the same for both model and observations).

Consequently, it is important to recognise that there are inherent uncertainties in both the observations and model output.

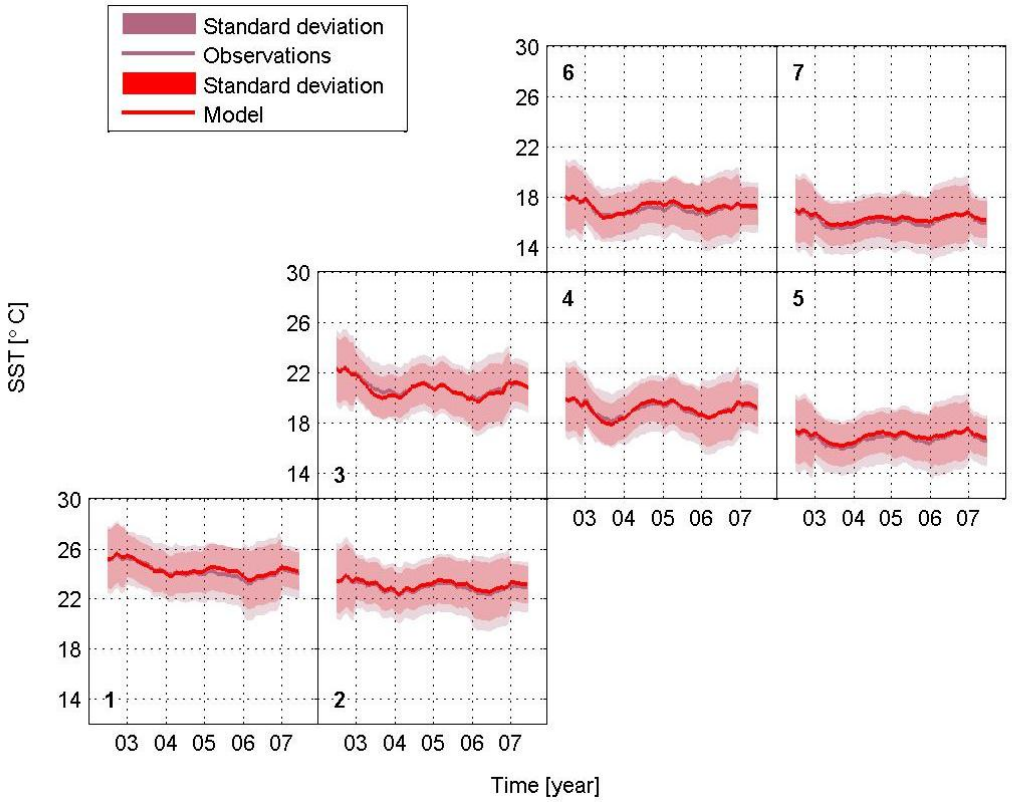

Figure 3-6: Inter-annual variability and standard deviation of the SST [°C] for the observations (dark red and shading respectively) and model output (red and shading respectively).

The very comparable SST pattern between the model and observations in the seven sub-regions does not equate to highly related surface water pCO_2 variability in all boxes (see Figure 3-5). For example, in boxes 6 and 7, in terms of the observations in particular, the decrease in surface water pCO_2 during 2004 is not mirrored by a decrease in SST. In fact, the SST increases during that time period. In addition, the steady increase in the surface water pCO_2 from 2005 through to 2007 in these boxes is not reflected in a steady SST increase.

The modelled surface water pCO_2 in these temperate regions do not show as much variability as the observations, but the co-variability between the modelled SST and modelled pCO_2 in this region is also not as great as in the subtropics (e.g. boxes 1 and 2). The main difference between model pCO_2 and model SST in the temperate regions stems from a slight decoupling of the pCO_2 from the SST during 2004 to

2006, with the SST increasing slightly but the pCO_2 either decreasing slightly (box 6) or remaining at a similar level during this time period (box 7).

Furthermore, also it is interesting to note that although the subtropics exhibit the highest SST (e.g. ranging between 22 and 28°C in box 1) with a steady decrease in the SST further north and east (see boxes 3 to 5 for example), this steady decrease is not reflected in the observed surface water pCO_2. In fact, the observed surface water pCO_2 inter-annual variability ranges between ~350 µatm to ~370 µatm in all boxes. This indicates that the SST is not the only factor controlling the variability of the pCO_2, even in the subtropics.

The magnitude of the modelled pCO_2 is greater than the observations in the subtropics (especially boxes 1 and 2), hinting that the model SST is the main parameter affecting the modelled pCO_2 in these regions. However, in boxes 3 to 5, whilst the model SST steadily decreases, the modelled pCO_2 does not and remains at similar levels seen in box 3, located within the subtropics. Thus, the model is also hinting at other variables that control the pCO_2 variability, albeit mainly outside of the subtropical regions.

3.3.1.3 Mixed layer depth

Mixed layer depth is another important parameter to consider, since it will affect the volume of carbon-rich subsurface water entrained to the surface, thereby increasing the surface water pCO_2. These waters are cold and hence will increase the solubility of CO_2 in seawater, thereby decreasing the surface water pCO_2. The net effect of cold versus carbon-rich water on the pCO_2 depends on the dominance of SST compared to DIC.

Figure 3-7 illustrates the inter-annual variability of the mixed layer depth (MLD) for both the observations and model output.

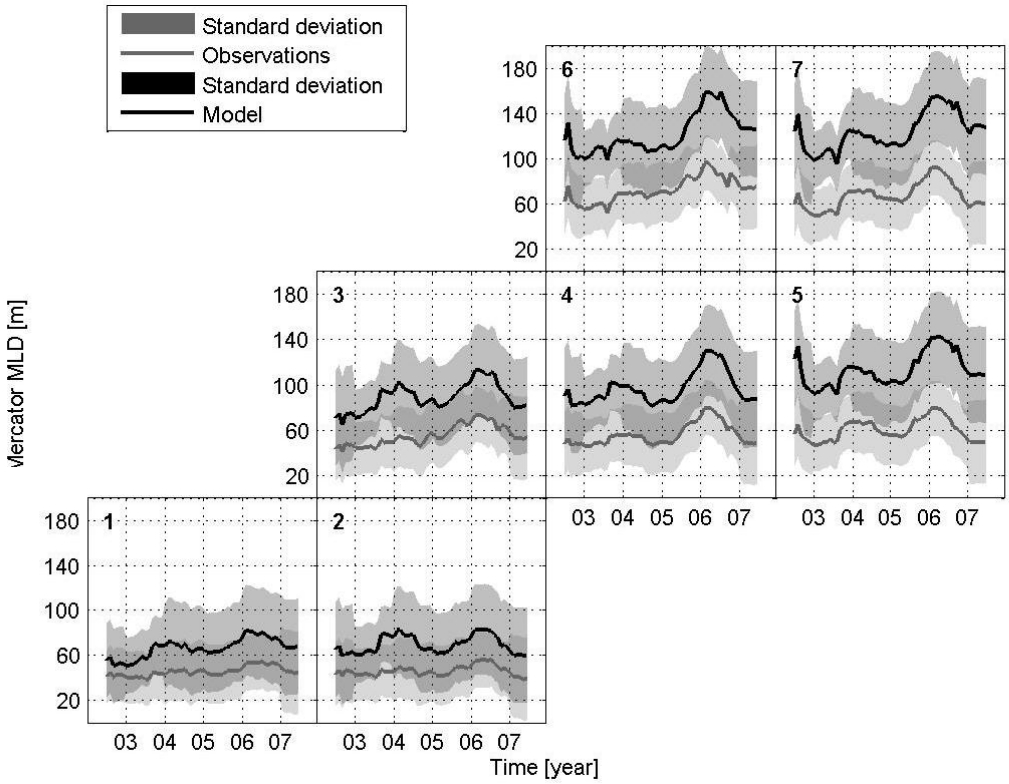

Figure 3-7: Inter-annual variability and standard deviation of the MLD [m] for the observations (grey line and lighter shading respectively) and model output (black line and darker shading respectively).

It is clear that the inter-annual variability of the MLD is in anti-phase with that of the SST (see Figure 3-6), with all boxes showing an increasing (deepening) trend of the MLD from 2002 to 2007. In addition, whilst the model output reveals a highly similar inter-annual pattern compared to the observations, the difference in magnitude of the MLD compared to the observations also increases from box to box. For example, in box 1 the modelled MLD ranges from ~10m to ~30m (i.e. compare 2002 to 2006) greater depth than the observations. In box 6, this difference increases to 60m at times (e.g. during 2002 and 2006).

Given that the criterion used to define the MLD in both the observations and the model is the same (section 2.4.2), this observed/model discrepancy is likely to stem from the accentuated differences in initial spatial resolution of this product between the observations and model output, with the observations' initial spatial resolution at 1/4° latitude by 1/4° longitude and the model output's at 1° latitude by 1° longitude (the temporal resolution is the same in this case). Thus, as described in section 3.3.1.2, even though the final spatial resolution between model and observations is the same, the regridding of the data from a 1/4° by 1/4° grid to 1° by 1° grid would

have taken more localized processes into account than the model. In addition, given that Steinhoff et al. (2010) show that the Mercator MLD product was one of the most accurate products (compared to the MLD estimated from Argo floats, it was only ~11m deeper based on 31 profiles), it is concluded that the observations are closer to the depiction of the MLD over the study region than the model.

At first glance it seems that the MLD is inversely proportional to the SST in all sub-regions. Hence, warmer waters will stratify the water column and colder waters will enable deep(er) winter mixing to take place. Whilst this applies to the subtropical regions (i.e. see how in boxes 1 and 2 the surface water pCO_2 variability (Figure 3-5) closely follows that of the SST variability (Figure 3-6)), this is not as clear cut in the temperate regions. For instance, in box 6, the pCO_2 increases during 2005, whilst the SST decreases. The MLD, however, increases in 2005, indicating that vertical mixing may be more important than SST in driving the pCO_2 enhancement that year. Thus, vertical mixing has an increasing influence on the surface water pCO_2 variability further north and east. However, it should also be noted that vertical mixing may also have contributed to the higher surface water pCO_2 in the subtropics during the winter of 2006/7 and thus may have also influenced the higher annual surface water pCO_2 during 2007. This will be further explored and discussed in Chapter 4 (seasonal anomalies) and Chapter 5 (inter-annual variability) respectively.

3.3.1.4 Chlorophyll-a

This section examines the observed and modelled chlorophyll-a (CHL). The CHL acts as a proxy for biological activity which has an important effect on the surface water pCO_2 variability, as mentioned in the Introduction, sections 1.6 and 1.7.

Figure 3-8 illustrates the observed and modelled CHL. As can be seen, the observed and modelled CHL patterns are different, especially within the temperate regions (i.e. boxes 4 to 7): the observations show that during 2002 and 2003 the CHL increases, then steadily decreases during 2004 to 2006. In boxes 5 and 7, the CHL continues to decrease during 2006, whilst it increases slightly in box 4 and 6 (relative to 2005).

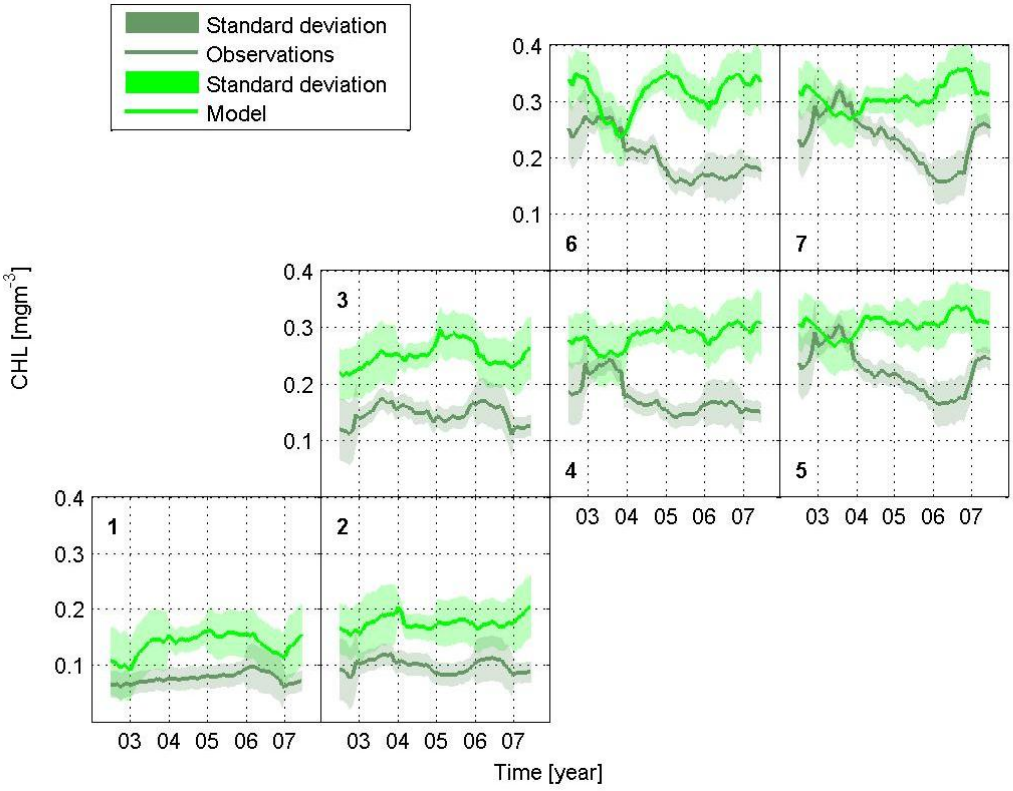

Figure 3-8: Inter-annual variability and standard deviation of the CHL [mg m^{-3}] for the observations (dark green and shading respectively) and model output (light green and shading respectively).

The model, on the other hand, almost shows the opposite within the temperate regions (boxes 4 to 7): after increasing in 2002, the CHL decreases during 2003, then increases until 2005 before either levelling off during 2005 until 2006 (box 4, 5 and 7) or decreasing again during 2005 until 2006 (box 6). This is followed by an increase in the CHL for all boxes in 2006 before it is either levelling off in 2007 (box 4 and 6) or decreasing slightly (box 5 and 7).

Both the observations and model output show a steady increase in the CHL concentration from box 1 (subtropical regions) to box 7 (temperate regions), however, as would be expected, from the oligotrophic subtropics to the more biologically active temperate regions (Longhurst et al. 1995).

It should be noted that the SeaWiFS CHL does not measure primary production but rather estimates the phytoplankton concentration as a function of the backscattered green light from the photosynthetic pigment of the phytoplankton, i.e. the total chlorophyll concentration (O'Reilly et al. 1998). Thus, it is widely used as a proxy for phytoplankton biomass (Huot et al. 2007). However, due to the pronounced

variability of its cellular content and its ratio with respect to phytoplankton carbon, the concentration of CHL is a biased estimator of phytoplankton biomass as organic carbon (Cullen, 1982). Thus, the CHL variability of the observations in Figure 3-8 does not equate to the phytoplankton biomass within the study regions and therefore cannot be used to understand changes in primary productivity Nevertheless, changes in CHL concentration are likely to infer changes in phytoplankton concentration since a shift from backscattered deep blue light from the ocean shifts to green as the phytoplankton concentration increases (Yentsch, 1960).

An increase in CHL concentration would usually equate to a decrease in surface pCO_2 due to the usage of DIC in the surface water by biology, and a decrease in CHL concentration would be marked by an increase in surface pCO_2 due to limited DIC usage. However, this very much depends on whether a) the CHL concentration is high enough for a decrease in pCO_2 to take place and b) the timing of the biological activity/phytoplankton blooms. This is because high SST may counteract the CHL signal, if it is not large enough. In addition, if the timing of the phytoplankton bloom coincides with the peak SST, this may also mask the CHL signal. Thus in both cases, a relatively high CHL concentration could give rise to higher than expected surface water pCO_2, but this would result from higher SST and not from high CHL. Higher surface water pCO_2 could also result from entrainment of high DIC water the previous winter. This is one of the main deficiencies in the model, particularly in the temperate regions, as will be explained in the following paragraphs and also in the seasonal variability section of this chapter.

In the subtropical regions (e.g. box 1), the observed and modelled CHL agree relatively well with a gradual increase in CHL concentration from 2002 up to and including 2005, a decrease in 2006 and a slight increase in 2007. The magnitude of the CHL concentration is low for both observations and model during the time period. Partially as a result, the surface water pCO_2 in this region is generally high and the inter-annual variability of the surface water pCO_2 is broadly in anti-phase with that of the CHL (especially between 2002 and 2006 where the surface pCO_2 decreases whilst the CHL concentration increases, compare Figure 3-5 with Figure 3-8). This pattern continues to be evident in boxes 2 and 3, albeit with a greater discrepancy between modelled and observed CHL (e.g. in box 2 and 3, the observed CHL decreases during 2004 and 2005 whereas the modelled CHL increases).

However, the modelled inter-annual variability of the CHL follows that of the modelled SST increasingly from boxes 4 to 7 (compare Figure 3-8 with Figure 3-5). Thus the CHL signal, even though it increases in magnitude, is masked more by the SST. The net effect this CHL masking has on the inter-annual variability of the surface water pCO_2 in the temperate regions is a stronger SST dependence than CHL. This is why the modelled pCO_2 co-varies closely with the modelled SST throughout the study region. The reason that the modelled SST is masking the modelled CHL is due to the timing of the phytoplankton blooms in the core summer months, when the SST is at its highest. This will be illustrated in the CHL section (section 3.3.2.4) of the seasonal variability part of this chapter.

The inter-annual CHL variability within the temperate regions (i.e. boxes 4 to 7) follows a broadly opposing pattern to the modelled CHL, with the observed CHL increasing, whilst the modelled CHL decreases (e.g. in boxes 4 through 7, the observed CHL increases during 2002 and much of 2003, whilst the modelled CHL decreases, see Figure 3-8). There are other examples of the opposing CHL patterns in the temperate zone between the observations and model, such as the increase in CHL concentration in the model between 2004 and 2005 in box 4, whilst the observations reveal a decrease.

The effect that these observed CHL patterns have on the observed inter-annual variability of the surface water pCO_2 is therefore different to that of the model output pCO_2 variability. For example, in Figure 3-5, boxes 4 to 7, but in particular from boxes 5 to 7, the surface water pCO_2 remains at a constant level during 2002 and 2003, whilst the CHL concentration is relatively high during this time period (~0.2 to 0.3 mg m^{-3}, see boxes 5 to 7, Figure 3-8). Therefore biological activity is likely to have dominated the inter-annual variability of the surface water pCO_2 during this time period.

During 2004, although the trend in CHL concentration tends to decrease in most boxes (e.g. boxes 2 to 7), it should be noted that the absolute CHL concentration of the observations in spring 2004 was either the 3rd or 4th highest of the entire study period (particularly in boxes 5 to 7, see Figure A-4 in the Appendix). (It should be noted that from here on, the suffix ‘A’, refers to the Appendix). Therefore, there would have still been a biological effect on the surface water pCO_2 during that time, contributing to the decreases observed in pCO_2 seen in all boxes that year. In addition, the SST summer values were suppressed in 2004 (relative to 2002 and

2003, see Figure A-2), although this relative decrease is not discernible in Figure 3-6, because it includes the winter increase in SST from 2002/3 to 2003/4, which counteracts the decrease in summer SST in 2004. Thus, on an annual basis, the winter increase in SST outweighs the summer decrease, therefore producing a slight increase in SST from 2003 to 2004. In any case, the summer SST decrease in 2004 likely contributed to the decline in surface water pCO_2 that year and was amplified by the still relatively high CHL concentration that year (despite the decreasing CHL trend during the year).

From 2005 to 2007, the CHL concentration in the observations within the temperate regions either slightly increases during 2005 to reach a high(er) level in 2007 (see Figure 3-8, boxes 4 and 6) or decreases during 2005 but steadily increases thereafter to also reach higher CHL concentrations in 2007. The surface water pCO_2 during this time period actually increases steadily to reach its highest levels of the entire study period in 2007. Thus, the biological activity is reduced compared to 2002 and 2003, thereby enabling the pCO_2 to increase. The MLD increased in all temperate regions during 2005, most likely resulting in enhanced winter vertical mixing, entraining higher DIC waters to the surface. This would have contributed to the pCO_2 increase in 2005. In 2006, the SST increased again and coupled with relatively high MLD (and thus higher surface DIC) may have enabled the pCO_2 to increase further in 2006. Thus, vertical mixing and SST are likely to have played a more decisive role than CHL in increasing the pCO_2 from 2005 to 2007 in the temperate regions.

The key similarities and differences between the observations and model output have been discussed with respect to the inter-annual variability of the surface water pCO_2 and related parameters. The following section discusses these with regards to the seasonal variability.

3.3.2 Seasonal variability

3.3.2.1 Surface water pCO_2

Figure 3-9 illustrates the mean seasonal cycle of both the observed and modelled surface water pCO_2. It shows that in the subtropics (i.e. boxes 1 to 3), there is a

clear seasonal cycle of the observed and modelled surface water pCO_2 with peaks in summer and troughs in winter.

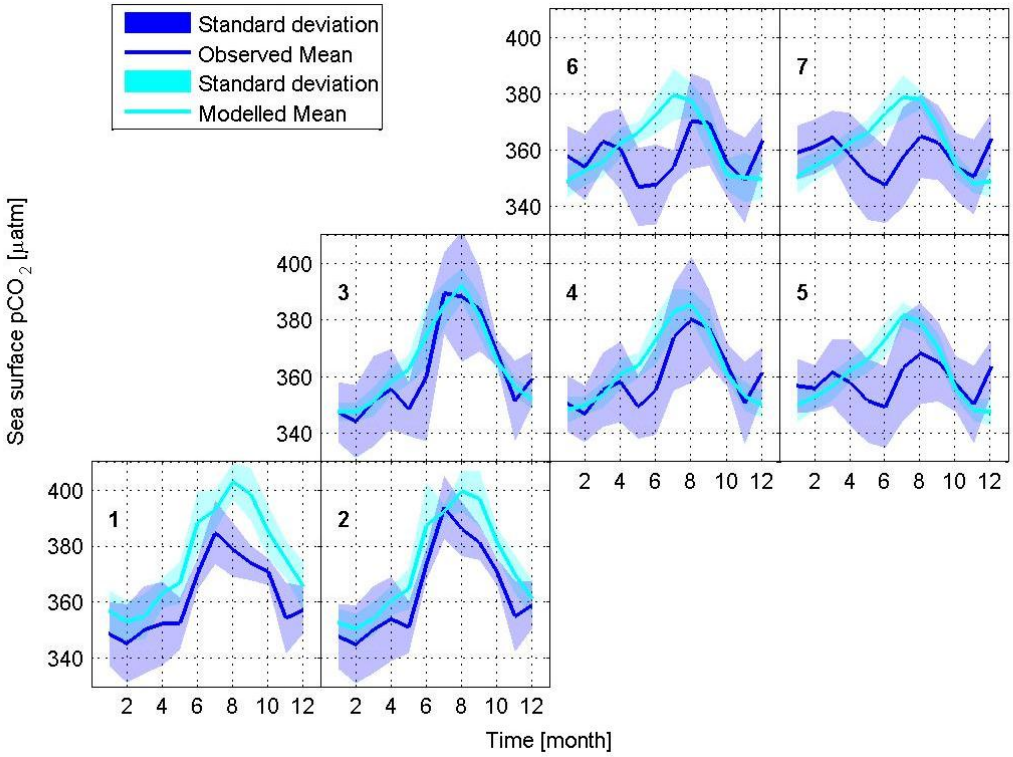

Figure 3-9: Mean seasonal cycle of the surface water pCO_2 [µatm] for both the observations (dark blue line) and standard deviation (dark blue shading) and the model (light blue line) and standard deviation (light blue shading).

In terms of the observations, this seasonal cycle becomes less pronounced further north and east in the observations with boxes 5 to 7 exhibiting a marked reduction in the summer (August) pCO_2 peak. In addition, there is an increasing late-winter (March) pCO_2 peak that develops from box 4 to 7. This winter peak reaches the summer pCO_2 peak levels in box 7 and is only slightly less than the summer pCO_2 peak in box 6. Furthermore, there is an increasing pCO_2 trough that develops between spring into early summer (e.g. April to June) from boxes 2 through to 7. This pCO_2 trough reaches its lowest point between May and June (boxes 4 and 6 for the former and boxes 5 and 7 for the latter). Interestingly, the summer peak pCO_2 in box 1 (July) is lower than that of box 2, although both boxes lie within the subtropics. An examination of the monthly means of the surface pCO_2 between these boxes shows that this is due to higher summer pCO_2 in box 2 during 2002 (see Figure A-1).

The model, on the other hand, reveals a seasonal cycle that is broadly similar to the subtropics, albeit with a decreasing amplitude from box 1 to box 7, due to a reduction in the summer peak pCO_2 from box 1 to box 7. It is unable to capture the development of a pCO_2 trough in spring in the temperate regions or a (smaller) stand-alone pCO_2 peak in late winter.

The reasons for this will be examined in the following sub-sections as the related parameters are focused upon.

3.3.2.2 Sea-surface temperature

Figure 3-10 reveals the mean seasonal cycle of the SST for the observations and model for all boxes. As can be seen, there is very good agreement between the observations and model output in terms of both the amplitude and phase of the SST seasonal cycle. Interestingly the model under-estimates the peak summer SST and over-estimates the late-winter SST slightly in all boxes, more so within the temperate regions (e.g. boxes 4 through to 7).

Both the observations and model output show a steady decrease in the SST from box 1 through to box 7, with box 1 exhibiting the highest SST, whilst box 7 displays the lowest, although still relatively warm. This explains the reduction in the summer peak of the modelled and observed surface water pCO_2 from boxes 1 to 7 in Figure 3-9, although in terms of the observations this reduction essentially starts from box 2 for reasons given in section 3.3.2.1.

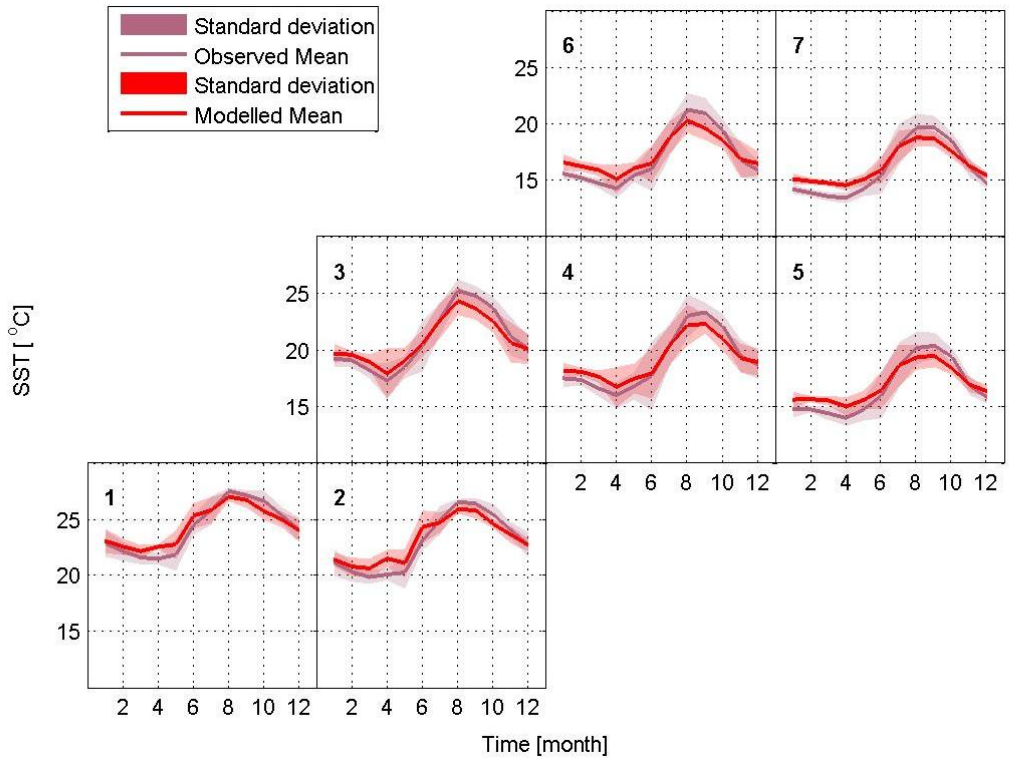

Figure 3-10: Mean seasonal cycle of the SST [°C] for both the observations (dark redline) and standard deviation (dark red shading) and the model (red line) and standard deviation (red shading).

However, during April and May, the observed surface pCO_2 in the temperate regions (i.e. boxes 4 to 7) decreases whilst the SST increases. Thus, as expected, the SST does not dominate the seasonal cycle of the surface water pCO_2 in the temperate regions in all seasons. Biological activity is the cause of this spring pCO_2 decrease in the temperate regions, as will be shown in section 3.3.2.4.

Importantly, the model output does not capture this key difference within the temperate zone: the SST seasonal cycle is very similar but the pCO_2 seasonal cycle mimics that of the SST, even in these more northerly regions. This is due to the incorrect timing of biological activity in these areas, which will be shown in section 3.3.2.4.

3.3.2.3 Mixed layer depth

Figure 3-11 illustrates the observed and modelled MLD for all boxes.

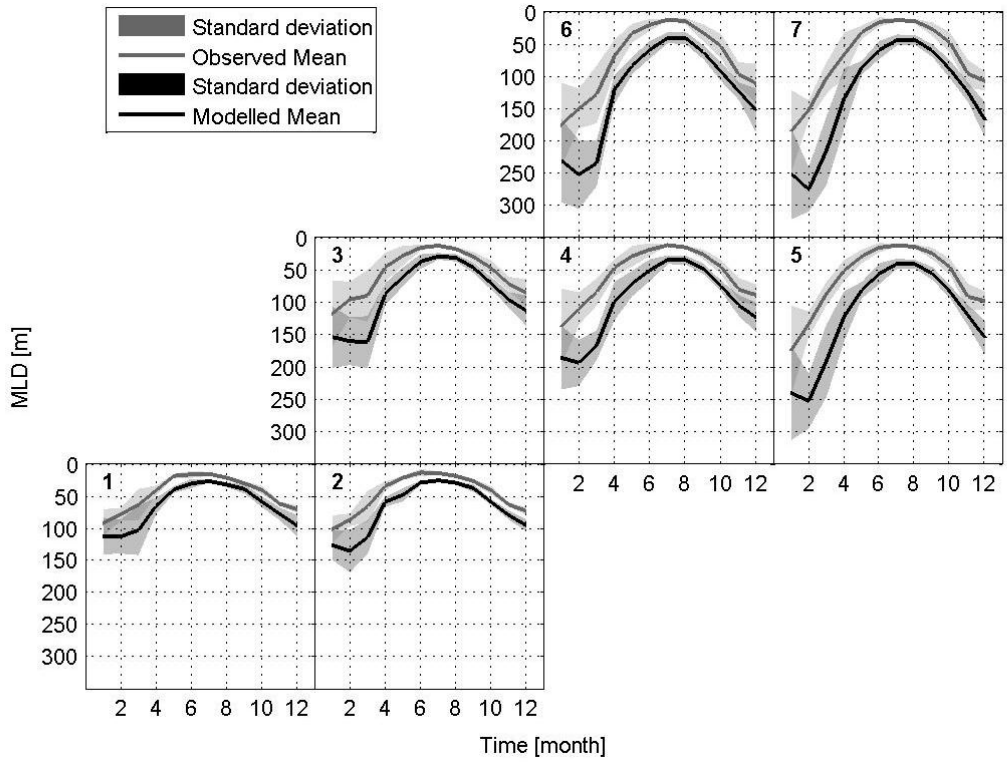

Figure 3-11: Mean seasonal cycle of the MLD [m] for both the observations (grey line) and standard deviation (grey shading) and the model (black line) and standard deviation (black shading).

Both observations and model output reveal broadly similar mean seasonal cycles of the MLD with the greatest MLD during winter and the lowest during summer. The amplitude and phase of the mean seasonal cycle between model and observations is generally very similar, although the maximum MLD occurs in January with respect to the observations, whilst it is February in the model. This is the month that shows the greatest difference between the model and observations, with the model generally over-estimating the MLD by up to 100 metres in the temperate regions compared to the observations (e.g. boxes 5, 6 and 7). As explained in section 3.3.1.3 for inter-annual variability, in this case the observations are likely to be more accurate given the findings of Steinhoff et al. (2010). Thus, the overestimation by the model on this seasonal timescale is likely to arise from differences in the spatial resolution of the modelled MLD, as also evident on the inter-annual timescale.

However, the model and observations do agree on the increase in surface pCO_2 during the late winter (i.e. February and March) in all boxes, which implies that entrainment of DIC-rich subsurface water to the surface is likely to increase the surface water pCO_2, despite cold subsurface waters (which would decrease the pCO_2). Given that the SST decreases from February to April (and the surface pCO_2

increases in all boxes during this time – see Figure 3-5 and Figure 3-6, respectively), DIC entrainment is likely to be occurring, which is increasing the pCO_2. The temperature versus non-temperature effects for both observations and model output on the surface pCO_2 will be highlighted in chapter 4 for the seasonal anomalies and in chapter 5 for the inter-annual variability. From this it will be possible to determine that the DIC is likely to cause the increase in surface pCO_2 during late-winter. In addition, the mean seasonal cycle of the model DIC can be viewed in Figure A-23, which clearly shows an increase in the DIC from January to April in most boxes, particularly in the temperate regions.

3.3.2.4 Chlorophyll-a

Figure 3-12 reveals the mean seasonal cycle of the CHL for both observations and model output.

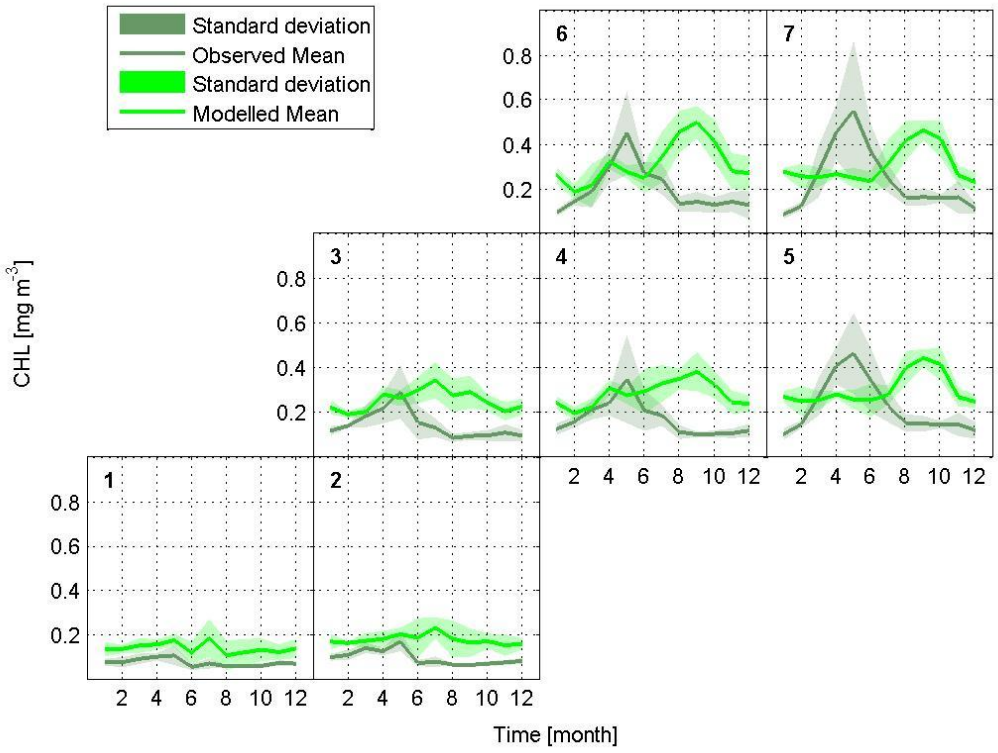

Figure 3-12: Mean seasonal cycle of the CHL [mg m^{-3}] for both the observations (dark green line) and standard deviation (dark green shading) and the model (light green line) and standard deviation (light green shading).

As can be clearly seen, the observed and modelled CHL mean seasonal cycles are different from one another, especially from boxes 2 through to 7. The difference arises from the timing of the peak phytoplankton bloom, which in the model is simulated to occur between July (boxes 1 to 3) and September (boxes 4 to 7). The observations, on the other, hand reveal that the peak phytoplankton bloom occurs between April and May throughout the seven sub-regions.

The net result of this misrepresentation of the CHL mean seasonal cycle is that the simulated pCO_2 in the temperate regions (e.g. boxes 4 to 7) during spring and early summer (i.e. April through to June) is over-estimated (see Figure 3-4, boxes 4 to 7). The observations reveal a pCO_2 trough that coincides with the peak CHL in these boxes, strongly suggesting that biological activity is decreasing the surface pCO_2 during that time period.

A possible reason for this misrepresentation of the modelled CHL is the result of the overestimation of the depth of the mixed layer (Figure 3-11). According to Behrenfeld (2010) as the mixed layer shoals in spring, this increases the grazing pressure since dilution from a deep winter mixed layer ceases. However, due to the increase in photosynthetically active radiation (PAR) during this time, the phytoplankton bloom reaches its peak despite this increase in grazing pressure (Behrenfeld, 2010). Since the model over-estimates the depth of the mixed layer year round, especially in winter and early spring particularly within the temperate regions (see Figure 3-11), this may reduce the availability of PAR and hence reduce the CHL concentration in the model in spring. The emergence of the modelled phytoplankton bloom in September may therefore result from a shallower mixed layer at that time compared to spring (Figure 3-11). This would enable sufficient PAR to enter the ocean surface and coupled with a sufficient nutrient reservoir promote a phytoplankton bloom.

This mistiming of the phytoplankton bloom (which incidentally coincides with the highest SST months) is likely to account for the large differences between the modelled and observed inter-annual variability of the surface pCO_2 in the temperate regions. Due to the late summer peak in SST, which coincides with that of the CHL, the inter-annual variability of the modelled pCO_2 follows that of the modelled SST to a large extent (see Figure 3-5 and Figure 3-6).

Capturing ecosystem dynamics is a known problem in many biogeochemical models (Manizza et al. 2010) and this needs to be improved so that the seasonal and inter-annual variability of surface water pCO_2 can be simulated more accurately. This will also enable better predictions of future surface water pCO_2 variability to be gauged.

It is therefore important to keep these points in mind, as the subsequent chapters make reference to the differences in SST dominance and CHL signature between observations and model output.

3.4 Summary

The mechanism hypothesised in the Introduction, with the ΔSSH acting as a proxy for the strength of the ocean circulation, has been proven here by coupling the zonal geostrophic velocity fields with the ΔSSH (see Figure 3-1 and Figure 3-2). In addition, the co-variability of the winter NAO index with the winter ΔSSH has been evidenced (see Figure 3-3 and Figure 3-4, respectively), thus enabling a connection between atmospheric forcing and ocean response to be made.

A data-model comparison of the surface water pCO_2 and related parameters has been undertaken in relation to their inter-annual (section 3.3.1) and seasonal variability (section 3.3.2). Deficiencies in the model have been highlighted which help explain some of the key differences between modelled and observed surface water pCO_2. In addition, uncertainties in the data have been highlighted, although it is still likely that the data provide a more accurate depiction of reality than the model (especially with respect to CHL).

A discussion of how the large-scale atmospheric and oceanic circulation affects the surface water pCO_2 through the related parameters follows in chapter 4 in terms of seasonal anomalies and in chapter 5 for inter-annual variability.

Chapter 4: Drivers of the seasonal anomaly of surface water pCO_2 in the North Atlantic Ocean

4.1 Introduction

This chapter highlights the importance of atmospheric and oceanic circulations in affecting the strength of the pCO_2 seasonal cycle, as outlined in the hypothesis (chapter 1, section 1.7). Both observational data and model output from a biogeochemical model (see Methods for a description of the observational data (section 2.4) and the model (section 2.2.2) are used to study the fundamental processes affecting the strength of the pCO_2 seasonal cycle.

As such, cross-correlation analysis was performed (see Methods section 2.7.2). The advantage of this type of analysis is that relationships between variables are discovered when one variable is leading or lagging the other by a certain time-period in addition to potential instantaneous relationships.

The main findings of this analysis are as follows:

- The atmospheric circulation in combination with the oceanic circulation affects the seasonal anomalies of the surface water pCO_2.
- The oceanic circulation, in response to the atmospheric circulation, affects the seasonal anomalies of the surface pCO_2 differently in the subtropical region compared to the temperate region in some years but not in others.
- The processes affecting the seasonal anomalies of the surface water pCO_2 are most prominent during the winter months, specifically December, January, February (DJF) and January, February and March (JFM).

The key points highlighted above will be discussed in detail below. Cross-correlations between the ΔSSH anomalies (a proxy for the large-scale oceanic circulation – see chapter 3, section 3.2.1 for a detailed explanation as to how the ΔSSH can be used in this way) and the surface water pCO_2 anomalies were performed to establish whether the oceanic circulation had an impact on the amplitude of the surface water pCO_2 seasonal cycle. Likewise, cross-correlations between the NAO index (an index widely used to measure the strength of the North Atlantic atmospheric circulation – see chapter 2, section 2.4.7 for a description of

the NAO) and the surface water pCO_2 anomalies were performed to determine the effect of the atmospheric circulation on the strength of the surface water pCO_2 seasonal cycle. The statistically significant correlation between the winter NAO index and winter ΔSSH anomalies (section 3.2.2) supports the hypothesis that the atmospheric circulation affects the oceanic.

It should also be noted that with regard to the hypothesis, the relationship between the winter parameters (such as SST) with the winter ΔSSH can still be tested, even though the real advantage of using the ΔSSH as a proxy for ocean circulation strength becomes evident in the longer-term (i.e. inter-annual variability in chapter 5). However, as already mentioned, the winter NAO index co-varies relatively well with the winter ΔSSH as shown in Figure 3-3, section 3.2.2, chapter 3. Thus, whilst the winter NAO index drives the winter ΔSSH, the effect on related parameters such as SST is likely to be mainly atmospheric during the winter months, with the oceanic circulation immediately responding to this forcing. However, the use of the ΔSSH anomalies in winter is justified, since it serves as a test of the potential atmospheric relationships between the related parameters and the surface pCO_2. In addition, given that the winter ΔSSH exhibits significantly less intra-seasonal variability than the winter NAO index (see Figure 3-3 in chapter 3), it may also aid in establishing new relationships and/or strengthening/supporting current ones.

The aim of this research is to focus on how the large-scale oceanic circulation (of which the ΔSSH are a proxy) and atmospheric circulation may affect the surface water pCO_2 variability. The statistically significant correlations apparent in Figure 4-1 at near-instantaneous and negative lag times supports the hypothesis of large-scale atmospheric and oceanic effects on the surface pCO_2 seasonal anomalies (section 1.7). There are also numerous statistically significant correlations between the ΔSSH anomalies and the surface pCO_2 anomalies at positive time lags (i.e. with the pCO_2 anomalies leading the ΔSSH anomalies – see Figure 4-1). These statistically significant relationships at positive lag time are unlikely to be controlled by the surface pCO_2. Figure A-18 in the Appendix illustrates that the SST anomalies cross-correlated with the ΔSSH anomalies also show statistically significant positive correlations at similar lag times with respect to Figure 4-1. Hence, it is more likely that the SST may be controlling the ΔSSH anomalies. A similar effect is evident with respect to the NAO index and surface pCO_2 anomalies, with the surface pCO_2 leading the NAO index. Figure A-19 reveals that the SST anomalies also statistically significantly positively correlate with the NAO index at positive time lags (i.e. with

the SST leading the NAO index), although these do not coincide with those of the surface pCO_2 anomalies. Previous studies (e.g. Marshall et al. (2001)), for example, have found that SST may exert an influence on the NAO index. Yet, these findings referred to decadal timescales, whereas the focus of this thesis is on seasonal to inter-annual timescales. Attempting to explain these relationships would therefore go beyond the scope of this thesis, which focuses on how the large-scale atmospheric and oceanic circulation affects the surface pCO_2 on seasonal to inter-annual timescales.

As discussed in chapter 2, section 2.7, two correlation coefficients can be calculated: the Pearson correlation coefficient and Spearman's rank correlation coefficient. Spearman's rank correlation coefficient is mostly discussed below as it provides a more robust determination of a correlation. However, where there are significant differences between the Spearman's and Pearson's correlation coefficient these are highlighted and the implications for the research explained.

The hypothesis of the drivers of the seasonal anomalies of surface water pCO_2 is tested in two steps (see section 2.7.2, of chapter 2): 1) cross-correlating a full set of anomalies and 2) cross-correlating three-month pairs of anomalies of the related parameters with the surface pCO_2. It should be noted that the figures in this chapter relating to step 1 are termed 3-month smoothed anomalies. The first step provides an idea of the strength of the correlation over the course of a year. However, it is not possible to deduce the driving season behind these correlations. The second step, on the other hand, enables identification of the driving season. It should be noted that the figures relating to this step are termed 3-month paired anomalies. These form a sub-set of the above-mentioned 3-month smoothed anomalies data.

However, once the driving season between both the NAO index and ΔSSH anomalies and the surface pCO_2 is established (section 4.2), the remainder of the chapter (section 4.3 and section 4.4) is devoted to establishing how the driving season affects the surface pCO_2 within that same season but also the following spring/summer and autumn seasons through the related parameters. As such, these sections focus on the three-month pair analysis described previously. Section 4.5 discusses the SST versus non-SST effects on the surface water pCO_2 variability and section 4.6 provides a summary of the main findings of this chapter.

4.2 Seasonal anomaly of surface pCO_2 in response to ΔSSH and the NAO index

4.2.1 ΔSSH anomalies with sea surface pCO_2 anomalies

In order to establish whether there is a coupling between the oceanic circulation and surface pCO_2 on a seasonal basis, cross-correlations were calculated between ΔSSH anomalies and surface water pCO_2 anomalies using a full set of seasonal anomalies. The Spearman's rank correlation coefficients are shown in Figure 4-1 for the original observations, the linearly interpolated observations, and the model output.

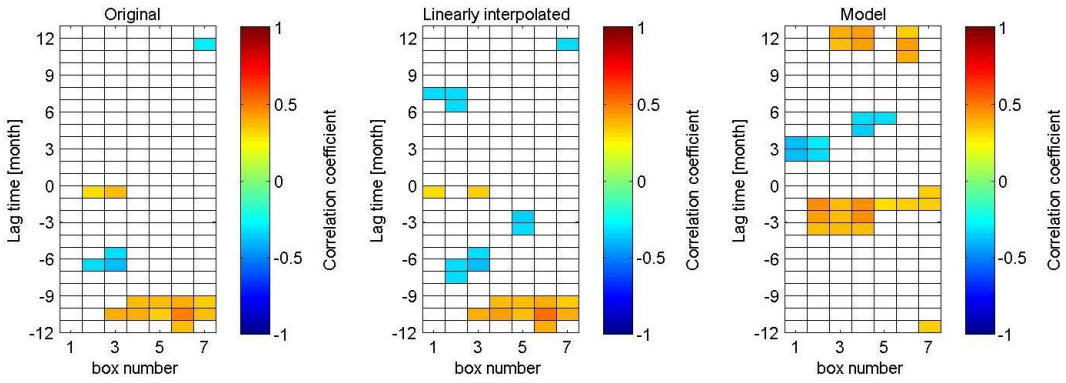

Figure 4-1: Spearman's rank correlation coefficient at lag times [months] versus box number of the observed 3-month smoothed ΔSSH anomalies and 3-month smoothed surface pCO_2 anomalies for the original observations (left), the linearly interpolated observations (middle) and model output (right). Statistically significant positive correlations are yellow to orange-red, whilst statistically significant negative correlations are light to dark blue. The ΔSSH anomalies lead the surface pCO_2 anomalies at negative lag times and the pCO_2 leads the ΔSSH at positive lag times.

The observations show that there are a number of statistically significant positive correlations between the ΔSSH anomalies and surface water pCO_2 anomalies: boxes 2 to 3 exhibit near-instantaneous correlations and boxes 3 to 7 reveal correlations between lag -9 months to lag -12 months. A similar picture is seen with the linearly interpolated data set, although no statistically significant positive correlation is apparent in box 2 and a statistically significant correlation is found in box 1. The model output also displays significant positive correlations at near-instantaneous lag (between lag 0 to lag -4) and in almost all boxes. There are also numerous statistically significant anti-correlations that are displayed in the observations between lags -6 months and -7 months (boxes 2 and 3) and between lags -3 months and -4 months (box 5). The model output shows does not show any

statistically significant anti-correlations in boxes 5, 6 and 7 however. In summary, there are statistically significant links between the proxy for large scale oceanic circulation, the ΔSSH anomalies, and the surface water pCO_2 anomalies. These only cover the subtropical regions.

However, with all months included, it is not possible to identify the main driving season behind these correlations. Hence, three-month paired correlations were undertaken to establish which season displays the strongest correlations. Only the lag time where the ΔSSH anomalies lead the pCO_2 anomalies were focused on in the seasonal correlations, since, according to the observations, it revealed a higher number of statistically significant correlations. As explained in chapter 2 (section 2.7.2), only the linearly interpolated observations were used.

The strongest correlations were found during the winter period, specifically during January, February and March (JFM) (see Figure 4-2).

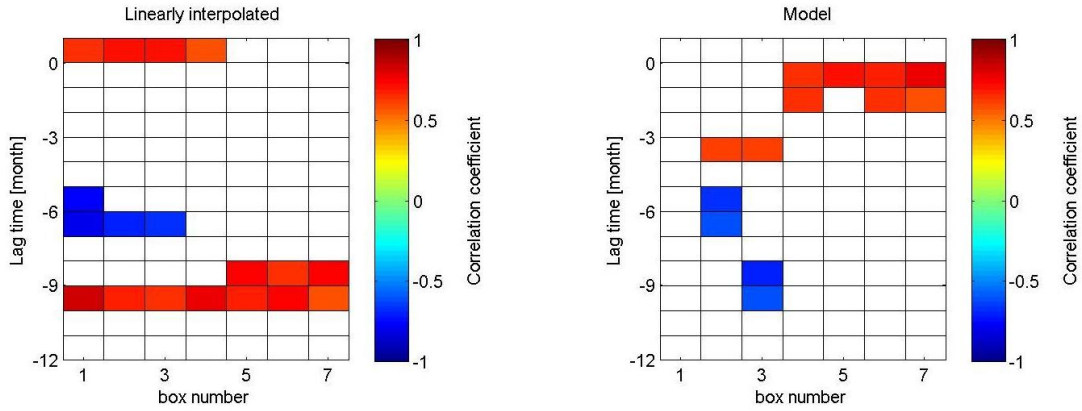

Figure 4-2: Spearman's cross-correlation coefficient at lag times [months] between the 3-month paired JFM ΔSSH anomalies and the 3-month paired surface water pCO_2 anomalies, for linearly interpolated observations (left) and model output (right). Statistically significant positive correlations are orange-red, whilst statistically significant negative correlations are light-dark blue. The ΔSSH anomalies lead the pCO_2 anomalies at negative lag times.

Instantaneous statistically significant positive correlations are evident in 4 out of the 7 boxes for the observations (boxes 1 to 4). This indicates a potential for a dynamical coupling between the proxy for ocean circulation and pCO_2 variability to be discernible during the winter months, specifically within the subtropical regions. The model output illustrates that statistically significant positive correlations are apparent for boxes 4 through to 7 and that significant positive correlations extend to

lag -1 and -2 months. Thus, in contrast to the observations, the model output suggests that the potential for a dynamical coupling between the surface pCO_2 anomalies and the proxy for ocean circulation is restricted to the temperate regions. In addition, the anti-correlations between the surface pCO_2 anomalies and the ΔSSH anomalies for the observations at lags -6 and -7 in boxes 1 to 3 are not reproduced in the model output. Furthermore, the model output does not reveal statistically significant positive correlations between the JFM ΔSSH anomalies and the surface water pCO_2 anomalies at lag -9 months to -10 months for all boxes.

Thus, the linearly interpolated observations reveal that the winter months are likely to explain the statistically significant correlations between the ΔSSH anomalies and the surface water pCO_2 anomalies in all months at instantaneous lag and at the negative lag times (see Figure 4-1). However, this seems to be restricted to the subtropical regions (i.e. boxes 1 to 4). Nevertheless, this highlights the importance of the JFM ΔSSH anomalies on the JFM surface water pCO_2 anomalies in the subtropics. In addition, the previous winter ΔSSH anomalies anti-correlate with the following summer (lags -6 to -7 months) in the subtropics and following autumn pCO_2 anomalies (lags -9 to -10 months) in both the subtropics and temperate regions. Thus, as hypothesised in the Introduction, section 1.7, the oceanic circulation in response to the atmosphere will affect the seasonal anomalies of the surface water pCO_2. These results suggest that this may only apply to the subtropics. However, the hypothesis that the winter NAO may affect the winter surface pCO_2 in both the subtropics and temperate regions will be tested in the following section.

4.2.2 Cross-correlations of NAO index with the surface water pCO_2 anomalies

In the previous section, it appears that the oceanic circulation affects the seasonal anomalies of the surface pCO_2 in the subtropics with winter as the driving season. However, as shown in section 3.2.2 in chapter 3, the winter NAO index drives the winter ΔSSH anomalies. Therefore, it would be expected that the surface water pCO_2 would also respond in a similar manner to the atmospheric circulation. As such, cross-correlations between the NAO index and the surface water pCO_2 were undertaken to establish whether this was the case. It should be noted that for the model output, the observed NAO index was used (since the model did not simulate

the behaviour of the NAO). Thus, caution must be used when comparing the model output with the observations in this instance.

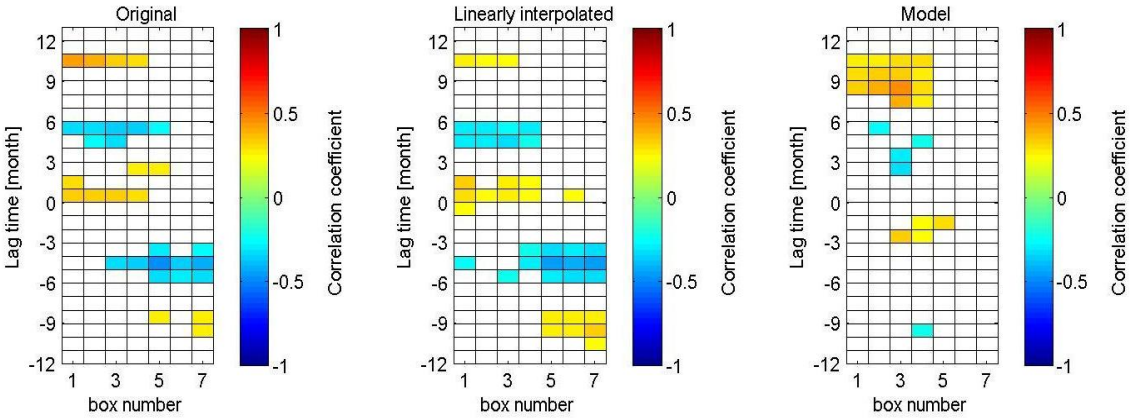

Figure 4-3: Spearman's correlation coefficient at lag times [months] versus box number for the observed NAO index and 3-month smoothed surface water pCO_2 anomalies, for the original observations (left), the linearly interpolated observations (middle) and the model output (right). Statistically significant positive correlations are orange-red, whilst statistically significant negative correlations are light-dark blue. The NAO index leads the pCO_2 at negative lag times and the pCO_2 leads the NAO index at positive lag times.

Using a full set of seasonal anomalies, statistically significant positive correlations are apparent at instantaneous and near-instantaneous lags between the NAO index and the surface water pCO_2 in the observations. This compares well with the cross-correlation of the ΔSSH anomalies with the surface water pCO_2 anomalies (Figure 4-1), although there are more numerous statistically significant correlations associated with the NAO index and surface water pCO_2 anomalies.

The model output results are less convincing, however. This may be due to the usage of the observed NAO index as opposed to a simulated version, which may produce different results.

The fact that the NAO index (with all months included and unsmoothed) statistically significantly correlates with the surface pCO_2 anomalies suggests that there is likely to be a dynamical coupling between the atmospheric circulation and the seasonal anomalies of surface water pCO_2 as hypothesised in section 1.7.

As previously shown with the ΔSSH anomalies and the surface pCO_2 anomalies, there is likely to be a seasonal dependence of the surface water pCO_2 anomalies on

the NAO index. Figure 4-4, which is based on the three-month-pairs seasonal anomalies, illustrates that such dependence does exist, with the winter months of JFM correlating the best.

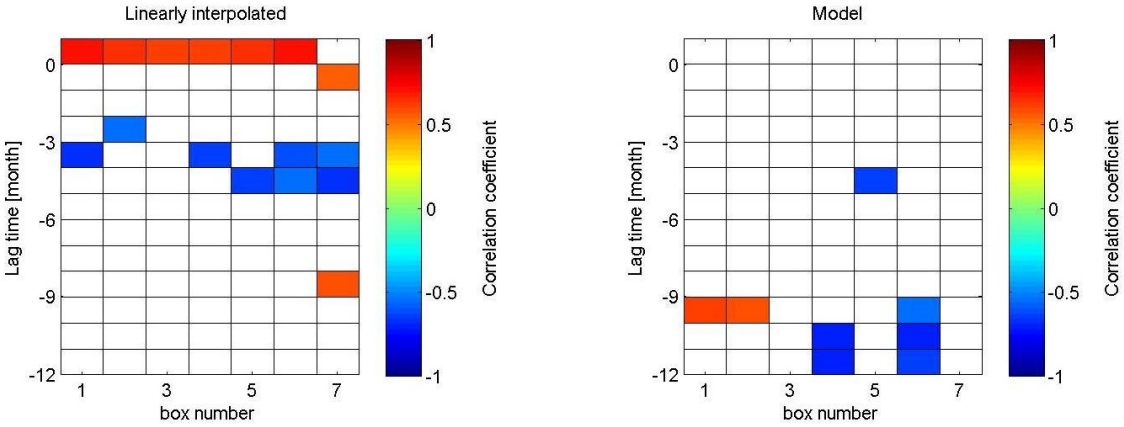

Figure 4-4: Spearman's cross-correlation coefficient at lag times [months] between the JFM NAO index and the 3- month paired surface water pCO_2 anomalies, for linearly interpolated observations (left) and model output (right). Statistically significant positive correlations are orange-red, whilst statistically significant negative correlations are light-dark blue. The NAO index leads the pCO_2 anomalies at negative lag times.

The observations reveal statistically significant positive correlations at instantaneous and lagged time periods, whereas the model output does not display instantaneous correlations. The seasonally lagged time periods broadly correspond to the lagged time periods observed with all months included in the correlations (see Figure 4-3) but with the temperate regions also showing statistically significant positive correlations. Thus, the winter NAO index is affecting the winter surface water pCO_2 anomalies but also the following spring and late summer (lags -4 and -5 months and lags -8 and -9 months respectively).

4.2.3 Summary

It has been shown that there are both statistically significant instantaneous and lagged correlations between the winter ΔSSH anomalies and winter surface pCO_2 anomalies as well as between the NAO index and surface pCO_2 anomalies. It is therefore concluded that both the atmospheric and oceanic circulation influence the strength of the seasonal cycle of pCO_2, with winter being the driving season. This confirms a key element of the thesis hypothesis, since it establishes that there are statistically significant links between the winter NAO index and winter ΔSSH

anomalies with the surface pCO_2 anomalies at both instantaneous and lagged time periods.

In order to understand why there is a link between the oceanic and atmospheric circulation and the seasonal anomalies of surface water pCO_2, it is necessary to examine other parameters that have a known effect on the surface water pCO_2, as detailed through the various relationships presented in the thesis hypothesis. These include SST (through its effect on the solubility of CO_2 in seawater (Takahashi et al, 1993)), the MLD via vertical mixing of nutrient and carbon-rich subsurface water as well as biological processes (represented by CHL as a proxy for net primary production). Section 4.3 will look at the relationships between the winter ΔSSH anomalies and the winter NAO index (as large scale parameters) and the above-mentioned parameters. Section 4.4 will then discuss the relationships between the latter parameters and surface water pCO_2.

4.3 Seasonal anomaly of related parameters in response to ΔSSH and the NAO index

4.3.1 Cross-correlations of the ΔSSH anomalies with the SST anomalies

Since it was found that the winter ΔSSH anomalies correlated with the winter surface pCO_2 anomalies, correlations between both the DJF and JFM ΔSSH anomalies with the SST anomalies were undertaken. Very few statistically significant correlations were found in both cases but with slightly more significant correlations when looking at the DJF time period (Figure 4-5).

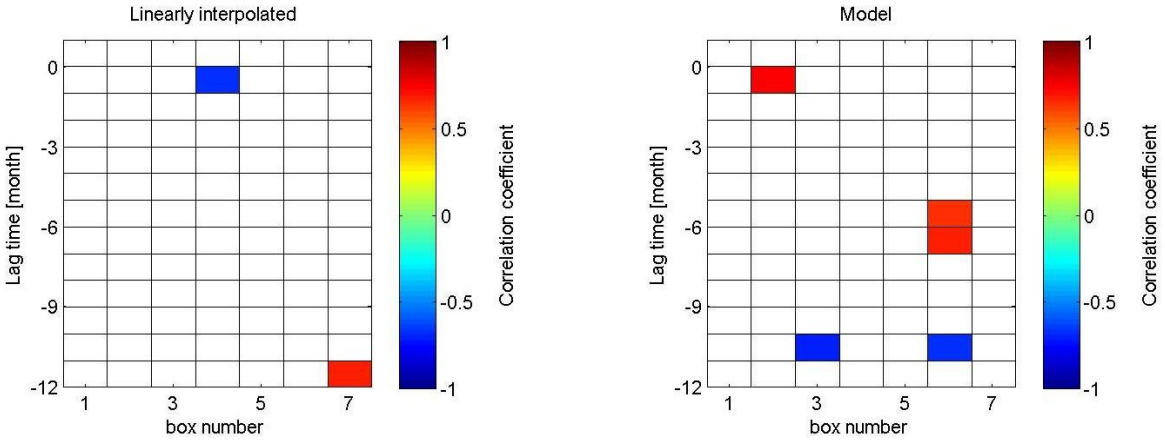

Figure 4-5: Spearman's cross-correlation coefficient at lag times [months] between the 3-month paired DJF ΔSSH anomalies and the 3-month paired SST anomalies, for linearly interpolated observations (left) and model output (right). Statistically significant positive correlations are orange-red, whilst statistically significant negative correlations are light-dark blue. The ΔSSH anomalies lead the SST anomalies at negative lag times.

With respect to the observations, only box 4 exhibits a statistically significant negative correlation in relation to the ΔSSH anomalies and the SST anomalies at lag -1 month whilst box 7 exhibits a statistically significant positive correlation at lag -12 months. In relation to the former, this could imply that a more active subpolar gyre circulation in winter reduced the winter SST in this temperate region. This may have been through the formation of the ENACWp mode water and its penetration further south into the temperate region, as discussed in section 1.6, during a positive winter NAO phase.

With regards to the statistically significant positive correlation in box 7 at lag -12 months, this could indicate a lagged SST response. As pointed out by Alexander and Deser (1995), it is possible to sustain either a positive or negative SST anomaly from one winter to the next (i.e. one year). The mechanism these authors propose is via a sequestering of the temperature anomaly below the mixed layer throughout the summer. In this way, when the mixed layer deepens once again the following winter, the same temperature anomaly seen the previous winter is apparent again. However, in this particular case this correlation is unlikely to be indicative of this mechanism because there is no statistically significant positive correlation between the ΔSSH anomalies and the SST anomalies at instantaneous or near-instantaneous lag. Therefore, it is not possible for the SST anomaly to re-emerge

the following winter since there is no SST anomaly the previous winter for that to happen.

The model output reveals a statistically significant positive correlation between the ΔSSH anomalies and the SST anomalies in box 2. This could indicate that in the subtropical regions, south of 40°N, an increase in ΔSSH anomalies in winter (DJF) may increase the SST anomalies there at lags -1 and -2 months (i.e. in box 2 during JFM and FMA). However, this has to be treated with caution since the observations do not substantiate this claim. It is surprising that the model output does not agree with the observations because both use the same SST source (i.e. NCEP-NCAR). This could originate from differences between the observed and modelled ΔSSH. This may impact on all correlations using modelled ΔSSH.

Thus, the research hypothesis that a high (low) NAO index winter would give rise to a negative (positive) SST anomaly in both the subtropics and temperate regions seems to be unlikely (see Figure 1-9 and Figure 1-10 respectively). However, it should be noted that only the winter ΔSSH anomalies have been tested in relation to the SST anomalies.

The following section analyses the winter NAO index and the winter SST anomalies.

4.3.2 Cross-correlations of the NAO index with the SST anomalies

It was discovered that the best winter-time cross-correlation between these variables occurred during DJF (as with the ΔSSH anomalies), and these are shown in Figure 4-6.

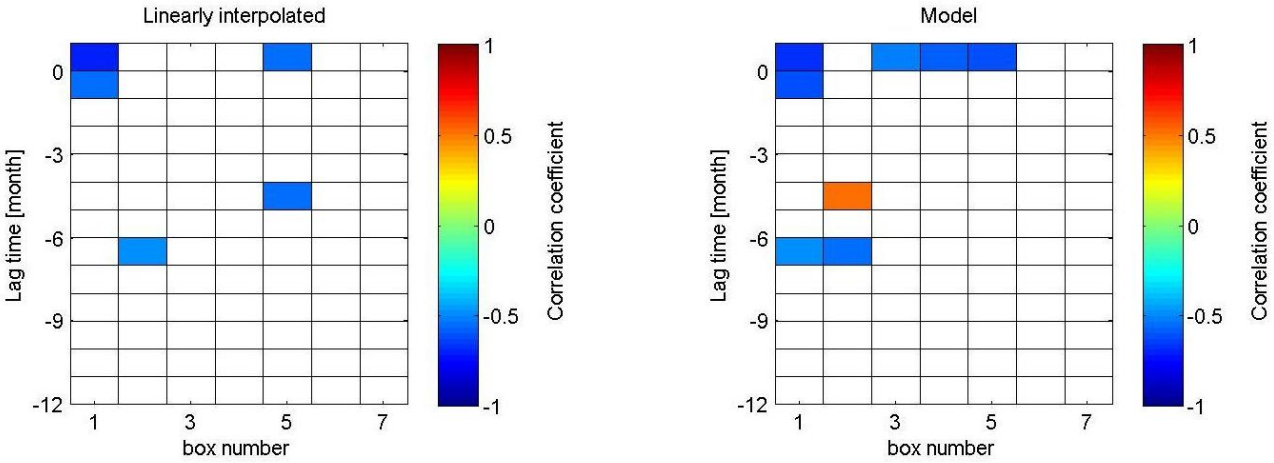

Figure 4-6: Spearman's cross-correlation coefficient at lag times [months] between the DJF NAO index and 3 month paired SST anomalies, for the linearly interpolated observations (left) and model output (modelled SST with observed NAO index) (right). Statistically significant positive correlations are orange-red, whilst statistically significant negative correlations are light-dark blue. The NAO index leads the SST anomalies at negative lag times.

As can be seen, there are numerous statistically significant anti-correlations that are apparent between the NAO index and the SST anomalies. At close to instantaneous time, the linearly interpolated observations (6, left panel) illustrate these to be manifested in box 1 and box 5 and the model output in box 1, 3, 4 and 5. Cross-correlations of the observations at lag times of -7 and -5 months are also occurring in boxes 2 and 5.

Thus, the anti-correlation between the winter NAO index and the winter SST anomalies seen in the subtropics is likely to be indicative of mode water formation infiltrating this region during the study time period during high NAO index winters, as hypothesised in the Introduction in section 1.7. Thus, even in the subtropics, DIC entrainment through more intense vertical mixing is likely to generate positive winter pCO_2 anomalies. This would partially explain the statistically significant positive correlations between both the winter NAO index and the winter ΔSSH anomalies with the winter pCO_2 anomalies in box 1. Figure 4-7 illustrates that mode water formation was likely to be present in the study region during the winter of 2006/7 as the SST anomalies were at their lowest then.

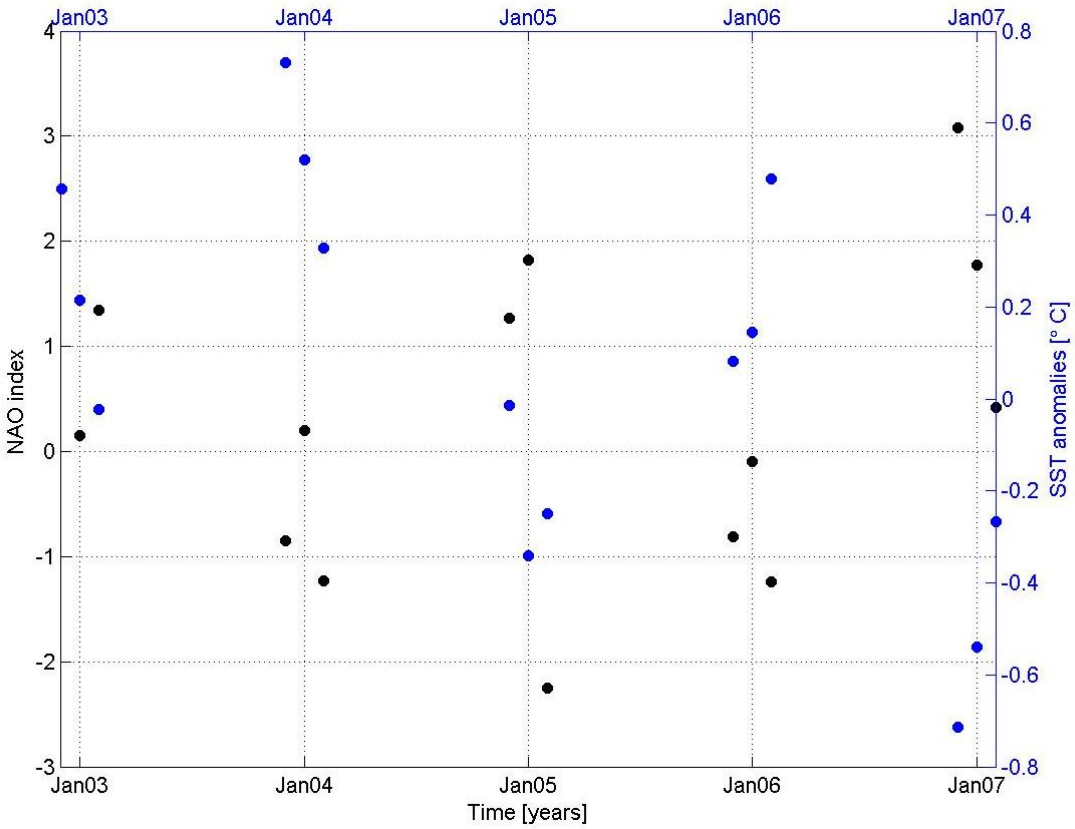

Figure 4-7: DJF NAO index with 3-month paired DJF SST anomalies in box 1 at lag 0 month for the linearly interpolated observations.

During the previous winters, the SST anomalies are either weakly positive (e.g. DJF 2002/3) or weakly negative (DJF 2004/5), with the exception of winter 2003/4 where the SST anomalies are moderately positive. The winter NAO index was generally weakly negative when the SST anomalies were weakly positive and vice-versa. Thus although mode water formation is likely to have infiltrated the subtropics during the winter of 2006/7, it is unlikely that the EDW penetrated the region prior to that winter. Instead, as a result of a possible decrease in the volume of high-DIC waters entrained to the surface prior to winter 2006/7, a net decreasing effect on the surface water pCO_2 may have occurred even if the SST anomalies were slightly negative (i.e. less negative than winter 2006/7) or even slightly positive. The reduced input of DIC to the surface may have enabled the relatively low SST water to dominate prior to the winter of 2006/7, thereby decreasing the surface pCO_2. Given that the mean winter surface pCO_2 is generally low in the subtropics (see Figure 3-9 in chapter 3) and that the mean winter SST follows the mean winter surface pCO_2 pattern (see Figure 3-10 in chapter 3), it is reasonable to assume this may have been the case. Section 4.5 of this chapter examines the SST versus non-

SST effects on the surface pCO_2, and it is shown that the contribution of these antagonistic effects on the surface pCO_2 is finely balanced in this region.

It should also be noted that the anti-correlation found here between the winter NAO index and the SST anomalies contradicts the findings of scholars such as Gruber et al. (2002), Thomas et al. (2008) and Ullman et al. (2009). In all cases, significant positive correlations between the winter NAO index and winter SST are found in the subtropics. However, Gruber et al. (2002) use an 18-year time period which included one of the strongest positive NAO phases during the 1990s. Thus the NAO signal was a lot stronger and thereby may have enabled the NAO-SST positive connection to be established in the subtropics. Therefore, the claim that mode water formation may occasionally affect the study region (as seen by the moderately negative SST anomalies during the winter of 2006/7), entraining high-DIC waters from the subsurface to the surface and thereby ultimately increasing the surface pCO_2, is certainly a possibility, even in the subtropics, as hypothesised in section 1.7, Figure 1-9. This is because there is a statistically significant positive correlation between both the winter NAO index and winter ΔSSH anomalies with the winter surface pCO_2 anomalies in box 1 (see Figure 4-4 and Figure 4-2 respectively).

The statistically significant anti-correlation found in box 5 at instantaneous lag between the winter NAO index and the winter SST anomalies is likely to be symptomatic of the occurrence of mode water formation in the temperate regions as already illustrated in section 4.3.1Although the mode water signature was found in box 4 in the aforementioned section, by cross-correlating the winter ΔSSH anomalies with the winter SST anomalies, given the close co-variability of the winter ΔSSH with the winter NAO index (see Figure 3-3, chapter 3), it is considered reasonable to assume that the anti-correlation between the winter NAO index and winter SST anomalies in box 5 is also likely to signal mode water formation. Thus further explanations are considered to be unnecessary for this significant correlation as a result.

The model output is in agreement with the linearly interpolated observations in box 1 with statistically significant anti-correlations between the NAO index and SST anomalies. Given the close co-variability between the observed and modelled SST seasonal cycle (see chapter 3, section 3.3.2.2), the explanations given for the potential meaning of these correlations are applicable to the model output as well.

There is also a statistically significant anti-correlation between the NAO index and the SST anomalies in box 2 at lag -7 and in box 5 at lag -5. Figure 4-8 illustrates the data points associated with the former box.

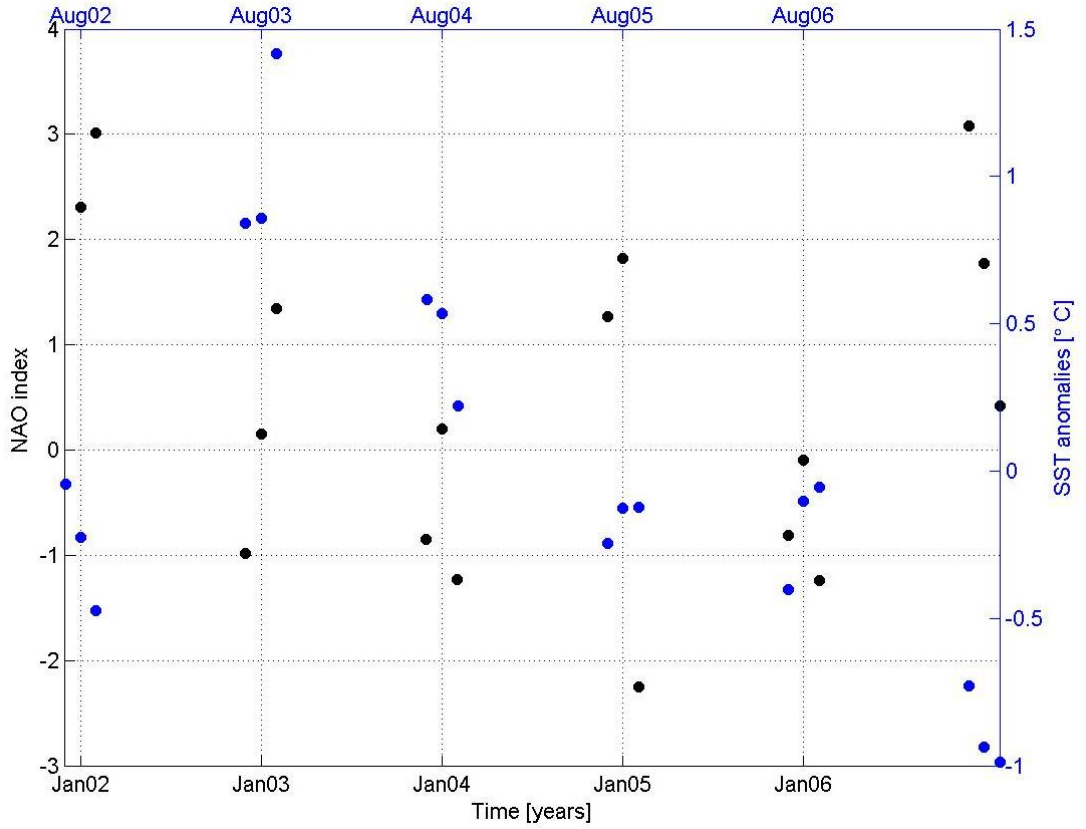

Figure 4-8: DJF NAO index with 3-month paired JAS SST anomalies in box 2 (lag -7 month) for the linearly interpolated observations.

Figure 4-8 shows that there are two summers in which the SST anomalies anti-correlate with the previous winter's NAO index, namely DJF 2001/02 with JAS 2002 and DJF 2006/7 with JAS 2007. However, attributing this anti-correlation to a specific physical process in this case is unwise because the NAO signal is strongest in winter, and therefore it would be expected that physical processes are affected within the winter time period and perhaps also the following spring. For example, a high NAO index winter may result in deeper vertical mixing in winter and entrain nutrients into the mixed layer, which may result in a stronger phytoplankton bloom the following spring. This will be returned to in section 4.3.8, when the NAO index and CHL are looked into. In addition, it should be borne in mind that summer SSTs in the subtropics generally range from 25°C to 28°C, so even a 1°C anomaly is still going to equate to a high absolute SST value. Therefore, the physical meaning of this anti-correlation at this time lag needs to be treated with caution.

As mentioned previously, box 5 also exhibits a statistically significant ant-correlation between the NAO index and SST anomalies but at an earlier lag time of -5 months (i.e. DJF NAO index with MJJ SST anomalies). Figure 4-9 illustrates the data points associated with these parameters.

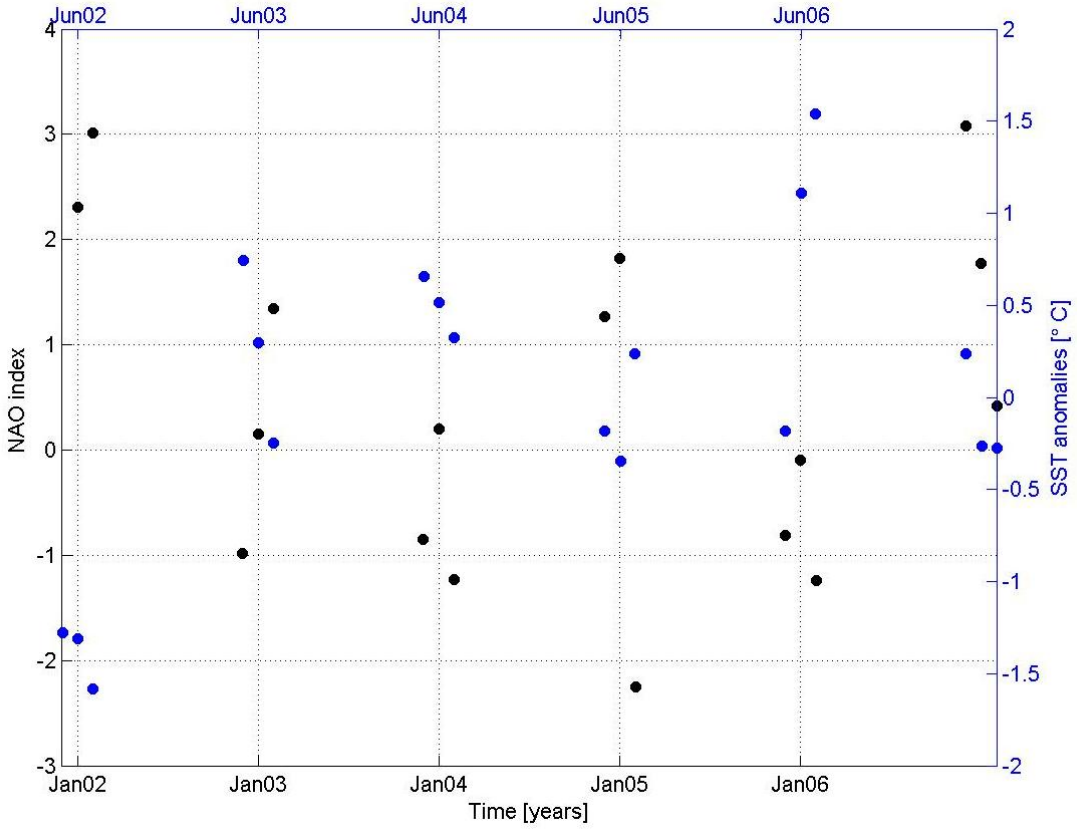

Figure 4-9: DJF NAO index with 3-month paired MJJ SST anomalies in box 5 (lag -5 months) for the linearly interpolated observations.

As can be seen, overall there is generally good agreement between the winter NAO index and the following late spring/early summer's SST anomalies. There is one notable exception, however, with MJJ 2002 exhibiting a significant reduction in SST (by ~1.5°C compared to what would be expected at this time of year). Given that this coincides with the peak in CHL observed in this region (i.e. May – see Figure 3-12, section 3.3.2.4), this could indicate a biological response to the previous winter NAO index: the presence of phytoplankton may have decreased the SST that late spring/early summer. Indeed, the absolute CHL concentration during May 2002 was relatively high (see Figure A-4). In addition, Figure 4-4 (winter NAO index with surface pCO_2 anomalies) between lags -5 and lag -3 months displays statistically

significant anti-correlations at this time lag. This could well imply that enhanced winter mixing may have entrained more nutrients to the surface allowing a stronger phytoplankton bloom to establish itself. This concept will be returned to later in the chapter when both the ΔSSH anomalies and the NAO index are examined with the CHL anomalies.

The model output reveals similar statistically significant anti-correlations between the NAO index and the SST anomalies at lag -7 months in boxes 1 and 2, and this is most likely due to the high SST agreement between the observations and model. The lack of a statistically significant anti-correlation in box 5 at lag -5 months may have more to do with the model's inability to simulate the correct timing of the phytoplankton bloom in the temperate regions (see chapter 3, section 3.3.2.4, for a discussion).

So far in this chapter, we have seen that the atmospheric circulation affects the oceanic, by altering the parameters that are known to affect the oceanic pCO_2, such as SST. We have established that the key season behind these pCO_2 changes manifests itself during the winter months. This confirms that a positive (negative) winter NAO gives rise to a negative (positive) SST anomaly, which is likely to indicate mode water formation in both the subtropics and temperate regions (see Figure 1-9 and Figure 1-10 respectively). How the large-scale atmospheric and oceanic circulation may alter the MLD has been inferred from the discussion on SST previously. However, this will now be analysed in the following section.

4.3.3 Cross-correlations of the ΔSSH anomalies with the MLD anomalies

Figure 4-10 displays the cross-correlations between the ΔSSH anomalies and the MLD anomalies. The best results were obtained during the DJF winter-period.

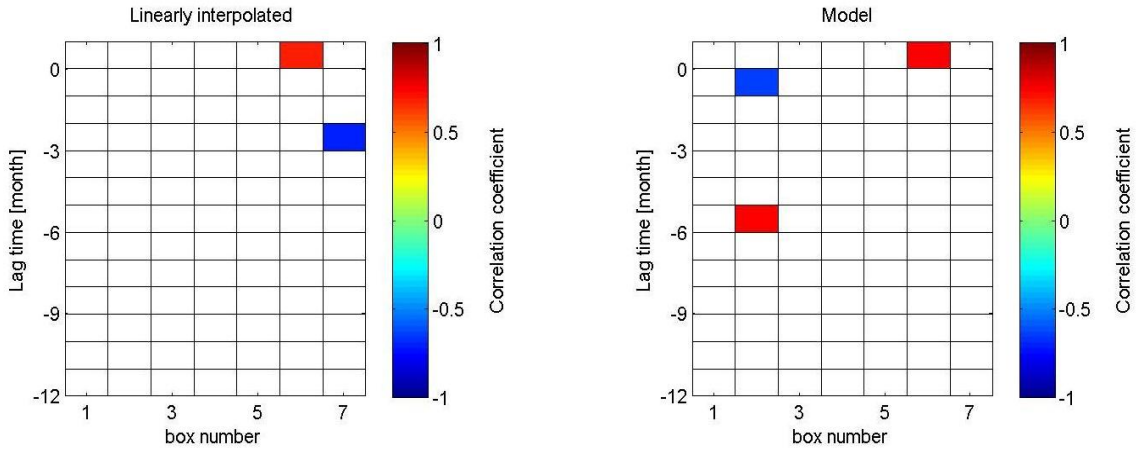

Figure 4-10: Spearman's cross-correlation at lag times [months] between the 3-month paired DJF ΔSSH anomalies and 3 month paired MLD anomalies (left) and co-located 3-month paired modelled MLD anomalies and 3-month paired modelled DJF ΔSSH (right). Statistically significant positive correlations are orange-red, whilst statistically significant negative correlations are light-dark blue. The ΔSSH anomalies lead the MLD anomalies at negative lag times.

As can be seen, only box 6 (within the temperate region) exhibits a statistically significant positive correlation between the DJF ΔSSH anomalies and the DJF MLD anomalies. The model output also illustrates this statistically significant link.

Therefore, this could indicate the formation of mode waters in the temperate region which would deepen the mixed layer during a positive NAO winter. In the subtropics, the lack of such a statistically significant relationship may seem to imply that formation of mode water is unlikely. However, in section 4.3.2, the NAO index anti-correlates with the SST anomalies during winter. Thus, this may also indirectly imply that the MLD deepened in response to the formation of mode waters in the subtropics.

Therefore, as hypothesised in the Introduction in section 1.7, enhanced surface cooling during a positive NAO winter is likely to lead to the formation of the subtropical and subpolar mode waters, thereby deepening the MLD as shown here. The high-DIC waters entrained to the surface would then lead to a net increase in the surface pCO_2, resulting in positive pCO_2 anomalies (see Figure 4-2 and Figure 4-4). Equally, during weakly negative to moderately negative NAO winters, it is likely

that the mixed layer does not deepen as extensively, thereby allowing the cold-SST waters to reduce the surface water pCO_2 (as a result of reduced DIC entrainment).

There are other statistically significant positive and negative correlations between the ΔSSH anomalies and the MLD anomalies in terms of the linearly interpolated observations. However these do not coincide with the ΔSSH anomalies and surface pCO_2 anomalies statistically significant correlations at these lag times (Figure 4-2) and therefore are not further discussed.

As stated in the hypothesis, during a positive NAO winter, surface cooling to the north of both the subtropics and temperate regions would aid in the formation of mode water. This, in turn would deepen the mixed layer and entrain high-DIC waters to the surface. The deepening of the mixed layer during high winter ΔSSH anomalies confirms this. Furthermore, the following autumn, it is possible that a surplus of DIC remains within the mixed layer, assuming that not all of it is used up by biology in spring. Thus coupled with the deepening of the mixed layer in autumn, a renewed DIC pool may emerge, thereby increasing the autumn pCO_2, as mentioned in the hypothesis. The statistically significant positive correlations between the winter ΔSSH anomalies and the following autumn pCO_2 anomalies (lag -9 months in most boxes, see Figure 4-2) certainly point toward this mechanism.

However, in order to place more confidence in this process, statistically significant positive correlations between either the winter ΔSSH anomalies or the winter NAO index and the following autumn's pCO_2 T_{norm}/DIC anomalies should be found. Whether the following autumn's mixed layer deepens anomalously in response to the previous winters atmospheric forcing will not make much difference to the re-entrainment of the 'old' DIC pool with new DIC waters. This is because, as can be seen in chapter 3, section 3.3.2.3, the MLD will be deep enough, particularly in the temperate regions, to allow for this renewal of DIC to take place. It is much more important to evaluate whether the pCO_2 T_{norm}/DIC anomalies are positive with respect to their monthly means the following autumn. This will be tested in section 4.3.5 and section 4.3.6, when both the winter ΔSSH anomalies and the winter NAO index are cross-correlated with the pCO_2 T_{norm}/DIC anomalies, respectively.

The following section briefly examines the relationships between the NAO index and the MLD anomalies.

4.3.4 Cross-correlations of the NAO index with MLD anomalies

Figure 4-11 illustrates both the Pearson and Spearman cross-correlations of the NAO index with the MLD anomalies.

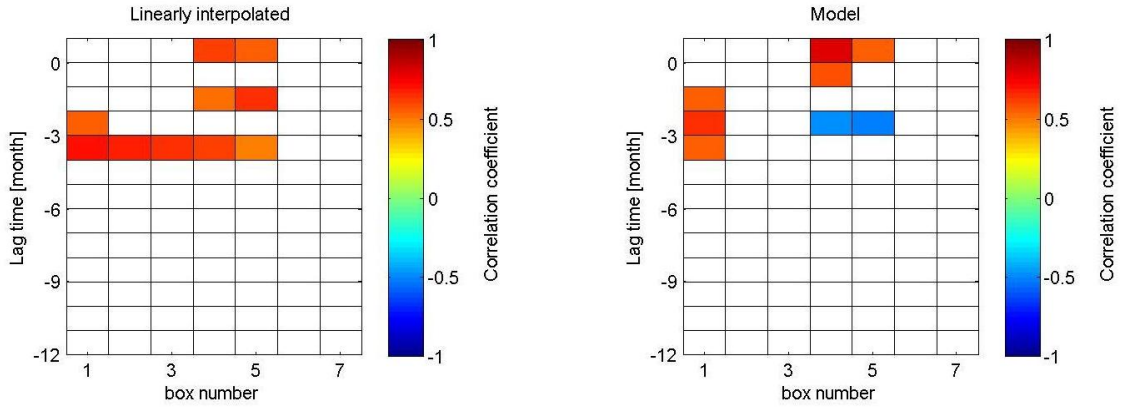

Figure 4-11: Spearman's cross-correlation at lag times [months] between the observed DJF NAO index and 3-month paired MLD anomalies (left) and co-located 3-month paired modelled MLD anomalies and observed DJF NAO index (right). Statistically significant positive correlations are orange-red, whilst statistically significant negative correlations are light-dark blue. The NAO index leads the MLD anomalies at negative lag times.

As can be seen, statistically significant positive correlations between the DJF NAO index and the MLD anomalies are apparent. . There are differences between Figure 4-10 (winter ΔSSH anomalies and winter MLD anomalies) and Figure 4-11. However, it is considered that these are likely to result from the greater intra-seasonal variability of the winter NAO index, as can be visualized in Figure 3-3 in chapter 3, rather than with key mechanistic differences between the winter ΔSSH anomalies and the winter NAO index. This is because Figure 3-3 in chapter 3 illustrates that the winter NAO index and winter ΔSSH are statistically significantly positively related.

The model output is also in good agreement with the observations, however this is expected, given the usage of the same observed NAO index and the same MLD product (albeit with differences due to the initial spatial resolution of the modelled MLD compared to the observations as highlighted in section 3.3.2.3 of chapter 3). This also explains slight differences between the occurrence of statistically

significant relationships between the model output and observations in relation to the parameters discussed here (see Figure 4-11).

Therefore, as hypothesised, the winter NAO index is likely to increase the MLD during positive NAO phases (and decrease the MLD during negative NAO phases) at instantaneous and near-instantaneous lag. This therefore will dictate the net effect on the surface pCO_2, with greater MLD during a positive NAO winter likely to entrain more DIC-rich water to the surface, thereby increasing the pCO_2 and shallower MLD during a negative NAO winter, enabling the cold-SST waters to dominate, and, as a result, decreasing the surface pCO_2. The statistically significant positive correlations at instantaneous lag between both the NAO index and ΔSSH anomalies and the surface pCO_2 (Figure 4-4 and Figure 4-2 respectively) are indicative of the effect the MLD (via DIC entrainment) is likely to have on the surface pCO_2.

However, MLD has been used so far as a proxy for DIC entrainment. It is necessary to evaluate whether the DIC itself (pCO_2 T_{norm} for the observations) responds in a similar manner to the large-scale atmospheric and oceanic circulation as the MLD does in order to verify the claim made so far that the mode water formation is likely to enhance the DIC entrained to the surface, thereby resulting in positive winter pCO_2 anomalies. The following section addresses this with respect to the ΔSSH anomalies (i.e. proxy for ocean circulation).

4.3.5 Cross-correlations of the ΔSSH anomalies with the pCO_2 T_{norm} /DIC anomalies

Given that no DIC measurements were made onboard the MV Santa Maria and MV Santa Lucia, a proxy for the DIC needed to be found so that an estimate of the carbon content of the water could be made. As mentioned previously, the vertical supply of DIC is likely to play an important role in the variability of surface water pCO_2, particularly in the winter months. The pCO_2 was therefore normalised to constant SST (hereafter referred to as pCO_2 T_{norm}). The procedure for undertaking this is described in the chapter 2 (section 2.4.4). Comparison with the modelled DIC was undertaken.

Figure 4-12 illustrates the cross-correlations between the DJF ΔSSH anomalies and the DJF pCO_2 T_{norm} anomalies and the DJF modelled ΔSSH anomalies with the DJF modelled DIC anomalies and their respective lagged correlations.

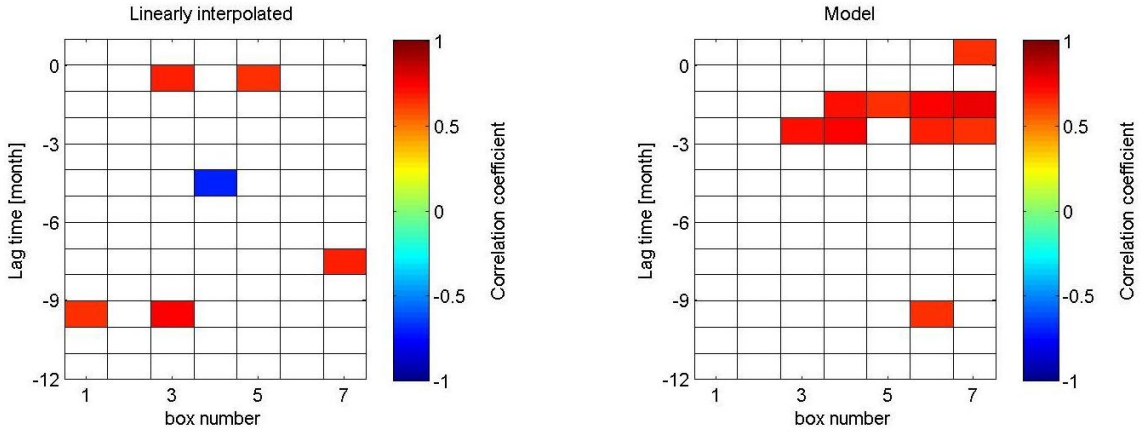

Figure 4-12: Spearman cross-correlation between the observed DJF ΔSSH anomalies and 3-month paired pCO_2 T_{norm} (left) versus lag time [months] and modelled DJF ΔSSH anomalies and modelled 3-month paired DIC anomalies(right). Statistically significant positive correlations are orange-red, whilst statistically significant negative correlations are light-dark blue. The ΔSSH anomalies lead the pCO_2 T_{norm}/DIC anomalies at negative lag times. An indication of the strength of the correlation is provided in the colorbar.

The above figure displays statistically significant positive correlations at lag -1 in boxes 3 and 5. There is also a significant anti-correlation that occurs in box 4 at lag -5 months. In addition, significant positive correlations between lags -8 (box 7) and lag -10 (boxes 1 and 3) are apparent. The model output also displays significant positive correlations at lag 0 in box 7, in addition to significant positive correlations at lag time of lag -2 to lag -3 months, extending this to box 3. There is also a significant positive correlation at lag -10 months in box 6.

Although the number of statistically significant correlations with respect to both the observations and model output is not large, the lag times at which they occur may hint at the proposed hypothesis identified in section 1.7. At instantaneous or near-instantaneous lag, the spin-up of the gyre circulation, in response to atmospheric forcing is likely to influence the amount of DIC-rich subsurface waters entrained to the surface and thereby increase the surface water pCO_2 in the temperate regions during a positive winter NAO index through mode water formation. The statistically significant positive correlations between both the winter ΔSSH anomalies and the winter NAO index with the surface pCO_2 anomalies in JFM is testament to this

claim. Thus, it is shown here that DIC entrainment through the deepening of the mixed layer may have occurred in response to the large-scale oceanic circulation, driven by the winter NAO index.

The absence of a statistically significant positive correlation in the subtropics (i.e. box 1 and 2) at these time lags does not automatically imply that DIC entrainment will not occur in these regions. The most likely meaning of this absence is that the cold-SST waters that are also entrained in addition to the high-DIC waters during a positive winter NAO index are likely to have an important decreasing effect on the surface pCO_2 in this region, perhaps more so than in the temperate regions. This will be discussed in section 4.5, when the SST versus non-SST effects on the surface pCO_2 are examined.

It should also be noted that whilst reference is made to a positive winter NAO, during negative winter NAO phases, the implication of the above significant correlation is that less DIC would be entrained, given that the MLD would not be as deep. However, the MLD would still be relatively deep, particularly in the temperate regions (see years 2003 to 2006 in Figure A-3) as a result of the southerly shift of the storm track in winter in response to a negative NAO winter (Hurrell 1995). Thus the net effect on the surface pCO_2 in winter in these years is more likely to be driven by the entrainment of cold-SST water to the surface than high-DIC waters.

The model output is in broad agreement with the location of the statistically significant correlations between the ΔSSH anomalies and the DIC anomalies and extends these correlations further south west (significant positive correlations are discernible in box 3 at lag -3 months). This signifies that the model output is able to replicate the observed effect that the ocean circulation has on the entrainment of DIC-rich subsurface waters in the temperate regions.

In terms of the effect of the previous winter's nutrient entrainment on the strength of the following spring blooms, the statistically significant anti-correlations between the ΔSSH anomalies and the pCO_2 T_{norm} anomalies at lags -4 months in box 4 may signify this mechanism. It should be noted, however, that the confidence one can place in such a mechanism, given the lack of significant negative correlations in the other boxes, is low. In addition, given that the JFM ΔSSH anomalies do not significantly anti-correlate with the surface pCO_2 between these time lags (i.e. -3 and -5 months), the claim that the previous winter's nutrient entrainment in response

to the large-scale ocean circulation affects the strength of the following spring bloom needs to be treated with caution. It could also be the case that this relationship is more clearly seen when the winter NAO index and pCO_2 T_{norm} anomalies/DIC are examined, given the close co-variability between the winter NAO index and winter ΔSSH (Figure 3-3, chapter 3). This will be evaluated in the following section.

With respect to the possibility of the DIC renewal mechanism occurring the following autumn under positive winter NAO conditions the previous winter, the statistically significant positive correlations between the winter ΔSSH anomalies and the pCO_2 T_{norm} anomalies the following autumn (i.e. at lags between -8 and -10 months) may be hinting at this mechanism. The observation that the winter ΔSSH anomalies statistically significantly positively correlate with the surface pCO_2 anomalies at similar lag times (i.e. generally between lags -9 and -10 months) lends credit to this claim.

The following section examines how the winter NAO index cross-correlates with the pCO_2 T_{norm} anomalies for the observations and DIC anomalies with respect to the model output.

4.3.6 Cross-correlations of the NAO index with the pCO_2 T_{norm} anomalies/DIC anomalies

Figure 4-13 reveals that statistically significant positive and negative correlations are apparent between the JFM NAO index and JFM pCO_2 T_{norm} anomalies. The model output also displays statistically significant positive correlations at instantaneous lag in boxes 2 and 3. It is interesting to note that when using the winter NAO index with the winter pCO_2 T_{norm} anomalies, statistically significant positive correlations between these parameters are now found in the subtropics, but not in the temperate regions, unlike the statistically significant positive correlations evident between the winter ΔSSH anomalies and pCO_2 T_{norm} anomalies. As mentioned on other occasions when this has occurred, this is more likely to result from slight differences within the winter NAO index compared to the winter ΔSSH anomalies rather than significant physical differences between the two variables. This is due to the statistically significant positive correlations between these two large-scale parameters that was shown to take place during winter (see Figure 3-3, chapter 3).

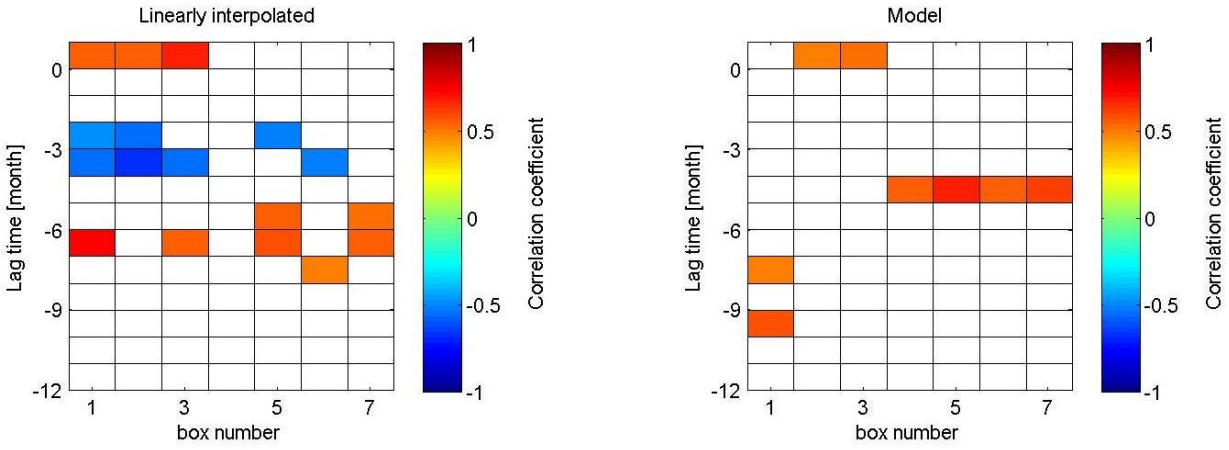

Figure 4-13: Spearman cross-correlation between the JFM NAO index and 3-month paired pCO_2 T_{norm} anomalies (left) versus lag time [months] and JFM NAO index and 3-month paired modelled DIC anomalies (right). Statistically significant positive correlations are orange-red, whilst statistically significant negative correlations are light-dark blue. The NAO index leads the pCO_2 T_{norm}/DIC anomalies at negative lag times. An indication of the strength of the correlation is provided in the colorbar.

Therefore, winter DIC entrainment is also likely to play an important role in the variability of surface pCO_2 in winter in the subtropics as advocated in Figure 4-10. The absence of significant correlations in the temperate regions (i.e. box 4 to 7) between these variables does not imply that DIC entrainment is not important in these regions, since significant correlations have been found between the ΔSSH anomalies (which is significantly related to the winter NAO index) and the pCO_2 T_{norm} anomalies (see box 5 at lag -1 month in Figure 4-12). Moreover, the statistically significant positive correlations between the NAO index and the surface pCO_2 anomalies in winter in all regions (Figure 4-4), coupled with the instantaneous correlations evident herein, indicate that mode water formation during a positive NAO winter will result in positive pCO_2 anomalies through mechanisms described in the Introduction, section 1.6 and illustrated in Figure 1-9 in section 1.7.

The model output is in broad agreement with the observations with respect to the statistically significant positive correlations found at instantaneous lag in the subtropics. This substantiates the claim that DIC entrainment occurs through deeper vertical mixing under a positive winter NAO scenario, since DIC is a term that is included in the model.

With respect to the potential effect of the previous winter's NAO index affecting the following spring's phytoplankton blooms, the statistically significant anti-correlations

between the winter NAO index and the pCO_2 T_{norm} anomalies at lags -3 to -4 months and in most regions of the study area is likely to indicate this effect. This is because almost identical statistically significant anti-correlations between the winter NAO index and the spring surface pCO_2 anomalies are apparent (see Figure 4-4). Thus, it has been shown here that during a high (low) winter NAO index, stronger (weaker) spring blooms are likely, thereby resulting in negative (positive) surface pCO_2 anomalies in spring. This confirms the hypothesis made in the Introduction regarding the mechanisms of seasonal anomalies of the surface pCO_2 under different winter NAO scenarios (see Figure 1-9 and Figure 1-10 for the subtropics and temperate regions respectively).

There also numerous statistically significant positive correlations between the winter NAO index and the following late summer/early autumn's pCO_2 T_{norm} anomalies (e.g. lags -6 to lags -8 months). As mentioned previously for the winter ΔSSH anomalies, (where a statistically significant positive correlation between them and the pCO_2 T_{norm} anomalies is evident at lags between -8 to -10 months), this is likely to be indicative of DIC renewal in autumn in response to the previous winter's high DIC entrainment.

There are seemingly slight differences in the lag times with respect to the winter NAO index and winter ΔSSH anomalies, with the significant positive correlation between the winter NAO index and the pCO_2 T_{norm} anomalies at lags -7 months corresponding to the August, September, October (ASO) period. The peak significant correlation with respect to the winter ΔSSH anomalies and the following autumn's pCO_2 T_{norm} anomalies is between lags -8 and -10 months (i.e. corresponding to the ASO period for lags -8 and October, November, December (OND) for lags -10). The actual difference between these statistically significant correlations is only 2 months, given that the best winter ΔSSH anomalies – pCO_2 T_{norm} anomalies links were found during the DJF time period whereas between the winter NAO index – pCO_2 T_{norm} anomalies this was in JFM (see Figure 4-12 and Figure 4-13 respectively). Thus, when the DJF time period is used, a lag time of -8 months corresponds to the ASO time period (ΔSSH anomalies with pCO_2 T_{norm} anomalies) as it would for the winter NAO index with pCO_2 T_{norm} anomalies, because the best correlations were found during the JFM period, hence a lag time of -8 months also corresponds to the ASO time period. The 1 month difference relates to the subtropical regions (boxes 1 to 3) where the significant correlations at lag -7 months in Figure 4-13 (winter NAO index with pCO_2 T_{norm} anomalies)

correspond to the ASO time period whereas the significant correlations at lag -10 months in Figure 4-12 (winter ΔSSH anomalies with pCO_2 T_{norm} anomalies) correspond to the OND time period.

However given the aforementioned relatedness between the winter NAO index and the winter ΔSSH anomalies, it is concluded here that both are symptomatic of the DIC renewal mechanism.

The main differences between the temperate and subtropical regions at the seasonal timescale are likely to be the magnitude of the SST versus non-SST effects on the surface pCO_2, with the subtropics more likely to be influenced by SST (more than the DIC) in all months than the temperate regions. This is due to the mean seasonal cycle of surface pCO_2 in the subtropics, which closely follows that of the SST, whereas in the temperate regions this is not the case (compare Figure 3-9 in chapter 3 with Figure 3-10 in chapter 3 for box 1 and box 6 respectively). However, this does not preclude that in certain years, where mode water formation occurs in the subtropics, DIC entrainment becomes more important. It would not be as regular a feature as in the temperate regions, however. This can be more clearly seen in section 4.5 of this chapter.

Section 4.3.5 and especially section 4.3.6 hint at the role of biology on the seasonal anomalies of the surface pCO_2 in both subtropical and temperate regions. This will be explored in greater detail in the following sections, when the winter ΔSSH anomalies and the winter NAO index are cross-correlated with the CHL anomalies.

4.3.7 Cross-correlations of the ΔSSH anomalies with the CHL anomalies

Figure 4-14 illustrates the cross-correlations between the winter ΔSSH anomalies and the CHL anomalies for the linearly interpolated observations and the model output.

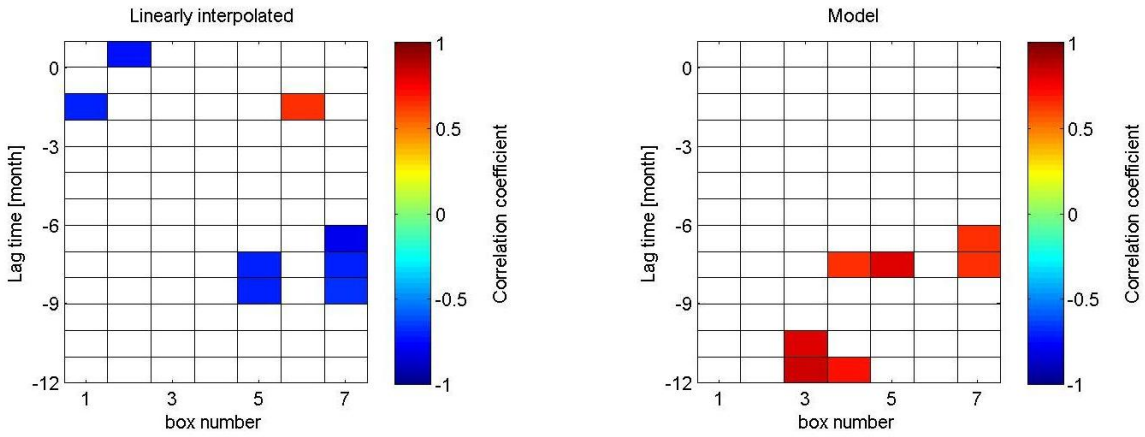

Figure 4-14: Spearman cross-correlation versus lag time [months] between the observed 3-month paired JFM ΔSSH anomalies and 3-month paired CHL anomalies (left) and modelled ΔSSH anomalies and 3-month paired modelled CHL anomalies (right). Statistically significant positive correlations are orange-red, whilst statistically significant negative correlations are light-dark blue. The ΔSSH anomalies lead the CHL anomalies at negative lag times.

The above figure illustrates that there are statistically significant correlations between the ΔSSH anomalies and the CHL anomalies at both instantaneous/near-instantaneous and lagged time periods. The model output also reveals statistically significant positive correlations but at lag -7 and -8 months in addition to -11 and -12 months. However, given that the model misplaces the timing of the spring bloom in the study region (see Figure 3-12 in chapter 3), the usefulness of the model output in this instance is low. Thus reference to the model output will not be made in this section.

The hypothesis states that during high NAO winters, stronger nutrient entrainment is likely to fuel more intense spring blooms particularly in the temperate regions where phytoplankton stocks are generally higher (Takahashi et al. 2002). Ideally then, a statistically significant positive correlation between the winter ΔSSH anomalies and the following spring CHL anomalies should be apparent. This means examining whether these significant correlations occur between lag -1 and lag -4, since these lags would correspond to the FMA to AMJ time period, when biology is expected to be at its peak, especially within the temperate regions where a CHL peak is discernible (see Figure 3-12, chapter 3). Given that lag times between lag -6 and lag -10 months have been discussed in relation to both the winter ΔSSH anomalies and the winter NAO index on the surface pCO_2 variability through the DIC renewal mechanism, it is considered irrelevant to discuss the statistically significant

correlations observed at these time lags between the winter ΔSSH anomalies and the CHL anomalies. This is because even if the CHL anomalies during the SON or OND time period are negative or positive in relation to the previous winter's ΔSSH anomalies, the fact that statistically significant positive correlations occur between the winter ΔSSH anomalies and the surface pCO_2 anomalies at lags -9 to -10 months illustrates that the CHL variability at that time is unlikely to be an important factor controlling the surface pCO_2. Rather, the DIC will have greater effect on the surface pCO_2 and is therefore likely to contribute to the statistically significant positive correlations in autumn via the DIC renewal mechanism discussed previously.

In addition, the fact that the mean CHL concentration during autumn is very low (in terms of the observations), even in the temperate regions (see Figure 3-12, chapter 3), further illustrates that any biology in autumn is unlikely to result in negative pCO_2 anomalies, due to entrainment of a renewed DIC pool. The observation that the pCO_2 T_{norm} mean seasonal cycle increases in autumn (i.e. OND), see Figure A-24, lends further credit to this statement.

In box 1 and to a certain extent box 2, a statistically significant anti-correlation is observed between lag times of 0 months and -3 months, the opposite of what would be expected to occur. However, in the temperate regions, on the other hand, a statistically significant positive correlation at lag times of -1 to -2 months is apparent. Therefore, in the temperate regions, as hypothesised, during high NAO winters, the spring bloom would intensify, with less intense spring blooms occurring during negative NAO winters. Negative surface pCO_2 anomalies would therefore be expected during or near to this time lag with respect to either the winter NAO index or winter ΔSSH anomalies. In relation to the latter, no such statistically significant relationship is apparent between lags -1 and lags -4. The former, however, does reveal a statistically significant relationship with the surface water pCO_2 in box 6 at lag -4 and lag -5 (i.e. within the MJJ and JJA time-period, see Figure 4-4).

The fact that this does not directly coincide with the significant positive correlations between the winter ΔSSH anomalies and the FMA and MAM CHL anomalies (lag -2 and -3 months) does not necessarily imply that the theory is disproved. This is because it is possible that the reduction in surface pCO_2 reaches its peak 2 to 3 months after the strongest CHL signal takes place. In the temperate regions, in particular in some years, the spring bloom lasts for several months and is not

restricted to April or May (although this is when the peak CHL signal is simulated in this region – see Figure 3-12, chapter 3). Therefore, the pCO_2 anomaly is more likely to reflect below normal values at the end of the spring bloom. Further discussion on the role of biology in the temperate region will be given in chapter 5, when the inter-annual variability of the surface water pCO_2 is focused upon.

It should also be noted here that the statistically significant anti-correlations between the winter ΔSSH anomalies and the surface water pCO_2 anomalies between lags -5 and -8 months in the study region (see Figure 4-2) are unlikely to represent negative (positive) pCO_2 anomalies in response to greater (smaller) phytoplankton blooms. This is because these anti-correlations occur in summer or early autumn (generally within the JAS to SON time period), with many of these significant correlations occurring in the subtropics where the SST in summer is likely to play an important role on surface pCO_2. In fact, Figure A-2 illustrates that in most boxes there was a noticeable peak in the absolute surface pCO_2 during the summer of 2005. Figure A-17 clearly shows that the surface pCO_2 anomalies were strongly positive at that time (and the previous winter ΔSSH anomalies negative). Although this is only shown for box 1, given the high absolute pCO_2 in the other boxes at the same time and a similar mean summer peak in pCO_2 (Figure 3-9, chapter 3), it is likely that the high absolute SST that year substantially contributed to the statistically significant anti-correlation to occur between the winter ΔSSH anomalies and the following summer pCO_2 anomalies (Figure 4-2).

However, whilst it is recognised that in the subtropics the spring bloom is less intense than that of the temperate regions, it is unclear as to why a statistically significant anti-correlation is evident between lags 0 and -3 months, as illustrated in Figure 4-14. This will now be explored. Figure 4-15 illustrates the data associated with box 1 at lag -1 month.

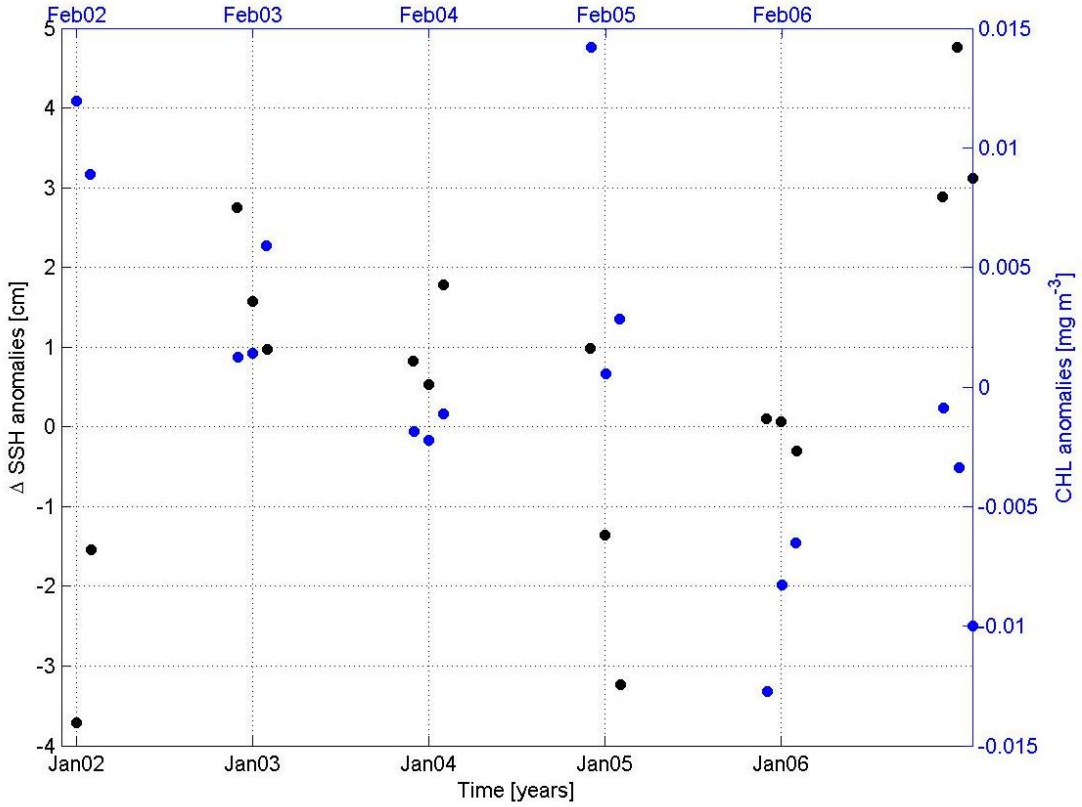

Figure 4-15: 3-month paired JFM ΔSSH anomalies versus 3-month paired FMA CHL anomalies at lag -1 month in box 1.

As can be seen, there is generally good co-variability associated with the above variables, with the exception of winter 2006/7, when the winter ΔSSH anomalies are positive and the late winter/early spring CHL anomalies are negative. However, the magnitude of this negative anomaly is very small. Thus, the physical implication of this statistically significant anti-correlation is debatable. It could well be that due to the deeper vertical mixing that occurred during the winter of 2006/7 (see the absolute MLD in box 1 in Figure A-3), the phytoplankton concentration decreased through entrainment of a larger portion of phytoplankton-free subsurface water into the surface layer – the winter dilution effect (Behrenfeld 2010). However, as already noted, given the very low magnitude of this negative anomaly, this cannot be unequivocally justified. It should also be noted that the positive anomalies are also of low magnitude. Therefore, it is more likely that the winter ΔSSH anomalies do not have a substantial effect on the spring bloom intensity in the subtropics. This is not to say that the spring bloom will not occur, just that due to the low standing stocks of phytoplankton in this region (Follows and Dutkiewicz 2001), large seasonal anomalies in the CHL signal is unlikely. This also implies that the spring bloom in

the subtropics, whilst likely to decrease the surface pCO_2, is unlikely to result in anomalously low surface pCO_2 levels.

Thus, as stated in the hypothesis, (see also Figure 1-9) under both positive and negative NAO scenarios, the spring bloom, although certainly present, is unlikely to lead to large negative pCO_2 anomalies in spring in the subtropics. This will also be tested when the small-scale parameters are cross-correlated with one another (i.e. surface pCO_2 with CHL).

The following section examines the winter NAO index and the CHL anomalies. Given the relatedness between the winter NAO index and the winter ΔSSH anomalies, where there are broadly similar statistically significant correlations, these will be highlighted in relation to the hypothesis.

4.3.8 Cross-correlations between the NAO index and the CHL anomalies

Figure 4-16 illustrates that there are broad similarities between the winter ΔSSH anomalies with the CHL anomalies (Figure 4-14) and the winter NAO index with CHL anomalies.

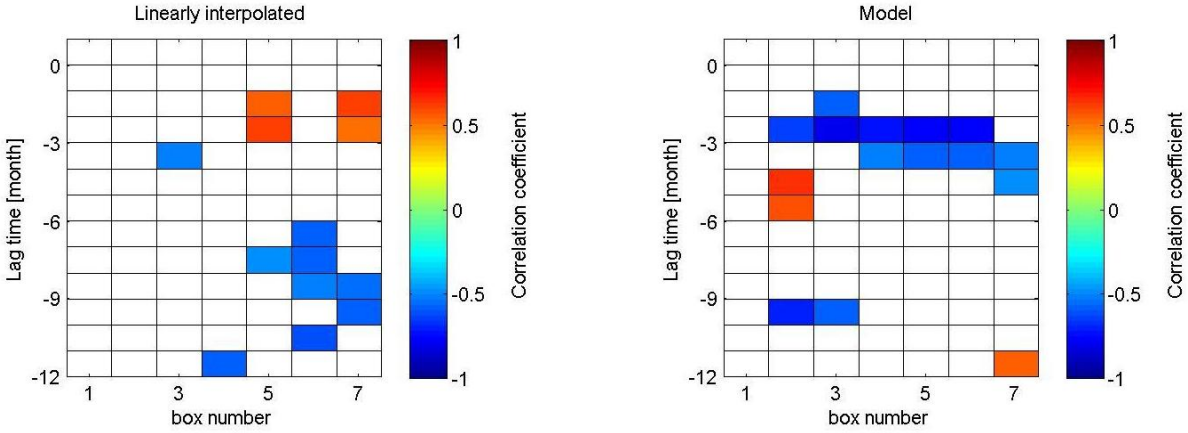

Figure 4-16: Spearman cross-correlation between the observed JFM NAO index and 3-month paired CHL anomalies (left) versus lag time [months] and observed JFM NAO index and 3-month paired modelled CHL anomalies (right). Statistically significant positive correlations are orange-red, whilst statistically significant negative correlations are light-dark blue. The NAO index leads the CHL anomalies at negative lag times.

Thus, the statistically significant positive correlations in the temperate regions (boxes 5 to 7) at lags of -2 to -3 months are also likely to be indicative of the previous winter's NAO index influence on the strength of the spring bloom. This has already been discussed in relation to the winter ΔSSH anomalies (which is dependent on the winter NAO index) and the following spring's CHL anomalies (section 4.3.6) and will therefore not be repeated here.

The effect of both the winter ΔSSH anomalies and the winter NAO index on the seasonal anomalies of the surface water pCO_2 has been examined through statistically significant relationships between the aforementioned parameters and the related parameters (e.g. SST, MLD and CHL). The key processes related to this variability have been described in the relevant sections in this chapter in addition to the Introduction (section 1.6) and illustrated with respect to both the subtropics (Figure 1-9) and temperate regions (Figure 1-10).

However, it is also important to evaluate how the 'small-scale' parameters (i.e. SST, MLD, CHL and pCO_2 T_{norm}/DIC) affect the surface water pCO_2 variability, since it is these parameters that will ultimately affect the surface pCO_2, through the effects of the large-scale atmospheric and oceanic circulation. Given that it has been established that winter is the driving season behind the seasonal anomalies of surface water pCO_2, the following sections focus on how the small-scale parameters affect the surface pCO_2 in winter. However, where a parameter clearly affects the surface pCO_2 in addition to winter (e.g. the pCO_2 T_{norm}/DIC) or only affects the surface pCO_2 in a particular season (e.g. CHL in spring), then a discussion focusing on those key seasons is also undertaken.

4.4 Seasonal anomaly of surface pCO_2 in relation to small-scale parameters

4.4.1 Cross-correlations of the SST anomalies with the surface pCO_2 anomalies

Figure 4-17 illustrates the cross-correlations of the winter SST anomalies with the surface water pCO_2 anomalies. It was found that the JFM rather than DJF winter SST anomalies correlated best with the surface water pCO_2 anomalies.

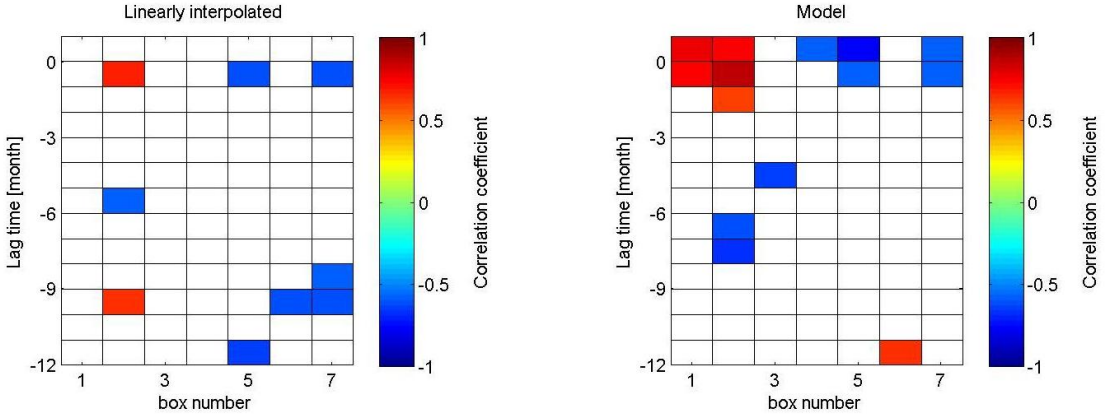

Figure 4-17: Spearman's cross-correlation coefficient at lag times [months] between the JFM 3 month paired SST anomalies and the 3 month paired surface water pCO_2 anomalies for the linearly interpolated observations (left) and the model output (right). Statistically significant positive correlations are orange-red, whilst statistically significant negative correlations are light-dark blue. The SST anomalies lead the surface water pCO_2 anomalies at negative lag times.

During JFM, the SST anomalies have a statistically significant effect on the pCO_2 anomalies throughout the study region, albeit in two opposing directions: in the subtropics, specifically box 2, the observations show a positive relationship at lag -1 months, such that positive/negative SST anomalies would result in positive/negative pCO_2 anomalies. The model output broadly agrees with this, albeit extends this effect to box 1 and at instantaneous lag (further west).

This seems to imply that in the subtropics, during high NAO winters, the surface pCO_2 anomalies may be positive and thereby indirectly suggest that mode water formation does not occur in these regions under a high NAO winter. However, it should be noted that there was no statistically significant positive correlation between either the winter ΔSSH anomalies or the winter NAO index and the winter SST anomalies in this box. In addition, in box 1, located further west, the winter

NAO index does anti-correlate with the winter SST anomalies, hinting at mode water formation in this region (see section 4.3.2).

The absence of a statistically significant anti-correlation in box 1 implies that the formation of the mode water may not occur as frequently as further north in the temperate regions, where the anti-correlation between the SST anomalies and surface pCO_2 anomalies is evident (box 5 and 7, Figure 4-17). This is because, although mode waters would be characterised by inherently low SST, they are also regions of intense mixing and will entrain high-DIC and nutrient waters from the depths to the surface. This latter process is likely to dominate under this scenario, as already explained and shown previously, especially for the temperate regions. This process is substantiated here as a result of the significant anti-correlations between the SST anomalies and surface pCO_2 anomalies in the temperate zone.

The statistically significant positive correlation in box 2 is thus more likely to suggest a reduced occurrence of mode water formation in this region compared to further west during high NAO winters. This may be due to the location of this box further east, which is therefore not as prone to the penetration of the EDW into the region, given that the core outcrop region of this mode water is located further west (Levine et al. 2011). In fact it may imply that high NAO winters increase the SST, thereby increasing the surface pCO_2, given the statistically significant positive correlation between the winter surface pCO_2 anomalies and the winter SST anomalies. However, given the absence of statistically significant correlations between either the winter NAO index and the winter ΔSSH anomalies with the SST anomalies in this region (box 2), this cannot be proven (see section 4.3.2 and section 4.3.1 respectively).

Equally, the absence of a statistically significant anti-correlation between the surface pCO_2 anomalies and the SST anomalies in winter in box 1 does not disprove the hypothesis of mode water formation. This is due to the winter NAO index and winter SST anomalies anti-correlating in this region. However, it is recognised that the absence of the former anti-correlation (between the SST anomalies and surface pCO_2 anomalies in winter) is likely to imply that the occurrence of mode water formation in this subtropical region is unlikely to be as frequent as in the temperate regions further north and east.

Thus, we have firmly established that DIC entrainment is likely to dominate in the temperate regions in winter rather than the low SST waters during a positive NAO winter. Under a negative NAO winter, it is more likely that the low SST waters dominate, given the decrease in DIC entrainment via a reduction in vertical mixing. Hence, Figure 4-17 supports the hypothesis of NAO control on the winter surface pCO_2 anomalies in the temperate regions as depicted schematically in Figure 1-10. However, within the subtropics, the absence of a statistically significant anti-correlation between the surface pCO_2 anomalies and SST anomalies (Figure 4-17, box 1) suggests that the NAO control on the winter surface pCO_2 anomalies is not as strong compared to the temperate regions.

As stated previously, the model output broadly agrees with the observations in terms of the location and sign of the statistically significant correlations between the winter SST anomalies and the surface pCO_2 anomalies. This further substantiates the observations in terms of the possible physical implications of these correlations, as described previously.

The statistically significant anti-correlations that occur at lagged time periods (between lags -9 and -12 months) in the temperate regions (i.e. boxes 5 to 7 in particular) between the SST anomalies and the surface water pCO_2 anomalies may act as a proxy for the DIC renewal mechanism described previously. This is because when SST is low, the pCO_2 T_{norm} is high and vice-versa (e.g. compare Figure 3-10 in chapter 3, section 3.3.2.2 with Figure A-24 for the observations). This also applies to the model output's SST versus DIC mean seasonal cycle (e.g. compare Figure 3-10 with Figure A-25). Therefore, when a statistically significant anti-correlation between the SST anomalies and surface pCO_2 anomalies occurs in winter, this implies that the pCO_2 T_{norm} anomalies/DIC anomalies must be positive, thereby substantially contributing to this anti-correlation. This means that DIC entrainment is likely to override the low SST effect, thereby resulting in positive pCO_2 anomalies, even though the SST anomalies are negative.

However, the fact that the previous winter's SST anomalies anti-correlate with the following autumn's and early winter surface pCO_2 anomalies (lags -9 to -12 months), suggests that the previous winter's DIC entrainment may have been sufficient for a renewed DIC pool to be entrained the following autumn, when the deepening of the mixed layer occurs. It should be noted that for this to occur, the depth of the mixed layer does not necessarily have to exceed its mean autumn levels, since the MLD

would be deep enough to re-entrain the previous winter's DIC alongside a new DIC pool, particularly in the temperate regions, where the mixed layer depth is deeper in autumn and winter than in the subtropics (see Figure 3-11, in chapter 3, section 3.3.2.3). Thus the surface pCO_2 anomalies would likely again have been positive despite negative SST anomalies, as a result of this mechanism. The above process would likely occur during a positive NAO winter, as described previously. Under negative NAO winters, DIC entrainment in winter would be less intense and hence the DIC renewal mechanism would therefore be unlikely to occur during these years, resulting in negative pCO_2 anomalies the following autumn. Hence, these significant anti-correlations support the hypothesis of anomalously high (low) surface pCO_2 anomalies the following autumn in response to high (low) NAO index winters in the temperate regions (see Figure 1-10). The model output does not reveal such significant anti-correlations at these lag times within the temperate regions. Given that the SST source of both the model output and observations is the same (i.e. NCEP-NCAR), it is more likely that this may be due to an underestimation of the modelled surface pCO_2 during autumn (see Figure 3-9, in boxes 6 and 7). Thus, the model may be overestimating the effect of low SST autumn waters decreasing the surface pCO_2, rather than DIC-rich autumn waters increasing the surface pCO_2 (as may be implied from the observations).

A statistically significant positive correlation between the previous winter SST anomalies and the following autumn pCO_2 anomalies is evident in the subtropics (e.g. box2 at a time lag of -10 months), thereby implying that this region would be more SST-driven. However, as described for the near-instantaneous statistically significant positive correlations in this region, this lagged correlation is more likely to imply that over the study period as a whole, the formation of mode water would not be as frequent. This would result in the SST co-varying with the surface pCO_2 overall but would certainly not exclude the possibility of mode water formation occurring within the region as explained previously. The statistically significant positive correlations between the previous winter's ΔSSH anomalies and the following autumn's pCO_2 T_{norm} anomalies in box 1 and box 3 (Figure 4-12, lags -10 months) is testament to this claim.

Furthermore, a statistically significant anti-correlation is also evident at lag -5 months in the subtropics (specifically box 2). As Figure A-20 illustrates, this simply indicates that the previous (cold) SST water (most years show a slight negative SST anomaly) anti-correlates with the usually high surface pCO_2 the following summer.

This is not considered to be important in terms of this research, however, as this is an expected relationship. The model output also reveals these anti-correlations in the subtropics.

The following section examines how the winter MLD may affect the winter surface pCO_2 variability.

4.4.2 Cross-correlations of the MLD anomalies with the surface pCO_2 anomalies

In this section, the effect of the winter MLD anomalies on the winter surface pCO_2 anomalies and the following spring/early summer and autumn pCO_2 anomalies is considered. This is because, as noted previously, deeper (shallower) vertical mixing in winter is also likely to impact the variability of surface pCO_2 the following spring through the usage of nutrients by biology. The volume of nutrients entrained in winter is likely to establish the sign of the surface pCO_2 anomalies the following spring, with higher (lower) nutrients due to deeper (shallower) winter MLD likely to lead to negative (positive) pCO_2 anomalies. In addition, deeper (shallower) MLD in winter is likely to result in positive (negative) pCO_2 anomalies the following autumn through the DIC renewal mechanism discussed previously. These processes will be driven by the sign of the winter NAO index, as stated previously. Figure 4-18 illustrates the cross-correlations associated with the DJF MLD anomalies and the surface pCO_2 anomalies.

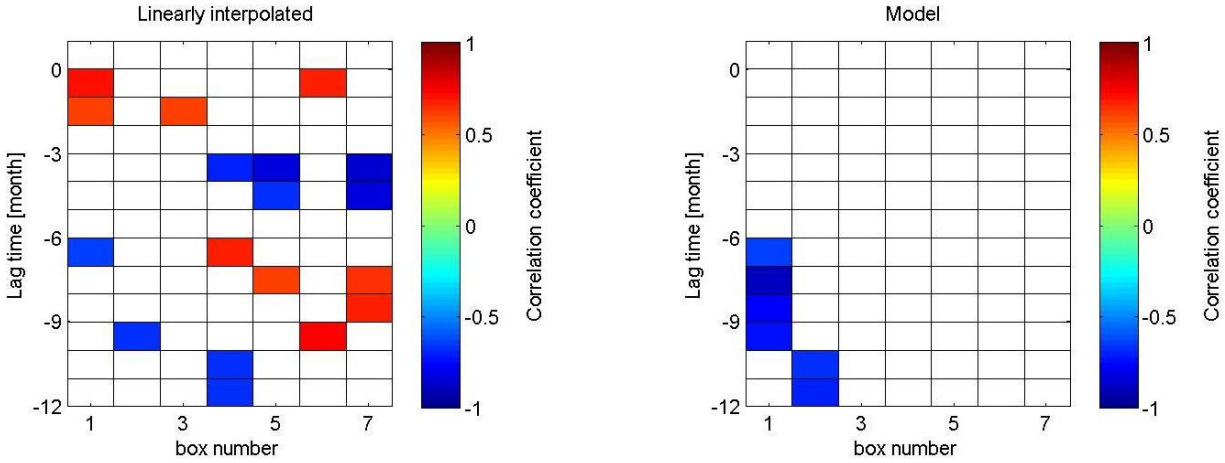

Figure 4-18: Spearman's cross-correlation coefficient at lag times [months] between the DJF 3-month paired MLD anomalies and the 3-month paired surface water pCO_2 anomalies for the linearly interpolated observations (left) and the model output (right). Statistically significant positive correlations are orange-red, whilst statistically significant negative correlations are light-dark blue. The MLD anomalies lead the surface water pCO_2 anomalies at negative lag times.

Figure 4-18 illustrates that there are numerous statistically significant correlations between the winter MLD anomalies and the surface water pCO_2 anomalies. In winter, i.e. at time lags between 0 and lag –2 months, there are statistically significant positive correlations apparent in boxes 1, 3 and 6. This therefore confirms that deeper (shallower) winter MLD will result in positive (negative) winter surface water pCO_2 anomalies through the volume of DIC entrained.

The fact that both the winter NAO index and winter ΔSSH anomalies statistically significantly positively correlate with the winter DIC anomalies in the subtropics (see section 4.3.3), and the winter DIC anomalies in the temperate regions, respectively, in addition to the above significant positive correlations, supports the hypothesis of winter surface water pCO_2 control through large-scale atmospheric and oceanic processes on the depth of the winter mixed layer through variations in DIC entrainment intensity as depicted schematically in Figure 1-9 for the subtropics and Figure 1-10 for the temperate regions.

The model output does not reveal any statistically significant positive correlations between the winter MLD anomalies and the winter pCO_2 anomalies at these time lags, however. This may be due to the over-estimation of the modelled winter MLD

(see Figure 3-11 in section 3.3.2.3), thereby potentially over-estimating the entrainment of low SST waters, decreasing the surface pCO_2.

The following spring and early summer (i.e. at lag times between -3 and -5 months), statistically significant anti-correlations between the previous winter MLD anomalies and the spring/early summer surface pCO_2 anomalies are apparent in the temperate regions. This is likely to be indicative of the spring blooms using the nutrients entrained the previous winter to photosynthesise, thereby resulting in negative surface pCO_2 anomalies. This would most likely explain the anti-correlation between the previous winter's MLD anomalies and the following spring/early summer pCO_2 anomalies in this region. However, this can only be confirmed in the following section, when the pCO_2 T_{norm}/DIC anomalies are cross-correlated with the surface water pCO_2 anomalies.

The absence of statistically significant anti-correlations between the previous winter MLD anomalies and the following spring pCO_2 anomalies in the subtropics is likely to indicate that the intensity of the spring bloom in this region will be weak(er) than in the temperate regions and hence probably not result in negative pCO_2 anomalies in spring in the subtropics. However, the likelihood of this will be confirmed in the following section where the pCO_2 anomalies are cross-correlated with the pCO_2 T_{norm}/DIC anomalies.

There are also numerous statistically significant correlations between lag times of -7 to -10 months in both temperate (boxes 4 to 7) and subtropical regions (boxes 1 to 3) with the temperate regions exhibiting positive correlations and the subtropics anti-correlations. The former is likely to indicate the DIC renewal mechanism described previously, since the previous winter MLD will act as a precursor of that winter's DIC entrainment, with greater DIC entrainment likely to result in positive pCO_2 anomalies in the same winter but also the following autumn.

The anti-correlations evident within the subtropics are likely to indicate that the DIC renewal mechanism may not apply to these regions, even though there may be a near-instantaneous effect of deeper MLD giving rise to greater DIC entrainment and thereby increasing the surface pCO_2 in winter. Thus, the cooler SST in this region may dominate during autumn, lowering the surface pCO_2. This is supported by the model output which also reveals statistically significant anti-correlations between the MLD anomalies and surface pCO_2 anomalies at similar lag times in boxes 1 and 2.

The following section explores the seasonal links between the pCO_2 T_{norm} anomalies and the DIC anomalies for the model output with respect to the surface pCO_2 anomalies.

4.4.3 Cross-correlations of the pCO_2 T_{norm} anomalies/DIC anomalies

Figure 4-19 illustrates that statistically significant correlations are apparent between the winter pCO_2 T_{norm} anomalies and the surface pCO_2 anomalies at both instantaneous and lagged time periods. This applies to both the observations and model output.

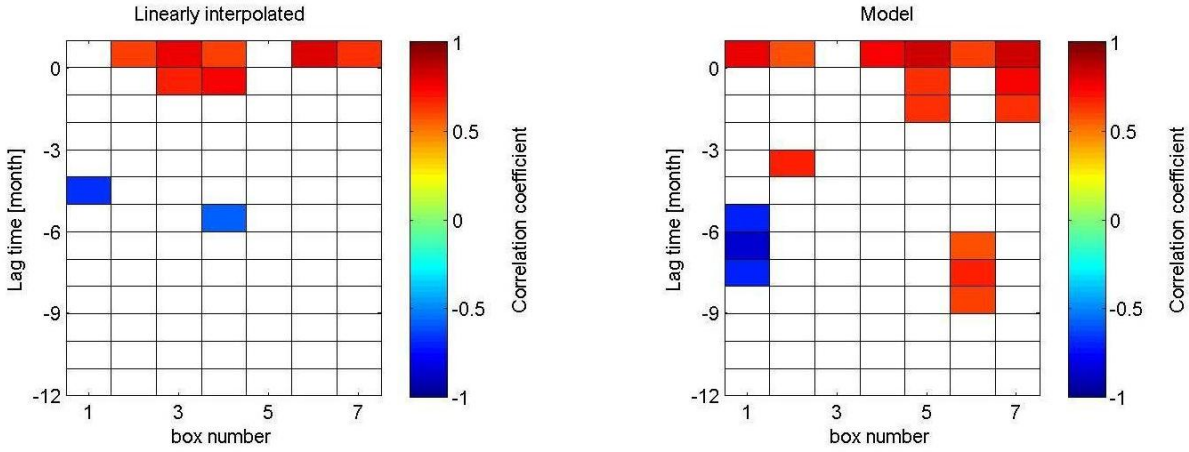

Figure 4-19: Spearman cross-correlation between the observed JFM 3-month paired pCO_2 T_{norm} anomalies and modelled JFM 3-month paired DIC anomalies with 3-month paired modelled pCO_2 anomalies (right). Statistically significant positive correlations are orange-red, whilst statistically significant negative correlations are light-dark blue. The pCO_2 T_{norm} /DIC anomalies lead the pCO_2 anomalies at negative lag times.

The instantaneous and near-instantaneous positive correlations in most regions are likely to indicate that DIC entrainment in winter is likely to control the surface pCO_2, with greater (lower) DIC entrainment giving rise to higher (lower) surface pCO_2. It is very encouraging to see that the co-located model output (right panel) reveals almost exactly the same statistically significant positive correlations at this time lag. The model output is able to estimate the DIC concentration, thus a similar outcome to the observations does suggest that DIC is an important parameter that affects the surface water pCO_2 during the winter months (even in the subtropics).

This provides further evidence to suggest that during high NAO winters, mode water formation in both the subtropics and temperate regions is likely to cause the entrainment of DIC to override that of the low SST, as seen by the positive response of the surface pCO_2 anomalies to the pCO_2 T_{norm}/DIC anomalies. During low NAO winters, it is likely that DIC entrainment reduces, with the low SST water overriding the DIC effect, thereby decreasing the surface pCO_2 and likely resulting in negative pCO_2 anomalies. Given that the winter NAO index declined from 2002/3 to 2005/6 (Figure 3-3, chapter 3), and the surface pCO_2 closely followed this decrease in most regions, a decrease in DIC entrainment may have reduced the surface pCO_2. This is likely to explain a significant fraction of the statistically significant positive correlations between the winter NAO index and winter ΔSSH anomalies with the surface pCO_2 at instantaneous lag (Figure 4-4 and Figure 4-2 respectively). Thus the winter fraction of the research hypothesis in both the subtropics and temperate regions (Figure 1-9 and Figure 1-10 respectively) is shown to be supported. However, even though in section 4.4.2, it was identified that the surface pCO_2 anomalies in spring significantly correlated with the previous winter's MLD anomalies in the temperate region (Figure 4-18), the winter MLD can only act as a proxy for DIC entrainment. Thus the absence of statistically significant anti-correlations between lags -3 and -4 months in both the subtropics and temperate regions does not support the hypothesis of anomalously high (low) surface pCO_2 the following spring in response to a high (low) NAO index the previous winter through anomalously high (low) biological activity.

There is also a statistically significant anti-correlation between the surface pCO_2 anomalies and the pCO_2 T_{norm} anomalies at a time lag of -5 months in box 1. However, given that this time lag corresponds to the June, July, August (JJA) time period), this may indicate that typically high surface water pCO_2 in summer (likely due to high summer SST) may anti-correlate with negative pCO_2 T_{norm} anomalies the previous winter in certain years. Thus, this is unlikely to show a biological response to the previous winter's DIC entrainment. Figure A-21 provides an example of this for box 1.

The model output also reveals statistically significant anti-correlations between the DIC anomalies and the surface water pCO_2 anomalies in the subtropics at similar lag times (i.e. between lags -5 and lag -9 months in box 1, for example), but this is also likely to imply a greater SST effect than a biological one, especially since the mean seasonal cycle of CHL in the model coincides with that of the SST. Hence,

even if higher CHL concentrations were simulated, the summer SST would have overridden this effect in the model.

With respect to the observations, there are no statistically significant positive correlations between the winter pCO_2 T_{norm} anomalies and the surface pCO_2 anomalies the following autumn in either the subtropics or temperate region (i.e. at lag times of -9 and -10 months). In section 4.4.2, Figure 4-17 illustrated that in the temperate region, statistically significant positive correlations between the previous winter MLD anomalies and the following autumn pCO_2 anomalies were apparent. It was therefore stated that this may be indicative of the DIC renewal mechanism within this region. Given the absence of significant positive correlations at similar lag times between the previous winter pCO_2 T_{norm} anomalies and the following autumn pCO_2 anomalies, the DIC renewal mechanism may not be taking place.

The model output does reveal statistically significant positive correlations at lag times of -9 months in the temperate region (box 6 specifically). However, given that the model over-estimates the MLD in winter in the temperate regions (see Figure 3-11), this implies that the model is predicting unrealistically high DIC concentrations the following autumn.

The observations therefore do not support the hypothesis of positive (negative) pCO_2 anomalies the following autumn within the temperate region in response to anomalously high (low) DIC entrainment the previous winter (see Figure 1-10). The lack of statistically significant positive correlations in the subtropics at this lag time hints that despite winters where DIC entrainment may have been higher, the volume may not have sufficed to enable a renewed positive surface pCO_2 anomaly to occur in the subtropics the following autumn, or that if this did occur, this positive anomaly was weak (and hence not statistically significant).

Even though it has been established in this section that it is unlikely for anomalously high (low) biological activity to take place in response to the previous winter's high (low) DIC entrainment, this will be explicitly examined in the following section.

4.4.4 Cross-correlations of the CHL anomalies with the surface water pCO_2 anomalies

Given that the peak CHL signal was established to occur during the AMJ time period (see Figure 3-12 in chapter 3), this section focuses on the instantaneous and near-instantaneous lag times between the CHL anomalies and the surface water pCO_2 anomalies. The model output will not be discussed in this section, given its limited use with respect to the CHL signal, as described previously. Statistically significant correlations outside of the lag 0 to -2 month lag time period will be ignored, given that the effect of biology on the surface pCO_2 manifests itself on an instantaneous or near-instantaneous time frame.

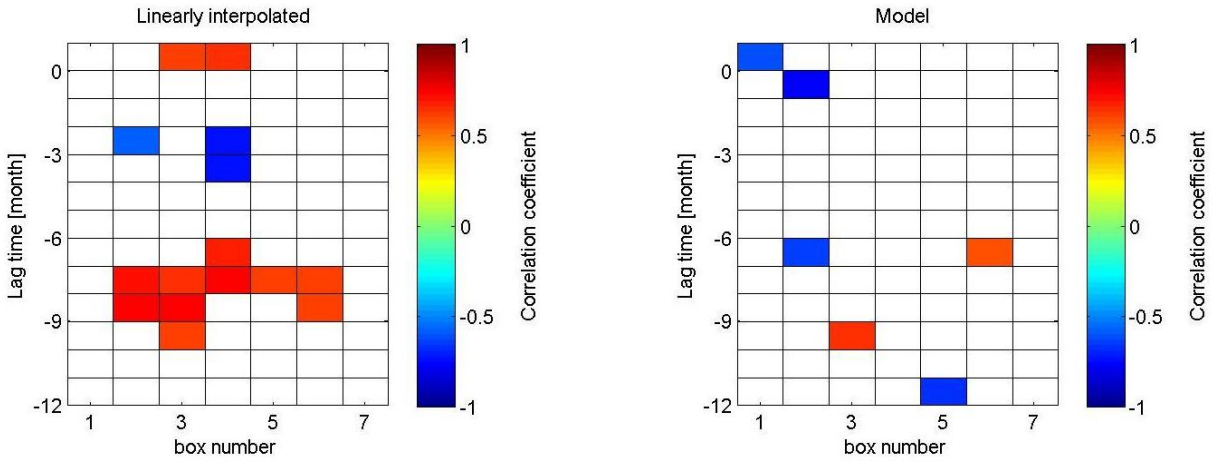

Figure 4-20: Spearman cross-correlation between the observed AMJ 3-month paired CHL anomalies with observed 3-month paired pCO_2 anomalies (left) and modelled AMJ 3-month paired CHL anomalies with 3-month paired modelled pCO_2 anomalies (right). Statistically significant positive correlations are orange-red, whilst statistically significant negative correlations are light-dark blue. The CHL anomalies lead the pCO_2 anomalies at negative lag times.

Statistically significant positive correlations are evident between the CHL anomalies and the surface water pCO_2 anomalies at instantaneous and near-instantaneous lag in boxes 3 and 4. At first glance, this is rather counterintuitive, since it would be expected that in spring, biology would decrease the surface pCO_2 and not increase it, as this correlation implies. However, the CHL anomalies are calculated with respect to their monthly mean. In AMJ in these regions, the mean CHL concentration reaches its peak (see Figure 3-12, chapter 3). At the same time, the mean surface water pCO_2 is either decreasing or also reaching a dip (see Figure

3-9, chapter 3). Thus, there is a discernible effect on the surface water pCO_2 from the phytoplankton blooms. Therefore, the above statistically significant positive correlation in both these boxes simply means that the two variables co-vary well. In this instance, this is unlikely to imply a biological connection over and above what is already known: that in spring, biology decreases the surface pCO_2. However, this implies that in relation to the previous winter's nutrient entrainment, the intensity of the spring bloom is unlikely to vary significantly. Consequently, the impact on the variability of the spring pCO_2 will be limited. The fact that this occurs in boxes 3 and 4 (neither in the core subtropics nor in the core temperate regions) is likely to imply that the CHL anomalies themselves are higher than they would be in the subtropics, and as such this leads to a statistically significant relationship, but in this case with limited biological implications, as explained. The absence of a statistically significant relationship in the core subtropical regions (i.e. box 1 and box 2) is therefore likely to imply that the CHL anomalies are very small and thus the impact on spring pCO_2 variability would be negligible in these regions.

However, the absence of statistically significant anti-correlations within the temperate regions once again indicates that despite anomalously high (low) nutrient entrainment the previous winter (as shown in Figure 4-19), this is unlikely to result in negative (positive) pCO_2 anomalies in the temperate region the following spring through biological activity.

The following section discusses the SST versus non-SST effects on the surface water pCO_2 variability.

4.5 Contributions of the SST versus non-SST effects on the surface pCO_2 anomalies

Figure 4-21 displays the surface water pCO_2 anomalies along with the pCO_2 T_{norm} anomalies (non-SST effect) and pCO_2 T anomalies (SST effect) for the linearly interpolated observations used throughout this chapter.

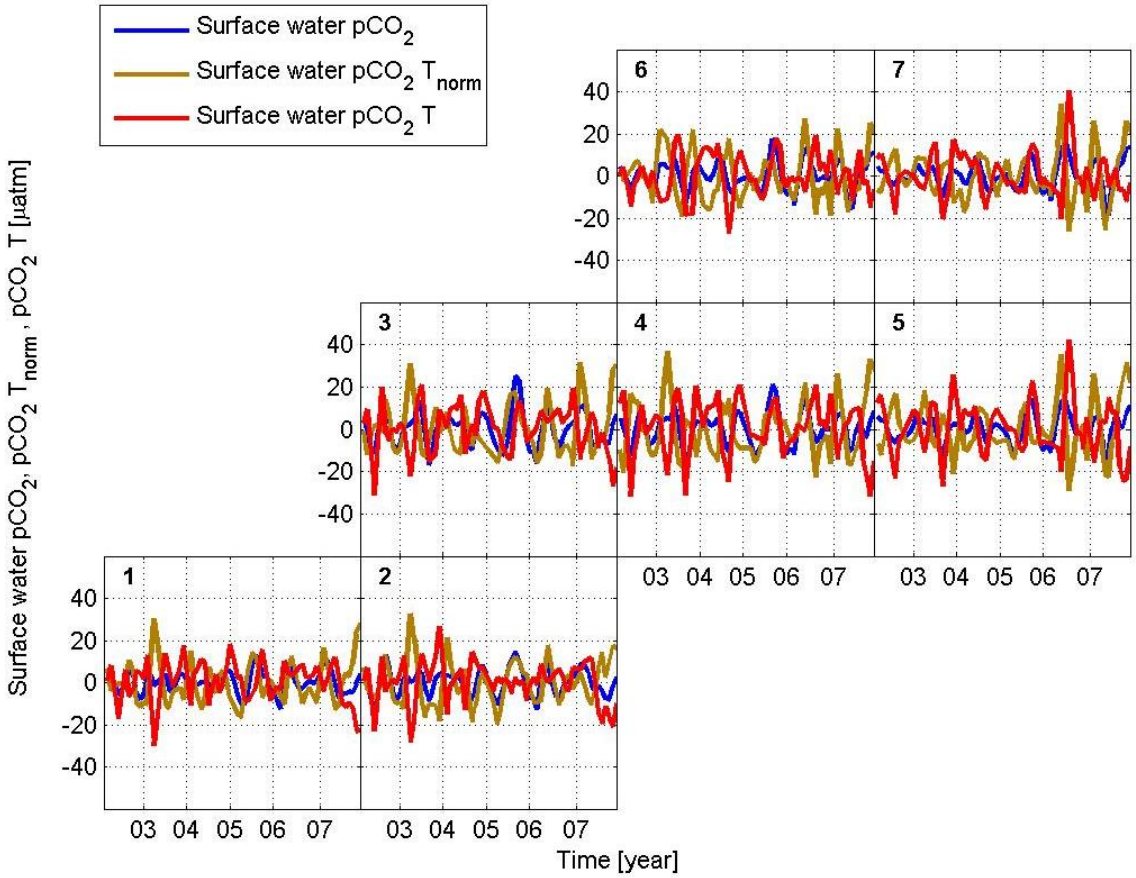

Figure 4-21: 3-month smoothed surface water pCO_2 anomalies (blue), 3-month smoothed surface water pCO_2 T_{norm} anomalies and 3-month smoothed surface pCO_2 T anomalies (red) for all boxes.

First and foremost, this figure illustrates that the contribution of the pCO_2 T_{norm} anomalies and pCO_2 T anomalies to the surface pCO_2 anomalies are both substantial throughout the time period with regard to the linearly interpolated observations. There are instances where both the pCO_2 T_{norm} anomalies and pCO_2 T anomalies are close to zero during the winter period (e.g. during 2002), indicative of low SST water decreasing the surface pCO_2 but equally of DIC-rich water increasing the surface pCO_2. However, the dominant process affecting the surface water pCO_2 anomalies in winter is likely DIC entrainment, since a statistically significant positive relationship between the winter NAO index and winter ΔSSH anomalies with the winter surface pCO_2 was found (Figure 4-4 and Figure 4-2 respectively). As already explained, this process is likely to be more important in the temperate regions, given the statistically significant anti-correlations between the winter SST anomalies and winter surface water pCO_2 anomalies (). However, even in the subtropics, DIC entrainment is likely to dominate at times, as seen in box 1 in

Figure 4-21 in early 2007. During January 2007, for example, the surface pCO_2 T_{norm} anomalies were positive, the surface pCO_2 T anomalies were slightly negative, but the surface pCO_2 anomalies were positive. Thus, the surface pCO_2 T_{norm} (non-SST effect) overrode the surface pCO_2 T (SST effect).

The contribution made by the absolute winter pCO_2 T became greater between 2003/4 and 2005/6 in both the subtropics and temperate regions, hence implying that the winter SST played a more dominant role overall during these years than DIC entrainment. This means that during negative NAO winters (e.g. winters 2003/4 to 2005/6), DIC entrainment will decrease due to shallower winter mixed layers (compared to positive NAO winters), thereby enabling the low-SST waters to decrease the surface pCO_2. This can be visualized in Figure A-7 in the Appendix where the difference between the absolute pCO_2 and absolute pCO_2 T (red) and absolute pCO_2 T_{norm} (brown) is shown. From 2002 to 2006, the difference between the absolute pCO_2 T and the absolute pCO_2 reduced whilst between the absolute pCO_2 T_{norm} and absolute pCO_2 the difference remained the same (i.e. between 40 µatm over-estimation in spring and 40 µatm under-estimation during late autumn). This also translates into weakly negative surface pCO_2 T anomalies (indicative of colder SST water) in addition to weakly negative surface pCO_2 T_{norm} anomalies (indicative of less DIC entrainment) and weakly negative surface pCO_2 anomalies especially during winter 2005/6 for most regions (Figure 4-21).

During spring, the mean pCO_2 T_{norm} value ranges from 370 to 430 µatm and within all regions of the study area. The mean pCO_2 T ranges from 310 to 330 µatm, so this is when the highest difference between the SST and DIC effects occurs (compare Figure A-24 with Figure A-25), with the SST generally the coldest at this time (decreasing the pCO_2) and the entrainment of DIC highest at this time (increasing the pCO_2). It is therefore not surprising that biological activity is highest in the spring months, given the availability of nutrients. Hence, the net effect that the biology has on the pCO_2 in spring is a reduction in pCO_2 due to usage of the nutrients. This is most clearly seen in the low absolute pCO_2 of the temperate regions during this time (e.g. box 6). Therefore, in this case, high pCO_2 T_{norm} will usually equate to low absolute pCO_2 due to biological activity (see Figure A-1).

In terms of the surface water pCO_2 anomalies at this time, Figure 4-21 captures this biological effect quite well during spring 2007. In the subtropics, the pCO_2 anomaly is less negative than in the temperate regions, but this is to be expected with regard

to the lower SST in spring further north and enhanced biological activity. In any case, there is a clear pCO_2 T_{norm} negative anomaly during April/May 2007 that coincides with that of the pCO_2 anomaly at that time. This implies that a strong phytoplankton bloom occurred, using up most of the nutrients upwelled from the previous winter's deep vertical mixing. Indeed, the absolute pCO_2, in particular from boxes 3 to 7, ranged from ~350 µatm (box 3) to ~330 µatm (box 7) during that time period. The fact that this effect is most clearly seen in spring 2007 and not during other similar time periods is down to the inability of the other spring time-periods to exhibit such low pCO_2. Thus, the spring pCO_2 anomaly may have been between 0 and ~-5 µatm (see Figure 4-21) in the temperate regions during 2002 to 2004, for instance, but in absolute terms the values would still have been relatively low (i.e. between ~340 and 360 µatm – see Figure A-1). It is therefore likely that these negative pCO_2 anomalies are too weak to robustly confirm the hypothesis of significant biological activity in spring in response to the previous winter's greater nutrient entrainment orchestrated through the NAO in both the subtropics and temperate region.

In relation to the DIC renewal mechanism described previously in this chapter, Figure 4-21 shows that after high NAO winter years, particularly the winter of 2006/7, the surface water pCO_2 anomalies the following autumn (e.g. SON 2007) were positive. There is a distinction, however, to how positive these surface water pCO_2 anomalies are in the subtropics compared to the temperate regions.

In the subtropics during this time period, even though the surface pCO_2 T_{norm} anomalies (non-SST effect) are positive, the surface pCO_2 anomalies are weakly negative (see boxes 1 and 2 for example). Given that the surface pCO_2 T anomalies (SST effect) are negative, the colder SST waters of autumn dominated the surface pCO_2 anomalies in this region during this time period.

In the temperate regions, however (e.g. box 6 and 7), during the same time period, both the surface water pCO_2 anomalies and the surface water pCO_2 T_{norm} anomalies are positive, whilst the surface pCO_2 T anomalies were negative. This therefore indicates that the non-SST effect (i.e. DIC entrainment through the deepening of the autumn mixed layer) is likely to have overridden the low SST waters at that time, thereby resulting in positive pCO_2 anomalies. However, this is clearest only during the autumn of 2007 within the temperate regions and whilst there are other positive surface pCO_2 anomalies during autumn in the temperate regions (e.g. box 7, early

2002), these are only weakly positive. Therefore, taking the time period as a whole, a robust correlation between the pCO_2 T_{norm}/DIC anomalies and the following autumn pCO_2 anomalies is not apparent. Thus, as noted earlier in this chapter (section 4.4.3), there is insufficient evidence to support the DIC renewal mechanism hypothesised to occur in the temperate regions.

During negative NAO winters (i.e. between 2003/4 and 2005/6), the surface water pCO_2 anomalies either close to zero (e.g. box 6; SON 2006) or even weakly negative (e.g. box 6, SON 2004). Therefore, a negative winter NAO will enable the following autumn SST effect to override the non-SST effects in the temperate regions.

In terms of the model output, Figure 4-22 displays the pCO_2 anomalies, pCO_2 T_{norm} anomalies and pCO_2 T anomalies in all regions.

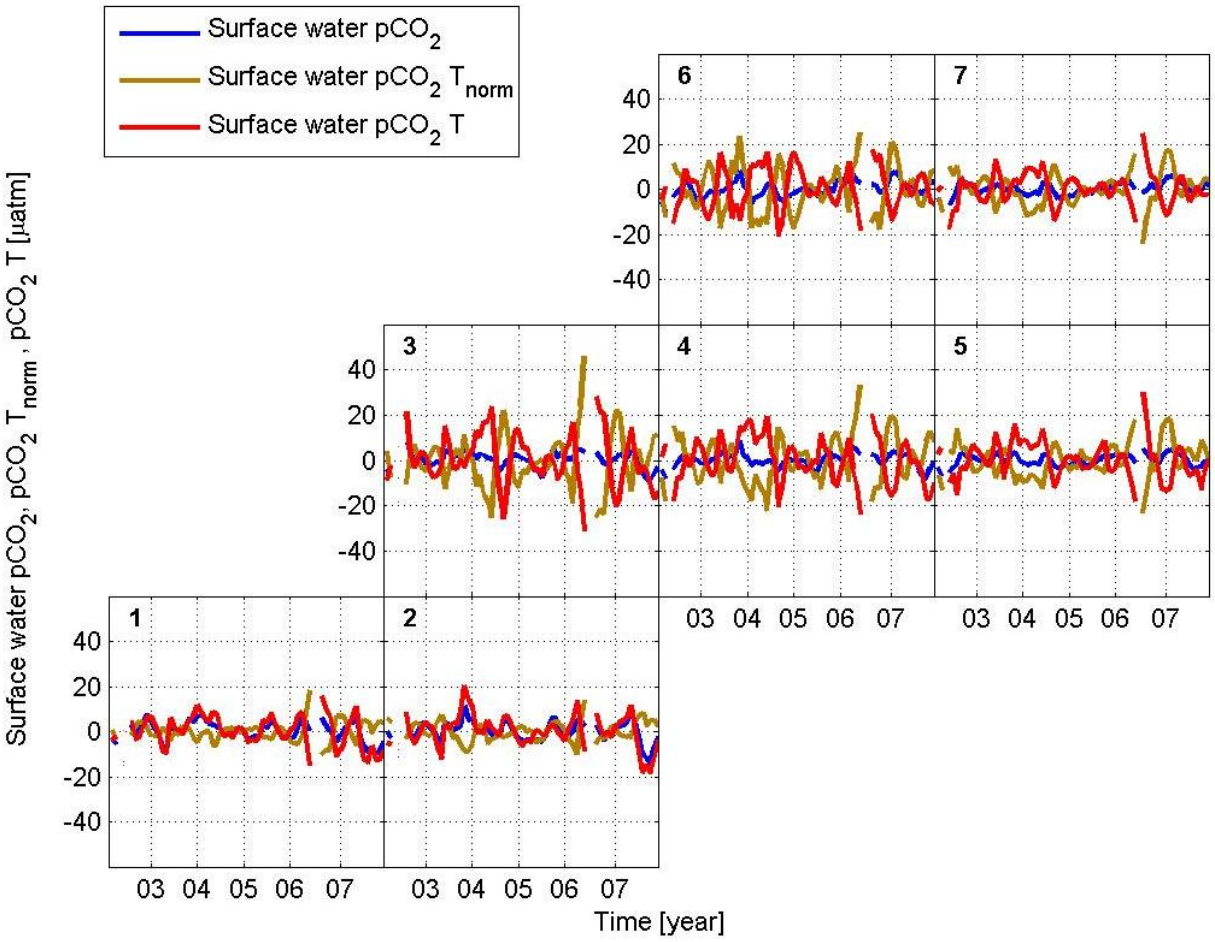

Figure 4-22: 3-month smoothed modelled surface water pCO_2 anomalies (blue), 3-month smoothed surface water pCO_2 T_{norm} anomalies and 3-month smoothed surface pCO_2 T anomalies (red) for all boxes.

Figure 4-22 clearly illustrates that the SST effect is strongly coupled (and over-estimated) in the subtropics with respect to surface water pCO_2 variability (in particular boxes 1 and 2), due to the high co-variability between the surface water pCO_2 anomalies (blue line) and the surface water pCO_2 T anomalies (red line). The SST effect decreases within the temperate regions with the pCO_2 T_{norm} and pCO_2 T opposing each other and thereby both contributing to the pCO_2 anomalies. However, as mentioned in chapter 3 section 3.3.2.4, the timing of the phytoplankton bloom coincides with that of the highest summer SST, and thus there is still likely to be an over-estimation of the contribution of the SST onto the surface water pCO_2 in late-spring summer compared to the observations (see Figure A-8). This is why the model simulates a clear pCO_2 seasonal cycle in the temperate regions, whereas in reality this is not the case (see chapter 3, section 3.3.2.1).

However, it should be noted that many of the models parameters agree with the observations (i.e. simulation of DIC entrainment in winter, and coupling with the large-scale oceanic and atmospheric circulation). This only serves to substantiate the claims made concerning the key mechanisms governing the seasonal surface pCO_2 variability discussed here in terms of the observations.

4.6 Summary

It is clear that there is likely to be a dynamical coupling between the winter atmospheric and winter oceanic circulation and the winter surface water pCO_2 variability throughout the study region (see Figure 4-4 and Figure 4-2 respectively). Although the study region can broadly be subdivided into subtropics (e.g. boxes 1 to 3) and temperate (boxes 4 to 7), the processes affecting the winter variability of the surface pCO_2 are similar in both of these sub-regions. For example, low SST waters as a result of winter vertical mixing are likely to decrease the surface water pCO_2 whilst DIC-rich subsurface waters will increase the surface water pCO_2. The net effect on the surface water pCO_2 will differ from winter to winter, with a gradual increase of the low SST effect (and a steady decrease of DIC entrainment) between JFM 2002 and JFM 2006, with the latter winter exhibiting moderately negative pCO_2 anomalies (see Figure A-16 for box 1 as an example, although similar co-variation is also seen in the temperate regions). Winter 2006/7 displayed positive pCO_2 anomalies in all regions, in addition to positive MLD and negative SST anomalies.

Thus, winter DIC entrainment had a net positive effect on the surface water pCO_2 anomalies at that time.

In terms of the lagged effects of the atmospheric and oceanic circulation on the surface water pCO_2, the statistically significant anti-correlations between the winter NAO index and the following spring surface pCO_2 anomalies in both subtropical and temperate regions (see Figure 4-4, lag times -3 to -4 months) seem to suggest that biological activity may be occurring in response to the nutrients entrained the previous winter, thereby resulting in negative pCO_2 anomalies in spring.

However, the absence of statistically significant anti-correlations between the winter pCO_2 T_{norm} anomalies and the following spring pCO_2 anomalies within the study region (see Figure 4-19) suggests that such a link is unlikely to be apparent. This is also confirmed in Figure 4-20 where there are no statistically significant anti-correlations between the spring pCO_2 anomalies and the spring CHL anomalies.

Thus, whilst there may be a potential for stronger phytoplankton blooms to occur in spring, following a high NAO index winter, this is not supported by the aforementioned lack of significant correlations between either the spring CHL anomalies with the spring pCO_2 anomalies nor from the previous winter's pCO_2 T_{norm} anomalies with the following spring's pCO_2 anomalies. Therefore, the hypothesis of biological control of the surface pCO_2 in both the temperate and subtropics in response to the winter NAO index is not supported by the aforementioned results.

It is unclear why this is the case, but one possibility is the antagonistic relationship between the SST and pCO_2 T_{norm} during spring: the SST begins to increase due to the enhanced incidence of solar radiation, whilst the pCO_2 T_{norm} decreases as a result of a decrease in vertical supply of DIC due to the shoaling of the MLD (see Figure 3-10 and Figure 3-11 respectively). These two effects may cancel each other out (the SST increase would increase the surface pCO_2 whilst the decrease in DIC would decrease the surface pCO_2) with the net effect on the surface pCO_2 to be negligible. Another possibility is that more data is required (i.e. at least 10 years rather than 6) to robustly evaluate the effect of biology on surface pCO_2 in the study region.

In addition, although the winter ΔSSH anomalies statistically significantly positively correlate with the following autumn's surface pCO_2 anomalies in both the subtropics

and temperate regions (see Figure 4-2 at lag times of -9 and -10 months), the winter pCO_2 T_{norm} anomalies do not significantly correlate with the following autumn's pCO_2 anomalies in either of these regions. Thus, whilst there are suggestions of a DIC renewal mechanism in response to the large scale oceanic circulation, this cannot be robustly supported given the absence of significant correlations associated with the local scale surface pCO_2 T_{norm} anomalies in winter and the surface pCO_2 anomalies the following autumn (Figure 4-19).

In conclusion, there is a robust link between the winter NAO index and winter surface pCO_2 variability that is most likely due to the effect of variations in vertical DIC entrainment. Thus, mode water formation in winter in both the subtropics and temperate regions is likely to play an important role in winter surface pCO_2 variability.

With respect to the lagged effects of biology and DIC renewal on the surface pCO_2 variability orchestrated through the winter NAO index, the local scale analysis (e.g.. surface pCO_2 T_{norm} anomalies with surface pCO_2 anomalies) does not support the elements of the research hypothesis, as explained.

The following chapter examines how these large-scale atmospheric and oceanic processes affect the inter-annual variability of the surface water pCO_2 in both the subtropics and temperate regions of the North Atlantic.

Chapter 5: Drivers of the inter-annual variability of surface water pCO_2 in the North Atlantic Ocean

5.1 Introduction

The chapter focuses on examining the atmospheric and oceanic circulation processes governing the inter-annual variability of the surface water pCO_2. Correlation analysis was again performed, this time by using the 12-month running mean in order to focus on the inter-annual variability. It should be noted that the first and last 6 months of the running means were not used, since these do not represent a full year of data. As in chapter 4, which discussed the seasonal anomalies of the surface water pCO_2, comparison between the observations and model output was undertaken.

The main findings of this chapter are as follows:

- That the inter-annual variability of atmospheric and oceanic circulation affects the inter-annual surface water pCO_2 variability, throughout the study region.
- That the subtropical regions inter-annual surface water pCO_2 variability is more likely to be influenced by SST and nutrient variability (and less by CHL) in response to the atmospheric and oceanic circulation.
- That the temperate regions inter-annual surface water pCO_2 variability is likely to be affected in a similar manner to the subtropics, but that biology is likely to play a greater role in these regions and will thereby also modulate the inter-annual variability of oceanic pCO_2.

Correlations between the ΔSSH (proxy for ocean circulation) and the surface water pCO_2 were performed, in addition to those of the SST, MLD, pCO_2 normalised to constant SST (proxy for DIC), DIC (model output) and CHL. Given that the NAO index exhibits its strongest signal in winter (Marshall et al. 2001), it was deemed that an analysis of the inter-annual variability of the NAO index on the inter-annual variability of the surface water pCO_2 would not yield representative results. However, the winter NAO index will have an effect on the inter-annual variability of the ocean circulation (see chapter 3 section 3.2.2). Therefore, where relevant, the

winter NAO index will be discussed here in relation to the inter-annual variability of either the related parameters or surface water pCO_2.

In order to demonstrate how the large-scale parameters affect the surface water pCO_2 and the key related parameters in both the subtropics and temperate regions, an analysis of box 1 (subtropics) and box 6 (temperate) will be made. The relevant plots and statistically significant correlations associated with the other boxes can be found in the Appendix (see Figure A-27 to Figure A-41).

5.2 Correlations of related parameters with surface water pCO_2 and of the related parameters and surface water pCO_2 with ΔSSH

5.2.1 Inter-annual variability in the subtropics

Figure 5-1 illustrates that there are statistically significant positive and negative correlations between the ΔSSH and SST and the ΔSSH and CHL respectively for the observations. In addition, the surface pCO_2 statistically significantly anti-correlates with the CHL. The model output however, only reveals a statistically significant positive correlation between the surface pCO_2 and the SST.

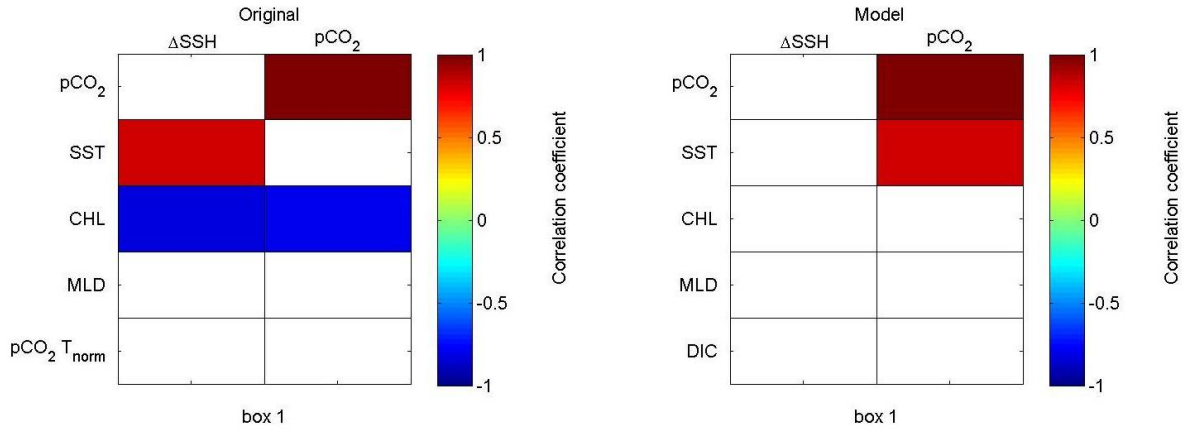

Figure 5-1: Spearman correlation coefficients between the ΔSSH and related parameters (left column) and surface water pCO_2 and related parameters (right column) for the observations (left panel) and model output (right panel) in box 1. Only coloured panels show statistically significant correlations.

This implies that the ΔSSH are likely to affect the inter-annual variability of the SST in the subtropics. This confirms an important element of the research hypothesis

(see Figure 1-9). The model output results suggest that the inter-annual variability of the surface pCO_2 is in turn strongly affected by the SST. This cannot be justified here, however, since there is no observed statistically significant correlation between the surface pCO_2 and SST. Thus, it cannot be firmly concluded that the ΔSSH affects the inter-annual variability of the surface water pCO_2 in the subtropics through SST, as stated in the research hypothesis (section 1.7, and depicted in Figure 1-9), even though there is a ΔSSH – SST link.

Nevertheless, it is evident in Figure 5-2 that the ΔSSH and surface pCO_2 co-vary relatively well between 2002 and 2005 (see the brown and dark blue lines respectively), which constitutes a large fraction of the study time period. Therefore as hypothesised in section 1.6, during high winter NAO events (see brown line in Figure 5-2 during 2002 and early 2003 as well as early 2007, in addition to Figure A-26 for the NAO index) the ΔSSH would increase. In the subtropics (e.g. box 1) this would be manifested as an increase in the SST (see red line in Figure 5-2 during 2002 and from 2006 to 2007). Box 1 is located within the centre of the subtropical gyre, thus when the ΔSSH are high, geostrophic velocities will be low (see section 3.2.1) and advection of water in the centre of the gyre is likely to be low. Therefore, stratification of the water column will be favoured, thereby increasing the SST (see red line) and decreasing the MLD (black line). The surface water pCO_2 would therefore increase in response to the higher SST during this period (i.e. 2002 in particular).

As the mean of the winter NAO index generally declined from 2003/4 to 2005/6 (with the exception of January 2005, see section 3.2.2), the ΔSSH slackened, reducing the degree of stratification and thus decreasing the SST and increasing the MLD in addition to the pCO2 Tnorm (see red line decreasing from 2003 to 2006 and the black line (MLD) and light blue line (pCO2 Tnorm) increasing during this time period). This is consistent with observational evidence at BATS (located only slightly further to the north and west of box 1), whereby neutral or negative NAO events coincide with deeper MLD and cooler SST (Gruber et al. 2002; Bates 2007; Bates 2012). Given that the SST effect usually dominates the surface water pCO_2 in the subtropics (Takahashi et al. 2002; Takahashi et al. 2009; Ullman et al. 2009), there was also a reduction in the surface water pCO_2 (see dark blue line).

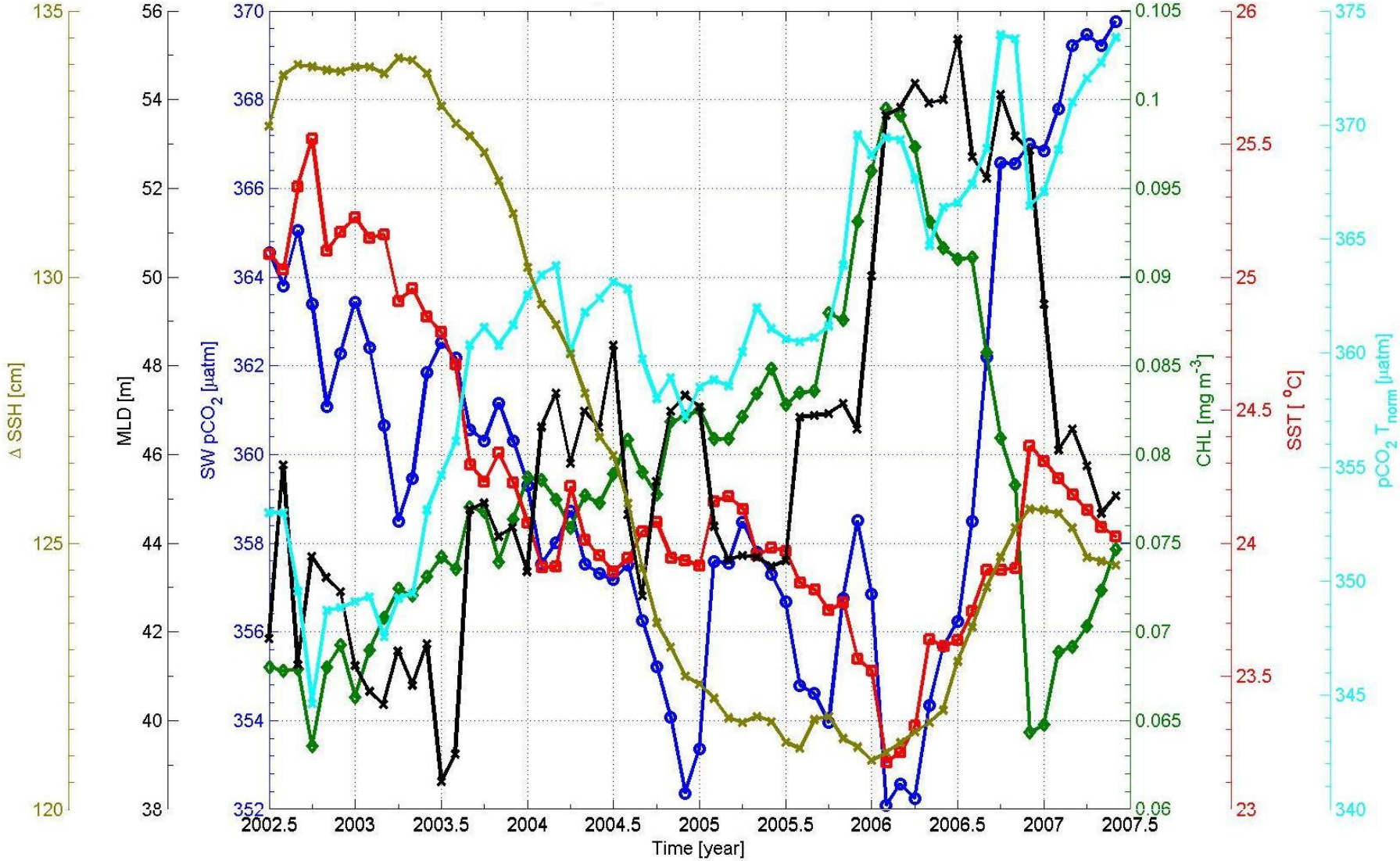

Figure 5-2: 12-month running means of the ΔSSH [cm] (brown), surface water pCO_2 T_{norm} [µatm] (light blue), surface water pCO_2 [µatm] (dark blue), SST [°C] (red), MLD [m] (black), CHL [mg m-3] (green) for the model output in box 1.

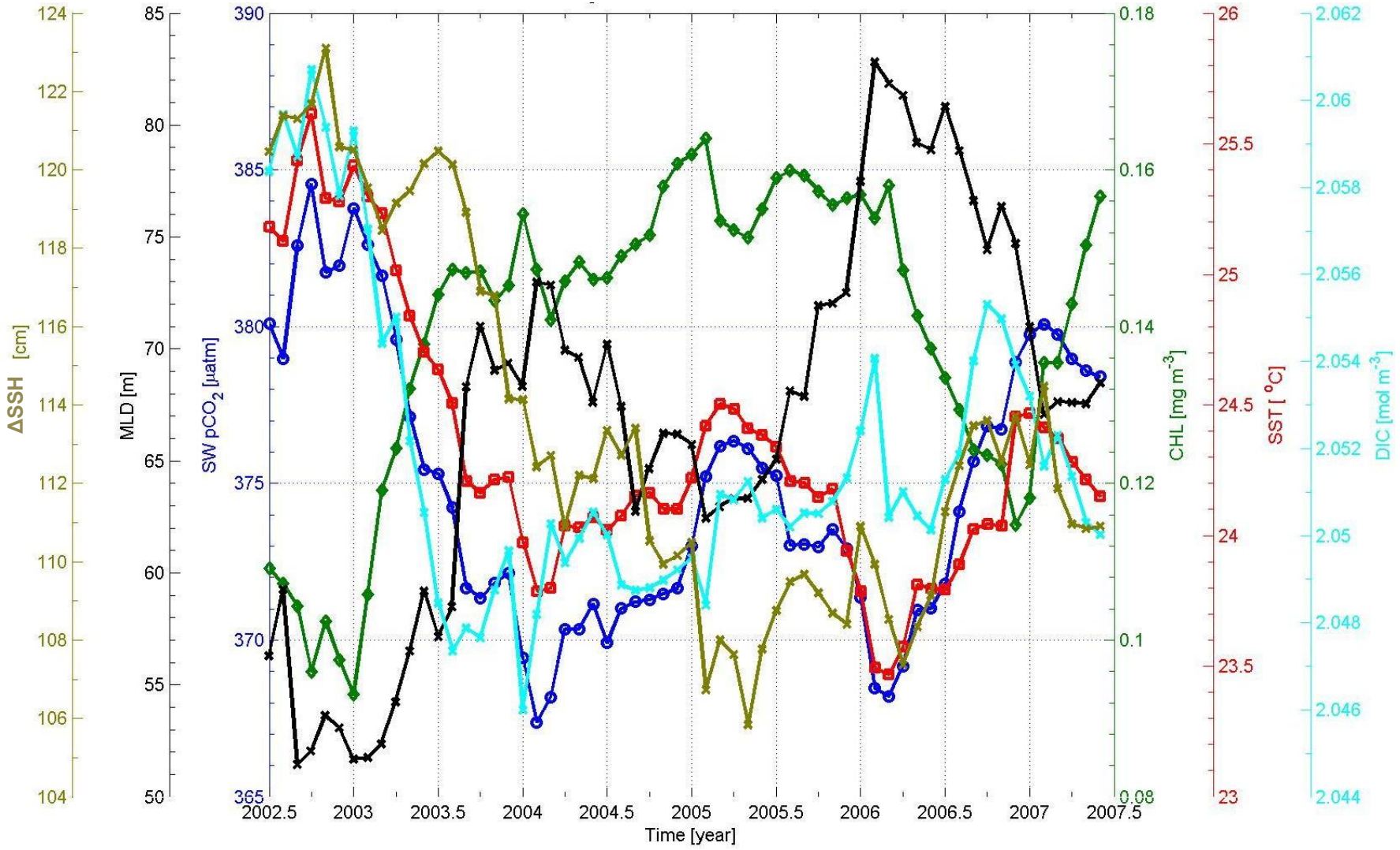

Figure 5-3: 12-month running means of the SSH differences [cm] (brown), DIC [mol m^{-3}] (light blue), surface water pCO_2 [µatm] (dark blue), SST [°C] (red), MLD [m] (black), CHL [mg m^{-3}] (green) for the model output in box 1.

In addition, from 2002 to 2006, there is a steady increase in the CHL concentration (although the magnitude of the absolute concentration is low), which follows the increase in MLD. Apart from the decrease in SST during this time period, the increase in CHL concentration may have also contributed to the decrease in surface water pCO_2, particularly during May 2006, when the highest CHL concentration in this region was reached (see peak in the green line in Figure 5-2, in addition to the low surface pCO_2).

From 2006, the ΔSSH increase once again, reaching a peak in early 2007. Although this is not as strong as in 2002/2003, rather than the MLD decreasing, as might be expected from the increase in SST, the MLD remains relatively high. This may be due to the infiltration of EDW in the region: the winter NAO index reached its highest values in 2006/7, and this may have initiated a meridional shift northwards of the EDW, but still affecting the study region (Levine et al. 2011; Bates 2012). The outcropping area and formation rates of EDW are strongest during positive NAO events (Levine et al. 2011), hence the consideration of this mechanism. The surface water pCO_2 increases dramatically during this period, thus hinting at carbon-rich water entrainment to the surface during this time. The dramatic increase in surface pCO_2 compared to the modest increase in the ΔSSH from 2006 most likely resulted in a reduction of the correlation coefficient between the ΔSSH and surface pCO_2 to insignificant levels, despite the good co-variation between the ΔSSH and surface pCO_2 between 2002 and 2006.

During 2007 itself, the surface water pCO_2 continues to increase and reaches its highest levels of the entire study period. This is due to the higher winter pCO_2 values combined with the typically high summer SST values driving up the pCO_2, which together increase the annual surface water pCO_2.

In terms of the model output, as noted earlier, a statistically significant link between the surface pCO_2 and SST is apparent. As seen in Figure 5-3, this is because both of these variables co-vary throughout the entire study period. Thus the model may be underestimating the potential effect of the EDW mode water infiltration into the subtropics during 2007, thereby enabling the surface pCO_2 (dark blue line) to co-vary well with the SST (red line). The model is thus overestimating the effect of the SST on the inter-annual variability of the surface pCO_2 in the subtropics. This will be further substantiated in section 5.2.3.2, when a comparison between the SST versus non-SST effects is examined for the model output.

5.2.2 Inter-annual variability in the temperate regions

Figure 5-4 illustrates that numerous statistically significant positive and negative correlations are apparent between both the observations and model output with the observations revealing statistically significant positive correlations between the ΔSSH and the CHL and between the surface water pCO_2 and pCO_2 T_{norm}. As explained in section 1.6 and hypothesised in section 1.7 (Figure 1-10), this suggests that when the gyre circulation is active (weak), in response to a positive (negative) winter NAO, increased (decreased) advection of high nutrients into the temperate region would occur thereby fuelling stronger phytoplankton blooms. This therefore confirms an important element of the research hypothesis in the temperate region (see Figure 1-10).

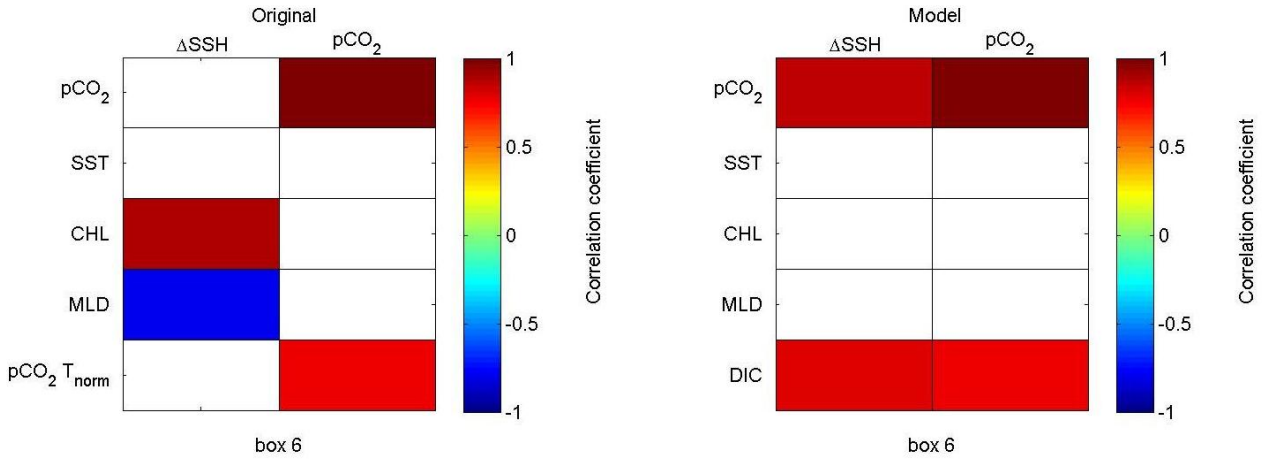

Figure 5-4: Spearman correlation coefficients between the ΔSSH and related parameters (left column) and surface water pCO_2 and related parameters (right column) for the observations (left panel) and model output (right panel) in box 6. Only coloured panels show statistically significant correlations.

However, there is no statistically significant anti-correlation between the ΔSSH and the surface pCO_2. Thus, even though there seems to be an association between the gyre circulation strength and biological activity, over the time period as a whole, this may not affect the inter-annual variability of the surface water pCO_2. Hence, the hypothesis of biological control of the surface pCO_2 on an inter-annual timescale cannot be supported (Figure 1-10).

The model output does not display this ΔSSH – CHL link but instead reveals a statistically significant link between the ΔSSH and the surface pCO_2 in addition to statistically significant positive correlations between the ΔSSH and the DIC.. Possible explanations for these significant correlations will be given later in this section.

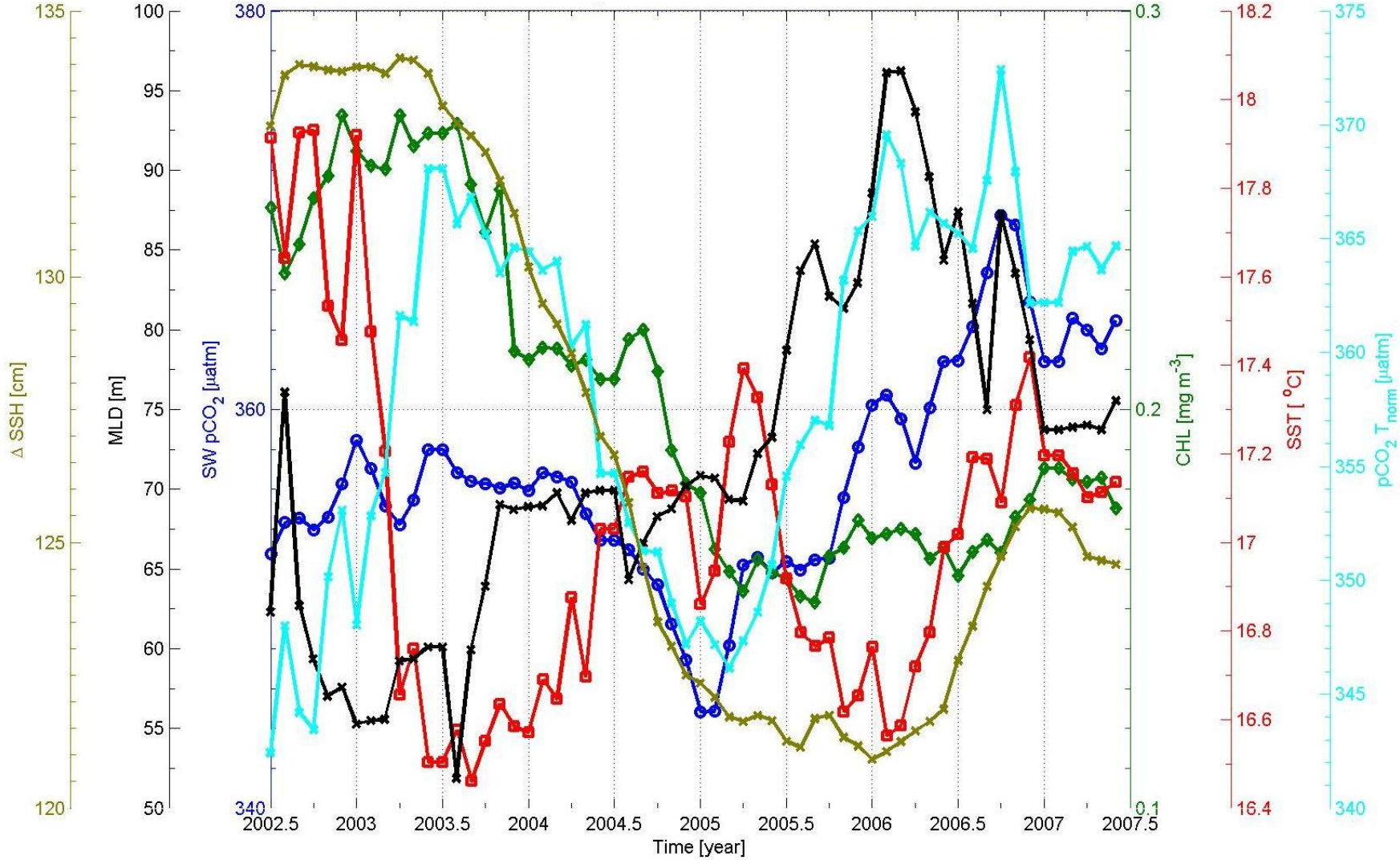

Figure 5-5: 12-month running means of the ΔSSH [cm] (brown), surface water pCO_2 T_{norm} [µatm] (light blue), surface water pCO_2 [µatm] (dark blue), SST [°C] (red), MLD [m] (black), CHL [mg m^{-3}] (green) for the observations in box 6.

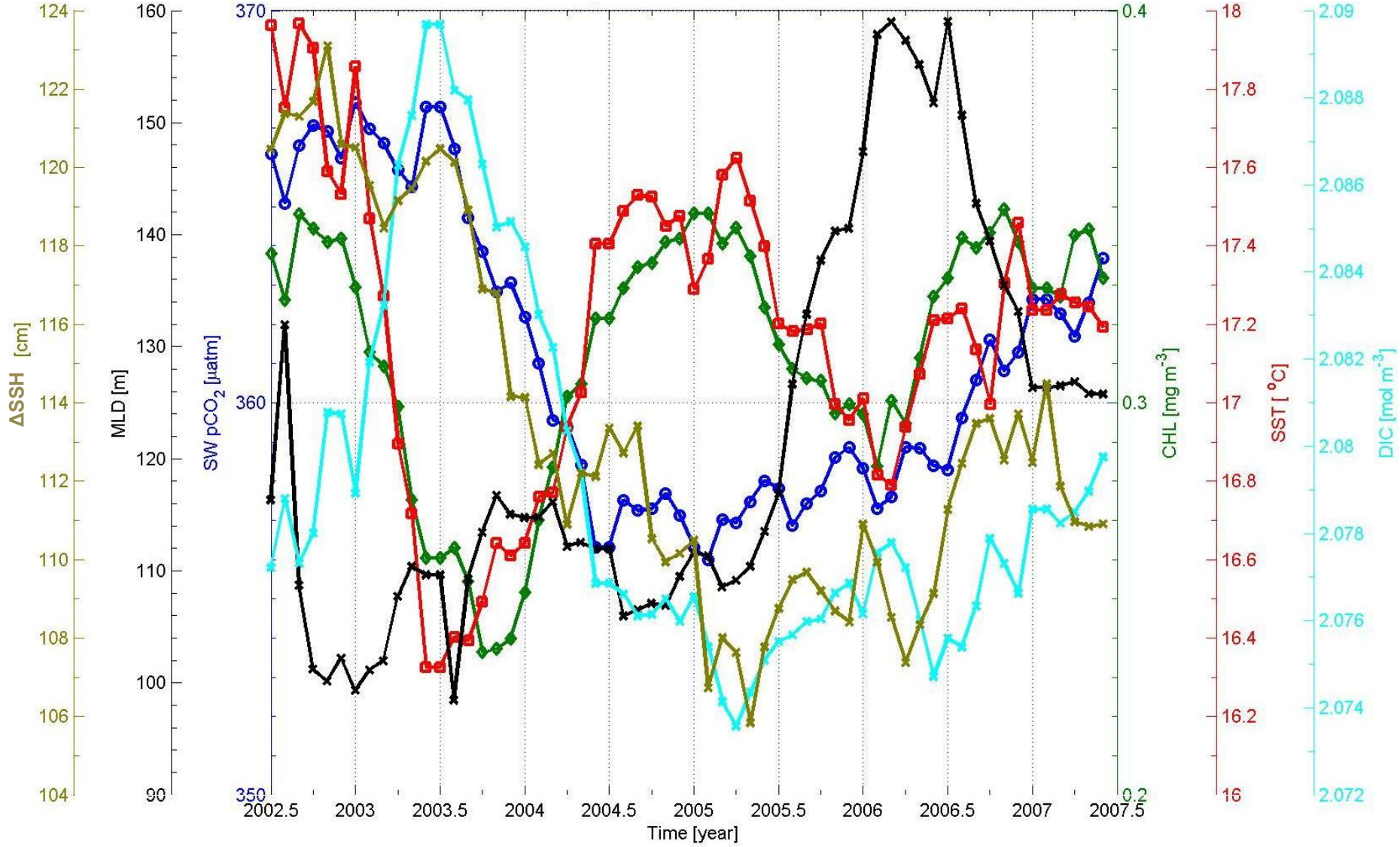

Figure 5-6: 12-month running means of the ΔSSH [cm] (brown), DIC [mol m^{-3}] (light blue), surface water pCO_2 [µatm] (dark blue), SST [°C] (red), MLD [m] (black), CHL [mg m^{-3}] (green) for the model output in box 6.

Figure 5-5, illustrates the patterns discernible in the temperate regions. Unlike the subtropics, the inter-annual co-variability between the surface water pCO2 and the ΔSSH is not robust (comparison of dark blue and brown lines), which is most likely due to the location of the temperate region within the transition zone between the subpolar and subtropical gyres. As described in section 1.6, colder nutrient-rich water masses from the north may infiltrate into this region, but likewise warm, nutrient-poor water from the south may also penetrate (Padin et al. 2011). This may be a reason for the fluctuating SST in the region (see red line), although local atmospheric conditions are also likely to play an important role.

For example, during the winter of 2001/2002, the NAO index was (strongly) positive and hence both the subpolar and subtropical gyres were well spun up. Given that the Icelandic Low would have been stronger than usual (as would the Azores High) during a positive NAO (Marshall et al. 2001), Ekman transport of the cold subpolar waters southward would have occurred (Flatau et al. 2003). In addition, formation of the ENACWp mode waters at ~44°N, -25°E during positive NAO phases has been documented with low SSTs and high nutrient waters in this region (Padin et al. 2011). SSTs during that winter were low in box 6 at ~ 13 - 15°C (see Figure A-2). The effect on the surface water pCO_2 was to maintain relatively high levels during the late winter months of February and March 2002 (~360 µatm) as a result of the formation of the ENACWp mode water entraining carbon-rich subsurface water. Equally, however, the low SST waters that were entrained would have decreased the oceanic pCO_2, highlighting the importance of both the SST and DIC components in driving the pCO_2.

The following summer, the gyre circulation would still be spun-up, since the NAO can affect the ocean circulation for up to 2 years (Curry and McCartney 2001; Flatau et al. 2003). During summer, although the NAO explains a minimum of Sea-Level Pressure (SLP) variability in the North Atlantic, the Azores High maintains its high central pressure and covers much of the North Atlantic (Hurrell and Deser 2009). Thus, the subtropical gyre would expand due to the increased surface convergence of warm waters into the gyre. Given the previous winter's high NAO state and the resulting spin-up of the gyre, which would likely continue for at least another year (Curry and McCartney 2001), the transport of warm subtropical SSTs might have been greater than during a neutral to weakly negative NAO winter. Therefore, summer SSTs would be higher than average during such intense subtropical gyre circulation and consequently increase the annual mean SST in this region; 2002 does show a high SST peak (see Figure 5-5, red line).

However, in these more temperate waters, SST would not dominate over the annual cycle of surface water pCO_2. As seen in Figure 5-5, dark blue line, the oceanic pCO_2 is rather low in

2002. During late spring/early summer, the monthly mean CHL concentration ranged from 0.28 mg m^{-3} to 0.45 mg m^{-3}, likely reducing the surface water pCO_2; the oceanic pCO_2 was ~349 and 339 µatm, respectively (see Figure A-4 and Figure A-1 for the absolute values of the aforementioned parameters).

From 2003 to 2005 there is a decrease in SST, although this is more marked in the summer months than during winter where there are slight increases (see Figure A-2). This slight winter SST increase explains the slight upward trend in the inter-annual SST from 2004 to 2005. Possible reasons are explored in section 5.2.3.1, but in broad terms the inter-annual SST was lower in 2005 than in 2002, which coincides with a weakening of the ΔSSH (red line in Figure 5-5 compared to brown line in Figure 5-5); a decrease in the intensity of the surface circulation during this time period may have reduced the volume of warm subtropical SSTs to penetrate in the region. Consequently, the surface pCO_2 remained low. Thus, the combination of high CHL levels (see green line in Figure 5-5) and lower SST (red line in Figure 5-5), may have accounted for a substantial fraction of the decrease in surface pCO_2 during this period. There is, however, an exception to this, namely the summer of 2005 (specifically July and August), where despite the decrease in ΔSSH, the SST increases (see red line peak in Figure 5-5). Possible reasons are explored in section 5.2.3.1.

It is interesting to note the very close co-variation between the ΔSSH and CHL (green line) in this region; hence, the statistically significant correlation between these two parameters in Figure 5-4, left panel. This suggests that the volume of nutrients and amount of carbon-rich water may be (strongly) related to the ocean circulation, with greater volumes of nutrients and carbon enabling stronger phytoplankton blooms to establish and vice-versa. This will naturally impact on the surface water pCO_2, decreasing it when CHL is high and increasing it when CHL is low. This could be through the aforementioned mechanism of mode water formation, but may also be due to the advection of nutrients from the subpolar regions to the south. In the latter case, deep winter vertical mixing may not be a necessary precursor to nutrient and carbon-rich waters infiltrating the region.

This decoupling between the MLD and ΔSSH is evident between 2003 and 2006, with the ΔSSH declining and the MLD increasing, which explains the statistically significant anti-correlation between the ΔSSH and the MLD (see Figure 5-3, left panel). It is likely that the decline in the winter NAO index between 2003 and 2006 had a significant role to play. As explained in section 1.5, in the western subtropics and temperate region (which would include box 1 and box 6 respectively), the ocean response to a negative NAO phase is a decrease in SST (Hurrell 1995; Marshall et al. 2001). This is visible in the data with a decline

in the SST between 2003 and 2006 (see red line in both Figure 5-2 and Figure 5-5). There is also a reduction in the strength of the gyre circulation (see decline in the ΔSSH – brown line in Figure 5-5). However, this decrease in SST is likely to initiate deeper vertical mixing through stronger surface cooling (Visbeck et al. 2003). Thus from 2003 to 2006, it is highly likely that the decline in SST through the decline in winter NAO index caused the MLD to steadily increase from 2003 to 2006. Thus, mode water formation may not account for the rise in MLD during this time period (see black line in Figure 5-5).

This is also likely to imply that the co-variation of the CHL with the ΔSSH during 2003 to 2006 may be due to Ekman transport of higher nutrient, carbon rich water moving southwards as a direct response to the oceanic circulation strength (Flatau et al. 2003). However, it remains unclear to what extent the advection of cold, nutrient rich water affected the MLD during 2002 and 2007 in comparison to mode water formation. This is because the ΔSSH and thus surface circulation were relatively high during these two years and so were the MLDs (particularly during 2007). Thus, it may be that both mode water formation (with its inherent high MLD, nutrients and carbon-rich subsurface water) and advection of nutrients and higher DIC affected the surface pCO_2, although it remains unknown as to whether one mechanism dominated over the other during 2002 and 2007.

In terms of the model output, there is a statistically significant positive correlation between the ΔSSH and the surface pCO_2 (see Figure 5-4, right panel). However, this cannot be attributed to the effect of SST on the surface pCO_2, since neither the ΔSSH nor the surface pCO_2 reveal statistically significant positive correlations with the SST (see Figure 5-4, right panel). Thus, the model output is able to capture other factors that may have an equal if not stronger effect on the surface pCO_2 than the SST.

For example, during 2002, the ΔSSH alongside SST and surface pCO_2 start high. Hence, the surface pCO_2 is likely to be dominated by the SST effect. Interestingly, the CHL levels are also high, yet the surface pCO_2 remains high. As described in section 3.3.2.4, the timing of the phytoplankton bloom in the model is incorrect, peaking at the same time as the SST (i.e. during summer). Hence, the net effect of biology on the surface pCO_2 in the model is likely to be negligible. The fact that the mean seasonal cycle of the modelled DIC peaks in spring (see Figure A-23), and that of the CHL peaks in summer (see Figure 3-12), 'enables' the surface pCO_2 to remain relatively high in spring in this region, given that the highest CHL signal is simulated in summer. This would therefore explain why, in the model, the peak in DIC (discernible during spring 2003 – see light blue line in Figure 5-6, in addition to Figure A-11), results in higher surface pCO_2 in the model than the observations. However, it should

be noted that the model simulates a greater contribution of the DIC to the surface pCO_2 than the SST during this time period with a large dip in the SST during early 2003 (see red line in Figure 5-6). Therefore, the model is correct in predicting higher DIC contributions on the surface pCO_2 than in the subtropics.

Thus, as described for the observations, in this more temperate region, the ΔSSH variability is likely to cause both cold(er) and warm(er) waters to become established throughout the region. The colder waters are more likely to occur when the ΔSSH is decreasing, reducing the volume of warm subtropical waters infiltrating the region (e.g. during 2003). Warmer waters conversely are likely to manifest themselves during periods of higher ΔSSH, such as 2002 or 2006. However, given the location of this region in the transition zone between the subpolar and subtropical gyres, it could be that both colder and warmer waters infiltrate the region simultaneously. This would explain why the co-variability between the SST and ΔSSH is not as evident as in the temperate regions. Furthermore, local atmospheric variations are also likely to play a role here, as will be explained in section 5.2.3.1. Consequently, the SST in response to the ΔSSH will not be as good a predictor of the inter-annual variability of the surface pCO_2 as it would be in the subtropics. This then explains the absence of statistically significant positive correlations between the ΔSSH and the SST.

The significant positive correlations between the ΔSSH and the DIC, on the other hand, demonstrate the importance of the DIC in this region on the inter-annual variability of the surface pCO_2. However, it should also be noted that the DIC effect is unlikely to dominate the inter-annual variability over the whole time period, just as the SST effect is also unlikely to do so. A comparison between the SST and non-SST effects will be given in the following section for both observations and model output.

5.2.3 Contributions of SST versus non-SST effects to the inter-annual variability of surface pCO_2

5.2.3.1 Observations

Figure 5-7 displays the surface pCO_2, pCO_2 T_{norm} and pCO_2 T components of the surface pCO_2 for all boxes. However, only boxes 1 and 6 will be focused upon, given that these are considered to represent the subtropical and temperate regions.

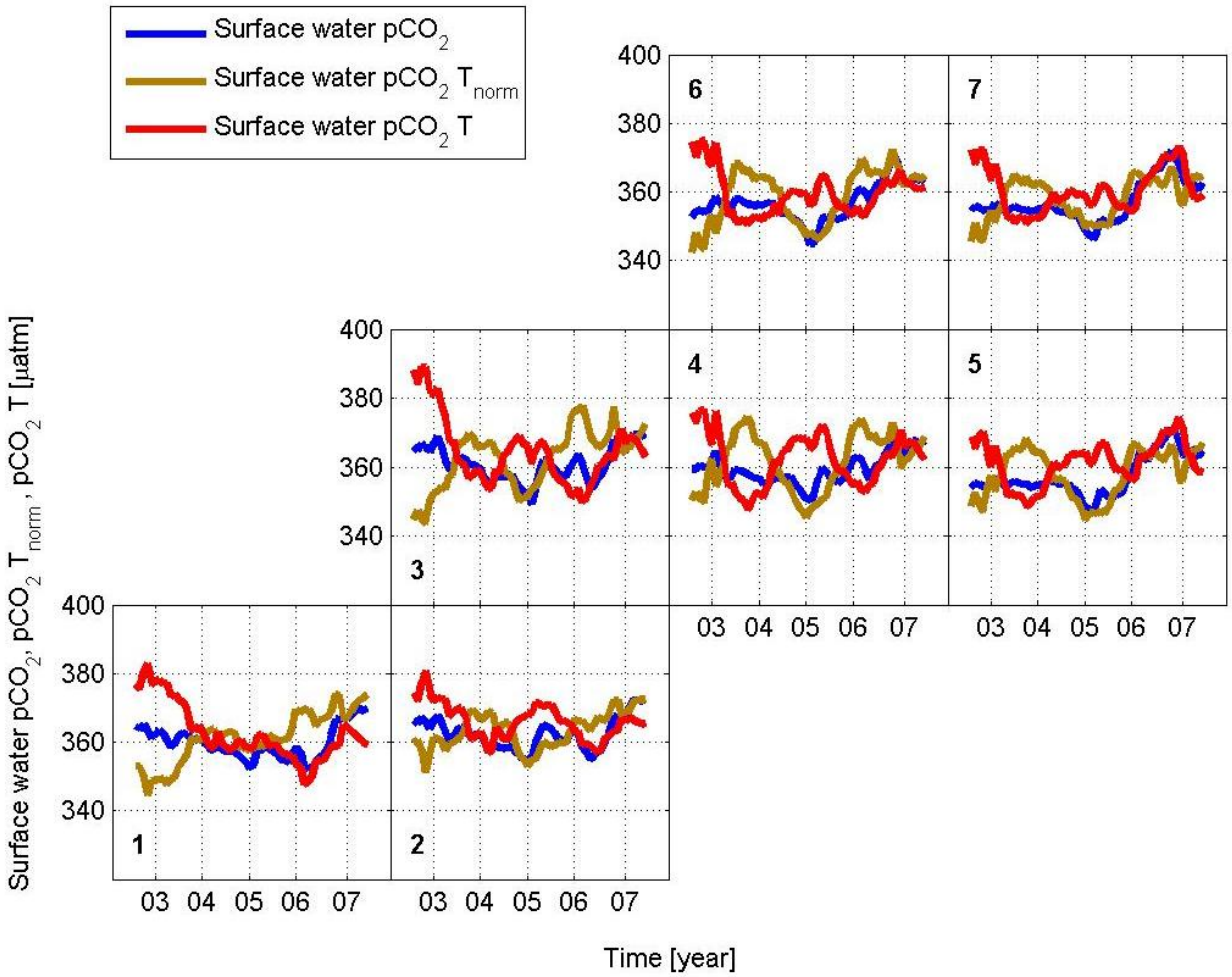

Figure 5-7: Inter-annual variability of the surface pCO_2, pCO_2 T_{norm} and pCO_2 T throughout the study region.

In the subtropics (box 1), during 2002, the surface pCO_2 starts off at ~ 365 µatm and decreases to ~ 360 µatm. The pCO_2 T_{norm} begins at ~ 355 µatm and declines to ~ 345 µatm. The pCO_2 T starts off at ~375 µatm and increases slightly to ~ 380 µatm. In winter and during early 2002, high surface pCO_2 T_{norm} is evident in this region with the absolute pCO_2 T_{norm} reaching ~430 µatm; in contrast, the pCO_2 T is ~310 µatm and surface water pCO_2 is between 350 and 370 µatm. Thus, low SST water will decrease the surface water pCO_2, whilst DIC entrainment from the depths will increase the surface water pCO_2. The net effect is a balance between the SST versus non-SST effect, with both the pCO_2 T_{norm} and pCO_2 T influencing the surface pCO_2 in approximately equal measures (see box 1, Figure A-7).

The peak pCO_2 T_{norm} is observed in winter with a large decrease in the summer pCO_2 T_{norm} component due to the peak in SST which results in high pCO_2 T values (see Figure A-6). This is the reason for the low annual pCO_2 T_{norm} and the high annual pCO_2 T during 2002.

However, if the SST effect would dominate entirely, the surface pCO_2 would be closer to the pCO_2 T (compare dark blue line with red line, respectively) in 2002. The fact that the surface pCO_2 is not as close to the pCO_2 T is evidence that DIC entrainment is an important contributor to the surface pCO_2 in the subtropics, as also discussed section 4.4.3.

From 2003 to 2005 inclusive, the surface pCO_2 decreases (see dark blue line in Figure 5-7); the pCO_2 T also decreases, whereas that of the pCO_2 T_{norm} increases. The decrease in the pCO_2 T is due to a decrease in the late winter pCO_2 T values (especially early 2003 and early 2006) as a result of lower winter SSTs during those two winters (see Figure A-6 and Figure A-2). However, the summer SST also decreased slightly from 2003 to 2004 (see Figure A-2), contributing to the decline in the pCO_2 T between 2003 and 2005. This decrease in both winter and summer SST is consistent with the supposition that a weaker subtropical gyre circulation would decrease the transport of warm subtropical water to the region, as previously explained in section 5.2.1. Consequently, the pCO_2 T_{norm} would have increased during the same time period (since cold waters would be richer in DIC than warmer waters). However, given that the surface pCO_2 decreased during this time in tandem with the pCO_2 T, it can be concluded that the net effect on the surface pCO_2 was the SST.

From 2006 to 2007 inclusive, the surface pCO_2 increases once more (see dark blue line in Figure 5-7, box 1). In this instance, however, the pCO_2 T_{norm} increases as well. This is due to the winter pCO_2 T_{norm} component increasing during this time (see Figure A-5). During 2006, the pCO_2 T component also increases and this is due to the summer increase of the pCO_2 T in 2006; the SST was slightly higher that summer (see Figure A-6 and Figure A-2). During 2007, however, there is a decrease in the pCO_2 T component, owing to a decline in the summer SST (see Figure A-6 and Figure A-2) during this time period. Thus once again, the SST follows the pattern of increasing ΔSSH during 2006 and decreasing ΔSSH during 2007; refer to Figure 5-2 for the inter-annual variability of the ΔSSH. Hence warmer (cooler) water will be transported to the region during stronger (weaker) subtropical gyre circulation, as already mentioned.

In the temperate regions, box 6 in this case, during 2002, the surface water pCO_2 remains at a lower level than in the subtropics; ranging from 355 to 360 µatm. During early 2002, as in the subtropics, the pCO_2 T_{norm} component was high indicative of DIC entrainment through deeper vertical mixing (see Figure A-5 and Figure A-3). The surface pCO_2 reached ~ 350 µatm thereby hinting at the decreasing effect on the surface pCO_2 of the low SST water in addition to the increasing effect of the DIC entrainment on the surface pCO_2.

During spring in this region, the nutrients entrained to the surface the previous winter will be used up by biology. The low absolute pCO_2 (see Figure A-1) in addition to the high CHL concentration (see Figure A-4) in April 2002, for example, is testament to this claim; hence the closer co-variability between the surface pCO_2 and pCO_2 T_{norm} in this region during 2002.

Between 2002 and 2004, there is a decline in the summer SST (see Figure A-2) and consequently the pCO_2 T component also decreases during this time (see box 6, Figure 5-7). As a result, the pCO_2 T_{norm} component increases (since the summer pCO_2 T_{norm} increases – see Figure A-5). Thus, in the temperate regions a decrease in the subtropical gyre circulation would reduce the volume of warm subtropical water that penetrates into the region.

However, it is also important to note that the local atmospheric conditions may also impinge on the SST. For example, between summer 2002 and summer 2004, there is a notable decrease in the SST (see Figure A-2), which contributed to the substantial decline in the inter-annual SST (see the marked decline of the red line in Figure 5-5). Although the NAO index is most active during the winter months (Marshall et al. 2001), the NAO climate mode is evident throughout the whole year (Barnston and Livezey 1987).

During the summer months, the Azores High pressure system strengthens and drifts northwards (Hurrell and Deser 2009). However, variations to the strength and northward extent of the Azores High do occur, and this has led some scholars to define a summer NAO (Folland et al. 2009). During summer 2002, specifically July and August, the NAO index was weakly negative (see Figure A-26). Although weakly negative NAO indices imply a southerly shift in the North Atlantic storm track (Marshall et al. 2001), this is mostly applicable to the winter season and thus may not automatically imply lower summer SST. Thus, during summer, a weak negative NAO may still result in high summer SST in the temperate region. This may arise from a more frequent incidence of above average sea-level pressure in the mid Atlantic also known as mid-Atlantic blocking and covering the temperate region (e.g. box 6). Figure 1c, right panel in Folland et al. (2009), depict a typical negative summer NAO set-up, and although the negative sea-level pressure anomalies extend into the study region, it is possible that the Azores High during July and August of 2002 exhibited a more meridional orientation (i.e. mid-Atlantic blocking). This could have explained the high summer SST in summer 2002, in addition to the strong surface circulation that would have transported high-SST subtropical water to the region.

The decline in summer SST in 2003 may have been brought about by a decrease in the occurrence of mid-Atlantic blocking. The NAO index was just as negative in August 2003 as it was the previous year (see Figure A-26), however, given the lower summer SST, it is plausible that in addition to a decrease in the gyre circulation (transporting less high-SST water to the region, a sea-level pressure set-up as described in Folland et al. (2009)), Figure 1c right panel became established with a southerly shift in the North Atlantic storm track. Thus, cooler, cloudier conditions would have increased in frequency during that time and may therefore (in combination with the decline in ΔSSH) explain the dramatic decrease of the inter-annual SST in the region during 2003 (see Figure 5-5). Given the deviation between the ΔSSH and the SST during this time period (although both are decreasing), the above mechanism may have explained the additional decrease in SST.

A similar mechanism may also have contributed to the decline in summer SST between 2003 and 2004 in this region (see Figure A-2), in addition to the continuing decline in gyre circulation strength (the ΔSSH declined as well – see brown line in Figure 5-5) albeit with stronger negative sea-level pressure anomalies in the study region more likely. However, the inter-annual SST actually increases (see red line during the latter part of 2003 into 2004, Figure 5-5). On closer inspection, this is due to the winter SST increase from 2002 to 2004 (see Figure A-2). A possible explanation for the winter SST increase during this period is that the formation of subpolar mode water, in response to a decline in the winter NAO index, decreased. Thus, low SST from further north would not have affected the study region as much, but rather local SST would have had more of an influence.

In addition, during the summer of 2005, and particularly August, even though the subtropical gyre circulation was decreasing (i.e. the ΔSSH – see Figure 5-5), the SST actually increased in this region. Thus, in this instance, it may be that higher sea-level pressure was present which would have led to reduced cloud-cover and hence higher SST. Therefore a pressure pattern depicted in Figure 1c, left panel in Folland et al. (2009) may have occurred. From 2006 to 2007, the increase in summer SST follows the increase in ΔSSH (see red line and brown line in Figure 5-5, respectively) thereby implying that the gyre circulation strength was more important during these years than in 2003 to 2005 in explaining inter-annual SST variability.

The above mechanism would explain the peak in the pCO_2 T observed during 2005 in this box (see Figure A-6). The surface water pCO_2 during 2005 only displays a modest increase due to the previous winter's low surface pCO_2 with the pCO_2 T_{norm} having reached its lowest point during the winter of 2004/5 (see Figure A-5), indicative of a greater SST effect,

resulting in a net decrease of the surface pCO_2. Even though the summer of 2005 exhibited the highest pCO_2 peak of the study period, this could not override the low winter pCO_2. From 2005 to 2006 inclusive, the surface water pCO_2 increases once again. This is due to an increase in DIC entrainment in the winter of 2005/6 (the pCO_2 T_{norm} increases relative to the previous winter – see Figure A-5) due to an increase in the MLD (see Figure A-3). In addition, the summer SST remains at a similar level to that of 2005 (see Figure A-2), thereby maintaining relatively high surface pCO_2, although not as high as during 2005. It is unclear as to why the surface pCO_2 during the summer of 2006 is less than that of the previous summer even though the SST remained at a similar level (i.e. ~22°C).

However, over the course of a year, it is clear that 2005 exhibited lower surface pCO_2 than 2006, and this is likely to be indicative of the effect of a negative NAO index (particularly during February and March 2005), decreasing the SST and hence the surface pCO_2 in early in 2005. Figure A-5 reveals that the absolute pCO_2 T_{norm} during early 2005 was the lowest of the entire study period, implying a greater SST effect on the surface pCO_2 at that time. The fact that the ΔSSH (i.e. gyre circulation) was weaker during 2005 than 2006 may also have reduced the transport of warm subtropical waters into the study region, particularly outside of the summer season when local atmospheric dynamics are likely to have been more important, as explained previously. However, the close co-variability between the ΔSSH and the SST during 2006 and early 2007 in addition to 2002 and early 2003 suggest that advection of subtropical waters into the temperate region is an important process that would affect the inter-annual variability of the surface water pCO_2 in this region.

During the winter of 2006/7, the MLD reached its deepest levels of the entire study period in this region (~280 m in January – see Figure A-3). Consequently, DIC entrainment also increased (see the pCO_2 T_{norm} (brown peak) just prior to 2007 in Figure 5-7 and the absolute pCO_2 T_{norm} during January to March 2007 in Figure A-5). Even though low SST water would have also been entrained to the surface, there was a net increase in the surface water pCO_2 (see blue line in Figure 5-7 and the absolute pCO_2 in January to March 2007 in Figure A-1).

The decline in surface pCO_2 during 2007 was a result of a strong phytoplankton bloom that occurred during April and May 2007, most likely due to the high volume of DIC entrained to the surface the previous winter (see Figure A-1). Although the CHL concentration was not as high during spring 2007 as spring 2003, the greater availability of nutrients and DIC (the pCO_2 T_{norm} is the highest of the entire study period, see Figure A-5) may have enabled the phytoplankton to photosynthesise more effectively, hence reducing the surface pCO_2 to one of its lowest concentrations of the study period in this region.

The following section discusses the findings of the model output's SST versus non-SST contributions on the inter-annual variability of the surface water pCO_2.

5.2.3.2 Model output

Figure 5-8 illustrates the contribution of the SST versus non-SST effects on the modelled surface pCO_2. As with the observations only boxes 1 and 6 will be focused upon.

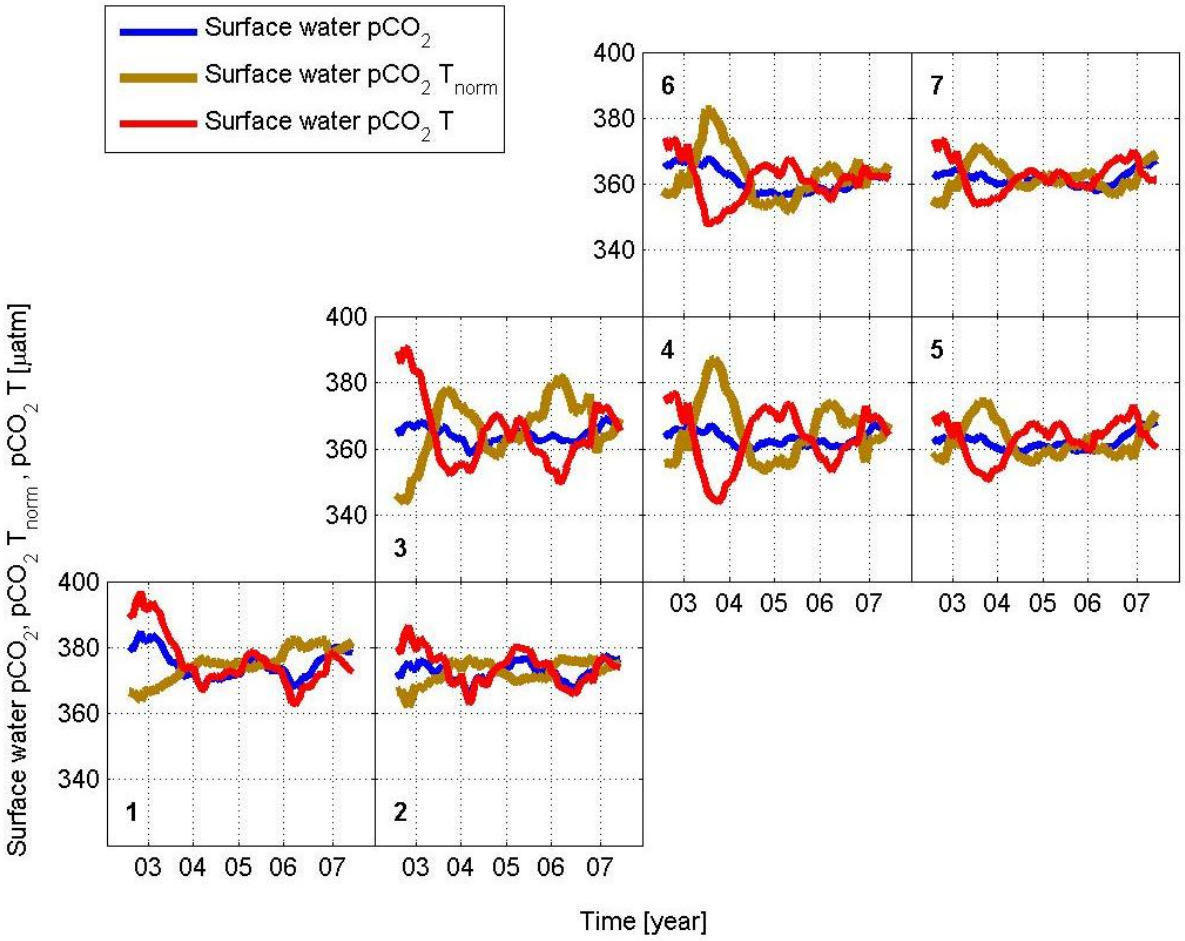

Figure 5-8: Inter-annual variability of the surface pCO_2, pCO_2 T_{norm} and pCO_2 throughout the study region for the model output.

Box 1 displays significant co-variability between the surface pCO_2 (blue line) and the surface water pCO_2 T (red line). This is further evidence of the model output's over-reliance on the SST effect on the surface water pCO_2 variability in the subtropics. Thus, changes in the ocean circulation strength are likely to affect the surface water pCO_2, primarily via SST, as discussed in section 5.2.1. This does not exclude DIC entrainment occurring during the

winter months, but the low SST water is likely to have a net decreasing effect on the surface pCO_2 during this season, as discussed in section 5.2.1 and section 3.3.2.4. Thus the processes described in section 5.2.1, with respect to the observations in the subtropics, also occurs in the model and will not be repeated here. The difference between model and observations is the degree to which the pCO_2 T (and hence SST) affects the inter-annual variability of the surface pCO_2 (e.g. compare box 1, Figure 5-8 with box 1, Figure 5-7).

In terms of the temperate regions, the model output reveals a greater dependency on non-SST effects (e.g. DIC entrainment) on the surface pCO_2 than in the subtropics, as illustrated by the differences between the blue line (surface pCO_2) and red line (pCO_2 T) in box 6 (Figure 5-8). Thus, as discussed in section 5.2.2, the model is in relatively good agreement with the observations as to the driving mechanisms of surface water pCO_2 variability in this region. However, although the model is successful in attributing non-SST factors to pCO_2 variability in the temperate region, it is unable to resolve the timing of the phytoplankton bloom, as also discussed in section 5.2.1, and section 3.3.2.4.

5.3 Summary

In the subtropics, it has been shown that on inter-annual timescales, the ΔSSH affect the inter-annual variability of the SST. The absence of a statistically significant positive correlation between the ΔSSH and the surface water pCO_2 suggests that the SST control on the surface pCO_2 may not be as significant as hypothesised. As explained in this chapter, it should be noted that good co-variation between the ΔSSH and the surface pCO_2 is evident for most of the time period (2002 to 2006), with 2007 exhibiting the largest differences. Thus, it is possible that with further data, significant links between the ΔSSH and the inter-annual variability of the surface pCO_2 could still be found, which are likely to relate to inter-annual SST variability. The model output agrees well with the observations with respect to the SST dominance of the surface water pCO_2 variability in the subtropics, although it over-estimates this SST effect. Other non-SST effects such as winter DIC entrainment also occur in the model, but this does not dominate the inter-annual surface water pCO_2 variability. The observations reveal that even in the subtropics, DIC entrainment is likely to impact upon the surface pCO_2 as illustrated by similar absolute differences between the surface pCO_2 and pCO_2 T_{norm} and pCO_2 T. The model output reveals a greater difference between the absolute pCO_2 and surface pCO_2 T_{norm}, compared to the surface pCO_2 T, highlighting the over-reliance of the SST effect on the pCO_2.

In the temperate regions, the SST dominance is reduced (but is still important) and winter DIC entrainment, spring biological activity in combination with summer SST, are all likely to play a part in regulating the inter-annual variability of the surface water pCO_2. However, given the absence of a statistically significant correlation between the ΔSSH and the surface water pCO_2, this needs to be treated with caution. This is likely to be orchestrated through the ocean circulation (ΔSSH) in response to the winter NAO index impacting on all of these variables at certain key times of the year. It has also been shown that in certain years, the NAO index may exert an influence on the surface pCO_2 during the summer (through SST changes) which may override the ocean circulation effect. Thus, the net effect on the surface water pCO_2 is likely to depend on the strength of each of these different variables. In some years, this is mostly dominated by the interplay between winter DIC entrainment and spring biology with summer SST not as important (e.g. 2002 to 2004), whilst in other years, a combination of all three can be of vital importance to dictating the inter-annual variability of the surface water pCO_2 (e.g. 2005 to 2007).

The temperate region variability is likely to be orchestrated through a combination of atmospheric and ocean processes. For example, during the winter periods of 2002, 2003 and 2007, a strong oceanic circulation may have induced subpolar mode water to be advected south into the region, thereby increasing the contribution of DIC entrainment on the surface pCO_2 and nutrient entrainment on biology. This may have enabled strong(er) phytoplankton blooms to occur the following spring, decreasing the surface pCO_2. In addition, a decreasing surface circulation during 2003 to 2005 would have contributed to a decline in SST and thus maintained low(er) surface pCO_2 in combination with the higher CHL in spring.

Furthermore, the winter NAO index declined during this time period (2003 to early 2006), which aided in the formation of deeper winter mixed layers. The storm track of Atlantic pressure systems shifts south during a negative NAO, hence there would have been an increase in the MLD. It should be noted that although the MLD increased this was not as deep as during early 2002 or 2003 when subpolar mode water formation likely took place with inherently deeper mixed layers. This also explains the slight increase in SST between the winters of 2003 and 2004; mode water SST would be colder than local SST. Initially, this MLD increase would have decreased the surface pCO_2 through cold water entrainment but as the MLD became deeper, the DIC entrainment would have counteracted the low SST water effect and aided in the modest increase in surface pCO_2 during early 2006. This seasonal forcing would impact upon the inter-annual variability of the surface pCO_2 however, through the combined effect of the SST, DIC and CHL on the surface pCO_2.

In general, the model output agrees with the observations on the importance of the inter-play between the SST, DIC and CHL in dictating the inter-annual variability of the surface water pCO_2 through the ocean circulation (i.e. ΔSSH). However, it over-estimates the SST effect in the subtropics. In the temperate regions, the model simulates phytoplankton blooms in the autumn, with no or very limited biological activity during the spring. This is in stark contrast to the observations. Furthermore, the model simulates high DIC concentrations in spring, but with no CHL peak at that time. In reality, high nutrient concentrations in spring correspond closely to peak CHL events (thus enabling the spring bloom to take place) and thus reduce surface pCO_2 by decreasing the DIC. This sometimes results in a model over-estimation of the SST effect on the surface water pCO_2 in spring.

Chapter 6: Conclusions and future research

6.1 Conclusions

The conclusions relating to this research are stated with respect to the seasonal anomalies of surface water pCO_2 (section 6.1.1) and the inter-annual variability of surface water pCO_2 (section 6.1.2). Recommendations for future work are outlined in section 6.2.

6.1.1 Seasonal surface water pCO_2 anomalies

Cross-correlation analysis has shown that a statistically significant positive relationship exists between the winter NAO index and the winter surface water pCO_2 anomalies in both the subtropics and temperate regions of the North Atlantic Ocean. Thus, the large-scale atmospheric circulation is likely to affect the winter surface water pCO_2 variability. The close co-variability between the winter NAO index and the winter ΔSSH illustrates that the large-scale oceanic circulation responds instantaneously to the atmospheric forcing and with positive sign (see Figure 3-3, chapter 3).

The mechanisms driving the surface water pCO_2 anomalies in the study region have been found to vary according to the sign of the winter NAO index. During positive NAO winters, stronger surface cooling in the northern subtropics in addition to the subpolar region will aid in the formation of mode waters through intense convective mixing. The deep MLD characteristic of these waters will penetrate these regions, causing high-DIC subsurface waters to be entrained to the surface, resulting in positive winter pCO_2 anomalies. As such, this research has shown that mode water formation is likely to play an important role in dictating the seasonal anomalies of surface water pCO_2 under positive NAO conditions in both the subtropical and temperate regions of the North Atlantic.

During negative NAO winters, surface cooling would be less extensive in the aforementioned regions, resulting in a reduction of the winter MLD. However, given that the North Atlantic storm track shifts south during negative NAO winters (Hurrell 1995), the depth of the winter mixed layer will still be relatively deep. The entrainment of high-DIC waters would still occur but not as extensively in comparison to the high winter NAO phase. Thus, compared to the positive winter NAO phase, the surface pCO_2 will decrease as a result of a reduction in the entrainment of high DIC waters to the surface. In addition, although surface cooling would be

less extensive compared to a positive winter NAO phase, the reduction in entrainment of high DIC waters would also enable the surface cooling to decrease the surface pCO_2.

Although it would be expected that a relationship between the winter NAO index and the following spring and early summer surface pCO_2 is evident (through vertical variations in DIC and nutrient entrainment), particularly in the temperate regions, there is insufficient evidence in this thesis to confirm that this is the case: a significant anti-correlation between the winter NAO index and the following spring surface pCO_2 anomalies was found. This was not supported by a statistically significant anti-correlation between the previous winter's pCO_2 T_{norm} anomalies (a proxy for DIC) and the following spring pCO_2 anomalies, however. Thus, this element of the research hypothesis cannot be justified for either the subtropics (Figure 1-9) or for the temperate region (Figure 1-10).

In addition, statistically significant positive correlations were found between the winter ΔSSH anomalies and the following autumn pCO_2 anomalies in both the subtropics and temperate regions. However, this was not supported by a statistically significant positive correlation between the previous winter's pCO_2 T_{norm} anomalies and the following autumn pCO_2 anomalies. Thus, whilst there is some evidence that may point towards a DIC renewal mechanism in the temperate region, this element of the research hypothesis also cannot be confirmed.

The model output that was used to compare the observations to shows broadly similar significant relationships (e.g. the statistically significant anti-correlations in the temperate regions between the winter NAO index and the winter SST). This is highly encouraging given that the model is forced with atmospheric physics which will mechanistically affect the calculation of the surface water pCO_2.

6.1.2 Inter-annual surface water pCO_2 variability

On longer time-scales, the effect of the winter NAO index clearly manifests itself onto the inter-annual variability of the ΔSSH, with a positive (negative) winter NAO index giving rise to higher (lower) ΔSSH. Since the ocean exhibits a large specific heat capacity, the ΔSSH can be used to establish the longer-term changes to the spin-up/down of the gyre circulation in the North Atlantic. As such, this forms another vital driver of surface water pCO_2 variability.

This research has determined that statistically significant relationships between the ΔSSH and SST are evident in the subtropics in relation to the observations. The model output reveals statistically significant relationships between the surface pCO_2 and SST in this region. Thus the model hints that the inter-annual variability of the surface water pCO_2 is SST driven in the subtropics. The observations reveal the importance of the gyre circulation in dictating the SST in this region and, as seen in chapter 5, this is observed to impact upon the inter-annual variability of the surface pCO_2 throughout much of the time period. However, given that there are (significant) differences between the ΔSSH and surface pCO_2 during 2007, this does not result in a statistically significant correlation between the ΔSSH and surface pCO_2. Thus, for the time period as a whole, this means that the research hypothesis of large-scale oceanic circulation control of the inter-annual variability of the surface pCO_2 in the subtropics through SST cannot be confirmed.

Conversely, in the temperate regions, statistically significant positive correlations between the ΔSSH and CHL have been found. Thus, the inter-annual variability of the surface water pCO_2 may be controlled by advection of high-DIC and nutrient waters from the subpolar region. However, the absence of statistically significant anti-correlations between the ΔSSH and surface water pCO_2 does not support the research hypothesis of biological control of the surface pCO_2 in this region (i.e. higher surface pCO_2 when biological activity is low and lower surface pCO_2 when biological activity is high). As already explained in chapter 5, in this region other processes are also likely to have an effect on the surface pCO_2, such as summer SST and winter DIC entrainment, which on an inter-annual timescale may well dampen the biological effect.

The model output does not reveal a significant link between the ΔSSH and CHL. This is likely to stem from its inability to simulate the timing of the phytoplankton bloom as discussed in chapter 3 and chapter 5.

Furthermore it has been pointed out that, although the oceanic circulation dominates on an inter-annual time period, local atmospheric forcing in summer may also affect the summer SST and thereby the summer pCO_2 within the temperate regions specifically. This may in turn influence the inter-annual variability of the surface water pCO_2, depending on the strength of this atmospheric forcing.

6.2 Recommendations for future work

Under future climate change, temperatures are set to rise between 1.1 to 6.4°C by the end of 2100 (IPCC 2007). How the marine carbon cycle and ocean circulation will respond to this increase needs to be understood so that better estimates of the oceanic sink for atmospheric CO_2 can be determined.

Coupled climate models forced by increased atmospheric CO_2 in the twenty-first century simulate a significant warming of the ocean surface (IPCC 2001). This, in turn could result in an enhanced stratification of the ocean, particularly at mid-to-high latitudes in both hemispheres (Sarmiento et al. 2004).

This ocean stratification would decrease the uptake of atmospheric CO_2 since warmer waters reduce the CO_2 solubility (Takahashi et al. 1993). In addition, a decrease in ocean vertical mixing is anticipated, which would decrease the global uptake of carbon by biology, although there are significant regional differences (Bopp and Le Quéré 2001). On the seasonal timescale, the winter ΔSSH anomalies have been shown to validate atmospheric relationships and vitally establish new mechanisms that will affect the seasonal anomalies of the surface water pCO_2.

Equally important is a need to understand the inter-annual variability of surface water pCO_2. The ΔSSH, a proxy of oceanic circulation strength will provide important information regarding to how the surface pCO_2 may respond to changes in temperature and biogeochemical alterations (e.g. through nutrient transport and subsequent biological activity).

As such, it is strongly recommended to utilise altimetry in conjunction with climate modes, such as the NAO, to further understand both the seasonal and inter-annual variability of surface water pCO_2.

This research was made possible through an automated in-situ pCO_2 measuring system placed onboard a VOS line. It is only through continued in-situ pCO_2 measurements that we will be able to further our understanding of the complexities of the marine carbon system.

The establishment of SOCAT version 1.5 (Pfeil et al. 2012), a worldwide database of ~ 6.3 million fCO_2 measurements from 1968 to 2007 collated from research vessels, commercial

ships as well as moored and drifting platforms (Bakker et al. 2012), will enable changes to the regional and global ocean carbon uptake to be assessed. Thus, longevity of this data set in addition to its global coverage will provide improved detection of long-term trends in the ocean carbon sink that may be attributed to anthropogenic warming as opposed to cyclical changes of this sink, which are likely to be affected by natural climate variability (e.g. Schuster and Watson 2007; Schuster et al. 2009; Thomas et al. 2008; Ullman et al. 2009). Indeed, McKinley et al. 2011, using in-situ pCO_2 data from 1981 to 2009 covering the North Atlantic, found evidence that linked the decrease in ocean uptake within the subtropical biome with anthropogenic warming.

However, in-situ pCO_2 data on its own is not enough. The continued development of coupled physical-biogeochemical models, particularly with respect to the ecosystem dynamics, is very important. Without this, accurate predictions of future surface water pCO_2 variability and hence the oceanic carbon sink will be difficult to carry out. The SOCAT data product will provide valuable initialization and validation fields for ocean carbon models. Therefore, more accurate predictions of both regional and global ocean carbon sinks can be made under future climate change. It is encouraging to see that White et al (2012) noted that improvements in their modelled surface ocean pCO_2 compared to the observations were evident after implementation of their data assimilation technique which incorporated SOCAT data.

Therefore, both in-situ pCO_2 data analysts and modellers within the marine carbon research community should continue to work closely together to ensure that models are both initialised and validated with in-situ fCO_2 measurements in addition to improving the modelled ocean carbon uptake through data assimilation of these in-situ fCO_2 measurements.

Appendix

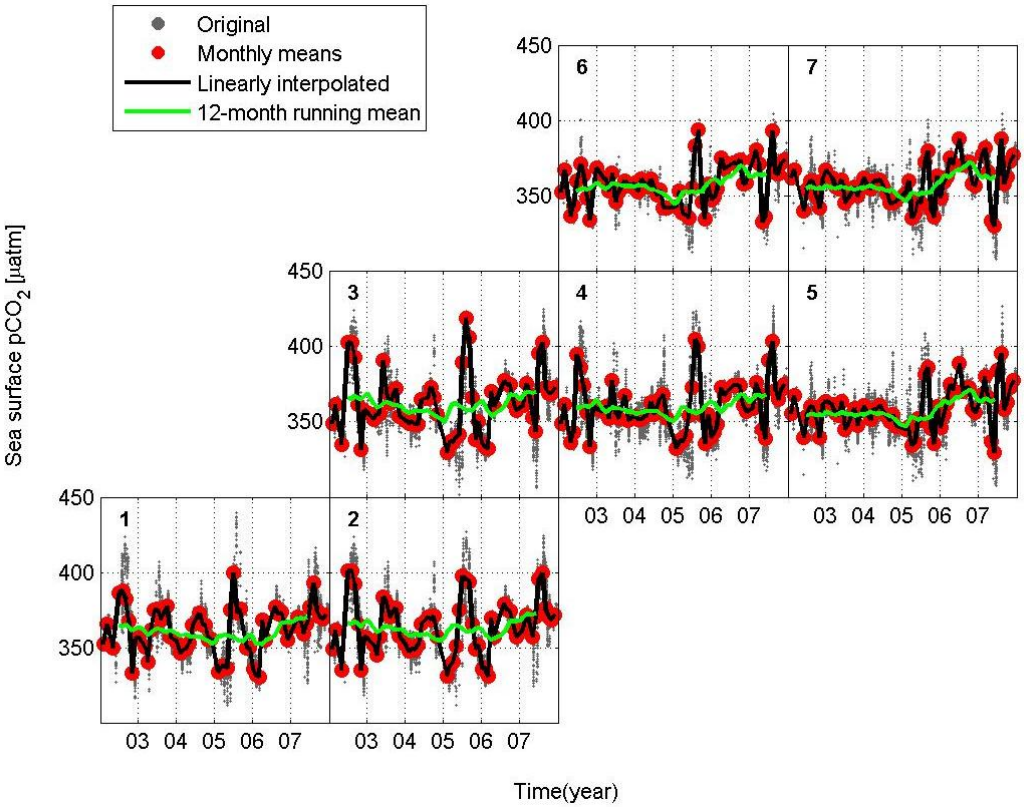

Figure A-1: Original (grey), monthly mean (red), linearly interpolated (black) and 12-month running mean of the ship's sea-surface pCO_2 measurements [µatm] in the seven sub-regions.

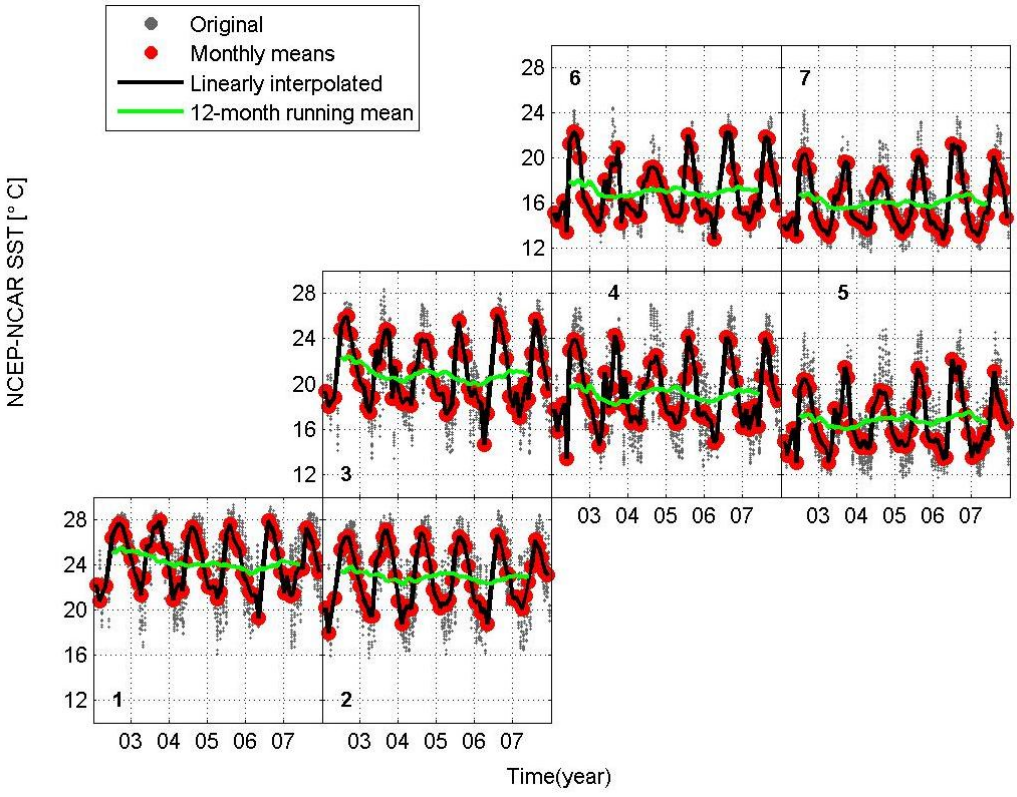

Figure A-2: Original (grey), monthly mean (red), linearly interpolated (black) and 12-month running mean of the NCEP-NCAR SST [°C] in the seven sub-regions.

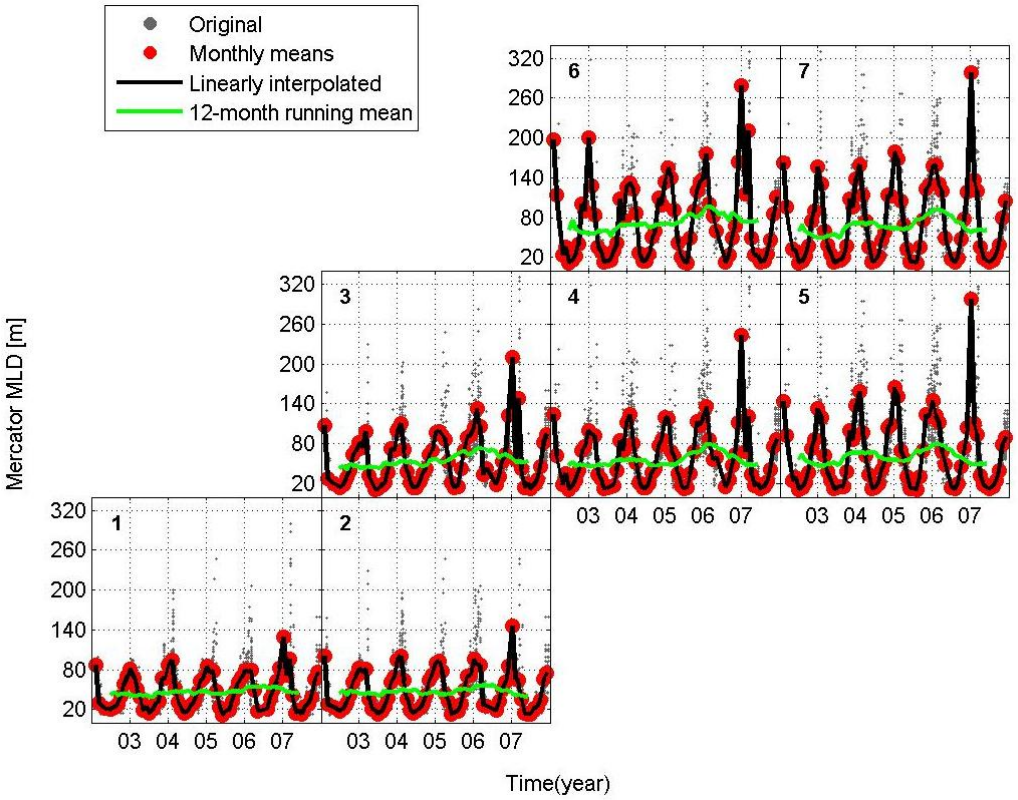

Figure A-3: Original (grey), monthly mean (red), linearly interpolated (black) and 12-month running mean of the Mercator MLD [m] in the seven subregions.

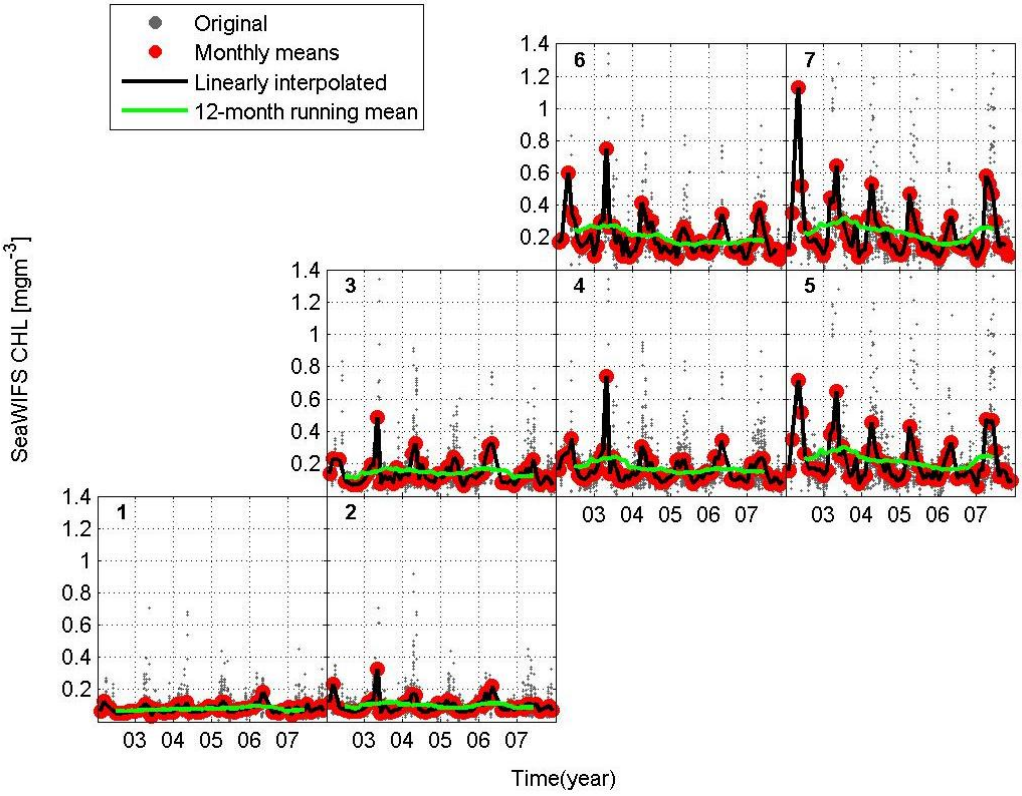

Figure A-4: Original (grey), monthly mean (red), linearly interpolated (black) and 12-month running mean of the SeaWiFS [mg m^{-3}] in the seven sub-regions.

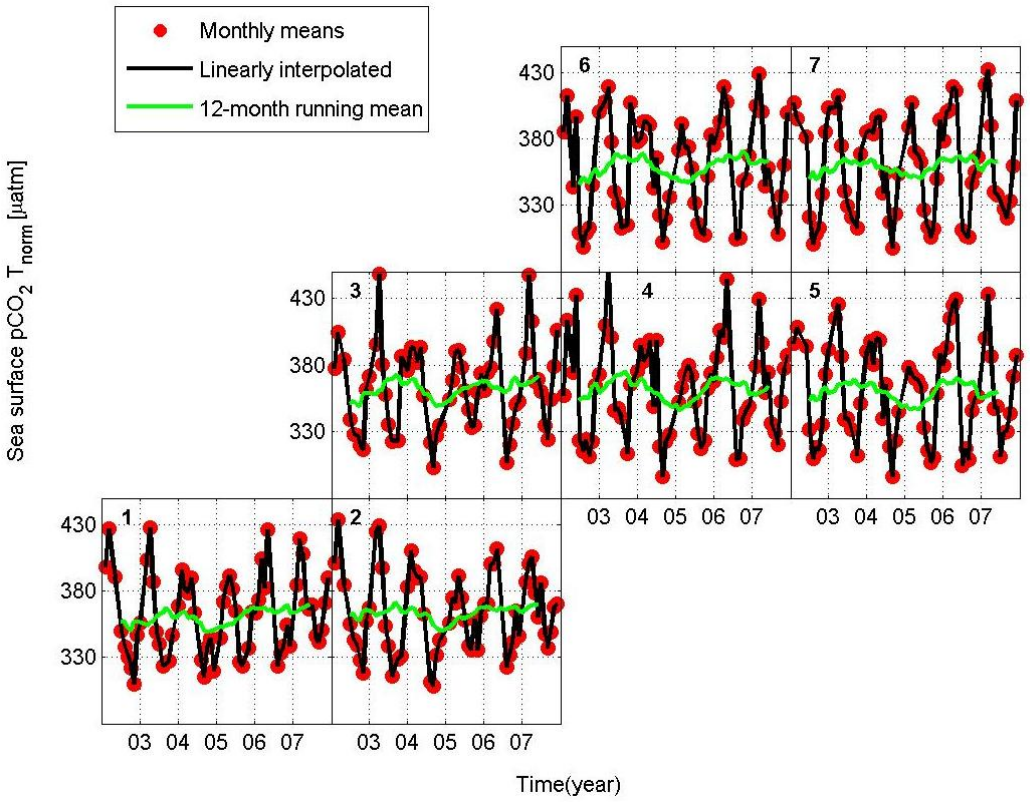

Figure A-5: Monthly mean (red), linearly interpolated (black) and 12-month running mean of the surface water pCO_2 T_{norm} [µatm] in the seven sub-regions.

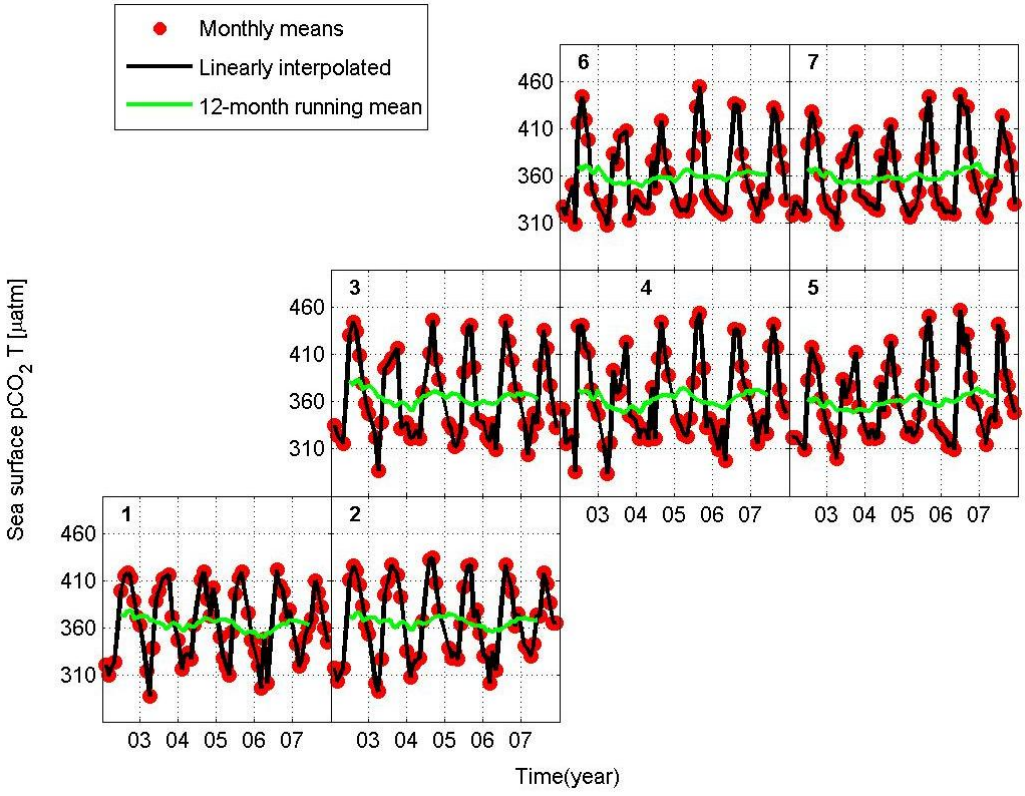

Figure A-6: Monthly mean (red), linearly interpolated (black) and 12-month running mean of the surface water pCO_2 T [µatm] in the seven sub-regions.

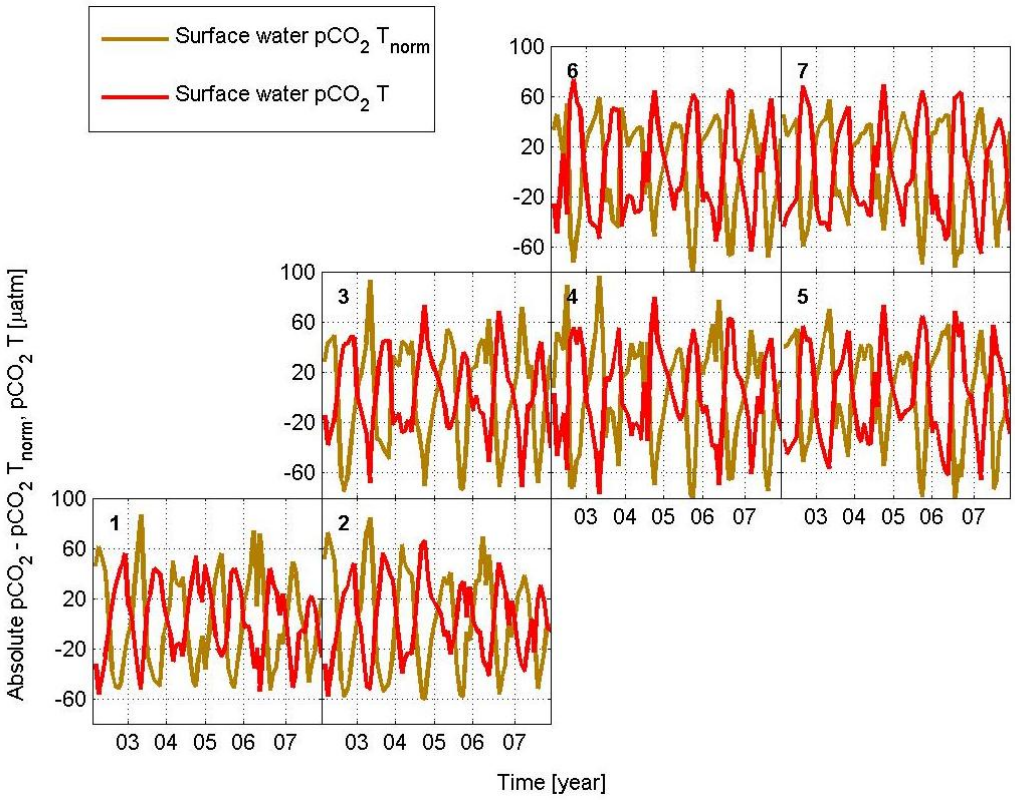

Figure A-7: Absolute difference between the linearly interpolated absolute surface pCO_2 and the linearly interpolated absolute pCO_2 T_{norm} (brown) and the linearly interpolated absolute pCO_2 T (red).

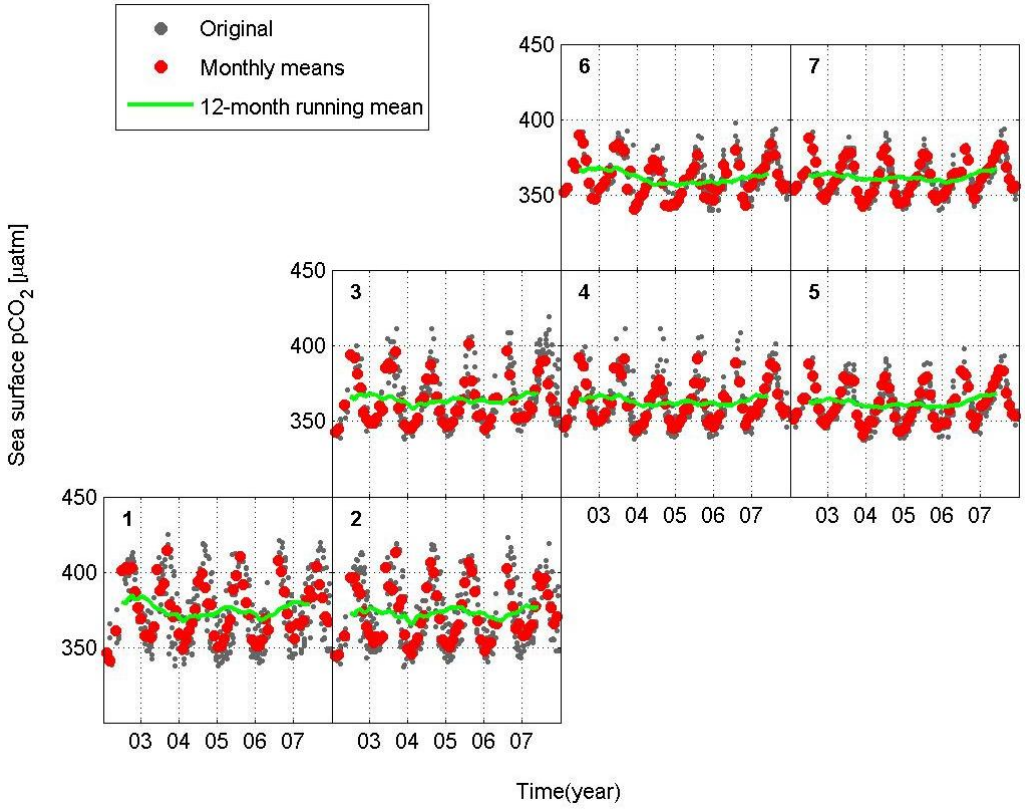

Figure A-8: Original (grey), monthly mean (red), and 12-month running mean of the NEMO-PlankTOM-5 model sea-surface pCO_2 [µatm] in the seven sub-regions.

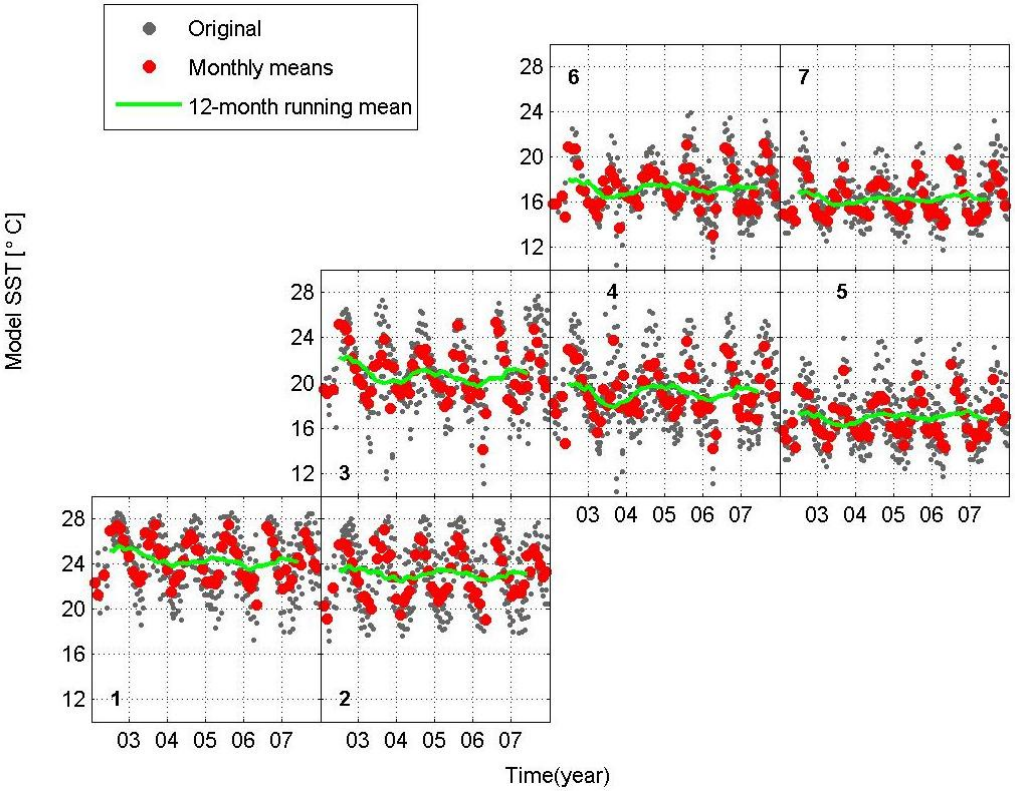

Figure A-9: Original (grey), monthly mean (red), and 12-month running mean of the NEMO-PlankTOM-5 model SST[°] in the seven sub-regions.

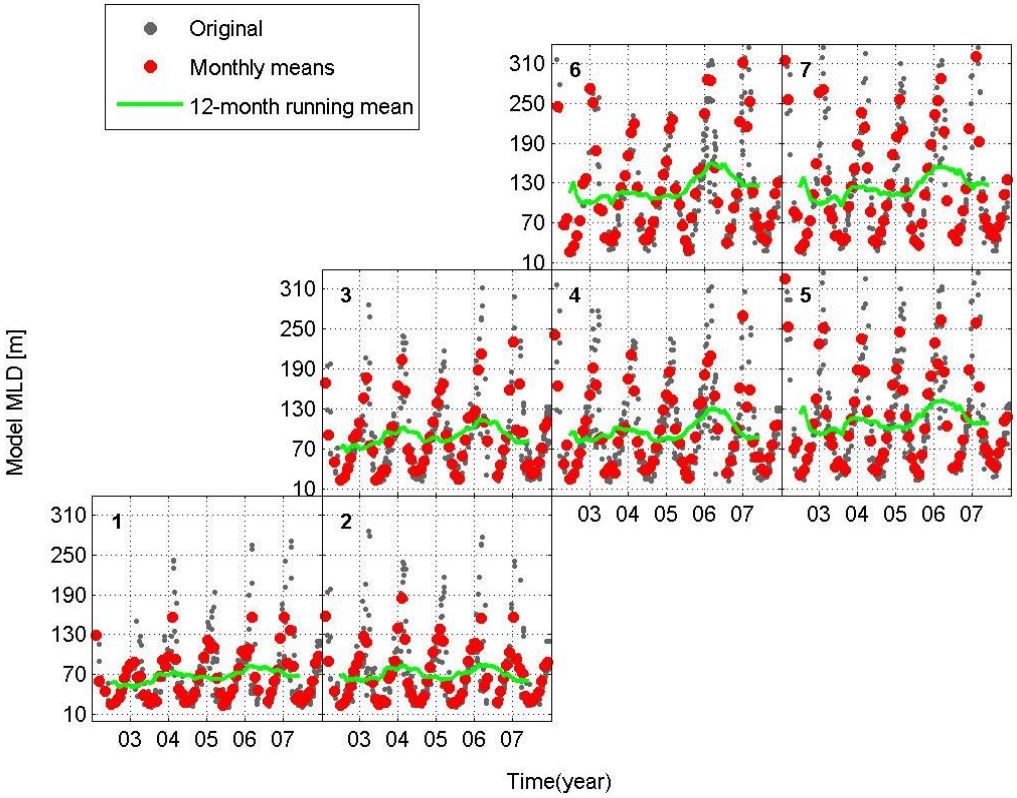

Figure A-10: Original (grey), monthly mean (red), and 12-month running mean of the NEMO-PlankTOM-5 model MLD [m] in the seven sub-regions

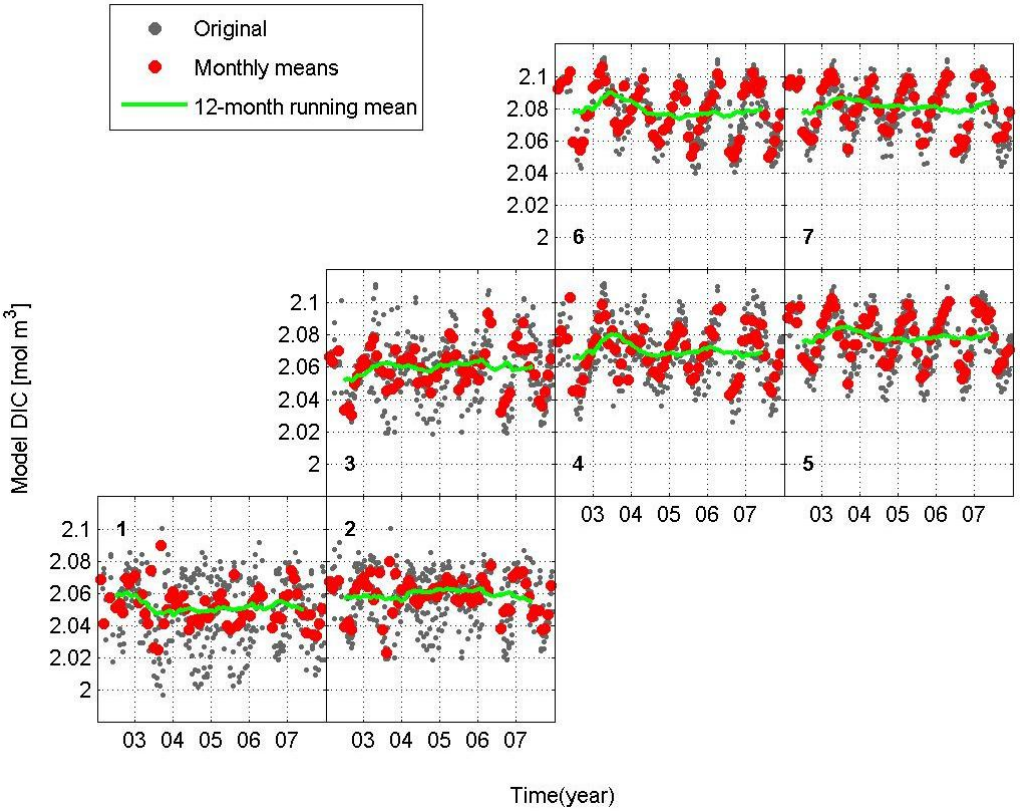

Figure A-11: Original (grey), monthly mean (red), and 12-month running mean of the NEMO-PlankTOM-5 model DIC [mol m^{-3}] in the seven sub-regions.

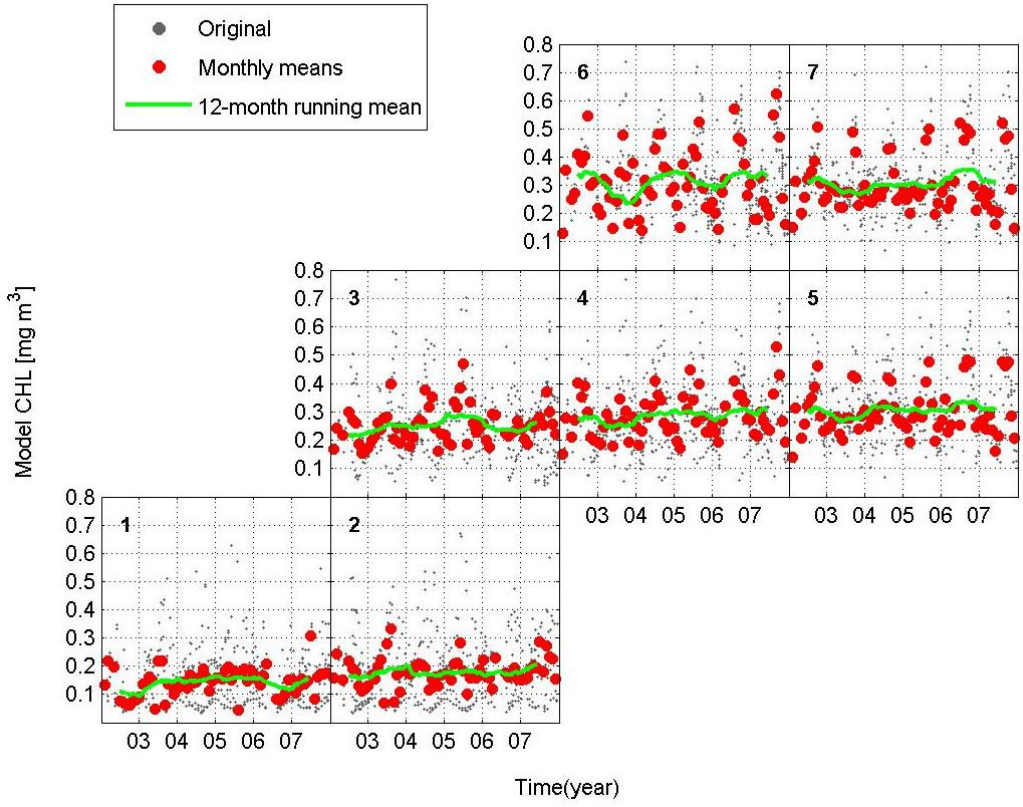

Figure A-12: Original (grey), monthly mean (red), and 12-month running mean of the NEMO-PlankTOM-5 model CHL [mg m^{-3}] in the seven sub-regions.

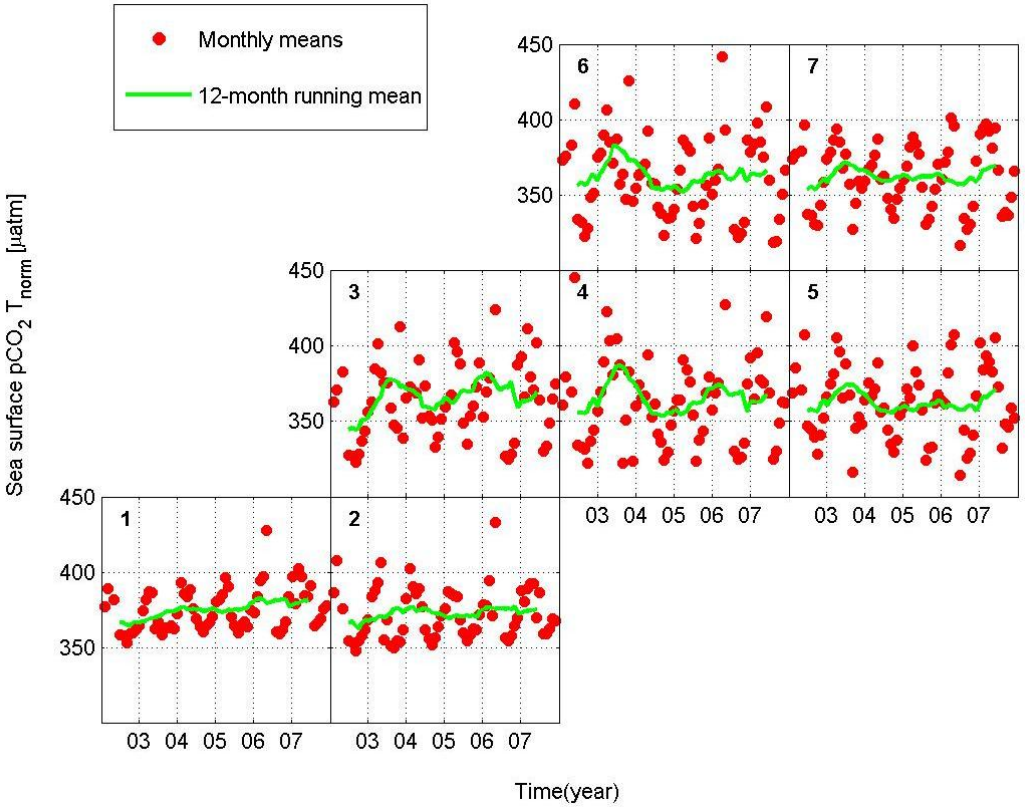

Figure A-13: Original (grey), monthly mean (red), and 12-month running mean of the NEMO-PlankTOM-5 model surface water pCO_2 T_{norm} [µatm] in the seven sub-regions.

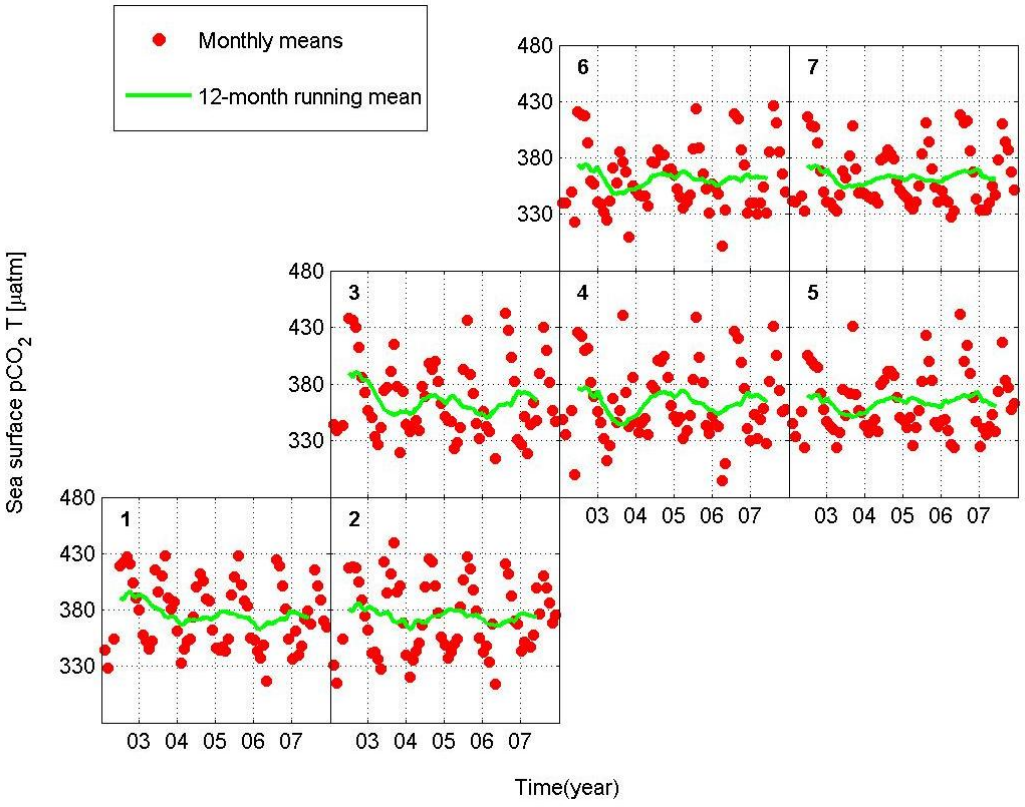

Figure A-14: Original (grey), monthly mean (red), and 12-month running mean of the NEMO-PlankTOM-5 model surface water pCO_2 T [µatm] in the seven sub-regions.

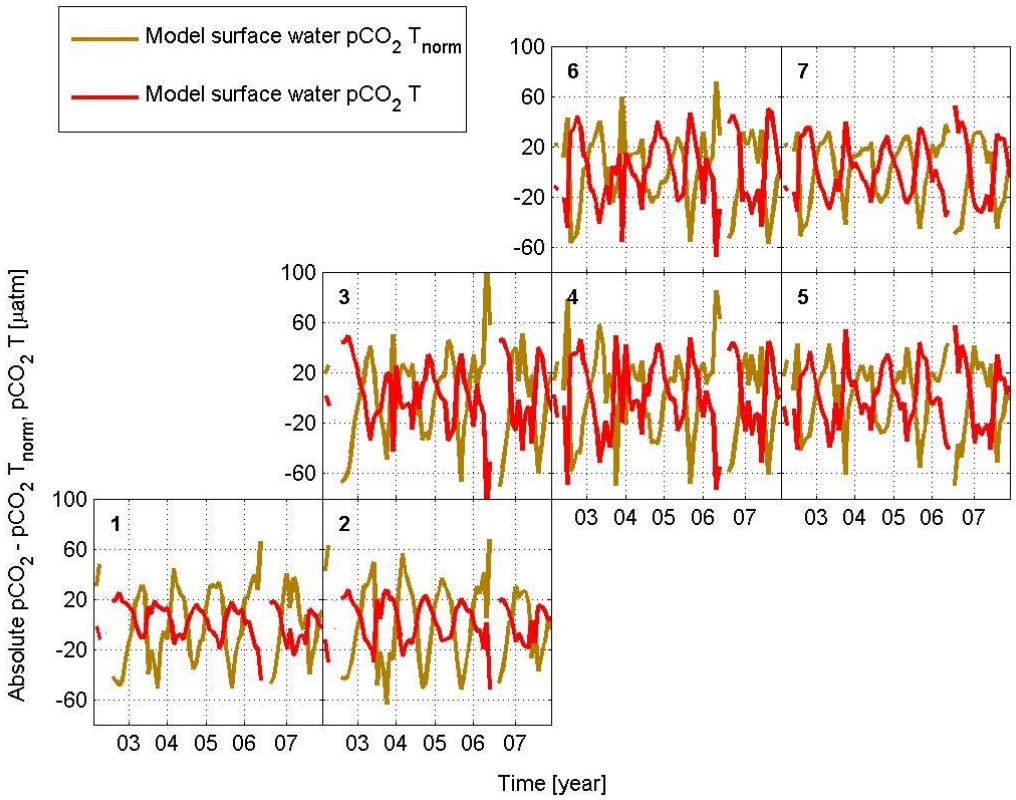

Figure A-15: Absolute difference between the modelled absolute surface pCO_2 and the modelled absolute pCO_2 T_{norm} (brown) and the modelled absolute pCO_2 T (red).

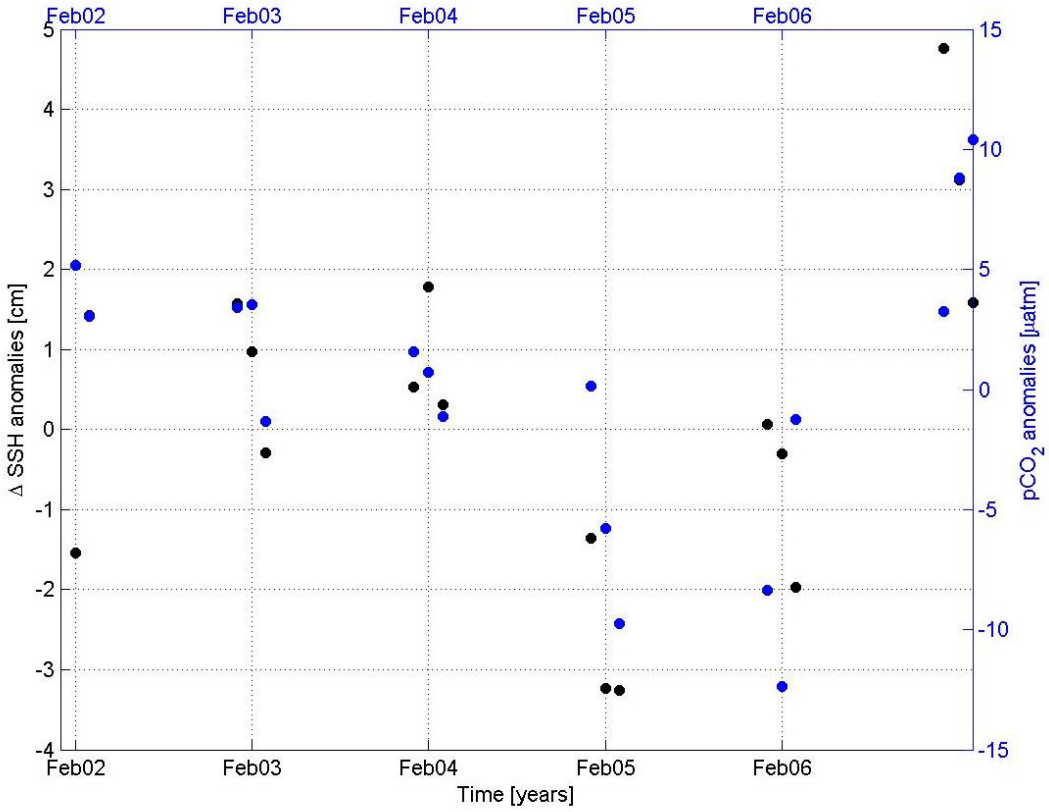

Figure A-16: JFM ΔSSH anomalies with JFM surface water pCO_2 anomalies in box 1 for the linearly interpolated observations.

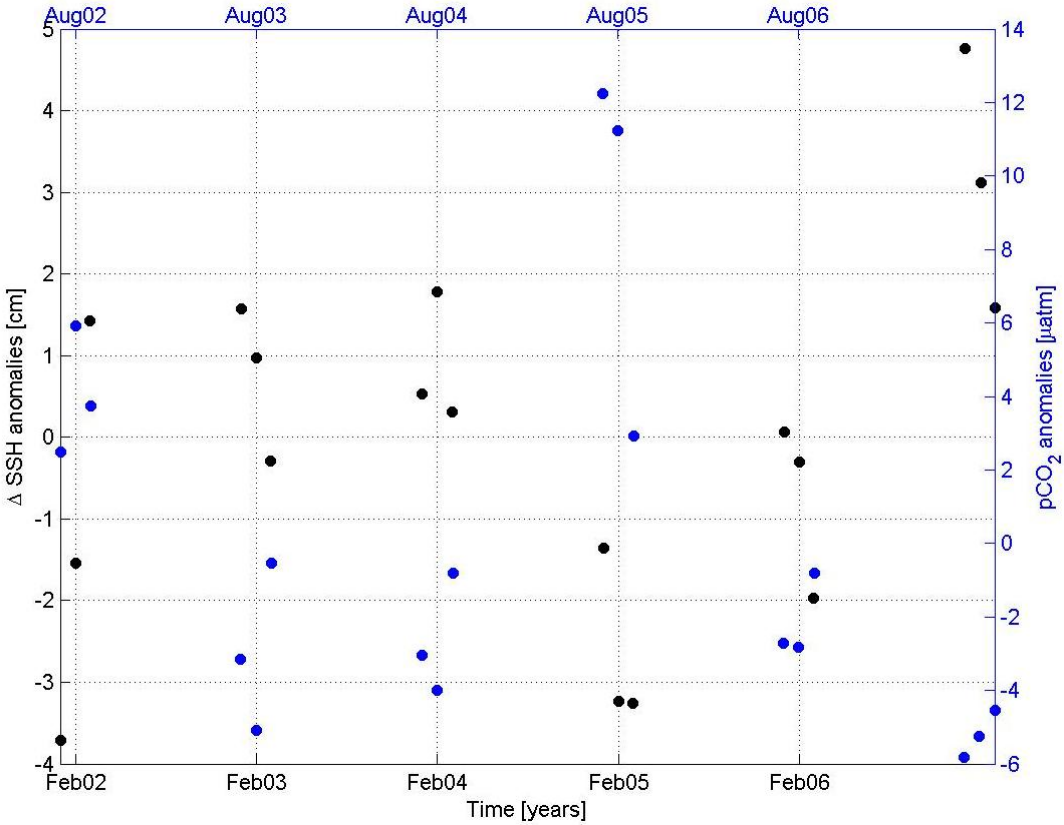

Figure A-17: JFM ΔSSH anomalies versus JAS pCO_2 anomalies at lag -6 months (ΔSSH anomalies leading the pCO_2 anomalies by 6 months) in box 1.

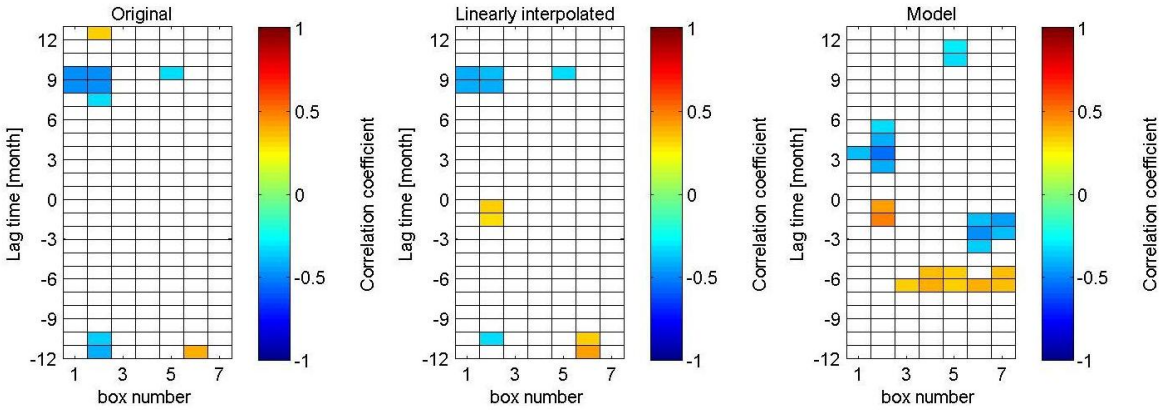

Figure A-18: Spearman's rank correlation coefficient at lag times [months] versus box number of the observed ΔSSH anomalies and SST anomalies for the original observations (left), the linearly interpolated observations (middle) and model output (right). Statistically significant positive correlations are yellow to orange-red, whilst statistically significant negative correlations are light to dark blue. The ΔSSH anomalies lead the SST anomalies at negative lag times and the SST leads the ΔSSH at positive lag times.

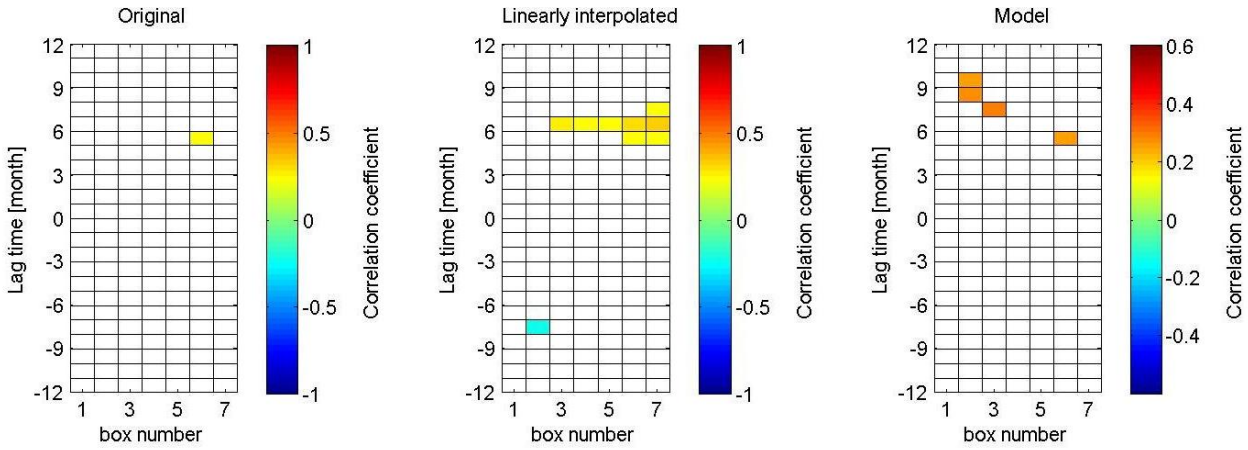

Figure A-19: Spearman's correlation coefficient at lag times [months] versus box number between the observed NAO index and SST anomalies, for the original observations (left), the linearly interpolated observations (middle) and the model output (right). Statistically significant positive correlations are orange-red, whilst statistically significant negative correlations are light-dark blue. The NAO index leads the SST at negative lag times and the SST leads the NAO index at positive lag times.

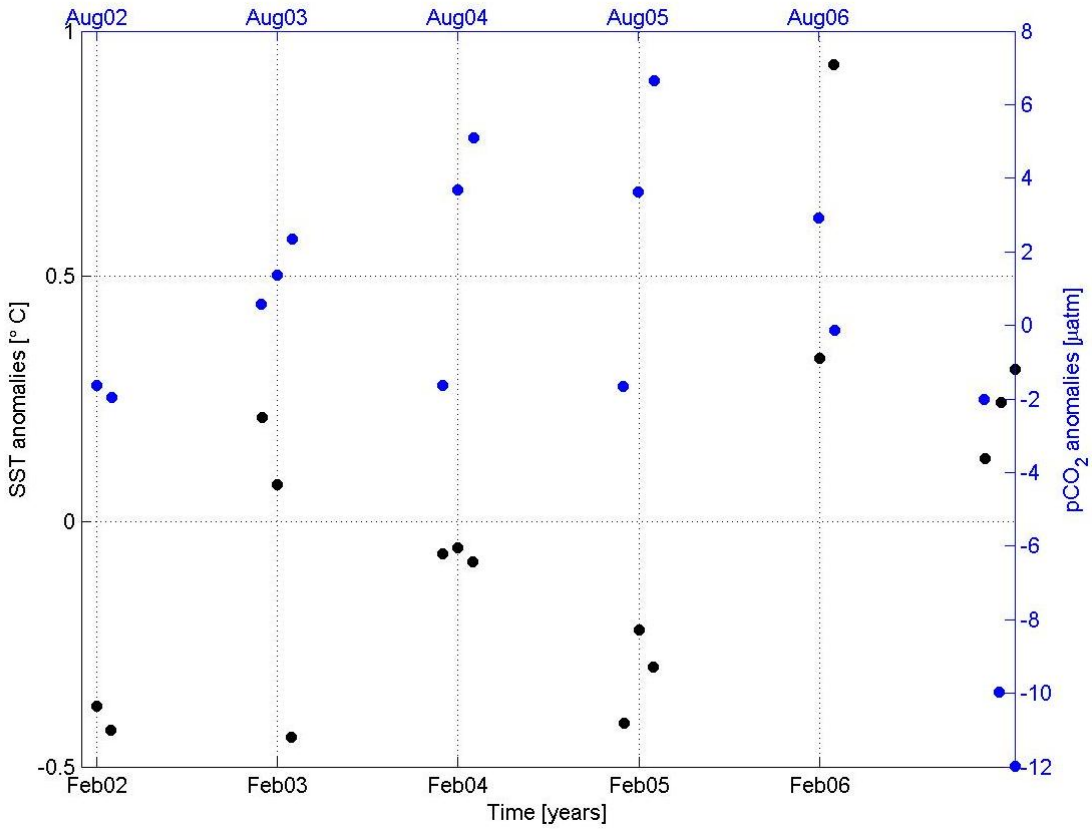

Figure A-20: JFM SST anomalies versus JAS pCO_2 anomalies at lag -6 months (SST anomalies leading the pCO_2 anomalies by 6 months) in box 2.

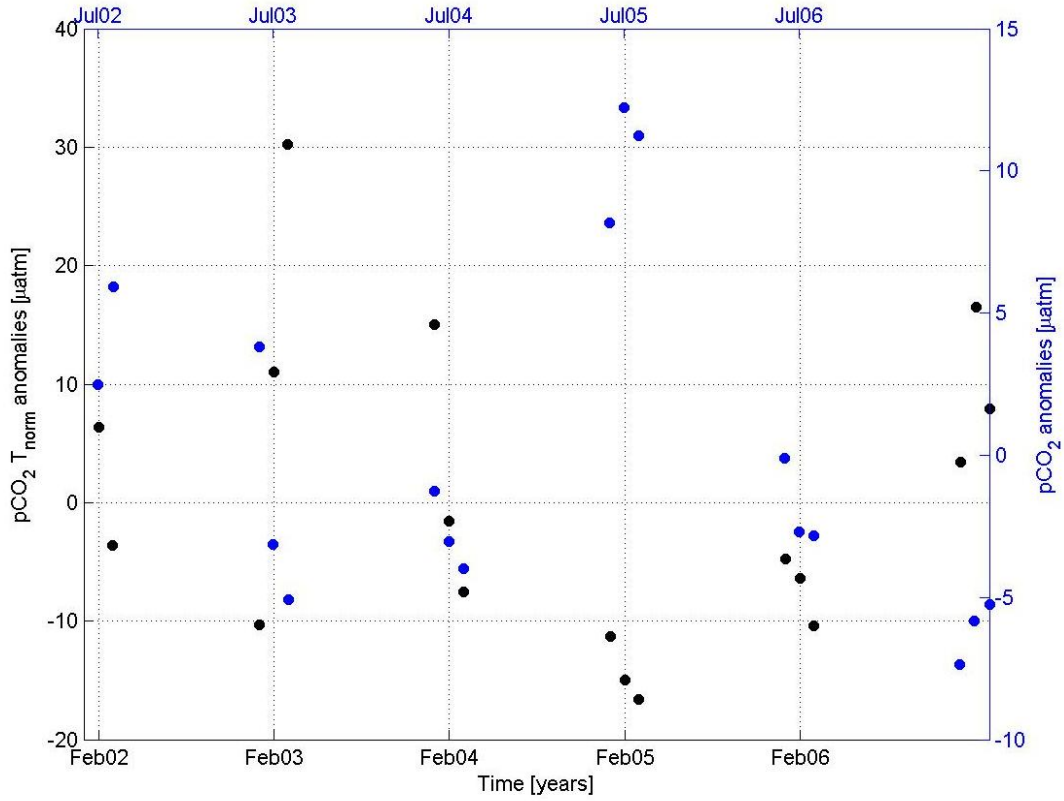

Figure A-21: JFM pCO_2 T_{norm} anomalies versus JJA pCO_2 anomalies at lag -5 months (pCO_2 T_{norm} anomalies leading the pCO_2 anomalies by 6 months) in box 1.

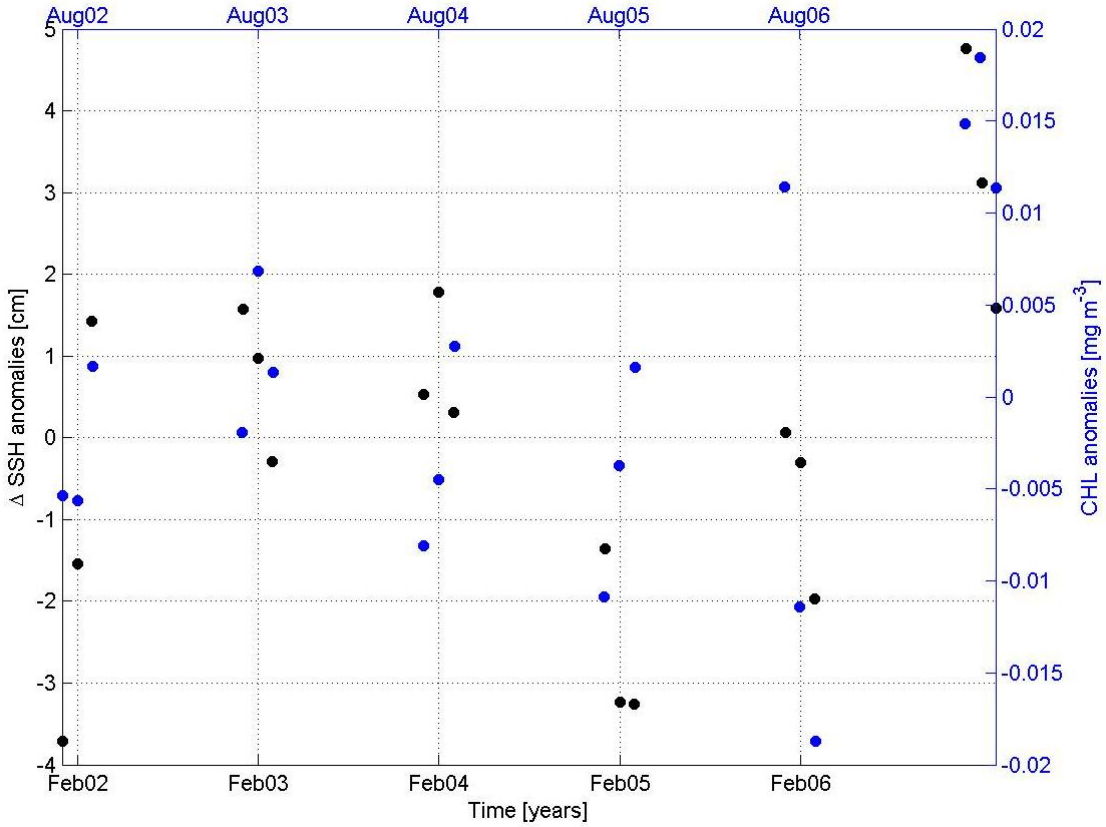

Figure A-22: JFM ΔSSH anomalies versus CHL anomalies at lag -6 months (ΔSSH anomalies leading the CHL anomalies by 6 months) in box 1.

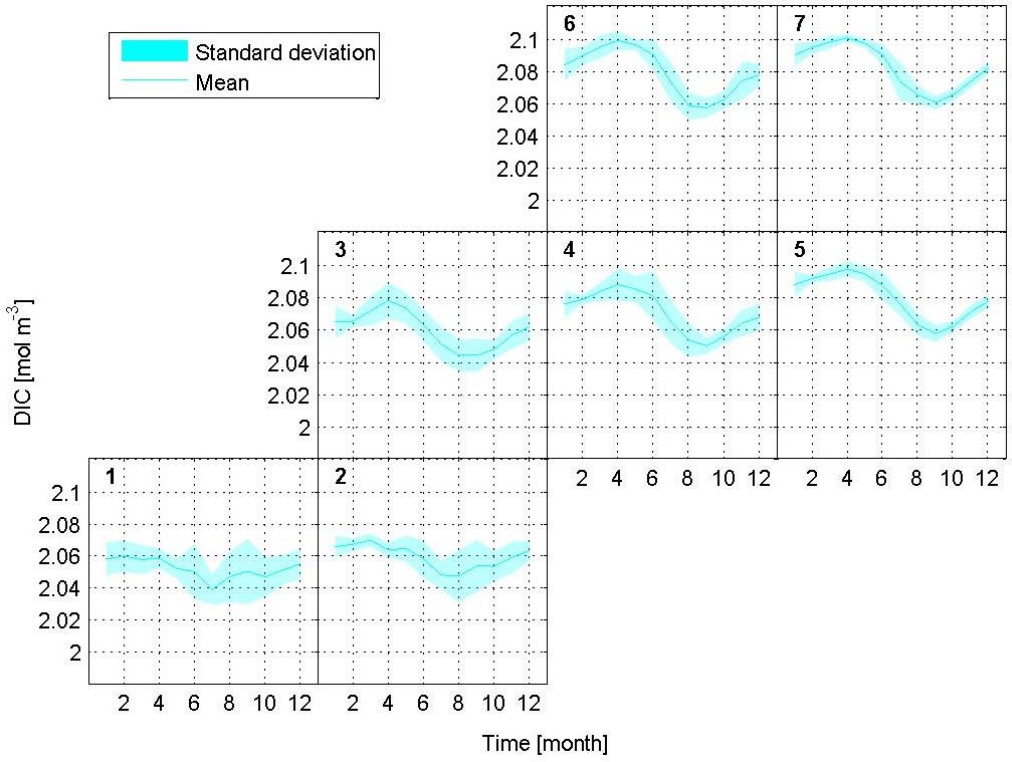

Figure A-23: Mean seasonal cycle of the modelled DIC [mol m^{-3}] in boxes 1 to 7.

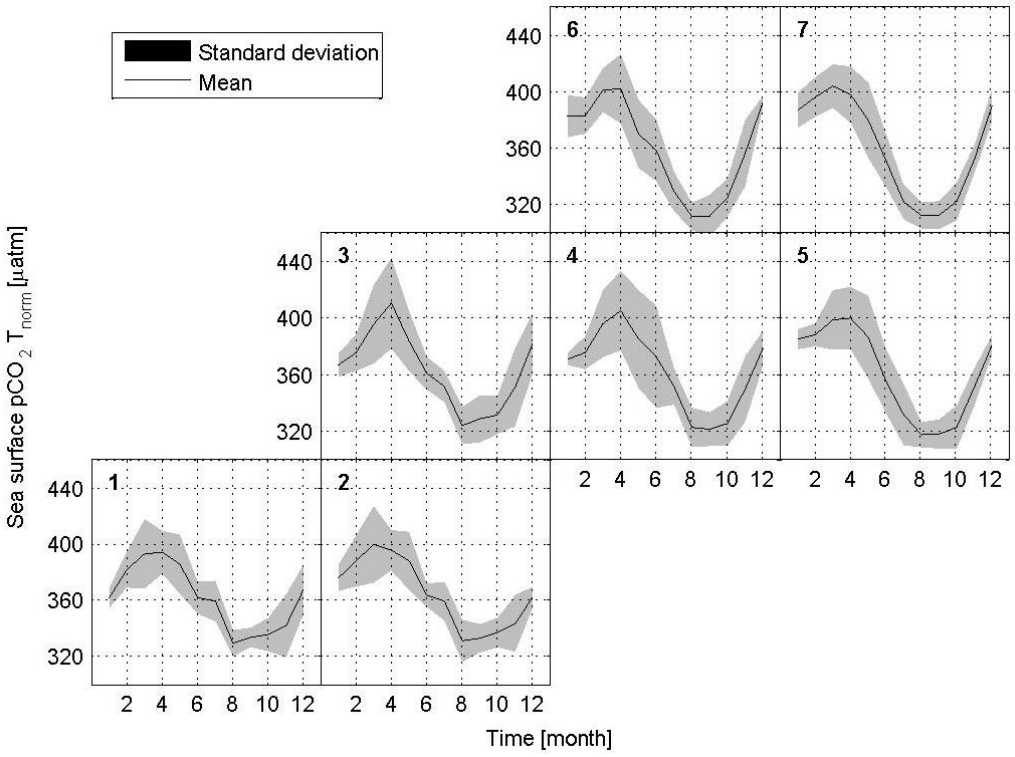

Figure A-24: Mean seasonal cycle of the observed pCO_2 T_{norm} [µatm] in boxes 1 to 7.

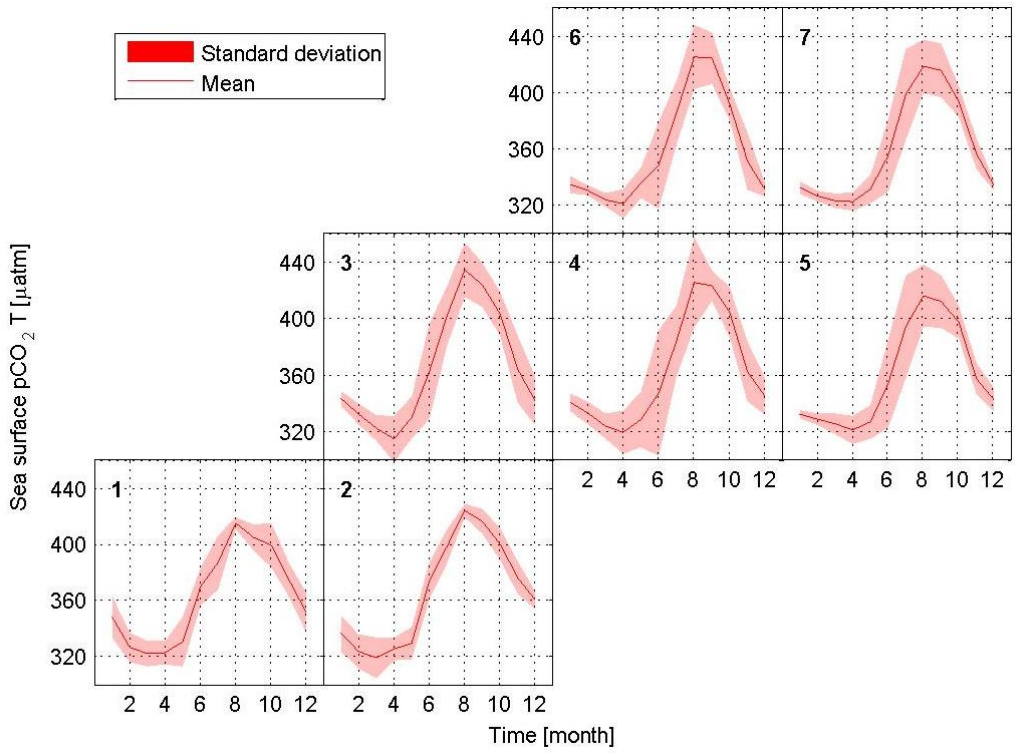

Figure A-25: Mean seasonal cycle of the observed pCO_2 T [µatm] in boxes 1 to 7.

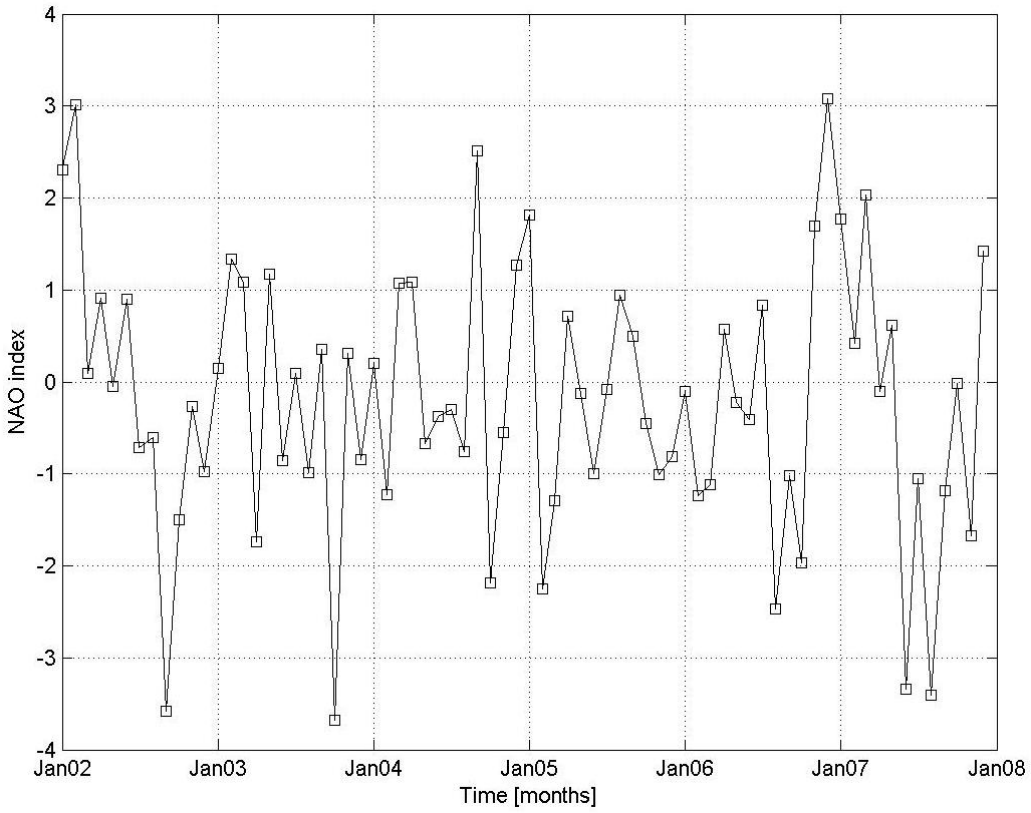

Figure A-26: The standardised sea-level pressure difference between Reykjavik, Iceland and Gibraltar, Spain (NAO index).

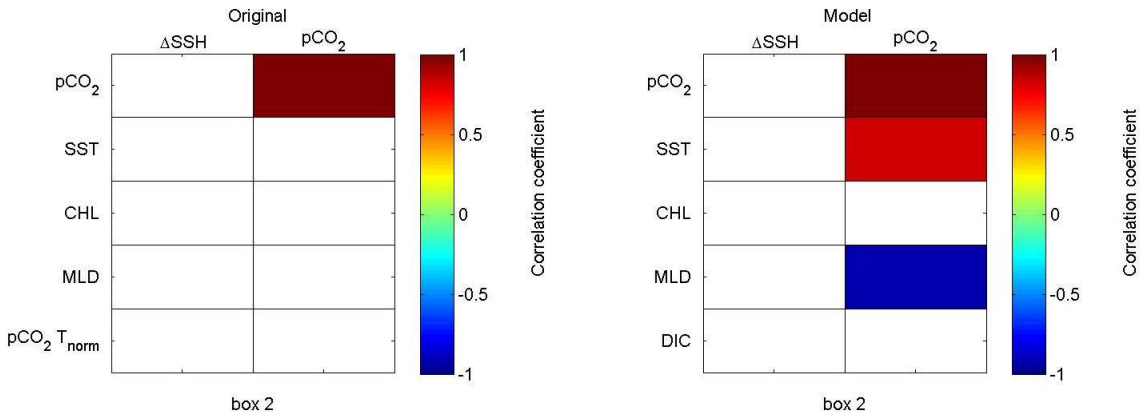

Figure A-27: Spearman correlation coefficients between the ΔSSH and related parameters (left column) and surface water pCO2 and related parameters (right column) for the observations (left panel) and model output (right panel) in box 2. Only coloured panels show statistically significant correlation coefficients.

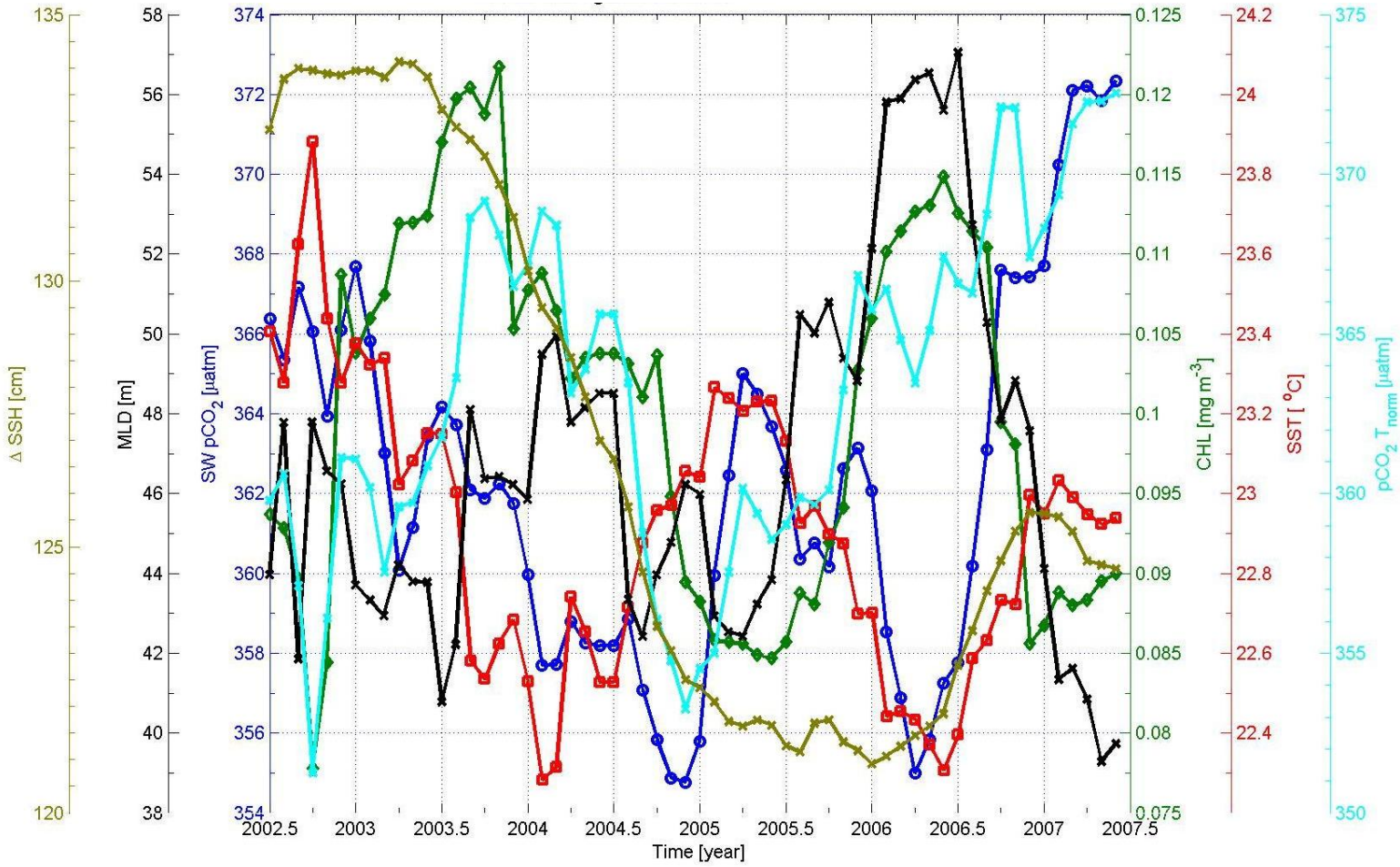

Figure A-28: 12-month running means of the ΔSSH [cm] (brown), surface water pCO_2 T_{norm} [µatm] (light blue), surface water pCO_2 [µatm] (dark blue), SST [°C] (red), MLD [m] (black), CHL [mg m^{-3}] (green) for the observations in box 2.

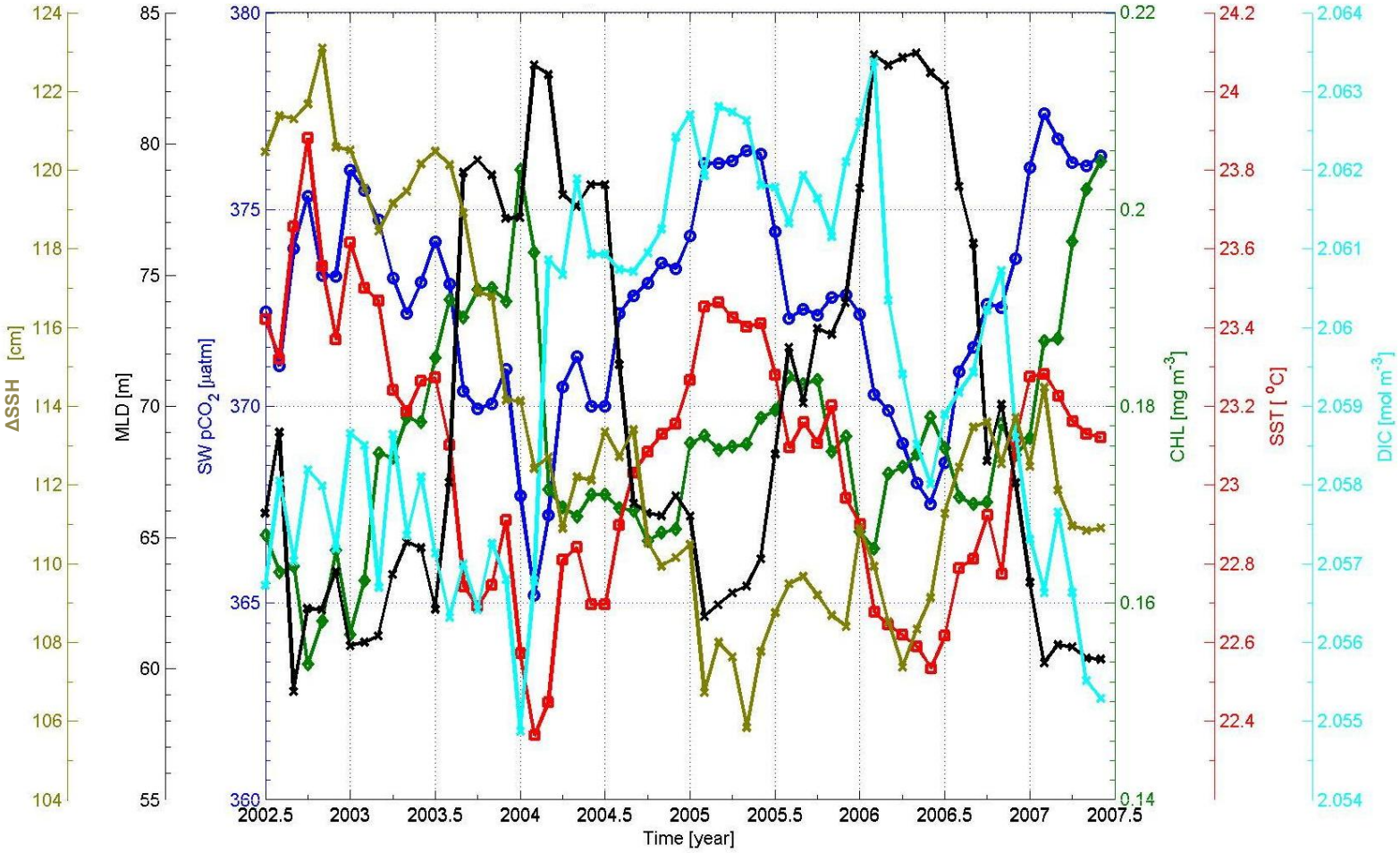

Figure A-29: 12-month running means of the ΔSSH [cm] (brown), DIC [mol m^{-3}] (light blue), surface water pCO_2 [µatm] (dark blue), SST [°C] (red), MLD [m] (black), CHL [mg m^{-3}] (green) for the model output in box 2.

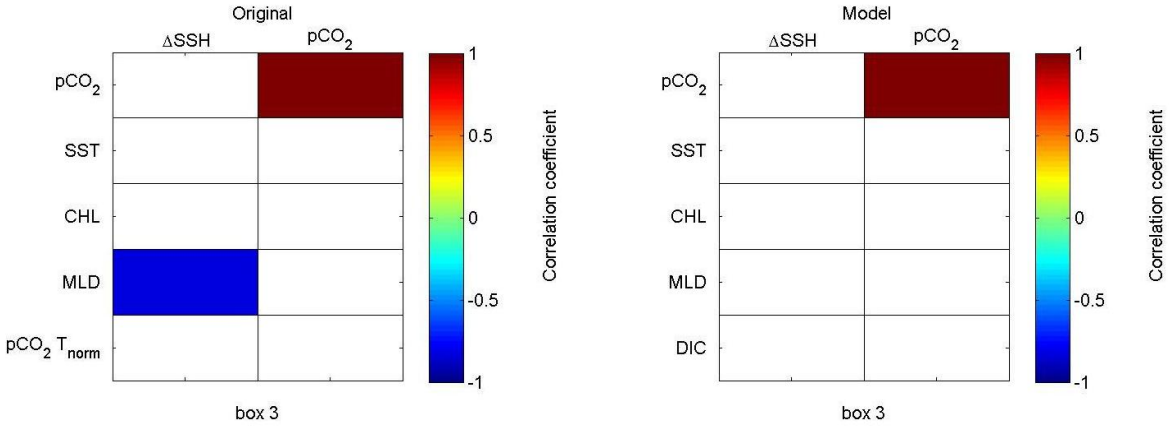

Figure A-30: Spearman correlation coefficients between the ΔSSH and related parameters (left column) and surface water pCO_2 and related parameters (right column) for the observations (left panel) and model output (right panel) in box 3. Only coloured panels show statistically significant correlation coefficients.

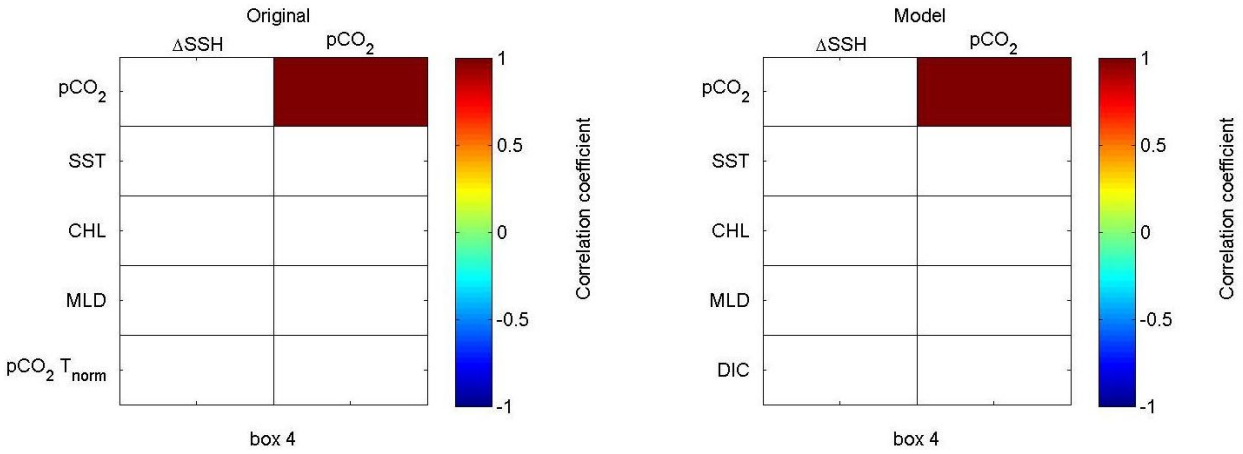

Figure A-31: Spearman correlation coefficients between the ΔSSH and related parameters (left column) and surface water pCO_2 and related parameters (right column) for the observations (left panel) and model output (right panel) in box 4. Only coloured panels show statistically significant correlation coefficients.

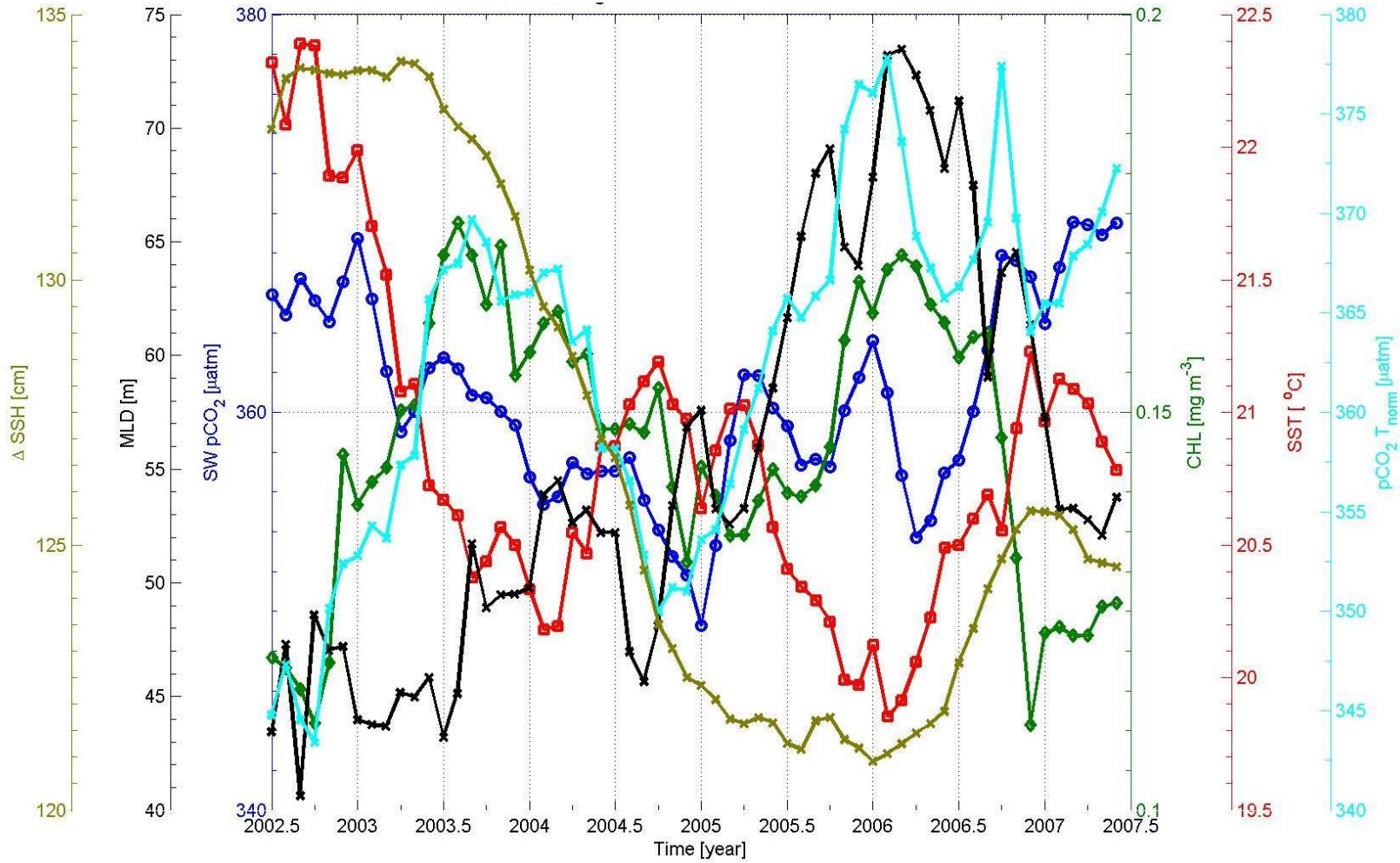

Figure A-32: 12-month running means of the ΔSSH [cm] (brown), surface water pCO_2 T_{norm} [µatm] (light blue), surface water pCO_2 [µatm] (dark blue), SST [°C] (red), MLD [m] (black), CHL [mg m^{-3}] (green) for the observations in box 3.

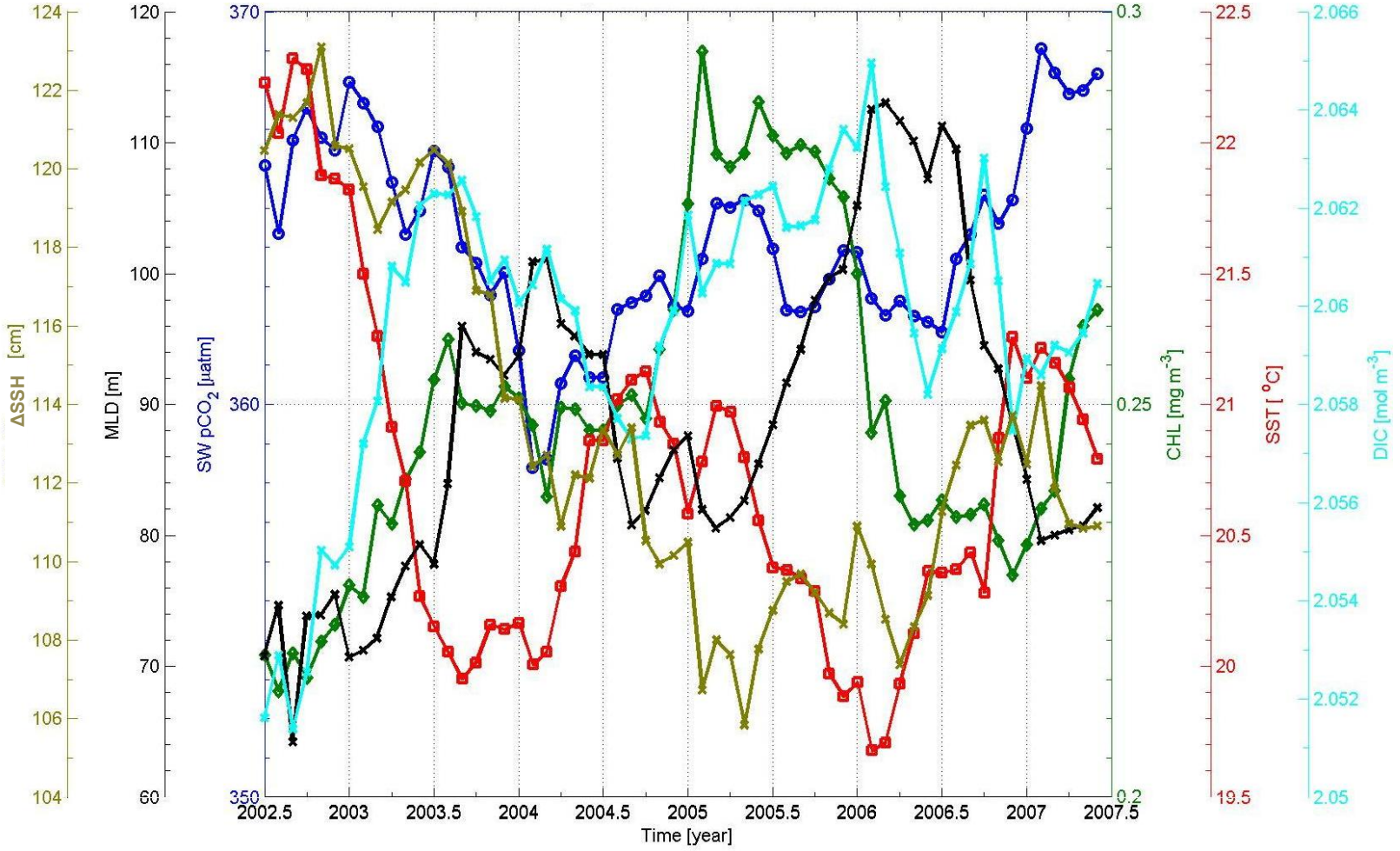

Figure A-33: 12-month running means of the ΔSSH [cm] (brown), DIC [mol m^{-3}] (light blue), surface water pCO_2 [µatm] (dark blue), SST [°C] (red), MLD [m] (black), CHL [mg m^{-3}] (green) for the model output in box 3.

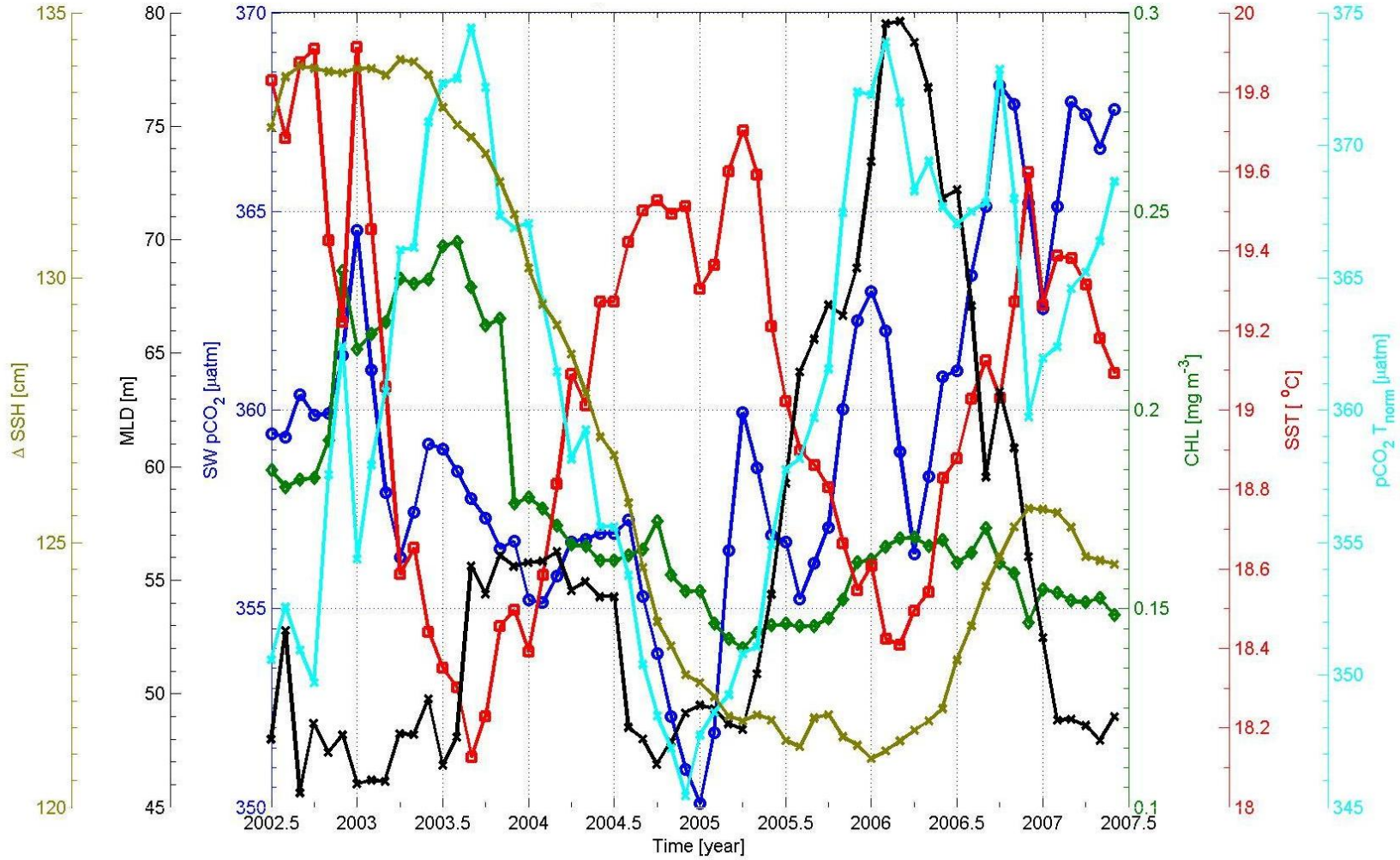

Figure A-34: 12-month running means of the ΔSSH [cm] (brown), surface water pCO_2 T_{norm} [µatm] (light blue), surface water pCO_2 [µatm] (dark blue), SST [°C] (red), MLD [m] (black), CHL [mg m^{-3}] (green) for the observations in box 4.

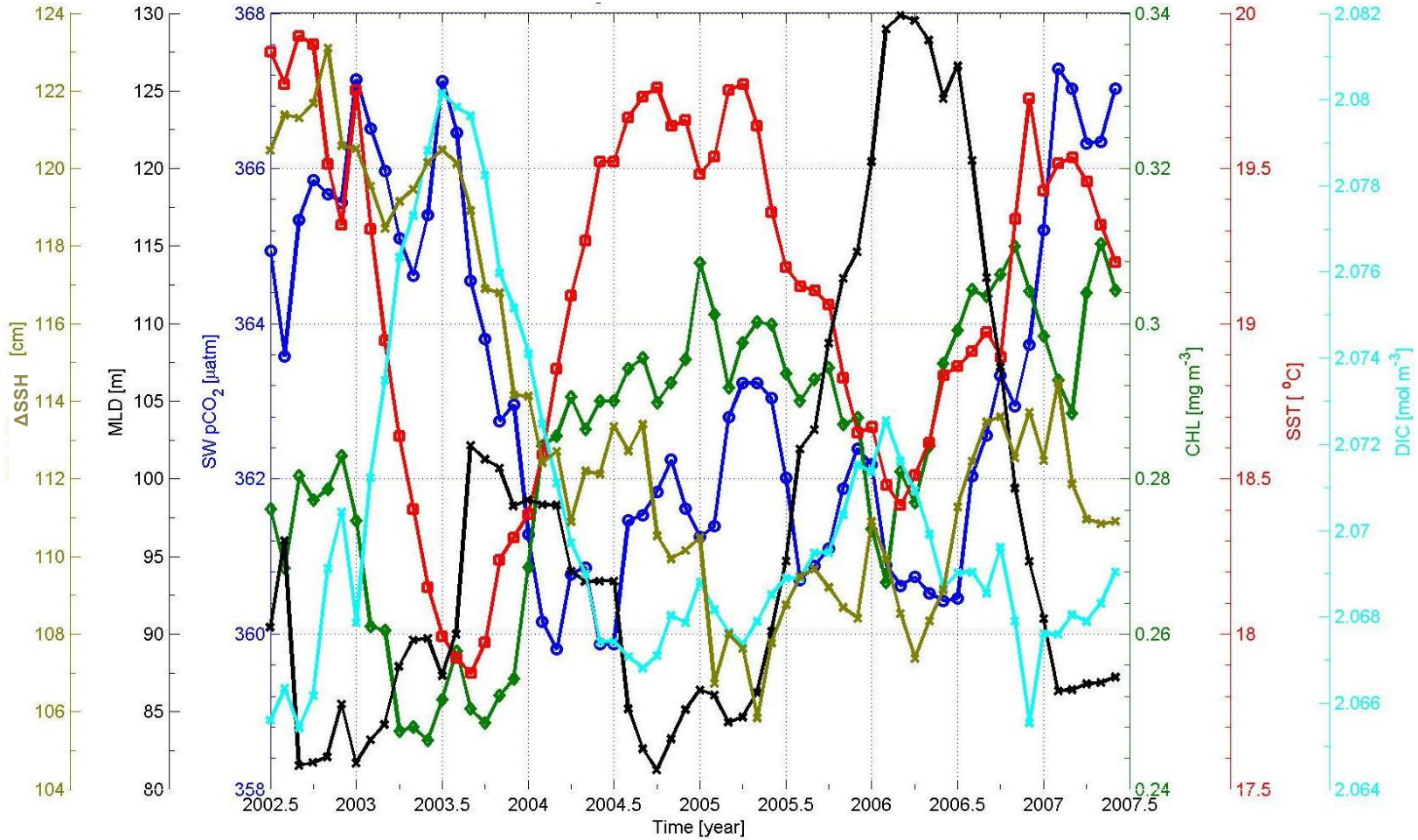

Figure A-35: 12-month running means of the ΔSSH [cm] (brown), DIC [mol m^{-3}] (light blue), surface water pCO_2 [µatm] (dark blue), SST [°C] (red), MLD [m] (black), CHL [mg m^{-3}] (green) for the model output in box 4.

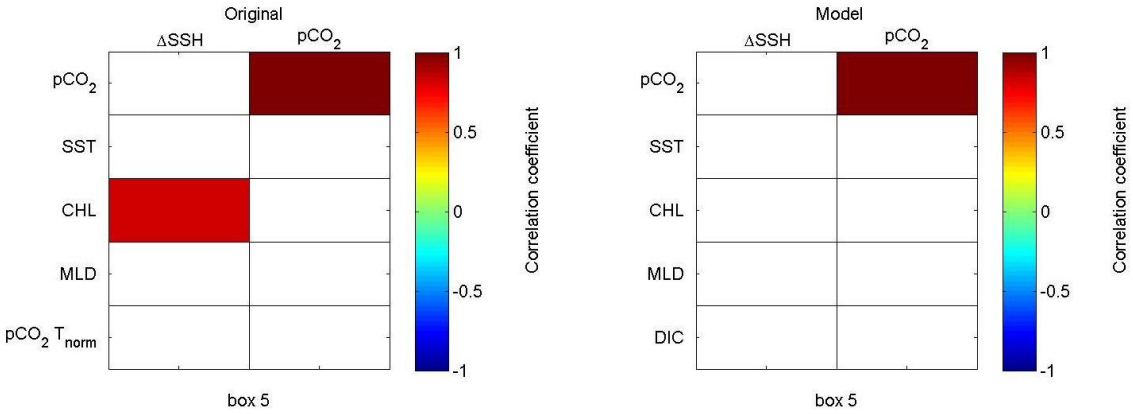

Figure A-36: Spearman correlation coefficients between the ΔSSH and related parameters (left column) and surface water pCO_2 and related parameters (right column) for the observations (left panel) and model output (right panel) in box 5. Only coloured panels show statistically significant correlation coefficients.

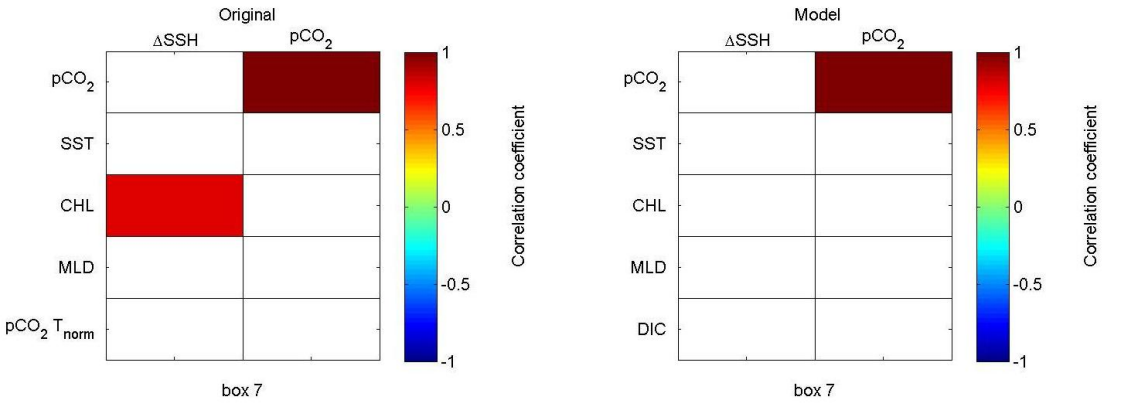

Figure A-37: Spearman correlation coefficients between the ΔSSH and related parameters (left column) and surface water pCO_2 and related parameters (right column) for the observations (left panel) and model output (right panel) in box 7. Only coloured panels show statistically significant correlation coefficients.

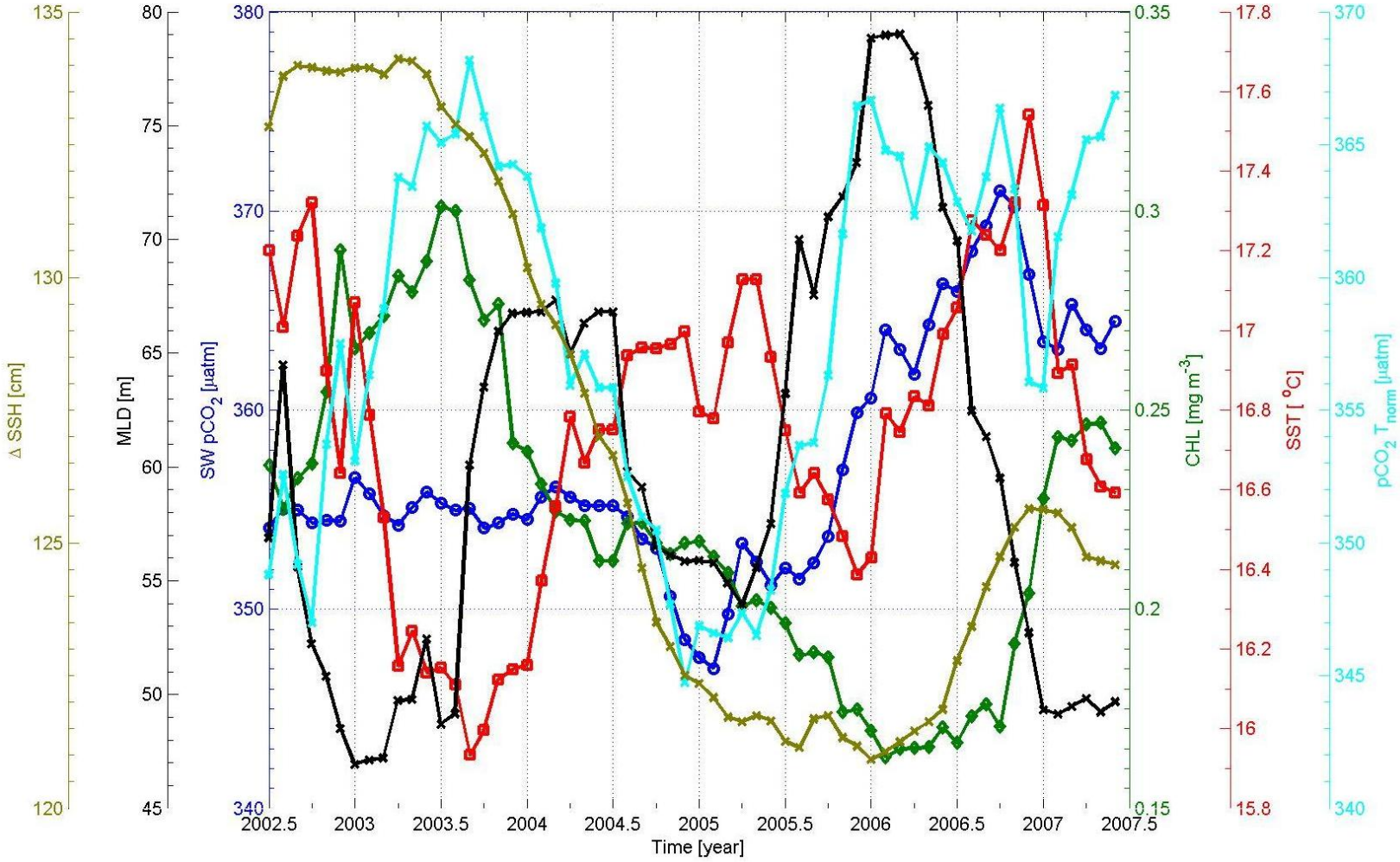

Figure A-38: 12-month running means of the ΔSSH [cm] (brown), surface water pCO_2 T_{norm} [µatm] (light blue), surface water pCO_2 [µatm] (dark blue), SST [°C] (red), MLD [m] (black), CHL [mg m^{-3}] (green) for the observations in box 5.

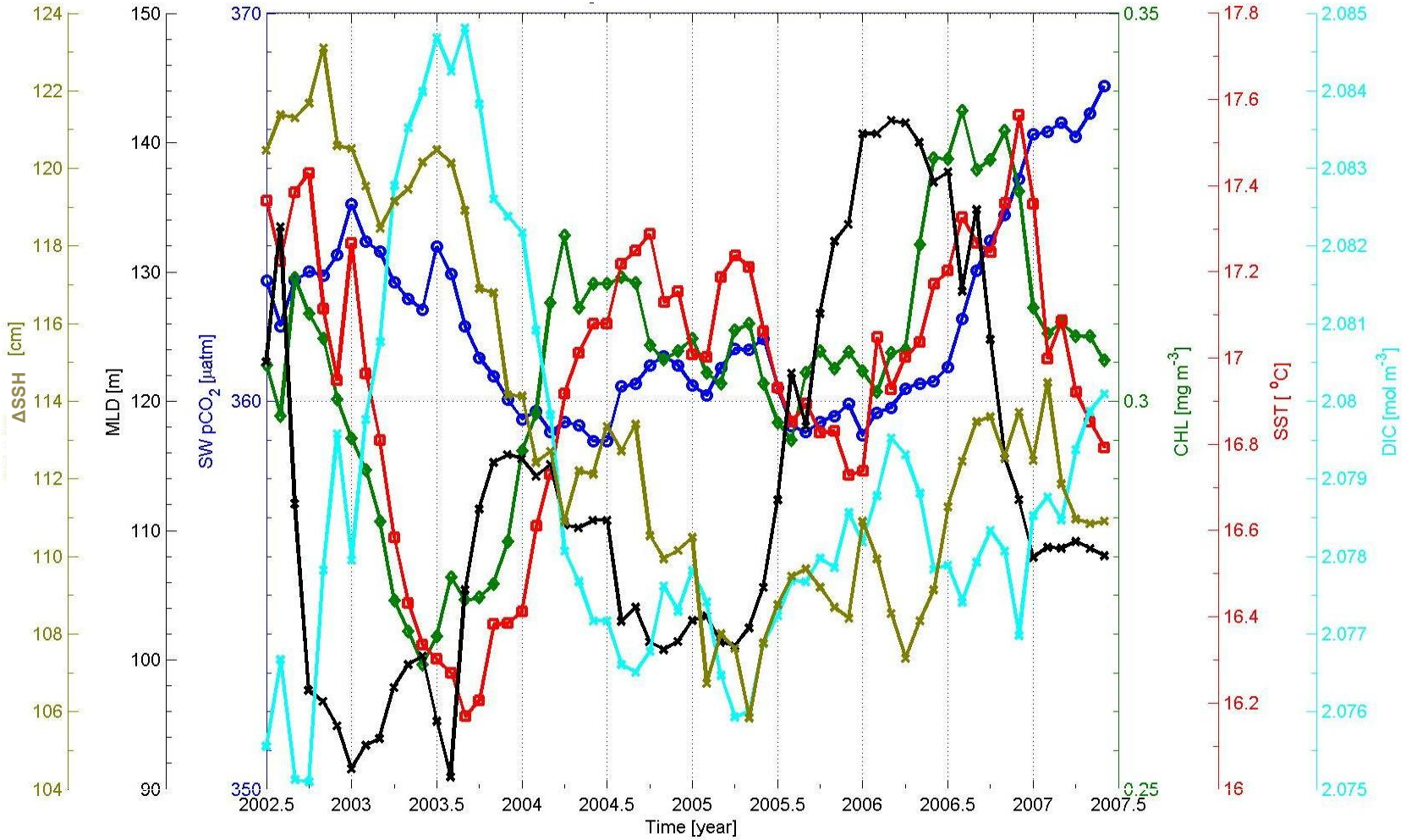

Figure A-39: 12-month running means of the ΔSSH [cm] (brown), DIC [mol m^{-3}] (light blue), surface water pCO_2 [µatm] (dark blue), SST [°C] (red), MLD [m] (black), CHL [mg m^{-3}] (green) for the model output in box 5.

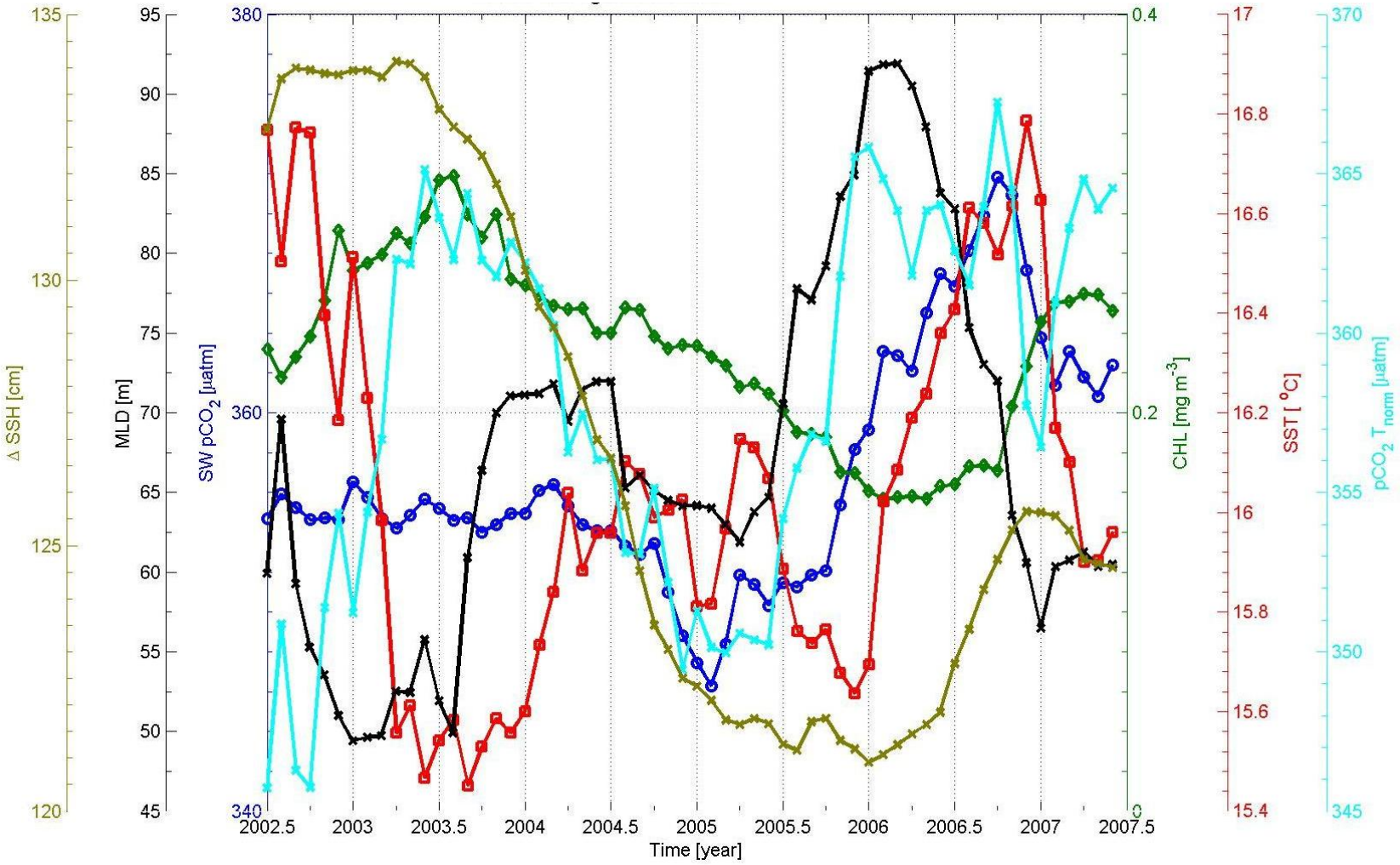

Figure A-40: 12-month running means of the ΔSSH [cm] (brown), surface water pCO_2 T_{norm} [µatm] (light blue), surface water pCO_2 [µatm] (dark blue), SST [°C] (red), MLD [m] (black), CHL [mg m^{-3}] (green) for the observations in box 7.

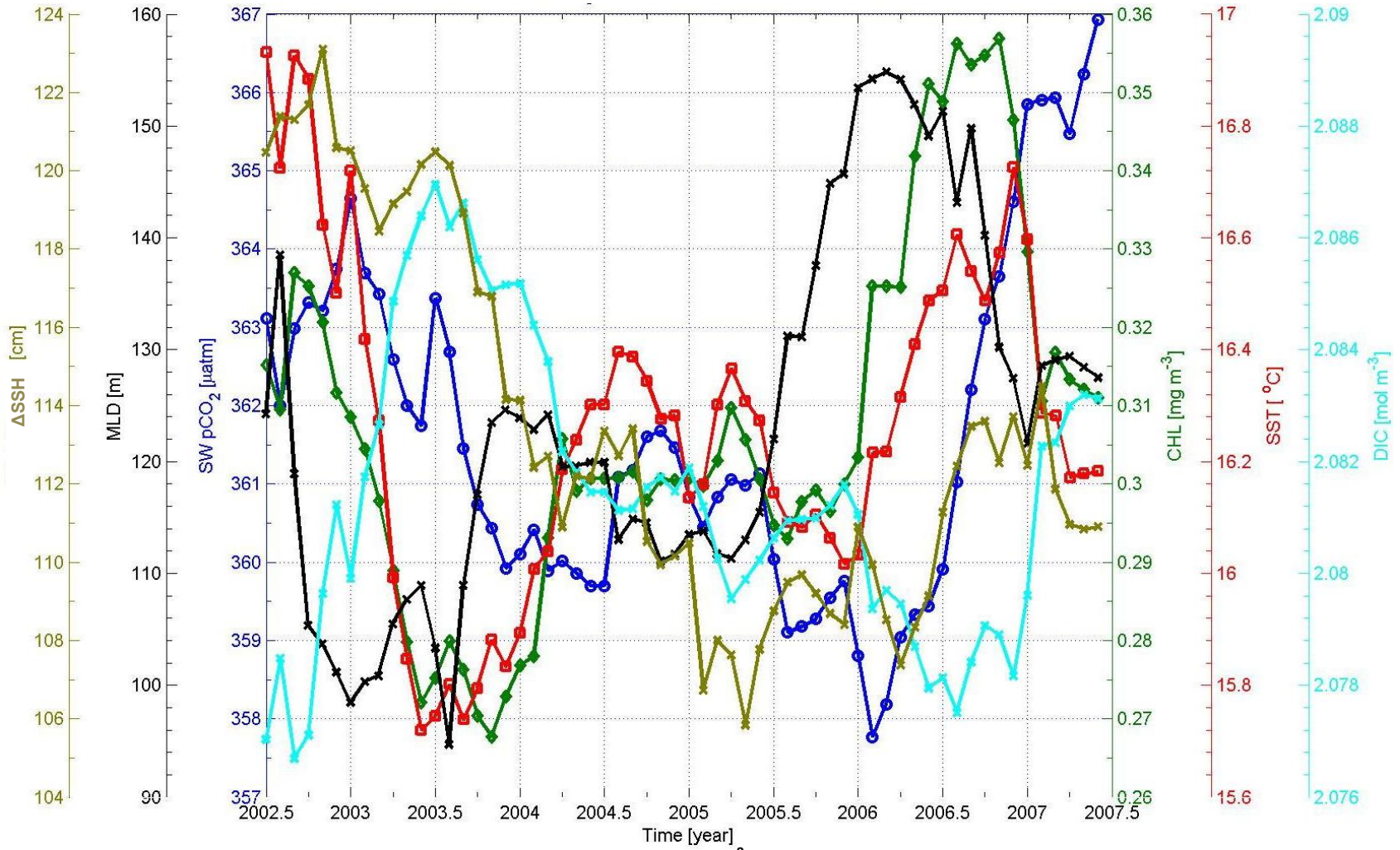

Figure A-41: 12-month running means of the ΔSSH [cm] (brown), DIC [mol m^{-3}] (light blue), surface water pCO_2 [µatm] (dark blue), SST [°C] (red), MLD [m] (black), CHL [mg m^{-3}] (green) for the model output in box 7.

List of abbreviations and acronyms

ALK - alkalinity
BATS - Bermuda Atlantic Time Series
CDOM - coloured dissolved organic matter
CHL - chlorophyll *a*
ΔSSH - SSH differences
DGOM - Dynamic Green Ocean Model
DIC - dissolved inorganic carbon
EDW - Eighteen Degree Water
ENACW - Eastern North Atlantic Central Water
ENACWt - subtropical Eastern North Atlantic Central Water
ENACWp - subpolar Eastern North Atlantic Central Water
ESTOC - European Station for Time Series in the Ocean
fCO_2 -fugacity of CO_2
MLD - mixed layer depth
NADW - North Atlantic Deep Water
NAO - North Atlantic Oscillation
pCO_2 - partial pressure of CO_2
pCO_2 T - temperature effect on CO_2
pCO_2 T_{norm} - non-temperature effect on CO_2
PFT - plankton functional type
SOCAT - Surface Ocean CO_2 Atlas
SPMW - subpolar mode water
SSH - sea surface height
SSS - sea surface salinity
SST - sea-surface temperature
VOS - voluntary observing ships

References

Alexander, M. A. and C. Deser (1995). "A mechanism for the recurrence of wintertime midlatitude SST anomalies." Journal of Physical Oceanography **25**(1): 122-137.

Antonov, J. I., R. A. Locarnini, T. P. Boyer, A. V. Mishonov and H. E. Garcia (2006). World Ocean Atlas 2005, Volume 2: Salinity. Washington, D. C., U.S. Government Printing Office.

Aumont, O., E. Maier-Reimer, S. Blain and P. Monfray (2003). "An ecosystem model of the global ocean including Fe, Si, P colimitations." Global Biogeochem. Cycles 17(2): 1060, doi:10.1029/2001GB001745.

Bakker, D. C. E., B. Pfeil, A. Olsen, C. L. Sabine, N. Metzl, S. Hankin, H. Koyuk, A. Kozyr, J. Malczyk, A. Manke and M. Telszewski (2012). "Global Data Products Help Assess Changes to Ocean Carbon Sink." EoS Transactions 93(12): 125-132.

Ballantyne, A. P., C. B. Alden, et al. (2012). "Increase in observed net carbon dioxide uptake by land and oceans during the past 50 years." Nature 488: 70-72.

Barnston, A. G. and R. E. Livezey (1987). "Classification, seasonality and persistence of low-frequency atmospheric circulation patterns." Monthly Weather Review 115(6): 1083-1126.

Bates, N. R., A. F. Michaels, et al. (1996). "Seasonal and interannual variability of oceanic carbon dioxide species at the U.S. JGOFS Bermuda Atlantic Time-series Study (BATS) site." Deep Sea Research II 43(2-3): 347-383.

Bates, N. R. (2007). "Interannual variability of the oceanic CO_2 sink in the subtropical gyre of the North Atlantic Ocean over the last 2 decades." J. Geophys. Res. 112: C09013, doi:10.1029/2006JC003759.

Bates, N. R. (2012). "Multi-decadal uptake of carbon dioxide into subtropical mode water of the North Atlantic Ocean." Biogeosciences Discuss. 8(6): 12451-12476.

Behrenfeld, M. J. (2010). "Abandoning Sverdrup's critical depth hypothesis on phytoplankton blooms." Ecology 91(4): 977-989.

Bigg, G. R. (2003). The Oceans and Climate, Second Edition. Cambridge, New York, Melbourne, Madrid, Cape Town, Singapore, São Paulo, Cambridge University Press.

Bingham, R. J., K. Haines, et al. (2008). "Calculating the ocean's mean dynamic topography from a mean sea surface and a geoid " Journal of Atmospheric and Oceanic Technology **25**: 1808-1822.

Bopp, L. and C. Le Quéré (2001). Ocean carbon cycle. Surface Ocean - Lower Atmosphere Processes. C. Le Quéré and E. S. Saltzmann. Washington, D.C., American Geophysical Union**:** 181-195.

Bretherton, C. S., M. Widmann, et al. (1999). "The effective number of spatial degrees of freedom of a time-varying field." Journal of Climate **12**: 1990-2009.

Buitenhuis, E. T., R. B. Rivkin, S. Sailley and C. Le Quéré (2010). "Biogeochemical fluxes through microzooplankton." Global Biogeochem. Cycles 24(4): GB4015, doi:10.1029/2009GB003601.

Cabanes, C., T. Huck and A. Colin de Verdière (2006). "Contributions of wind forcing and surface heating to interannual sea level variations in the Atlantic Ocean." Journal of Physical Oceanography 36(9): 1739-1750.

Canadell, J. G., C. Le Quéré, M. R. Raupach, C. B. Field, E. T. Buitenhuis, P. Ciais, T. J. Conway, N. P. Gillett, R. A. Houghton and G. Marland (2007). "Contributions to accelerating atmospheric CO_2 growth from economic activity, carbon intensity, and efficiency of natural sinks." Proc. Natl Acad. Sci. USA 104: 18866-18870.

Chatfield, C. (2004). The Analysis of Time Series: An Introduction. New York, CRC Press LLC.

Chelton, D. B. (1982). "Statistical reliability and the seasonal cycle: comments on 'Bottom pressure measurements across the antarctic circumpolar current and their

relation to the wind'." Deep Sea Research Part A. Oceanographic Research Papers 29(11): 1381-1388.

Cooper, D. J., A. J. Watson and R. D. Ling (1998). "Variation of pCO_2 along a North Atlantic shipping route (UK to the Caribbean): A year of automated observations." Marine Chemistry 60(1-2): 147-164.

Corbière, A., N. Metzl, G. Reverdin, C. Brunet and T. Takahashi (2007). "Interannual and decadal variability of the oceanic carbon sink in the North Atlantic subpolar gyre." Tellus B 59: 168-179.

Cotrim da Cunha, L., E. T. Buitenhuis, C. Le Quéré, X. Giraud and W. Ludwig (2007). "Potential impact of changes in river nutrient supply on global ocean biogeochemistry." Global Biogeochem. Cycles 21(4): GB4007.

Cullen, J. J. (1982). "The deep chlorophyll maximum: comparing vertical profiles of chlorophyll a." Canadian Journal of Fisheries and Aquatic Sciences 39: 791–803.

Curry, R. G. and M. S. McCartney (2001). "Ocean gyre circulation changes associated with the North Atlantic Oscillation." Journal of Physical Oceanography 31(12): 3374-3400.

Deser, C., M. A. Alexander, S.-P. Shang-Ping Xie and A. S. Phillips (2010). "Sea surface temperature variability: Patterns and mechanisms." Annual Review of Marine Science 2: 115–43.

Dibarboure, G., O. Lauret, F. Mertz, V. Rosmorduc and C. Maheu (2009). SSALTO/DUACS User Handbook : (M)SLA and (M)ADT Near-Real Time and Delayed Time Products. Ramonville St Agne, AVISO.

Dickson, A. G. (1981). "An exact definition of total alkalinity and a procedure for the estimation of alkalinity and total inorganic carbon from titration data." Deep Sea Research 28: 609-623.

Dickson, A. G., C. L. Sabine and J. R. Christian (2007). Guide to best practices for ocean CO_2 measurements. PICES Special Publication 3: 191pp.

Esselborn, S. and C. Eden (2001). "Sea surface height changes in the North Atlantic Ocean related to the North Atlantic Oscillation." Geophysical Research Letters 28(18): 3473-3476.

Ferry, N., S. Masina, A. Storto, K. Haines, M. Valdivieso, B. Barnier and J.-M. Molines. (2011). "Product User Manual GLOBAL-REANALYSIS-PHYS-001-004-a and b." from http://catalogue.myocean.eu.org/static/resources/user_manual/myocean/USER_MANUAL_GLOBAL_001_004_v1.0.pdf.

Flatau, M. K., L. Talley and P. P. Niiler (2003). "The North Atlantic Oscillation, surface current velocities, and SST changes in the subpolar North Atlantic." Journal of Climate 16(14): 2355-2369.

Folland, C. K., J. Knight, H. W. Linderholm, D. Fereday, S. Ineson and J. W. Hurrell (2009). "The Summer North Atlantic Oscillation: Past, Present, and Future." Journal of climate 22(5): 1082-1103.

Follows, M. and S. Dutkiewicz (2001). "Meteorological modulation of the North Atlantic spring bloom." Deep Sea Research Part II: Topical Studies in Oceanography 49(1-3): 321-344.

Frankignoul, C., G. de Coëtlogon, T. M. Joyce and S. Dong (2001). "Gulf Stream Variability and Ocean-Atmosphere Interactions." Journal of Physical Oceanography 31(12): 3516-3529.

Gaspar, P., Y. Grégoris and J.-M. Lefevre (1990). "A Simple Eddy Kinetic Energy Model for Simulations of the Oceanic Vertical Mixing: Tests at Station Papa and Long-Term Upper Ocean Study Site." J. Geophys. Res. 95(C9): 16179-16193.

Gent, P. R. and J. C. McWilliams (1990). "Isopycnal Mixing in Ocean Circulation Models." Journal of Physical Oceanography 20(1): 150-155.

Gregg, W. W. and M. E. Conkright (2002). "Decadal changes in global ocean chlorophyll." Geophysical Research Letters 29(15): 1730, doi:10.1029/2002GL014689.

Gruber, N., C. D. Keeling and N. R. Bates (2002). "Interannual variability in the North Atlantic Ocean carbon sink." Science 298(5602): 2374-2378.

Häkkinen, S. and P. B. Rhines (2004). "Decline of subpolar North Atlantic circulation during the 1990s." Science 304(5670): 555-559.

Häkkinen, S. and P. B. Rhines (2009). "Shifting surface currents in the northern North Atlantic Ocean." J. Geophys. Res. 114: C04005, doi:10.1029/2008JC004883.

Huot, Y., M. Babin, F. Bruyant, C. Grob, M. S. Twardowski and H. Claustre (2007). "Does chlorophyll a provide the best index of phytoplankton biomass for primary productivity studies?" Biogeosciences Discussions **4**(707–745).

Hurrell, J. W. (1995). "Decadal trends in the North Atlantic Oscillation - regional temperatures and precipitation." Science 269(5224): 676-679.

Hurrell, J. W. and C. Deser (2009). "North Atlantic climate variability: The role of the North Atlantic Oscillation." Journal of Marine Systems 79(3-4): 231-244.

Imawaki, S., H. Uchida, H. Ichikawa, M. Fukasawa, S. Umatani and t. A. Group (2001). "Satellite altimeter monitoring the Kuroshio transport south of Japan." Geophysical Research Letters **28**(1): 17-20.

IPCC (2001). Climate Change 2001: The Scientific Basis. Contribution of Working Group I to the Third Assessment Report of Intergovernmental Panel on Climate Change. J. T. Houghton, Y. Ding, D. J. Griggset al. Cambridge, Cambridge University Press.

IPCC (2007). Climate Change 2007: The Physical Science Basis. Contribution of Working Group I to the Fourth Assessment Report of the IPCC. Cambridge and New York, Cambridge University Press.

Jones, S. D., C. Le Quéré and C. Rödenbeck (2012). "Autocorrelation characteristics of surface ocean pCO2 and air-sea CO2 fluxes." Global Biogeochemical Cycles **26**: GB2042.

Kalnay, E., M. Kanamitsu, R. Kistler, W. Collins, D. Deaven, L. Gandin, M. Iredell, S. Saha, G. White, J. Woollen, Y. Zhu, M. Chelliah, W. Ebisuzaki, W. Higgins, J. Janowiak, K. C. Mo, C. Ropelewski, J. Wang, A. Leetmaa, R. Reynolds, R. Jenne and D. Joseph (1996). "The NCEP/NCAR 40-year reanalysis project." Bull. Am. Meteorol. Soc. 77: 437-471.

Keeling, C. D., R. B. Bacastow, A. E. Bainbridge, C. A. Ekdahl, P. R. Guenther and L. S. Waterman (1976). "Atmospheric carbon dioxide variations at Mauna Loa Observatory, Hawaii." Tellus **28**: 538-551.

Kubryakov, A. A. and S. V. Stanichny (2011). "Mean Dynamic Topography of the Black Sea, computed from altimetry, drifter measurements and hydrology data." Ocean Science **7**: 745-753.

Le Quéré, C., S. P. Harrison, I. C. Prentice, E. T. Buitenhuis, O. Aumont, L. Bopp, H. Claustre, L. Cotrim Da Cunha, R. Geider, X. Giraud, C. Klaas, K. E. Kohfeld, L. Legendre, M. Manizza, T. Platt, R. B. Rivkin, S. Sathyendranath, J. Uitz, A. J. Watson and D. Wolf-Gladrow (2005). "Ecosystem dynamics based on plankton functional types for global ocean biogeochemistry models." Global Change Biology 11: 2016–2040.

Le Quéré, C., C. Rödenbeck, E. T. Buitenhuis, T. J. Conway, R. Langenfelds, A. Gomez, C. Labuschagne, M. Ramonet, T. Nakazawa, N. Metzl, N. Gillett and M. Heimann (2007). "Saturation of the Southern Ocean CO2 sink due to recent climate change." Science **316**: 1735-1737.

Lefèvre, N., A. J. Watson, A. Olsen, A. F. Rios, F. F. Perez and T. Johannessen (2004). "A decrease in the sink for atmospheric CO_2 in the North Atlantic." Geophysical Research Letters 31(7): L07306, doi:10.1029/2003GL018957.

Levine, N. M., S. C. Doney, I. Lima, R. Wanninkhof, N. R. Bates and R. A. Feely (2011). "The impact of the North Atlantic Oscillation on the uptake and accumulation of anthropogenic CO_2 by North Atlantic Ocean mode waters." Global Biogeochem. Cycles 25(3): GB3022, doi:10.1029/2010GB003892.

Liss, P. S. and L. Merlivat (1986). Air-sea gas exchange rates: Introduction and synthesis. The Role of Air-Sea Exchange in Geochemical Cycling. P. Buat-Menard. Dordrecht, Reidel Publishing: 113-127.

Locarnini, R. A., A. V. Mishonov, J. I. Antonov, T. P. Boyer and H. E. Garcia (2006). World Ocean Atlas 2005, Volume 1: Temperature. Washington, D.C., U.S. Government Printing Office.

Longhurst, A., S. Sathyendranath, T. Platt and C. Caverhill (1995). "An estimate of global primary production in the ocean from satellite radiometer data." Journal of Plankton Research 17(6): 1245-1271.

Madec, G. (2008). NEMO Ocean Engine. Pole Model Note 27. Paris.

Manizza, M., E. T. Buitenhuis and C. Le Quéré (2010). "Sensitivity of global ocean biogeochemical dynamics to ecosystem structure in a future climate." Geophys. Res. Lett. 37(13): L13607, doi:10.1029/2010GL043360.

Marshall, J. and R. A. Plumb (2007). Atmosphere, Ocean and Climate Dynamics: An Introduction. Burlington, MA, Academic Press.

Marshall, J., R. Ferrari, G. Forget, G. Maze, A. Andersson, N. Bates, W. Dewar, S. Doney, D. Fratantoni, T. Joyce, F. Straneo, J. Toole, R. Weller, J. Edson, M. Gregg, K. Kelly, S. Lozier, J. Palter, R. Lumpkin, R. Samelson, E. Skyllingstad, K. Silverthorne, L. Talley and L. Thomas (2009). "The Climode Field Campaign: Observing the Cycle of Convection and Restratification over the Gulf Stream." Bulletin of the American Meteorological Society 90(9): 1337-1350.

Marshall, J., Y. Kushner, D. Battisti, P. Chang, A. Czaja, R. Dickson, J. Hurrell, M. McCartney, R. Saravanan and M. Visbeck (2001). "North Atlantic climate variability: Phenomena, impacts and mechanisms." International Journal of Climatology 21(15): 1863-1898.

Mason, E., S. Coombs and P. B. Oliveira (2006). An overview of the literature concerning the oceanography of the eastern North Atlantic region. Relatórios Científicos e Técnicos. Lisbon, INIAP.

McClain, C. R., M. L. Cleave, G. C. Feldman, W. W. Gregg, S. B. Hooker and N. Kuring (1998). "Science quality SeaWiFS data for global biosphere research." Sea Technology **39**(9): 10–16.

McKinley, G. A., A. R. Fay, T. Takahashi and N. Metzl (2011). "Convergence of atmospheric and North Atlantic carbon dioxide trends on multidecadal timescales." Nature Geoscience **4**: 606-610.

Metzl, N., A. Corbière, G. Reverdin, A. Lenton, T. Takahashi, A. Olsen, T. Johannessen, D. Pierrot, R. Wanninkhof and S. R. Ólafsdóttir (2010). "Recent acceleration of the sea surface fCO_2 growth rate in the North Atlantic subpolar gyre (1993–2008) revealed by winter observations." Global Biogeochem. Cycles 24: 1992–2006.

O'Reilly, J. E., S. Maritorena, B. G. Mitchell, D. A. Siegel, K. L. Carder, S. A. Garver, M. Kahru and C. R. McClain (1998). "Ocean color chlorophyll algorithm for SeaWiFS." J. Geophys. Res. **103**: 24 937–24 953.

Olsen, A., A. M. Omar, R. G. J. Bellerby, T. Johannessen, U. Ninnemann, K. R. Brown, K. A. Olsson, J. Olafsson, G. Nondal, C. Kivimäe, S. Kringstad, C. Neill and S. Olafsdottir (2006). "Magnitude and origin of the anthropogenic CO_2 increase and 13C Suess effect in the Nordic seas since 1981." Global Biogeochem. Cycles 20: GB3027, doi:10.1029/2005GB002669.

Omar, A. M. and A. Olsen (2006). "Reconstructing the time history of the air-sea CO_2 disequilibrium and its rate of change in the eastern subpolar North Atlantic, 1972-1989." Geophysical Research Letters 33: L04602, doi:10.1029/2005GL025425.

Osborn, T. J. (2011). "Winter 2009/2010 temperatures and a record-breaking North Atlantic Oscillation index." Weather **66**(1): 19-21.

Oschlies, A. (2001). "NAO-induced long-term changes in nutrient supply to the surface waters of the North Atlantic." Geophys. Res. Lett. 28(9): 1751-1754.

Padin, X. A., C. G. Castro, A. F. Ríos and F. F. Pérez (2011). "Oceanic CO_2 uptake and biogeochemical variability during the formation of the Eastern North Atlantic

Central water under two contrasting NAO scenarios." Journal of Marine Systems 84(3-4): 96-105.

Pfeil, B., A. Olsen, D. C. E. Bakker, S. Hankin, H. Koyuk, A. Kozyr, J. Malczyk, A. Manke, N. Metzl, C. L. Sabine, J. Akl, S. R. Alin, R. G. J. Bellerby, A. Borges, J. Boutin, P. J. Brown, W.-J. Cai, F. P. Chavez, A. Chen, C. Cosca, A. J. Fassbender, R. A. Feely, M. González-Dávila, C. Goyet, N. Hardman-Mountford, C. Heinze, M. Hood, M. Hoppema, C. W. Hunt, D. Hydes, M. Ishii, T. Johannessen, S. D. Jones, R. M. Key, A. Körtzinger, P. Landschützer, S. K. Lauvset, N. Lefèvre, A. Lenton, A. Lourantou, L. Merlivat, T. Midorikawa, L. Mintrop, C. Miyazaki, A. Murata, A. Nakadate, Y. Nakano, S. Nakaoka, Y. Nojiri, A. M. Omar, X. A. Padin, G.-H. Park, K. Paterson, F. F. Perez, D. Pierrot, A. Poisson, A. F. Ríos, J. M. Santana-Casiano, J. Salisbury, V. V. S. S. Sarma, R. Schlitzer, B. Schneider, U. Schuster, R. Sieger, I. Skjelvan, T. Steinhoff, T. Suzuki, T. Takahashi, K. Tedesco, M. Telszewski, H. Thomas, B. Tilbrook, J. Tjiputra, D. Vandemark, T. Veness, R. Wanninkhof, A. J. Watson, R. Weiss, C. S. Wong and H. Yoshikawa-Inoue (2012). "A uniform, quality controlled Surface Ocean CO_2 Atlas (SOCAT)." Earth Syst. Sci. Data Discuss. 5: 735-780.

Roullet, G. and G. Madec (2000). "Salt conservation, free surface, and varying levels: a new formulation for ocean general circulation models." J. Geophys. Res. 105(C10): 23927-23942.

Sabine, C. L., R. A. Feely, N. Gruber, R. M. Key, K. Lee, J. L. Bullister, R. Wanninkhof, C. S. Wong, D. W. R. Wallace, B. Tilbrook, F. J. Millero, T. H. Peng, A. Kozyr, T. Ono and A. F. Rios (2004). "The oceanic sink for anthropogenic CO_2." Science 305(5682): 367-371.

Sarmiento, J. L. and N. Gruber (2006). Ocean Biogeochemical Dynamics. Princeton, Princeton University Press.

Sarmiento, J. L., R. Slater, R. Barber, L. Bopp, S. C. Doney, A. C. Hirst, J. Kleypas, R. Matear, U. Mikolajewicz, P. Monfray, V. Soldatov, S. A. Spall and R. Stouffer (2004). "Response of ocean ecosystems to climate warming." Global Biogeochemical Cycles **18**(3): GB3003.

Schuster, U., G. A. McKinley, N. Bates, F. Chevallier, S. Doney, A. R. Fay, E. F. González-Dávila, N. Gruber, S. Jones, J. Krijnen, P. Landschützer, N. Lefèvre, M. Manizza, J. Mathis, N. Metzl, A. Olsen, A. F. Rios, C. Rödenbeck, J. M. Santana-Casiano, T. Takahashi, R. Wanninkhof and A. J. Watson (2012). "Atlantic and Arctic sea-air CO_2 fluxes, 1990 - 2009 " Biogeosciences Discuss. 9: 10669 - 10724.

Schuster, U. and A. J. Watson (2007). "A variable and decreasing sink for atmospheric CO_2 in the North Atlantic." Journal of Geophysical Research-Oceans 112: C11006, doi:10.1029/2006JC003941.

Schuster, U., A. J. Watson, N. R. Bates, A. Corbiere, M. Gonzalez-Davila, N. Metzl, D. Pierrot and M. Santana-Casiano (2009). "Trends in North Atlantic sea-surface fCO_2 from 1990 to 2006." Deep Sea Research Part II: Topical Studies in Oceanography 56(8-10): 620-629.

Sinha, B., E. T. Buitenhuis, C. Le Quéré and T. R. Anderson (2010). "Comparison of the emergent behaviour of a complex ecosystem model in two ocean general circulation models." Progress in Oceanography **84**: 204-224.

Steinhoff, T., T. Friedrich, S. E. Hartman, A. Oschlies, D. W. R. Wallace and A. Körtzinger (2010). "Estimating mixed layer nitrate in the North Atlantic Ocean." Biogeosciences (BG) 7: 795-807.

Strom, S., C. Miller and B. Frost (2000). "What sets lower limits to phytoplankton stocks in high-nitrate, low chlorophyll regions of the open ocean?" Marine Ecology Progress Series 193: 19-31.

Takahashi, T., J. Olafsson, J. G. Goddard, D. W. Chipman and S. C. Sutherland (1993). "Seasonal variation of CO_2 and nutrients in the high-latitude surface oceans: A comparative-study." Global Biogeochemical Cycles 7(4): 843-878.

Takahashi, T., S. C. Sutherland, R. A. Feely and R. Wanninkhof (2007). "Decadal change of the surface water pCO2 in the North Pacific: a synthesis of 35 years of observations." J. Geophys. Res. 111: C07S05.

Takahashi, T., S. C. Sutherland, C. Sweeney, A. Poisson, N. Metzl, B. Tilbrook, N. Bates, R. Wanninkhof, R. A. Feely, C. Sabine, J. Olafsson and Y. Nojiri (2002).

"Global sea-air CO_2 flux based on climatological surface ocean pCO_2, and seasonal biological and temperature effects." Deep-Sea Research Part Ii-Topical Studies in Oceanography 49(9-10): 1601-1622.

Takahashi, T., S. C. Sutherland, R. Wanninkhof, C. Sweeney, R. A. Feely, D. W. Chipman, B. Hales, G. Friederich, F. Chavez, C. Sabine, A. Watson, D. C. E. Bakker, U. Schuster, N. Metzl, H. Yoshikawa-Inoue, M. Ishii, T. Midorikawa, Y. Nojiri, A. Körtzinger, T. Steinhoff, M. Hoppema, J. Olafsson, T. S. Arnarson, B. Tilbrook, T. Johannessen, A. Olsen, R. Bellerby, C. S. Wong, B. Delille, N. R. Bates and H. J. W. de Baar (2009). "Climatological mean and decadal change in surface ocean pCO_2, and net sea-air CO_2 flux over the global oceans." Deep Sea Research Part II: Topical Studies in Oceanography 56(8-10): 554-577.

Thomas, H., A. E. F. Prowe, I. Lima, S. Doney, R. Wanninkhof, R. J. Greatbatch, U. Schuster and A. Corbiere (2008). "Changes in the North Atlantic Oscillation influence CO_2 uptake in the North Atlantic over the past two decades." Glob. Biogeochem. Cycles 22: GB4027.

Tjiputra, J., A. Olsen, K. Assmann, B. Pfeil and C. Heinze (2012). "A model study of the seasonal to long-term North Atlantic surface pCO_2 variability." Biogeosciences 9: 907-923.

Tomcak, M. and J. S. Godfrey (2001). Regional Oceanography: An Introduction, Daya Publishung House, Delhi.

Ullman, D. J., G. A. McKinley, V. Bennington and S. Dutkiewicz (2009). "Trends in the North Atlantic carbon sink: 1992 - 2006." Global Biogeochem. Cycles 23: GB4011, doi:10.1029/2008GB003383.

van Sebille, E., L. M. Beal and A. Biastoch (2010). "Sea surface slope as a proxy for Agulhas Current strength." Geophysical Research Letters **37**: L09610.

Visbeck, M., E. P. Chassignet, R. G. Curry, T. L. Delworth, R. R. Dickson and G. Krahmann (2003). The ocean's response to North Atlantic Oscillation variability. The North Atlantic Oscillation: Climatic Significance and Environmental Impact. Washington, DC, AGU. 134: 113-145.

Volk, T. and M. I. Hoffert (1985). Ocean carbon pumps: analysis of relative strengths and efficiencies in ocean-driven atmospheric CO_2 changes. The Carbon Cycle and Atmospheric CO_2: Natural Variations Archean to Present. E. T. Sundquist and W. S. Broecker. Washington D.C., American Geophysical Union: 99-110.

Wanninkhof, R. (1992). "Relationship between wind speed and gas exchange over the ocean." Journal of Geophysical Research 97: 7373-7383.

Watson, A. J. and J. C. Orr (2003). Carbon dioxide fluxes in the global ocean. Ocean Biogeochemistry: The role of the ocean carbon cycle in global change. M. J. R. Fasham. Berlin, Springer: 123-143.

Watson, A. J., U. Schuster, D. C. E. Bakker, N. R. Bates, A. Corbiere, M. Gonzalez-Davila, T. Friedrich, J. Hauck, C. Heinze, T. Johannessen, A. Kortzinger, N. Metzl, J. Olafsson, A. Olsen, A. Oschlies, X. A. Padin, B. Pfeil, J. M. Santana-Casiano, T. Steinhoff, M. Telszewski, A. F. Rios, D. W. R. Wallace and R. Wanninkhof (2009). "Tracking the Variable North Atlantic Sink for Atmospheric CO_2." Science 326(5958): 1391-1393.

Weiss, R. F. (1974). "Carbon dioxide in water and seawater: the solubility of a non-ideal gas." Marine chemistry 2(3): 203-215.

Wheater, C. P. and P. A. Cook (2000). Using Statistics to Understand the Environment, Routledge, Taylor and Francis Group.

While, J., I. Totterdell and M. M. Martin (2012). "Assimilation of pCO_2 data into a global coupled physical-biogeochemical ocean model." Journal of Geophysical Research **117**: C03037.

Woolf, D. K., P. E. Land, J. D. Shutler and L. M. Goddijn-Murphy (2012). "Thermal and haline effects on the calculation of air-sea CO_2 fluxes revisited." Biogeosciences Discuss. **9**: 16381–16417.

Yentsch, C. S. (1960). "The influence of phytoplankton pigments on the colour of seawater." Deep Sea Research **7**: 1-9.